Bioconvection Flow of a Nanofluid Past an Inclined Wavy Surface

A thesis submitted to
NATIONAL INSTITUTE OF TECHNOLOGY WARANGAL, (T.S.)
for the award of the degree of
DOCTOR OF PHILOSOPHY
in
MATHEMATICS

by
KALAKUNTLA SITA RAMANA
(Roll No. 718070)

UNDER THE SUPERVISION OF
Prof. D. SRINIVASACHARYA

DEPARTMENT OF MATHEMATICS
NATIONAL INSTITUTE OF TECHNOLOGY
WARANGAL - 506 004, INDIA

AUGUST 2021

C E R T I F I C A T E

This is to certify that the thesis entitled " **Bioconvection Flow of a Nanofluid Past an Inclined Wavy Surface** " submitted to National Institute of Technology Warangal, for the award of the degree of ***Doctor of Philosophy***, is the bonafide research work done by **Mr. KALAKUNTLA SITA RAMANA** under my supervision. The contents of this thesis have not been submitted elsewhere for the award of any degree.

Dr. D. Srinivasacharya
Professor
Department of Mathematics
National Institute of Technology,
Warangal, T.S., INDIA

.

DECLARATION

This is to certify that the work presented in the thesis entitled **"Bioconvection Flow of a Nanofluid Past an Inclined Wavy Surface"**, is a bonafide work done by me under the supervision of **Prof. D. SRINIVASACHARYA** and has not been submitted elsewhere for the award of any degree.

I declare that this written submission represents my ideas in my own words and where others' ideas or words have been included, I have adequately cited and referenced the original sources. I also declare that I have adhered to all principles of academic honesty and integrity and have not misrepresented or fabricated or falsified any idea / data / fact /source in my submission. I understand that any violation of the above will be a cause for disciplinary action by the Institute and can also evoke penal action from the sources which have thus not been properly cited or from whom proper permission has not been taken when needed.

Kalakuntla Sita Ramana

Roll No. 718070

Date:_____

Dedicated to

My Parents

Dr. K. Kodanda Ramacharyulu , Shakunthala

&

Lord Sri Venkateshwara Swamy

ACKNOWLEDGEMENTS

It is a rare privilege and boon that I could associate myself with Dr. D. Srinivasacharya, Professor of Mathematics, National Institute of Technology Warangal, India, for pursuing my research work. I sincerely record my gratitude for his invaluable guidance and constant encouragement throughout the preparation of this thesis and his involvement and meticulous supervision while my work was in progress. With his inimitable qualities as a good teacher, he chiseled my path towards perfection. He has been a perpetual source of inspiration, spiritual guidance, encouragement, and enlightenment since I first met him. He is the one who ensured that the duration of my research work was both educational and fun. He has been a great source of motivation and inspiration. The thesis would not have seen the light of the day without his unrelenting support and cooperation. I deem it a privilege to have worked under his amiable guidance. My vocabulary is inadequate to express my gratitude. I also thank madam Smt. D. Jaya Srinivasacharya for her hospitality and patience during our elongated discussions with my supervisor.

I am grateful to Dr. P. Muthu, Head, and Prof. D. Srinivasacharya, Prof. Debashis Dutta, former Heads, Department of Mathematics for providing necessary help and support throughout my research period.

I take this opportunity to thank Prof. Y. N. Reddy, and Prof. J. V. Ramana Murthy, Department of Mathematics for their valuable suggestions, moral support and encouragement during my stay.

I thank the members of the Doctoral Scrutiny Committee, Prof. K. N. S. Kasi Viswanadham and Dr. Ch. Ramreddy, Department of Mathematics, and Dr. T. V. Appa Rao, Department of Physics for their valuable suggestions, moral support, and encouragement while my work was in progress.

I place on record my gratitude to all the faculty members of the Department of Mathematics, for their constant encouragement.

I express my sincere thanks to the Director, National Institute of Technology, Warangal for providing me QIP Fellowship (AICTE, GoI) to carry out my research work.

I thank Dr. P. Jagadeeshwar, Dr. P. Naveen, Dr. I. Sreenath, Dr. Pavankumar Reddy, Dr. Shivakumar Reddy, Mr. Dipak Barman, Mr. Abhinav Srivasthav, Mr. R. Shravan Kumar, Mr. B. Rajendar and all other research colleagues in the Department of mathematics and my friends, who helped me during my Ph.D. for being cooperative and also for making my stay in the NITW campus fruitful and enjoyable every moment.

I am ever grateful to Sri. P. Usha Kiran Kumar, Chairman, Vijaya Engineering College, Khammam, for his ever encouraging nature and the moral support given to me to complete this research work.

I feel it my privilege to honor Sri R. Atma Ram Rao, Formal Principal, Kavitha Degree College, Khammam, and my well-wisher for his ever-ending blessings.

I greatly acknowledge Sri N. B. Rama Rao, Dr. Ch. Radha Krishna, T. Rama Chandra Rao, M. Srinivasa Rao, and Dr. B. Raja Gopal (Late) for their constant encouragement.

I owe my special thanks to Dr. R. E. P. Koundinya (Late) and G. L. N. Sarma, my classmates, for all their continuous encouragement while doing my research work.

My heartfelt gratitude goes to my parents, Dr. K. Kodanda Ramacharyulu and Smt. K. Shakunthala (Janaki), whose encouragement and blessings inspired me to finish my job ahead of schedule. I am overjoyed to thank my family members for their contributions to the completion of this job. All of their prayers, support, love, and affection have been the driving force behind what has happened.

Kalakuntla Sita Ramana

A B S T R A C T

Bioconvection is due to microscopic convection generated by the density gradient produced by the collective motion of self-propelled motile microorganisms within the fluid. Several researchers have been enticed in the study of bioconvection in Newtonian and non-Newtonian fluids due to the multifaceted range of applications in biological systems and biotechnology. Although the combination of nanofluid elements along with the bioconvection is important, very little work has been reported in the literature. The purpose of this thesis is to study the bioconvection flow of nanofluids past an inclined wavy surface.

This thesis consists of Ten chapters. Chapter - 1 provides an introduction to the concepts and a review of the pertinent literature. Chapter-2 deals with the Computational analysis of double diffusive bioconvection of a nanofluid past an inclined wavy surface. In Chapter - 3, the Thermal radiation and double-diffusive effects on bioconvection flow of a nanofluid past an inclined wavy surface is considered. Chapter - 4 presents the mixed convection of a nanofluid past an inclined wavy surface in the presence of gyrotactic microorganisms. Chapter - 5 considers the mixed convection of a nanofluid past an inclined wavy surface in the presence of gyrotactic microorganisms and magnetic field. In Chapter - 6, the Effect of variable properties on the bioconvection in a nanofluid flow past an inclined wavy surface is studied. Chapter - 7 provides the Natural convection of nanofluid flow past an inclined wavy surface in the presence of gyrotactic microorganisms with activation energy. In Chapter - 8, the Radiation effect on mixed convection of a nanofluid past an inclined wavy surface in the presence of gyrotactic microorganisms with variable properties are analyzed. Chapter - 9, handles the Bioconvection in a nanofluid past a moving inclined wavy surface with convective boundary conditions.

In all the above chapters, A coordinate transformation is applied to convert the wavy surface to a plane surface. The equations governing the flow and the accompanying boundary conditions are non-dimensionalized employing pseudo-similarity variables and then linearized by utilizing the local linearization method. The bivariate Chebyshev pseudo-spectral collocation procedure is implemented to solve the resulting linear equations

The last chapter, Chapter - 10, gives a summary and overall conclusions and scope for future work.

NOMENCLATURE

A	Angle of the wavy plate.
Bi	Biot Number
b_c	Chemotaxis constant.
C	Concentration of the fluid.
Cf_x	Skinfriction number.
C_∞	Ambient concentration.
D_B	Brownian diffusion coefficient.
D_{CT}	Soret type diffusivity.
D_n	Diffusivity of the microorganisms.
D_S	Solutal diffusion coefficient.
D_T	Thermophoretic diffusion coefficient of the microorganisms.
D_{TC}	Dufour type diffusivity.
E	Activation energy parameter.
E_a	Coefficient of activation energy.
E_c	Eckert number.
f	Dimensionless stream function.
g	acceleration due to gravity.
Gr	Grashof Number.
Ha	Magnetic induction parameter.
J_0	Joule heating parameter.
k	Thermal conductivity.
K_e	Mean absorption coefficient.
k_0	Thermal conductivity.
L	wavelength associated with the wavy surface.
Le	regular Lewis Number.
Ln	Nanoparticle Lewis Number.
M	Density of the motile microorganism.
M_∞	Ambient density of motile microorganism.
N_b	Brownian motion parameter.
N_c	regular double diffusive buoyancy Ratio.
N_d	Modified Dufour Number.
N_r	Nanofluid Buoyancy Ratio.
N_t	Thermophoresis parameter.
NSh_x	Nanoparticle Sherwood number.
Nu_x	Local Nusselt number.
P	Pressure.
Pe	Bio-convection Peclet number.
P_n	Pearson number.
Pr	Prandtl number.
Q_x	Motile microorganism Density Number.
q_m	Mass flux.
q_n	Surface motile microorganisms flux.
q_{np}	Nanoparticle Mass Flux.
q_w	Heat Flux.
Re	Rayleigh number.
R_b	Bio-convection Rayleigh number.
R_d	Radiation Parameter.
Ri	Mixed convection parameter.

Sc Bio-convection Schmidt number.

Sh_x Local Sherwood number.

S_r Soret Number.

T Fluid Temperature.

T_w Wall temperature.

T_∞ Ambient Temperature.

U_∞ Free stream velocity.

U Velocity component in X direction.

V Velocity component in Y direction.

$\widetilde{V}$ Average Swimming velocity.

w_c Maximum cell swimming speed.

Greek Symbols

α Amplitude associated with the wavy surface.

α_m Thermal diffusivity of the fluid.

β Temperature dependent thermal conductivity parameter.

β_C Coefficient of Solutal expansion.

β_M Coefficient of Microorganism expansion.

β_T Coefficient of Thermal expansion.

γ Nanofluid heat capacity ratio.

δ Temperature ralative parameter.

δ_1 Reaction rate parameter.

$\delta\chi$ Constant.

η Non-dimensional variable / Similarity variable.

$\sigma(x)$ Wavy surface of the plate.

σ_1 Reaction rate parameter.

σ_2 Stefan Boltzman constant.

θ Dimensionless temperature.

κ Boltzman constant.

μ Dynamic Viscosity of the fluid.

μ_∞ Absolute Viscosity of the fluid.

ν Magnetic diffusivity/kinetic viscosity.

ξ Non-dimensional variable / dimensionless distance.

ρc_f Heat capacity of the fluid.

ρ_f Density of the fluid.

ρ_p Density of the nanoparticles.

Φ Nanoparticle volume fraction.

φ Dimensionless fluid concentration.

χ Dimensionless microorganism.

ϕ Dimensionless Nanoparticle Volume fraction.

Φ_∞ Ambient nanoparticle volume fraction.

ψ Stream function.

Subscripts

w wall condition.

∞ Ambient condition.

Superscript

$\prime$ Partial differentiation with respect to η.

Contents

[1]Published in "**International Journal of Applied and Computational Mathematics**",7, No. 4, 173 (2021)

[2]Published in "**Thermal Science and Engineering Progress**", 22 (2021): 100830

[3]Published in "**Heat Transfer**", Early View, 2021, DOI: 10.1002htj.22291

[4]Communicated to "**Pramana Journal of Physics**"

[5]Communicated to "**Computational Thermal Sciences**"
[6]Communicated to "**International Journal of Engineering Systems Modelling and Simulation**"
[7]Communicated to "**Journal of Applied Nonlinear Dynamics**"
[8]Communicated to "**International Journal of Applied Mechanics and Engineering**"

Chapter 1

Preliminaries and Review

1.1 Introduction

The study of microorganisms and their swimming behaviour, which can lead to cell aggregation, can provide insight into the lifecycle of these cells. Furthermore, studies of group motion caused by cell swimming may reveal insights into phenomena such as self-ordering or cell migration, and the findings of these studies can be used to explore other problems involving many species and organisms. Many of these microorganisms have applications in industry and commerce. Some species of microorganisms yield ethanol as a consequence of intracellular photosynthesis and respiration and have a variety of applications such as wastewater treatment plants, fertilisers, plastics, and solid fuels. Recently, various microorganisms have been used to produce hydrogen gas and biodiesel, acting as an efficient source of biofuels or biodiesel industry. As a result, they can serve as a potential source of renewable energy, reducing our reliance on depleting fossil fuel reservoirs and biofuels derived from edible crops such as corn, maze, coconut, palm, and so on.

Flow and heat transfer over irregular surfaces are frequently encountered in many engineering applications to improve heat transfer, such as in a microelectronic device cooling system, flat-plate condensers flat-plate and solar collectors in refrigerators, electric machinery, underground cable systems, etc. Roughened surfaces could also be used to cool electrical and nuclear components where the wall heat flux is known. Sometimes surfaces are deliber-

ately roughened to improve heat transfer. The existence of roughness elements disrupt the flow past a flat surface and changes the rate of heat transfer.

Engineered suspensions of nanoparticles in liquids, known as nanofluids, have stimulated the interest of many investigators because of their ability to enhance heat transfer rates in engineering systems while minimising, or possibly eliminating, erosion, sedimentation, and clogging issues that crippled previous solid-liquid mixtures with larger particles. Nanofluids can be employed in a variety of technical applications, medicinal applications, power plant cooling systems, and computer systems. The convection caused by heated/cooled objects of various geometries in a nanofluid under diverse physical conditions offers one of the most essential situations for heat and mass transfer theory and is thus of great theoretical and practical relevance.

Nanofluid bioconvection is the study of the formation of the spontaneous pattern by simultaneous interaction of denser self-propelled microorganisms, buoyancy forces, nanoparticles, and density stratification. The mixing nanoparticles issue may be overcome and mass transport in micro volumes might be improved by using bioconvection motion in nanofluids ([123], [63]). On the other hand, adding micro-organisms to a nanofluid increases its stability as a suspension [62], and could avoid nanoparticles from agglomerating and accumulating.

1.2 Nanofluids

A class of fluids, referred to as nanofluids, are a mixture of nanoparticles (particles of size 1-100nm) and a base fluid. Choi [28] first explored the term 'nanofluid' by presenting a detailed model to improve the thermal properties of the base fluids. Nanoparticles are small in size having very large surface areas. The nanoparticles used in nanofluids are typically made of oxide ceramics ($Al_2O_3, Fe_3O_4, TiO_2, SiO_2, CuO, ZnO$), metals ($Au, Ag, Cu, Al, Fe$), metal carbides ($SiC$, TiC, graphite, diamond, graphene,), nitrides (AlN, SiN) etc. Base fluids may be water, ethylene or tri-ethylene-glycols and other coolants, oil and other lubricants, bio-fluids, and polymer solutions. The addition of nanoparticles to a base liquid improves its thermal characteristics, resulting in significant improvements in various thermal extrusion systems. It was demonstrated experimentally [65, 128, 36] that these fluids provide a significant improvement in thermal properties when compared to other fluids.

Several models and methods for studying the convective flows of nanofluids have been proposed by various authors. Two models namely, the Tiwari-Das model [121] and the

Buongiorno model [19] are more frequently used by several researchers to investigate the heat transfer improvement in a nanofluid. Tiwari and Das developed a model to analyze the behaviour of nanofluids by taking the volumetric fraction of nanoparticles into consideration. Buongiorno considered seven slip mechanisms, namely, inertia, Brownian diffusion, thermophoresis, diffusiophoresis, Magnus effect, fluid drainage, and gravity that can produce a relative velocity between nanoparticles and the base fluid. In the absence of turbulent effects, he concluded that only Brownian diffusion and thermophoresis are important slip mechanisms in nanofluids. Based on this observation, Buongiorno proposed a mathematical model for the nanofluid based on these effects. **Brownian motion** refers to the arbitrary movement of nanoparticles within the base fluid. This is caused by continuous collisions between nanoparticles and base fluid molecules. The phenomenon of particle diffusion under the influence of a temperature gradient is known as **thermophoresis** and is the particle equivalent of the renowned Soret effect for gaseous or liquid mixtures.

The basic governing equations of a nanofluid using the Buongiorno model are

$$\nabla \cdot \vec{V} = 0, \tag{1.1}$$

$$\rho_{\mathrm{f}} \left(\frac{\partial \vec{V}}{\partial t} + \vec{V} \cdot \nabla \vec{V} \right) = \rho_f \vec{\mathrm{g}} - \nabla p + \mu \, \nabla^2 \vec{V}, \tag{1.2}$$

$$\left(\frac{\partial T}{\partial t} + \vec{V} \cdot \nabla T \right) = \alpha_m \, \nabla^2 T + \gamma \left[D_B \left(\nabla \Phi . \nabla T \right) + \frac{D_T}{T_m} \left(\nabla T . \nabla T \right) \right], \tag{1.3}$$

$$\left(\frac{\partial \Phi}{\partial t} + \vec{V} \cdot \nabla \Phi \right) = D_B \left(\nabla^2 \Phi \right) + \frac{D_T}{T_m} \left(\nabla^2 T \right), \tag{1.4}$$

where $\vec{V}$ is the velocity vector, T is the temperature of the nanofluid, Φ is the nanoparticle volume fraction, D_B is the Brownian diffusion coefficient, D_T is the thermophoretic diffusion coefficient, T_{m} is the reference temperature, μ is the viscosity of the fluid, $\vec{\mathrm{g}}$ is the gravitational acceleration, $\alpha_m = \frac{k_m}{(\rho c)_f}$ is the thermal diffusivity of the fluid and $\gamma = \frac{(\rho c)_p}{(\rho c)_f}$ is the nanofluid heat capacity ratio.

The thermophysical properties of the nanofluid, namely the density, heat capacity and volumetric expansion coefficient of the nanofluid depend on the particle volume fraction ϵ and are given by [19]

$$\rho_{nf} = (1 - \epsilon)\rho_f + \epsilon \rho_p,$$

$$(\rho\beta)_{nf} = (1 - \epsilon)(\rho\beta)_f + \epsilon(\rho\beta)_p,$$

$$(c)_{nf} = \frac{(1-\epsilon)(\rho c_p)_f + \epsilon(\rho c_p)_p}{\rho_{nf}}.$$

The Brownian and thermophoretic diffusion coefficients are given by

$$D_B = \frac{K_{BO}T}{3\pi\mu_f d_p} \quad \text{and} \quad D_T = 0.26\frac{k_f}{2k_f + k_p}\frac{\mu_f}{\rho_f}$$

respectively. The subscripts, f and p and refer to as base fluid and nanoparticle, respectively. Moreover, d_p is the nanoparticle diameter ($1nm \leq d_p \leq 100nm$) and K_{BO} is the Boltzmann constant .

Thermophysical properties of different base fluids and nanoparticles are presented in the Table.(1.1)

Table 1.1: Thermophysical properties of base fluids and different nanoparticles

	Water	Alumina (Al_2O_3)	Titanium oxide (TiO_2)	Silver (Ag)
$\rho(kg/m^3)$	997.1	3970	4250	10500
$c_p(J/kg.K)$	4179	765	686.2	235
$k(W/m.K)$	0.613	40	8.9538	429
$\beta \times 10^{-5}(K^{-1})$	21	0.86	1.9	1.89
$\frac{\mu_{nf}}{\mu_f}$	1	$1 + 39.11\epsilon + 533.9\epsilon^2$ [89]	$1 + 5.45\epsilon + 108.2\epsilon^2$ [89]	$1.005 + 0.497\epsilon - 0.1149\epsilon^2$ [37]
$\frac{k_{nf}}{k_f}$	1	$1 + 7.47\epsilon$ [89]	$1 + 2.92\epsilon - 11.99\epsilon^2$ [89]	$0.9508 + 0.9692\epsilon$ [37]

Nanofluids have several applications in engineering, which includes microelectronics, micro-fluidics, high power X-rays, transportation, scientific measurement, solid-state lighting, material synthesis, material processing, and coolant in heat exchangers, electronic cooling system (flat plate) [104], Vertical galvanizing furnace [74], photovoltaic-thermal collector or solar power tower plant [94, 134], etc and radiators. These fluids are additionally utilized in the manufacturing of nanostructured substances for cleansing oil from surfaces due to their exquisite wetting and spreading behaviour. The nanofluids containing some precise nanoparticles will show off biomedical properties if the nanoparticles have drug transport properties or antibacterial activities.

1.3 Bioconvection

Microorganisms, also called microbes, are microscopic organisms. Microorganisms include bacteria, archaea, fungi, and protists. Microbes contribute to human culture and wellness in a number of ways, such as digesting food and purifying waste, as well as manufacturing

fuel, enzymes, and other bioactive compounds. Microbes have been employed in biological warfare and bioterrorism and are essential model organisms in biology. Microbes are an important part of a healthy soil ecosystem. Microorganisms in the human body make up the microbiota, which includes the essential intestinal flora. Considering microbes are the source of many infectious diseases, they are the focus of hygiene initiatives.

The term bioconvection pertains to a macroscopic convection motion of fluid-induced by a density gradient generated by motile microorganisms swimming together. These self-propelled motile microorganisms cause bioconvection by increasing the density of the base fluid by swimming in a specific direction[92, 57]. It is found in closely packed cultures of free-swimming microorganisms in suitable aqueous systems such as rivers, oceans, puddles, and droplets. Its characteristic feature is the spontaneous self-organization or self-concentration of swimmers into a macroscopic pattern.

Based on the mechanism of directional motion, or taxis (arrangement)of the cells, bioconvective systems can be distinguished and classified. Taxis can also include the change in surroundings along with the mechanisms of an organisms movement as a response to that change in its surroundings. Generally, in the absence of taxis, organisms move randomly. Most organisms use a combination of random movement and taxis. Moving microorganisms include chemotaxis or oxytactic microorganisms, gyrotactic microorganisms, and negative gravitaxis. As some micro-organisms are bottom-heavy, they swim upwards (geotaxis or gravitaxis). The oxygen concentration gradient, which is caused by the cells' oxygen consumption and supply from the air interface, can cause upward swimming towards regions of higher oxygen concentration (aerotaxis, oxygen taxis, or, in general, chemotaxis). The movement of organisms towards or away from a light source (phototaxis). The balance of gravitational and viscous torques determines the direction in which microorganisms swim, and they swim due to the displacement between the cell centre of mass and buoyancy (Gyrotaxis). Gyrotaxis might work to extract more and more nutrients from the bed of a pond in the absence of wind shear or thermal convection, than a mere geotactic instability.

In biological systems and biotechnology, bioconvection has numerous applications. Thermo-bioconvection is used to colonise hot springs by a motile microorganism known as thermophiles, or heat-loving microorganisms. Another application is microbial enhanced oil recovery, which involves inserting microorganisms and nutrients into oil-bearing layers to control permeability fluctuation. Several investigators have analyzed different aspects of bioconvection concerns.

The first comprehensive theory for bioconvection of gravitactic swimmers was presented

by Childress *et al.* [26]. Their equations took into consideration both the directional and stochastic components of swimming velocity, but not the effect of local vorticity on swimming direction. The Navier-Stokes equation with the Boussinesq approximation and the conservation equation for motile microbe concentration are used in this theory. Pedley *et al.* [90] developed a continuum model for bioconvection in a suspension of swimming gyrotactic microorganisms, demonstrating that gyrotaxis aids in the development of convection instability. Later, Pedley and Kessler [91] discussed the hydrodynamic phenomena in the suspension of swimming microorganisms.

Governing equation for the motile microorganisms is given by :

$$\frac{\partial M}{\partial t} - \nabla \cdot (D_m \nabla M) + \vec{V} \cdot \nabla M + \nabla (M \cdot \bar{v}) = 0 \tag{1.5}$$

where M is the concentration of motile microorganism, D_m is the rate of diffusion of motile microorganism (which is a constant), $\vec{V}$ is the fluid velocity and $\bar{v}$ is the average velocity of swimming of the motile microorganism.

1.4 Basic Terminology

Convective Heat Transfer

The exchange of internal energy between particular constituents or regions of the medium under consideration is referred to as heat transfer. It always happens in a downward direction from a higher to a lower temperature location. There are three modes by which heat transfer occurs. They are conduction, convection, and radiation. The molecular transport of heat in bodies or between bodies in the thermodynamical system is referred to as conduction. Heat transfer caused by the movement of fluid from one region of the medium to another is called convection. Radiation heat transfer is a mechanism in which the internal energy of a substance is converted into radiant energy. The transport of heat by convection together with conduction is known as *convective heat transfer*. Forced convection, free convection, and mixed convection are the three types of convective heat transfer. Forced convection is caused by an external agent unrelated to heating effects that causes fluid to flow over the heated body. Natural forces such as buoyancy forces, which originate from density variations in a fluid, cause free or natural convection. The temperature gradients within the fluid cause these density variances. In Mixed Convection the order magnitude of the buoyancy force is

comparable with the externally maintained pressure drop to force the flow.

Radiation

Thermal radiation is the transfer of heat caused by the emission of electromagnetic waves. The importance of radiation becomes intensified at high absolute temperature levels. It is well known that the thermal radiation heat transfer does not require any intermediate medium. Thus thermal radiation is of great importance in vacuum and space applications.

The radiation heat flux is q_r, under the Rosseland approximation [115] can be written as

$$q_r = -\frac{4\sigma^*}{3k^*}\frac{\partial T^4}{\partial y} \tag{1.6}$$

where σ^* is Stefan-Boltzman constant and k^* is the coefficient of mean absorption. This approximation is good only for intensive absorption and is valid at points optically far from the bounding surface,i.e., for an optically thick boundary layer.

Magnetohydrodynamics

Magnetohydrodynamics (MHD) is the branch of continuum mechanics which deals with the mutual interaction between the magnetic field and electrically conducting fluid. When a magnetic field is there in an electrically conducting and incompressible fluid, it interacts with the fluid through body force and body couple per unit mass. In the absence of gravitational effects, the regular magneto-fluid dynamics assumption is $\rho\vec{f} = \rho_e\vec{E} + \vec{J}\times\vec{B}$, where ρ_e is the free charge density, $\vec{E}$ is the electric field, $\vec{B}$ is the total magnetic field, and $\vec{J}$ is the current density and given by the Ohm's law $\vec{J} = \sigma\Big[\vec{E} + \vec{q}\times\vec{B}\Big]$. Since $\vec{J}\times\vec{B} \gg \rho_e E$, the later can be neglected. Hence, by adding the electromagnetic force term to the momentum equation of the fluid, the fluid dynamical aspects of MHD can be studied.

The total magnetic field in the medium is the sum of the applied magnetic field and induced magnetic field due to the motion of a conducting liquid in an applied magnetic field. The magnetic Reynolds number describes the relative strength of the induced magnetic field. When the magnetic Reynolds number is modest, it is reasonable to ignore the induced magnetic field. The motion of a conducting fluid through a magnetic field induces electric currents and the fluid experiences a force. This force is called Lorenz force ($\vec{J}\times\vec{B}$) and it alters the motion of the fluid.

Double diffusive convection

Double diffusive convection is a fluid dynamics phenomena that explains a type of convection that is caused by two separate density gradients with differing diffusion rates. Oceanography is a good example of double diffusive convection because heat and salt concentrations have separate gradients and diffuse at different speeds.

Arrehenius Equation

At higher temperatures, chemical reactions are expected to happen more quickly, while at lower temperatures, they are expected to take longer. At the molecular level, thermal energy is directly related to motion. Molecules travel quicker and collide more violently as the temperature rises, dramatically increasing the possibility of bond cleavages and rearrangements. The Arrhenius activation energy is the smallest amount of energy required to start a chemical reaction. Between unreacted and reacted molecules or atoms, activation energy acts as a barrier. Once this barrier is crossed, a chemical reaction will occur, and only those molecules or atoms with greater energy than the fence will be able to pass through. The Arrhenius equation [11], which combines the notions of activation energy and the Boltzmann distribution law, is one of the most fundamental relationships in physical chemistry. The equation is given by

$$k = Ae^{\frac{-E_a}{RT}} \tag{1.7}$$

where k is rate constant of the reaction, E_a is the Activation energy for the reaction, T is the absolute temperature, R is the universal gas constant and A is the pre-exponential factor,a constant. The alternative form of the equation is given by

$$k = Ae^{\frac{-E_a}{\kappa T}} \tag{1.8}$$

where κ is the Boltzmann constant. This equation provides us the temperature dependence of reaction rates.

Variable fluid properties

In most engineering applications, the thermophysical properties of the fluid, especially viscosity and thermal conductivity may vary with temperature. Therefore, to predict the heat transfer rate accurately, it is necessary to take into account this variation of viscosity and thermal conductivity. Different researchers have taken the variations of the viscosity and thermal conductivity as different functions of temperature, time, etc. Batchelor and Batchelor [14] assumed that the fluid viscosity μ, the thermal conductivity k are considered as linear functions of temperature and are given by

$$\mu(T) = \mu_\infty \left[1 + A(T_w - T)\right] \qquad \text{and} \qquad k(T) = k_0 \left[1 + B(T - T_\infty)\right] \tag{1.9}$$

where μ_∞ is the absolute viscosity of the fluid, k_0 is the thermal conductivity and A and B are constants whose values depends on the fluid under consideration.

Oberbeck-Boussinesq Approximation

A convenient and simple way to define the density difference $\rho - \rho_\infty$ in the buoyancy part of the momentum equation for nanofluids is given by

$$\rho = \Phi\rho_{\mathrm{p}} + (1 - \Phi)\rho_{\mathrm{f0}}[1 - \beta_{\mathrm{T}}(T - T_0)], \tag{1.10}$$

where ρ_{p} is the nanoparticle density, T_0 is the reference temperature and ρ_{f0} is the fluid density at reference temperature at some point in the medium, β_{T} is the coefficient of thermal expansion. The Eq. (1.10) is an approximation for the variation of the density, and it is known as the Oberbeck-Boussinesq approximation

If the density ρ varies linearly with T over the range of values of the physical quantities encountered in the transport process, β_{T} in Eq. (1.10) are given by

$$\beta_{\mathrm{T}} = -\frac{1}{\rho}\left(\frac{\partial\rho}{\partial T}\right)_{\mathrm{p,C}}.$$

Isothemral/Flux conditions

In most cases, heat transfer occurs when a fluid moves near a wall that is heated or cooled to a temperature other than the fluid's temperature. The boundary conditions are expressed

at the fluid/solid interface in this case. One of the following simplified assumptions is used in the most common conditions:

1. The fluid/solid interface is at a uniform temperature : $T_{\text{fluid}} = T_{\text{solid}} = \text{constant}$
2. The heat flux is uniform on the interface : $q_w = -K_f\,(\hat{n} \cdot \nabla T)$.

where $\hat{n}$ is the unit normal to the surface.

Convective Boundary Conditions

Many researchers have recently become interested in a unique heating mechanism is known as the convective boundary condition, in which heat is given to the convecting fluid through a bounding surface with a finite heat capacity. Furthermore, the rate of heat transmission through the surface is related to the local temperature differential from ambient conditions. [76].

$$-K_f\,(\hat{n} \cdot \nabla T) = h(T_{\text{surface}} - T_\infty)$$

where h is the heat transfer coefficient, T_∞ is the ambient temperature.

1.5 Bivariate Pseudo Spectral Local Linearisation Method

The bivariate pseudo-spectral local linearisation method (BPSLLM) is initialized by Motsa [81] and developed by Magagula and Motsa [67, 82]. In his article Motsa [81] solved a coupled system of non-linear ordinary differential equations by linearizing the equations about one dependent variable at a time in the sequential order and was labelled as the local linearisation method (LLM). Later, Magagula and Motsa [67, 82] extended it to system of partial differential equations wherein spectral collocation method was applied in both directions of independent variables. The local linearisation method for partial differential equations along with spectral collocation method is called as bivariate pseudo-spectral local linearisation method (BPSLLM).

1.5.1 Local Linearisation Method

By using this technique, the iteration process is attained by linearizing the non-linear part of differential equations about one dependent variable at a time using Taylor series expansion.

If there are n nonlinear differential equations in n unknown functions Z_i, $(i = 1, 2, \cdots, n)$, then the k^{th} nonlinear differential equation is locally linearized about $Z_{k,r}$ (the previous iteration) assuming that all the remaining $Z_{i,m}$ $(i \neq k)$ are known. To find the solution Z_k at the present iteration level $(Z_{k,m+1})$, the updated values Z_s $(s < k)$ obtained as solutions of the previous $k = 1, 2, \cdots, s$ equations are used.

To understand more, let us consider a system of equations in three unknowns, say f, g, and h. Let, f_{m+1}, g_{m+1}, and h_{m+1} be an approximate solution at the current iteration and f_m, g_m, and h_m be the solution at the previous iteration of the system of equations. The first equation is linearized at the present iteration (f_{m+1}) using the values of the functions at the previous iteration i.e. g_m, h_m. The second equation is linearized at the current iteration (g_{m+1}) using the updated value of f at the current iteration i.e. f_{m+1} and the values of the remaining functions at the previous iteration h_m. Similarly the third equation is linearized at the present iteration (h_{m+1}) using the updated value of f and g i.e., f_{m+1} and g_{m+1} . On applying this procedure to all the equations, we obtain the set of linear differential equations.

The system of equations thus obtained, can be solved by using Chebyshev spectral collocation method in both directions of the independent variables, since the each unknown function is a function of two independent variables.

1.5.2 Bivariate Chebyshev Spectral Collocation Method

The bivariate Chebyshev spectral collocation method ([20, 35, 122]) is based on the Chebyshev polynomials defined on the domain $[-1, 1] \times [-1, 1]$.

In this method, to solve the partial differential equation in two variable ζ and τ, consider the Chebyshev-Gauss - Lobatto points in both the directions ζ and τ defined as

$$\zeta_i = \cos\frac{\pi i}{N},\ i = 0, 1, \ldots, N \quad \tau_j = \cos\frac{\pi j}{M},\ j = 0, 1, \ldots, M \tag{1.11}$$

The functions that are to be determined are interpolated at the collocation points described by (1.11), using the following bivariate Lagrange interpolation polynomial.

$$f(\zeta, \tau) \approx \sum_{m=0}^{N}\sum_{j=0}^{M} f(\zeta_m, \tau_j) L_m(\zeta) L_j(\tau),$$

where $L_m(\zeta)$ and $L_j(\tau)$ are Lagrange polynomials given by

$$L_m(\zeta) = \prod_{\substack{m=0 \\ m\neq k}}^{N} \frac{\zeta - \zeta_k}{\zeta_m - \zeta_k} \ , \ L_m(\zeta_k) = \delta_{mk} = \begin{cases} 0 & if \ m \neq k \\ 1 & if \ m = k \end{cases}$$

and

$$L_j(\tau) = \prod_{\substack{j=0 \\ j\neq k}}^{M} \frac{\tau - \tau_k}{\tau_j - \tau_k} \ , \ L_j(\tau_k) = \delta_{jk} = \begin{cases} 0 & if \ \mathrm{j} \neq k \\ 1 & if \ \mathrm{j} = k \end{cases}$$

The p^{th} order derivative of the unknown function $f(\zeta, \tau)$ with respect to ζ, at (ζ_k, τ_i) is given by

$$\left.\frac{\partial^p f}{\partial \zeta^p}\right|_{(\zeta_k,\tau_i)} = \frac{2}{\eta_\infty} \sum_{r=0}^{N} \sum_{j=0}^{M} f(\zeta_j, \tau_r) \frac{d^p L_r(\zeta_k)}{d\zeta^p} L_j(\tau_r) \ = \ \mathbf{D}^p \mathbf{F}_i \tag{1.12}$$

Here, $\mathbf{D} = \frac{2}{\zeta_\infty}\mathcal{D}$, $\mathcal{D}$ is the $(N+1)^{th}$ order Chebyshev spectral differentiation matrices [122], and the vector $\mathbf{F}_i$ is given by $\mathbf{F}_i = [f(\zeta_0, \tau_i), f(\zeta_1, \tau_i), f(\zeta_2, \tau_i), \cdots, f(\zeta_N, \tau_i)]^T$

Similarly the derivative of $f(\zeta, \tau)$ with respect to τ, at (ζ_k, τ_i) is

$$\left.\frac{\partial f}{\partial \tau}\right|_{(\zeta_k,\tau_i)} = \frac{2}{\xi_\infty} \sum_{r=0}^{N} \sum_{j=0}^{M} f(\zeta_j, \tau_r) \frac{dL_{jr}(\tau_i)}{d\tau} L_r(\zeta_k) \ = \ \frac{2}{\xi_\infty} \sum_{j=0}^{M} \mathbf{d}_{i,j} \mathbf{F}_j \tag{1.13}$$

where $\mathbf{d}_{i,j}$ is the element of the chebyshev matrix of order $(M+1) \times (M+1)$ for the first derivative.

Substituting the above derivative in the given differential equations, we get the following system of equations.

$$\mathbf{A}_{r-1}\mathbf{X}_r = \mathbf{R}_{r-1}, \tag{1.14}$$

in which A_{r-1} is a square matrix of order $(M+1)\times(M+1)$ while X_r and R_{r-1} are $(M+1)^{th}$ order column vectors. Also each element of the matrix is a diagonal matrix of order $N \times N$. Writing the boundary conditions in terms of Chebyshev polynomials, incorporating them in the above system of equations and solving the reduced system of algebraic equations, we obtain the solution of the given differential equation. If the domain is $[a, b]\times[c, d]$, then it will be transformed to the domain $[-1, 1] \times [-1, 1]$ by using the using suitable transformation.

1.6 Literature Review

Nanofluids have attracted a lot of attention in the last decade because of their numerous applications in biomedical, microelectronics, transportation, space, nuclear, and defence industry, radioactive waves, cooling processes, alternate sources of energy, solar energy systems and chemo-therapy. Choi *et al.* [28] demonstrated that adding a modest amount (less than 1% by volume) of nanoparticles to standard heat transfer liquids improved the fluid's thermal conductivity. A book by Das *et al.* [32] on nanofluids gives a comprehensive introduction and applications. Menni *et al.* [75] compiled the investigations on nanofluid flow in complex geometries. Guo [40] presented a review on heat transfer enhancement with nanofluids. Wang *et al.* [127]reviewed the literature on heat transfer of nanofluid by applied electric/ magnetic field. The literature on convective heat transfer characteristics of nanofluids including the magnetic effect on heat transfer enhancement has been reviewed by Narankhishig *et al.* [86]. These reviews examine in detail the work done on convective transport in nanofluids.

The analysis of flow, heat and mass transfer over irregular surfaces (wavy surfaces) is one of the fundamental important research areas due to its occurrence in many practical situations. An alternative approach for improving heat or mass or microorganism transfer is the modification to the geometry of the surface adjacent to the transport medium. Instances of this modification to the geometry of the surface consist of irregular or wavy surfaces, which have been efficiently used in a wide range of scientific and industrial applications. In the framework of biofuel cell design, plenty of the latest developments within the structure of wall surfaces and polymers have empowered engineers to discover wavy heat transfer as a feasible enhanced system that might significantly improve fuel productivity. Yao [131] was the first to initiate the study of natural convection along a vertical wavy surface. He obtained numerical results for a sinusoidal surface. His results revealed that the local heat transfer rate changes periodically along the wavy surface, with a frequency equal to double the frequency of the surface. Later, Moulic and Yao [83] considered the natural convection along a vertical wavy surface with uniform heat flux. Thereafter, several authors investigated the convective heat and mass transfer along a wavy surface embedded in a nanofluid under various physical conditions. Sameh and Aziz [4] studied transient convection on a vertical wavy surface with a thermal non-equilibrium model of a nanofluid. Kabir *et al.* [55] considered the effects of stress work on MHD natural convection flow along a vertical wavy surface with joule heating. Mehmood *et al.* [72] analysed the heat transfer in the MHD flow near the wavy rough plate. Rashid *et al.* [97] considered numerically the magnetic field effect on the mixed convective nanofluid flow over a sinusoidal wall. Gorla and Kumari [38] presented

a boundary layer analysis for the warm, laminar nanoliquid flow to a melting vertical wavy surface in a stagnant nanoliquid. Kameswaran *et al.* [56] studied the impact of convective boundary conditions, thermal stratification, and non-linear Boussinesq approximation on a wavy surface in a non-Darcy porous medium saturated with nanofluid. Mehmood and Iqbal [70] examined the impact of heat source in the free convective nanofluid flow along a vertical wavy surface. Javed *et al.* [54] investigated the radiation effect on hydromagnetic flow along a vertical impermeable wavy texture heated with uniform flux. Srinivasacharya *et al.* [116] examined the consequence of thermophoresis and variable fluid properties on the convection over a sinusoidal surface in a porous medium. Shenoy *et al.* [108] attempted to unify the information on the convective flow and heat transfer from a wavy surface in different fluids along with nanofluid in the form of a book. Siddiqa *et al.* [110] discussed the impact of thermal radiation on the heat and mass transfer features of free convection flow over a wavy surface. Hassan et al. [42] studied the convective flow of nanofluid over a wavy surface immersed in a porous medium. Siddiqa *et al.* [111] discussed the impact of thermal radiation on the natural convection along a wavy surface. Mehmood *et al.* [73] analysed the irreversibility phenomenon, in the presence of nanoparticles in the base fluid, in viscous flow caused by the uniform motion of a wavy plate. Mustafa and Javed [84] examined the improvement of heat transfer in natural convection flow of nanofluid past a vertical wavy plate with a changing heat flux. Roy and Siddiqa [102] considered the effect of nanofluid on heat transfer enhancement for mixed convection flow over a corrugated surface. Iqbal *et al.* [51] provided a computer simulation of the effects of dissipation on the hydromagnetic convective flow of hybrid nanofluids along a wavy plate. Zeeshan *et al.* [133] investigated numerically the effects of MHD, viscous dissipation, Joule heating on the radiative heat and mass transfer of nanofluid flow towards a vertical wavy surface.

The convective heat transfer over an inclined surface is the topic of interest for the investigators taking into account its applications in industry and technology. DAlessio *et al.* [30] analyzed the film flow overheated wavy inclined surfaces. Cheng [24] investigated the double-diffusive free convection across an slanted wavy surface embedded in a porous medium. Srinivasacharya and Vijay Kumar [118] studied the mixed convection flow of a nanofluid past an inclined wavy surface in a porous medium. Srinivasacharya and Vijay Kumar [119] investigated the effect of radiation on natural convection flow of nanofluid over an inclined wavy surface in a non-Darcy porous medium. Das *et al.* [33] considered the natural convection over an inclined plate implanted in a porous medium suffused with nanofluid. Srinivasacharya and Vijay Kumar [117] considered the problem of mixed convection along an inclined wavy surface embedded in a nanofluid saturated porous medium. Ziaei-Rad *et*

al. [135] considered the nanofluid flow on a permeable inclined flat plate. Siddiqa *et al.* [110] discussed double diffusive free convection over a wavy surface embedded in the non-absorbing medium. Nandal and Bhargava [85] discussed convectively heated inclined plate in a nanofluid for variable fluid properties and magnetic field. Goyal *et al.* [39] examined numerically natural convective boundary layer flow of a nanofluid past a heated inclined plate in the presence of magnetic field Bhat and Samanta [16] analyzed the linear stability of a contaminated fluid flow down a slippery inclined plane. Prasad *et al.* [93] considered the significance of thermal diffusion on unsteady convective transport over an accelerated wavy plate in a porous medium with a traverse magnetic field. Amit and Kundu [8] studied the passive control of nanoparticles and double-diffusive effects on the flow past a permeable inclined plate in a porous medium. Rashed *et al.* [96] analyzed the effects of uniform magnetic field and solar radiation on the natural convective flow of nanofluid near to the inclined plate embedded in the porous medium under. Mjankwi [77] examined the unsteady magnetohydrodynamics flow of a nanofluid in the presence of chemical reaction and thermal radiation over an inclined stretching sheet with variable fluid properties. Khademi *et al.* [58] analysed numerically the impact of magnetic field on the convective flow of nanofluid over an inclined flat plate ingrained in a porous medium. Reddy and Sreedevi [98] presented the magnetic, thermal radiation and chemical reaction effects on the mixed convection flow of Buongiorno's model nanofluid over an inclined porous vertical plate. Barik *et al.* [13] studied numerically the MHD characteristics of nanofluid past an inclined stretching sheet. Roy [101] investigated the influence of magnetic field on the natural convection flow past a sinusoidal surface with temperature variations.

The study of bioconvection problems attains significant attention due to its applications in biotechnology, the pharmaceutical industry, biosensors, microbial enhanced oil recovery, biological polymer synthesis, and medical sciences. Bioconvection is presumed to be an impulsive unicellular microbe movement within fluids created by a density gradient that has been formed by the directional collective swimming of self-propelled microorganisms. In practical applications such as hydrogen and biodiesel processing, gyrotactic microorganisms are found and are considered to be one of the most useful energy tools in water treatment plants. Nanofluid bioconvection is the study of the formation of the spontaneous pattern by simultaneous interaction of denser self-propelled microorganisms, buoyancy forces and nanoparticles and density stratification. Pedley *et al.* [90] established a model for the suspension of swimming gyrotactic microorganisms. Since then many findings have been reported on several characteristics of bioconvection related in different geometries. Ahmed and Mahdy [5] studied magnetohydrodynamic (MHD) bioconvection near a vertical wavy surface embedded

in an incompressible electrically conducting nanofluid saturated porous medium containing gyrotactic microorganisms. Dhanai *et al.* [33] considered the bioconvection of a nanofluid comprising gyrotactic microorganisms over an inclined permeable layer. Siddiqa *et al.* [112] investigated the heat and mass transfer characteristics of bioconvection flow of a water-based nanofluid over a vertical wavy surface. Uddin *et al.* [125] examined natural convective boundary layer flow past a wavy surface embedded in a water-based bio-nanofluid containing gyrotactic microorganisms using Buongiornos nanofluid model. Chamkha *et al.* [23] considered the effects of radiation on the natural bioconvection flow of a nanofluid containing gyrotactic microorganisms past a vertical plate with streamwise temperature variation. Nanofluid bioconvection with variable thermophysical properties was studied by Begum *et al.* [15] for the geometry of uniformly heated vertical cone. Rehman *et al.* [100]investigated the various aspects of bioconvection related to the internal/external flows in different geometries. Sivaraj *et al.* [114] provides an observation of microbes influence on CuO-water nanofluid by considering an upper horizontal surface of a paraboloid of revolution with thermoelectric effects. Amirsom *et al.* [7] studied the impact of melting, dissipation, and magnetic field on the nanofluid bioconvection with variable thermophysical properties and second-order slip. Shukla *et al.* [109] investigated analytically the influence of oblique magnetic field on the non-similar bioconvection flow of a nanofluid using the homotopy analysis method. Khan *et al.* [61] addressed the impact of gyrotactic microorganisms on nonlinear mixed convective MHD flow of thixotropic nanoliquids by considering Brownian motion and thermophoresis diffusion effects.

1.7 Aim and Scope

It is not always physically realistic to consider the flow past the vertical or horizontal surface. The inclinations are always possible, and hence, there is a need to frame a generalized mathematical model involving the inclination of the surface to carry out the investigation. With such a generalized model, it gets easier to switch to either of the two cases, horizontal surface or vertical surface.

The aim of present thesis is to understand the mathematical model for the bioconvection flow of nanofluids past an inclined wavy surface. The characteristics such as magnetic effects, thermal radiation effects, Double diffusion effects are also included in some of the problems. The effects of various flow governing parameters on the skin friction, nusselt number, sherwood number, nanoparticle sherwood number and density number of motile microorganism

are also studied here.

1.8 Overview of the Thesis

The thesis consists of Ten chapters.

The first chapter serves as an introduction and motivation for the research conducted throughout the thesis. A review of relevant literature is provided, emphasising the significance of the problems presented in the thesis. The basic equations governing the Nanofluid with the density of the motile microorganisms are presented in this chapter.

Chapters 2 to 9 (Eight chapters) deals with the bioconvection flow of a nanofluid past an inclined wavy surface containing the microorganisms. In all these chapters, we considered the incompressible, steady, and laminar flow of a nanofluid consisting of motile microorganisms over a semi-infinite inclined wavy surface. The wavy surface is inclined at an angle A ($0^o \leq A \leq 90^o$) to the horizontal line.

In Chapter - 2, the double-diffusive bioconvection of nanofluids flow past an inclined wavy surface is considered. The non-dimensional Skin friction coefficient, Nusselt number, Sherwood number, Sherwood number for nanoparticles and density number of motile microorganisms profiles for different values of bioconvection Peclet number, bioconvection Rayleigh number, angle of inclination, the amplitude of the wavy surface, nanofluid buoyancy ratio, regular double-diffusive buoyancy ratio, bioconvection Schmidt number, nanoparticle Lewis number, Soret number, modified Dufour number and microorganism slip parameter were studied through graphs. The results obtained are compared with the previously published results and are in good agreement with them.

Chapter - 3 deals with thermal radiation and double-diffusive effects on bioconvection flow of a nanofluid past an inclined wavy surface. Along with other effects studied in the earlier chapter, we analyzed the effect of radiation parameters on the local Nusselt number, Sherwood number, nanoparticle Sherwood number, and density number of motile microorganisms.

the mixed convection of a nanofluid past an inclined wavy surface in the presence of gyrotactic microorganisms is considered for study in chapter - 4. The obtained results are exhibited graphically to demonstrate the influence of various flow governing physical parameters, like mixed convection parameter along with the other effects on the coefficient

of skin friction, Nusselt number, nanoparticle Sherwood number, and density number of motile microbes.

Chapter - 5 considers the mixed convection of a nanofluid past an inclined wavy surface in the presence of gyrotactic microorganisms and magnetic field. Here, concentration is to examine the effect of Eckert number, magnetic induction parameter, Joule heating parameter, mixed convection parameter on Nusselt number, nanoparticle Sherwood number, and density number of motile microbes along with the other effects.

In Chapter - 6, an attempt has been made to study the effect of variable properties on the bioconvection flow of nanofluid over an inclined wavy surface. The focus of this investigation is to analyze the effect of variable viscosity parameter, variable thermal conductivity parameter apart from the other effects considered in previous chapters, on the coefficient of skin friction, Nusselt number, nanoparticle Sherwood number, and density number of motile microbes. The results obtained are compared with the previously published results and are in good agreement with them.

In Chapter - 7, the natural convection of nanofluid flow past an inclined wavy surface in the presence of gyrotactic microorganisms with activation energy. The influence of activation energy parameter, temperature relative parameter, reaction rate parameter, fitted rate constant along with the other parameters, on the coefficient of skin friction, Nusselt number, nanoparticle Sherwood number, and density number of motile microbes are obtained and are shown graphically.

Chapter - 8, is devoted to studying the radiation effect on mixed convection of a nanofluid past an inclined wavy surface in the presence of gyrotactic microorganisms with variable Properties. Here, we analyzed the mixed convection parameter, radiation parameter, Pearson number, and temperature-dependent thermal conductivity parameter on the coefficient of skin friction, Nusselt number, nanoparticle Sherwood number, and density number of motile microbes, which are explained through graphs.

Chapter - 9, explores the bioconvection in a nanofluid past a moving inclined wavy surface with convective boundary conditions. The main discussion in this chapter is on the effect of Biot number, along with the other effects on the coefficient of skin friction, Nusselt number, nanoparticle Sherwood number, and density number of motile microbes, which are explained graphically.

Chapter - 10, consists of the main conclusions of the thesis and the directions in which further investigations may be carried out.

In all the above chapters (Chapter 2 to Chapter 9), the coordinate transformations are employed to convert the wavy surface to a plane surface. The governing system of partial differential equations describing the total mass, momentum, thermal energy, mass diffusion, and microorganisms that are non-linear modified into dimensionless differential equations using pseudo-similarity variables along with their boundary conditions and then linearized using the local linearization method [81]. Thus obtained linear equations are solved using the Bivariate Chebyshev pseudo-spectral collocation method [20].

A list of references is given at the end of the thesis and is arranged in alphabetical order.

A considerable part of the work in the thesis is published/accepted for publication in reputed International Journals. The remaining part is communicated for publications. The details are presented below.

List of papers Published

1. "Thermal radiation and double diffusive effects on bioconvection flow of a nanofluid past an inclined wavy surface", *Thermal Science and Engineering Progress*, Vol.22 (2021), pages.100830.

2. "Computational Analysis of Double Diffusive Bioconvection of a Nanofluid Past an Inclined Wavy Surface ", *International Journal of Applied and Computational Mathematics*, Vol. 7, (2021) paper id :173.

3. "Mixed Convection of a Nanofluid Past an Inclined Wavy Surface in the presence of Gyrotactic Microorganisms", *Heat Transfer*, Early View, DOI: 10.1002htj.22291, 2021.

List of papers communicated

4. "Mixed Nano-bioconvection flow Past an Inclined Wavy Surface in the presence of Gyrotactic Microorganisms and Magnetic Field ", Communicated to *Pramana-Journal of Physics*.

5. "Effect of variable properties on the Bio-convection in a Nanofluid Flow Past an Inclined Wavy Surface", Communicated to *Computational Thermal Sciences*.

6. "Natural Convection of Nanofluid flow Past an Inclined Wavy Surface in the presence of Gyrotactic Microorganisms with Activation Energy ", Communicated to *International Journal of Engineering Systems Modelling and Simulation*.

7. "Radiation effect on Mixed Convection of a Nanofluid Past an Inclined Wavy Surface in the presence of gyrotactic microorganisms with Variable Properties"Communicated to *Journal of Applied Nonlinear Dynamics*.

8. "Bioconvection in a Nanofluid Past a Moving Inclined Wavy Surface with Convective Boundary Conditions "Communicated to *International Journal of Applied Mechanics and Engineering*.

Chapter 2

Computational Analysis of Double Diffusive Bioconvection of a Nanofluid Past an Inclined Wavy Surface [1]

2.1 Introduction

The analysis of convective flows with double-diffusion has received significant consideration during the last several years because of its manifestation in a wide spectrum of natural and technological situations. Double-diffusive convection is an essential fluid dynamic phenomenon that includes motions driven with the aid of two unique density gradients diffusing at distinctive rates [79]. Several investigations have been reported in the literature on double-diffusive convection. Siddiqa *et al.* [110] discussed double diffusive free convection over a wavy surface embedded in the non-absorbing medium. Das *et al.* [31] considered the natural convection over an inclined plate in a porous medium suffused with nanofluid. Amit and Kundu [8] studied the passive control of nanoparticles and double-diffusive effects on the flow past a permeable inclined plate in a porous medium.

In this chapter, the effects of double diffusion on the nanofluid flow past an inclined wavy surface in the presence of gyrotactic microorganism is considered. The Buongiorno model used for nanofluids. The governing partial differential equations are solved using the bivariate pseudo-spectral local linearization method (BPSLLM). The BPSLLM introduced

[1] Published in "**International Journal of Applied and Computational Mathematics**",7, No. 4, 173 (2021)

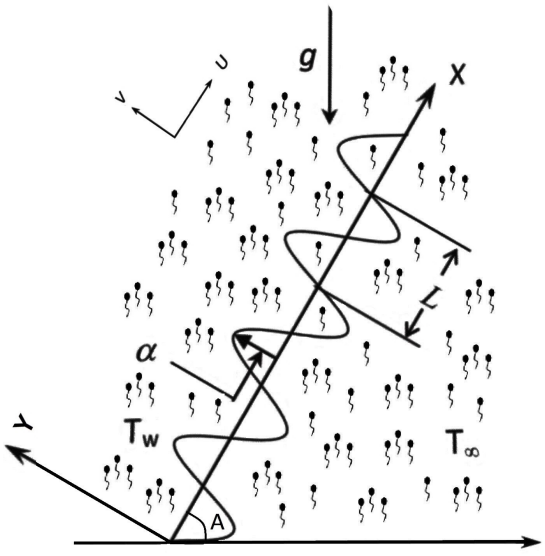

Figure 2.1: "Physical model and coordinate system".

by [67, 82] is a modification of the spectral local linearization method [81, 113] to solve non-linear partial differential equations in two dimensions. The effects of various parameters governing the flow and geometry on the skin friction, heat transfer rate, mass transfer rate, nanoparticle mass transfer rate, and density number of the microorganism are presented through graphs and discussed.

2.2 Mathematical Formulation

Consider the flow of a nanofluid consisting of motile microorganisms past an inclined wavy surface. The equation for the wavy surface is given by

$$Y = \sigma(X) = \alpha \sin(\frac{\pi X}{L})$$

where $2L$ and α are the characteristic length and amplitude associated with the wavy surface. The wavy surface is inclined at an angle A ($0^o \leq A \leq 90^o$) to the horizontal line as depicted in Fig. (2.1). $A = 0^o$ corresponds to horizontal surface and $A = 90^o$ corresponds to vertical surface. In formulating the problem the following assumptions are made and are considered throughout the thesis.

- The flow is two-dimensional, steady, laminar, and incompressible.
- The movement of nanoparticles is independent of the direction of swimming microbes.
- The nanoparticle suspension is assumed to be stable.
- The volume fraction of the microorganisms is adequately small such that their impact on the viscosity and inertia of the fluid - microbe suspension is insignificant.
- The wavy surface is maintained at a uniform temperature T_w, nanoparticle volume fraction Φ_w, concentration C_w and density of the motile microorganism M_w respectively.
- The temperature, nanoparticle volume fraction, concentration and density of motile microbes under ambient conditions are T_∞, Φ_∞, C_∞, M_∞ respectively. Here $T_w > T_\infty$, $\Phi_w > \Phi_\infty$, $C_w > C_\infty$, $M_w > M_\infty$.
- All the fluid properties are considered to be constant except for the density in the buoyancy component.

The equations governing the flow [90, 14, 19] with the above assumptions are

$$\frac{\partial U}{\partial X}+\frac{\partial V}{\partial Y}=0, \tag{2.1}$$

$$\rho_{f\infty}\left(U\frac{\partial U}{\partial X}+V\frac{\partial U}{\partial Y}\right)=-\frac{\partial P}{\partial X}+\mu\left(\frac{\partial^2 U}{\partial X^2}+\frac{\partial^2 U}{\partial Y^2}\right)+[(1-\Phi_\infty)\beta_T\rho_{f\infty}(T-T_\infty) \tag{2.2}$$
$$+(1-\Phi_\infty)\beta_C\rho_{f\infty}(C-C_\infty)-(\rho_p-\rho_{f\infty})(\Phi-\Phi_\infty)-\beta_M(\rho_m-\rho_{f\infty})(M-M_\infty)]\,g\sin A,$$

$$\rho_{f\infty}\left(U\frac{\partial V}{\partial X}+V\frac{\partial V}{\partial Y}\right)=-\frac{\partial P}{\partial Y}+\mu\left(\frac{\partial^2 V}{\partial X^2}+\frac{\partial^2 V}{\partial Y^2}\right)+[(1-\Phi_\infty)\beta_T\rho_{f\infty}(T-T_\infty) \tag{2.3}$$
$$+(1-\Phi_\infty)\beta_C\rho_{f\infty}(C-C_\infty)-(\rho_p-\rho_{f\infty})(\Phi-\Phi_\infty)-\beta_M(\rho_m-\rho_{f\infty})(M-M_\infty)]\,g\cos A,$$

$$U\frac{\partial T}{\partial X}+V\frac{\partial T}{\partial Y}=\alpha_m\left(\frac{\partial^2 T}{\partial X^2}+\frac{\partial^2 T}{\partial Y^2}\right)+\gamma\left\{D_B\left(\frac{\partial\Phi}{\partial X}\frac{\partial T}{\partial X}+\frac{\partial\Phi}{\partial Y}\frac{\partial T}{\partial Y}\right)\right. \tag{2.4}$$
$$\left.+\frac{D_T}{T_\infty}\left[\left(\frac{\partial T}{\partial X}\right)^2+\left(\frac{\partial T}{\partial Y}\right)^2\right]\right\}+D_{TC}\left(\frac{\partial^2 C}{\partial X^2}+\frac{\partial^2 C}{\partial Y^2}\right)$$

$$U\frac{\partial\Phi}{\partial X}+V\frac{\partial\Phi}{\partial Y}=D_B\left(\frac{\partial^2\Phi}{\partial X^2}+\frac{\partial^2\Phi}{\partial Y^2}\right)+\frac{D_T}{T_\infty}\left(\frac{\partial^2 T}{\partial X^2}+\frac{\partial^2 T}{\partial Y^2}\right), \tag{2.5}$$

$$U\frac{\partial C}{\partial X}+V\frac{\partial C}{\partial Y}=D_S\left(\frac{\partial^2 C}{\partial X^2}+\frac{\partial^2 C}{\partial Y^2}\right)+D_{CT}\left(\frac{\partial^2 T}{\partial X^2}+\frac{\partial^2 T}{\partial Y^2}\right), \tag{2.6}$$

$$U\frac{\partial M}{\partial X}+V\frac{\partial M}{\partial Y}+\frac{\partial}{\partial X}\left(M\widetilde{V}\right)+\frac{\partial}{\partial Y}\left(M\widetilde{V}\right)=D_n\left(\frac{\partial^2 M}{\partial X^2}+\frac{\partial^2 M}{\partial Y^2}\right), \tag{2.7}$$

where $(U(X,Y),V(X,Y),0)$ is the velocity vector. $T(X,Y)$ is the temperature, $\Phi(X,Y)$ is the nanoparticle volume friction, $C(X,Y)$ is the concentration, $M(X,Y)$ is the density of the motile microorganism. μ is the viscosity, g is the acceleration due to gravity, $\rho_{f\infty}$ is the density of the base fluid, ρ_p is the density of the nanoparticles, $(\rho c)_f$ is the heat capacity of the fluid, ρ_m is the density of the microorganisms and $(\rho c)_p$ is the effective heat capacity of the nanoparticles, k_m is the thermal conductivity, β_T, β_C and β_M are the volumetric thermal, solutal and microorganisms expansion coefficients, D_B is the Brownian diffusion coefficient, D_T is the thermophoretic diffusion coefficient, D_S is the solutal diffusivity, D_{TC} is the Dufour type diffusivity, D_{CT} is the Soret type diffusivity and D_n diffusivity of the microorganisms. $\widetilde{V}$ is the average swimming velocity of microorganism and is given by $\widetilde{V}=\dfrac{b_c w_c}{\Phi_w-\Phi_\infty}\dfrac{\partial \Phi}{\partial Y}$ where b_c is the Chemotaxis constant and w_c is the maximum cell swimming speed.

The associated boundary conditions are :

$$\left.\begin{array}{l} U=0,\ V=0,\ T=T_w,\ \Phi=\Phi_w,\ C=C_w,\ M=M_w \text{ at } Y=Y_w=\sigma(X),\\ U\to 0,\ T\to T_\infty,\ \Phi\to\Phi_\infty,\ C\to C_\infty,\ M\to M_\infty \text{ as } Y\to\infty. \end{array}\right\} \tag{2.8}$$

The irregular wavy surface is transformed to a flat surface using the following transformations [131].

$$\left.\begin{array}{l} \xi=\dfrac{X}{L},\quad \eta=\dfrac{Y-\sigma}{L\xi^{\frac{1}{4}}}Gr^{\frac{1}{4}},\quad \psi=\dfrac{\mu Gr^{\frac{1}{2}}\xi^{\frac{3}{4}}}{\rho_{f\infty}}f(\xi,\eta),\quad p=\dfrac{PL^2Gr^{-1}}{\rho_{f\infty}\nu^2},\\ \theta(\xi,\eta)=\dfrac{T-T_\infty}{T_w-T_\infty},\ \phi(\xi,\eta)=\dfrac{\Phi-\Phi_\infty}{\Phi_w-\Phi_\infty},\ \varphi(\xi,\eta)=\dfrac{C-C_\infty}{C_w-C_\infty},\ \chi(\xi,\eta)=\dfrac{M}{M_w}, \end{array}\right\} \tag{2.9}$$

where

$$Gr=\frac{g(1-\Phi_\infty)\beta_T(T_w-T_\infty)L^3}{\nu^2}$$

is the Grashof number. Here ψ is the stream function given by

$$U=\frac{\partial\psi}{\partial Y},\quad V=-\frac{\partial\psi}{\partial X}. \tag{2.10}$$

Substituting Eq. (2.9) and (2.10) in the governing equations (2.1) to (2.7) and invoking the boundary layer approximation, we get

$$\left(1+\sigma_\xi^2\right) f''' + \frac{3}{4} f f'' - \left[\frac{1}{2} + \frac{\xi\sigma_\xi\sigma_{\xi\xi}}{1+\sigma_\xi^2}\right](f')^2 + \frac{(\theta + N_c\varphi - N_r\phi - R_b\chi)}{(1+{\sigma_\xi}^2)}(\sin A + \sigma_\xi \cos A) = \xi\left[f'\frac{\partial f'}{\partial \xi} - \frac{\partial f}{\partial \xi} f''\right], \tag{2.11}$$

$$\frac{\left(1+\sigma_\xi^2\right)}{\mathrm{Pr}}\left[\theta'' + N_b\phi'\theta' + N_t(\theta')^2 + N_d\varphi''\right] + \frac{3}{4} f\theta' = \xi\left[f'\frac{\partial\theta}{\partial\xi} - \theta'\frac{\partial f}{\partial\xi}\right], \tag{2.12}$$

$$\frac{\left(1+\sigma_\xi^2\right)}{Le}\left[\phi'' + \frac{N_t}{N_b}\theta''\right] + \frac{3}{4} f\phi' = \xi\left[f'\frac{\partial\phi}{\partial\xi} - \phi'\frac{\partial f}{\partial\xi}\right], \tag{2.13}$$

$$\frac{\left(1+\sigma_\xi^2\right)}{Ln}\left[\varphi'' + S_r\theta''\right] + \frac{3}{4} f\varphi' + = \xi\left[f'\frac{\partial\varphi}{\partial\xi} - \varphi'\frac{\partial f}{\partial\xi}\right], \tag{2.14}$$

$$\frac{\left(1+\sigma_\xi^2\right)}{Sc}\chi'' - \frac{Pe}{Sc}(1-\sigma_\xi)(\chi\phi'' + \chi'\phi') + \frac{3}{4} f\chi' = \xi\left[f'\frac{\partial\chi}{\partial\xi} - \chi'\frac{\partial f}{\partial\xi}\right], \tag{2.15}$$

and the non-dimensional form of the conditions on the boundary are

$$\left.\begin{array}{l} f(\xi,0) = -\frac{4}{3}\xi\frac{\partial f}{\partial\xi},\ f'(\xi,0)=0,\ \theta(\xi,0)=1,\ \phi(\xi,0)=1,\ \varphi(\xi,0)=1,\ \chi(\xi,0)=1 \\ f'(\xi,\infty)=0,\ \ \theta(\xi,\infty)=0,\ \ \phi(\xi,\infty)=0,\ \ \varphi(\xi,\infty)=0,\ \ \chi(\xi,\infty)=\frac{M_\infty}{M_w}=\delta\chi, \end{array}\right\} \tag{2.16}$$

where the prime denotes partial derivative with respect to η, σ_ξ and $\sigma_{\xi\xi}$ are the first and second derivative of σ with respect to ξ. The parameters Prandtl number Pr, bioconvection Peclet number Pe, Lewis number Le, nano particle Lewis number Ln, bioconvection Schmidt number Sc, Brownian motion parameter N_b, regular double diffusive buoyancy ratio N_c, modified Dufour number N_d, nanofluid buoyancy ratio N_r, thermophoresis parameter N_t, bioconvection Rayleigh number R_b and Soret number S_r are defined by

$$Pr = \frac{\nu}{\alpha_m}, \quad Pe = \frac{b_c w_c}{D_n} \quad Le = \frac{\nu}{D_B}, \quad Sc = \frac{\nu}{D_n}, \quad Ln = \frac{\nu}{D_S}, \quad N_b = \frac{\gamma D_B(\Phi_w - \Phi_\infty)}{\alpha_m},$$

$$R_b = \frac{\gamma(\rho_m - \rho_{f\infty})M_w}{(1-\Phi_\infty)\beta_T\rho_{f\infty}(T_w - T_\infty)}, \quad N_c = \frac{\beta_C}{\beta_T}\frac{(C_w - C_\infty)}{(T_w - T_\infty)}, \quad N_d = \frac{\sigma_1 D_{TC}(C_w - C_\infty)}{\alpha_m(T_w - T_\infty)}$$

$$N_r = \frac{(\rho_p - \rho_{f\infty})}{(1-\Phi_\infty)\beta_T\rho_{f\infty}}\frac{(\Phi_w - \Phi_\infty)}{(T_w - T_\infty)}, \quad N_t = \frac{\gamma D_T(T_w - T_\infty)}{\alpha_m T_\infty}, \quad S_r = \frac{D_{CT}(T_w - T_\infty)}{D_S(C_w - C_\infty)}. \tag{2.17}$$

The objective of this study is to estimate the parameters of the engineering interest, namely the skin friction coefficient, Nusselt number, Sherwood number, nanoparticle Sherwood number, and motile microorganism density number.

The local skin friction coefficient, heat, mass, nanoparticle mass flux, and motile microorganism density flux can be obtained from

$$\begin{aligned} C_f = \frac{2\mu\rho L^2}{\mu_\infty^2 Gr}\left(\hat{n}\cdot\nabla U\right), \quad q_w = -k_m(\hat{n}\cdot\nabla T) \\ q_m = -D_S(\hat{n}\cdot\nabla C) \quad q_{np} = -D_B(\hat{n}\cdot\nabla\phi) \quad q_M = -D_n(\hat{n}\cdot\nabla M), \end{aligned} \tag{2.18}$$

where $\hat{n} = \left(\frac{-\sigma_x}{\sqrt{1+\sigma_x^2}}, \frac{1}{\sqrt{1+\sigma_x^2}}\right)$ is the unit normal to the wavy surface.

The non dimensional skin friction coefficient Cf_x, Nusselt number Nu_x, Sherwood number Sh_x, nanoparticle Sherwood number NSh_x and motile microorganism density number Q_x are given by

$$\begin{aligned} \frac{1}{2}(Cf_\xi)(Gr_\xi^{1/4}) &= \xi\sqrt{1+\sigma_\xi^2}\left.\frac{\partial^2 f}{\partial\eta^2}\right|_{(\xi,0)}, \\ \frac{Nu_\xi}{Gr_\xi^{1/4}} = -\sqrt{1+\sigma_\xi^2}\left.\frac{\partial\theta}{\partial\eta}\right|_{(\xi,0)}, &\quad \frac{Sh_\xi}{Gr_\xi^{1/4}} = -\sqrt{1+\sigma_\xi^2}\left.\frac{\partial\varphi}{\partial\eta}\right|_{(\xi,0)}, \\ \frac{NSh_\xi}{Gr_\xi^{1/4}} = -\sqrt{1+\sigma_\xi^2}\left.\frac{\partial\phi}{\partial\eta}\right|_{(\xi,0)}, &\quad \frac{Q_\xi}{Gr_\xi^{1/4}} = -\sqrt{1+\sigma_\xi^2}\left.\frac{\partial\chi}{\partial\eta}\right|_{(\xi,0)}. \end{aligned} \tag{2.19}$$

2.3 Method of Solution

The system of differential equations (2.11) - (2.15) along with the boundary conditions (2.16) are solved using the bivariate pseudo-spectral local linearisation method (BPSLLM)([82]). By using this method, the iteration scheme is obtained by linearizing the non-linear component of differential equations about one dependent variable at a time.

Let f_{m+1}, θ_{m+1}, ϕ_{m+1}, φ_{m+1} and χ_{m+1} be an approximate solution at the current iteration and f_m, θ_m, ϕ_m, φ_m and χ_m be the solutions at the previous iteration of the system of equations (2.11) - (2.15). The first equation Eq. (2.11) is linearized at the current iteration (f_{m+1}) using the values of the functions at the previous iteration i.e. θ_m, ϕ_m, φ_m and χ_m. The second equation Eq. (2.12) is linearized at the current iteration (θ_{m+1}) using the updated value of f at the current iteration i.e. f_{m+1} and the values of the remaining functions at the

previous iteration ϕ_m, φ_m and χ_m and so on. On applying this procedure to the equations (2.11) - (2.15), we get the following system of linear differential equations.

$$a_{1,m}f'''_{m+1} + a_{2,m}f''_{m+1} + a_{3,m}f'_{m+1} + a_{4,m}f_{m+1} + a_{5,m}\frac{\partial f'_{m+1}}{\partial \xi} + a_{6,m}\frac{\partial f_{m+1}}{\partial \xi} = R_{1,m}, \tag{2.20}$$

$$b_{1,m}\theta''_{m+1} + b_{2,m}\theta'_{m+1} + b_{3,m}\frac{\partial \theta_{m+1}}{\partial \xi} = R_{2,m}, \tag{2.21}$$

$$c_{1,m}\phi''_{m+1} + c_{2,m}\phi'_{m+1} + c_{3,m}\frac{\partial \phi_{m+1}}{\partial \xi} = R_{3,m}, \tag{2.22}$$

$$d_{1,m}\varphi''_{m+1} + d_{2,m}\varphi'_{m+1} + d_{3,m}\frac{\partial \varphi_{m+1}}{\partial \xi} = R_{4,m}, \tag{2.23}$$

$$e_{1,m}\chi''_{m+1} + e_{2,m}\chi'_{m+1} + e_{3,m}\chi_{m+1} + e_{4,m}\frac{\partial \chi_{m+1}}{\partial \xi} = R_{5,m}, \tag{2.24}$$

where the coefficients are

$$a_{1,m} = 1 + \sigma_\xi^2, \quad a_{2,m} = \frac{3}{4}f_m + \xi\frac{\partial f_m}{\partial \xi}, \quad a_{3,m} = -\left[\frac{1}{2} + \frac{\xi\sigma_\xi\sigma_{\xi\xi}}{1+\sigma_\xi^2}\right]2f'_m - \xi\frac{\partial f'_m}{\partial \xi},$$

$$a_{4,m} = \frac{3}{4}f''_m \quad a_{5,m} = -\xi f'_m \quad a_{6,m} = \xi f''_m,$$

$$R_{1,m} = \xi f''_m\frac{\partial f_m}{\partial \xi} - \left[\frac{1}{2} + \frac{\xi\sigma_\xi\sigma_{\xi\xi}}{1+\sigma_\xi^2}\right](f'_m)^2 + \frac{3}{4}f_m f''_m - \xi f'_m\frac{\partial f'_m}{\partial \xi}$$
$$-\frac{(\theta_m + N_c\,\varphi_m - N_r\phi_m - R_b\chi_m)}{(1+{\sigma_\xi}^2)}(\sin A + \sigma_\xi \cos A),$$

$$b_{1,m} = \frac{1+\sigma_\xi^2}{\Pr}, \quad b_{2,m} = \frac{1+\sigma_\xi^2}{\Pr}N_b\phi'_m + \frac{1+\sigma_\xi^2}{\Pr}2N_t\theta'_m + \frac{3}{4}f_{m+1} + \xi\frac{\partial f_{m+1}}{\partial \xi},$$

$$b_{3,m} = -\xi f'_{m+1}, \quad R_{2,m} = \frac{1+\sigma_\xi^2}{\Pr}\left[N_t(\theta'_m)^2 - N_d\varphi''_m\right],$$

$$c_{1,m} = \frac{1+\sigma_\xi^2}{Le}, \quad c_{2,m} = \frac{3}{4}f_{m+1} + \xi\frac{\partial f_{m+1}}{\partial \xi}, \quad c_{3,m} = -\xi f'_{m+1},$$

$$R_{3,m} = -\frac{1+\sigma_\xi^2}{Le}\frac{N_t}{N_b}\theta''_{m+1}, \quad d_{1,m} = \frac{1+\sigma_\xi^2}{Ln},$$

$$d_{2,m} = \frac{3}{4}f_{m+1} + \xi\frac{\partial f_{m+1}}{\partial \xi}, \quad d_{3,m} = -\xi f'_{m+1}, \quad R_{4,m} = -\frac{1+\sigma_\xi^2}{Ln}\theta''_{m+1},$$

$$e_{1,m} = \frac{1+\sigma_\xi^2}{Sc}, \quad e_{2,m} = -\frac{Pe}{Sc}(1-\sigma_\xi)\,\phi'_{m+1} + \frac{3}{4}f_{m+1} + \xi\frac{\partial f_{m+1}}{\partial \xi},$$

$$e_{3,m} = -\frac{Pe}{Sc}\left(1-\sigma_\xi\right)\phi''_{m+1}, \quad e_{4,m} = -\xi f'_{m+1}, \quad R_{5,m} = 0.$$

The corresponding boundary conditions are

$$\left.\begin{array}{l} f'_{m+1}(\xi,0) = 0, \quad f_{m+1}(\xi,0) = -\dfrac{4}{3}\xi\left.\dfrac{\partial f}{\partial \xi}\right|_{(\xi,0)}, \quad \theta_{m+1}(\xi,0) = 1, \\ \phi_{m+1}(\xi,0) = 1, \quad \varphi_{m+1}(\xi,0) = 1, \ \chi_{m+1}(\xi,0) = 1, \ f'_{m+1}(\xi,\infty) = 0, \\ \theta_{m+1}(\xi,\infty) = 0, \ \phi_{m+1}(\xi,\infty) = 0, \ \varphi_{m+1}(\xi,\infty) = 0, \ \chi_{m+1}(\xi,\infty) = \delta\chi. \end{array}\right\} \tag{2.25}$$

The system of linearized equations (2.20) to (2.24) are solved using the Chebyshev pseudo spectral method in both ξ and η directions [20]. To apply this method, first the semi-infinite domain $[0,\infty)\times[0,\infty)$ is truncated to $[0,\xi_\infty]\times[0,\eta_\infty]$, where η_∞ is the finite value that is introduced to facilitate the application of the numerical method at infinity and ξ_∞ is the largest values of ξ used in the numerical computations. This domain is then transformed to $[-1,1]\times[-1,1]$ by the transformation $\zeta = \frac{2\xi}{\xi_\infty} - 1$, $-1 \le \zeta \le 1$ and $\tau = \frac{2\eta}{\eta_\infty} - 1$, $-1 \le \tau \le 1$. Now, the problem is solved in the domain $[-1,1]\times[-1,1]$.

The functions that are to be determined are approximated by the bivariate Lagrange interpolation polynomial in such a manner that they are collocated at the Gauss - Lobatto points defined as

$$\zeta_i = \cos\frac{\pi i}{N}, \ i = 0,1,\ldots,N \quad \tau_j = \cos\frac{\pi j}{M}, \ j = 0,1,\ldots,M \tag{2.26}$$

The functions that are to be determined i.e. $f_{m+1}(\eta,\xi)$, $\theta_{m+1}(\eta,\xi)$, $\phi_{m+1}(\eta,\xi)$, $\varphi_{m+1}(\eta,\xi)$, and $\chi_{m+1}(\eta,\xi)$ are interpolated at the collocation points described by (2.26), using the

following bivariate Lagrange interpolation polynomials.

$$
\begin{aligned}
f_{m+1}(\xi,\eta) &\approx \sum_{m=0}^{N}\sum_{j=0}^{M} f_{m+1}(\zeta_m,\tau_j)L_m(\zeta)L_j(\tau),\\
\theta_{m+1}(\xi,\eta) &\approx \sum_{m=0}^{N}\sum_{j=0}^{M} \theta_{m+1}(\zeta_m,\tau_j)L_m(\zeta)L_j(\tau),\\
\phi_{m+1}(\xi,\eta) &\approx \sum_{m=0}^{N}\sum_{j=0}^{M} \phi_{m+1}(\zeta_m,\tau_j)L_m(\zeta)L_j(\tau),\\
\varphi_{m+1}(\xi,\eta) &\approx \sum_{m=0}^{N}\sum_{j=0}^{M} \varphi_{m+1}(\zeta_m,\tau_j)L_m(\zeta)L_j(\tau),\\
\chi_{m+1}(\xi,\eta) &\approx \sum_{m=0}^{N}\sum_{j=0}^{M} \chi_{m+1}(\zeta_m,\tau_j)L_m(\zeta)L_j(\tau),
\end{aligned}
\tag{2.27}
$$

where $L_m(\zeta)$ and $L_j(\tau)$ are well-known Lagrange polynomials.

The derivatives of the unknown functions with respect to η and ξ at the collocation points ζ_k and τ_i are given by

$$
\left.\frac{\partial^m f_{m+1}}{\partial \eta^m}\right|_{(\zeta_k,\tau_i)} = \mathbf{D}^m\mathbf{F}_i, \quad \left.\frac{\partial f_{m+1}}{\partial \xi}\right|_{(\zeta_k,\tau_i)} = \frac{2}{\xi_\infty}\sum_{j=0}^{M}\mathbf{d}_{i,j}\mathbf{F}_j. \tag{2.28}
$$

where m is the order of differentiation, $d_{i,j}(i,j=12,\cdots M)$ are the entries of the matrix $\mathbb{D}=\frac{2}{\xi_\infty}[d_{i,j}]$ and $\mathbf{D}=\frac{2}{\eta_\infty}\mathcal{D}$, $\mathbb{D}$ and $\mathcal{D}$ being the Chebyshev spectral differentiation matrices [122] of order $(M+1)\times(M+1)$ and $(N+1)\times(N+1)$ respectively. The vector $\mathbf{F}_i$ is defined as $\mathbf{F}_i=[f(\zeta_0,\tau_i),f(\zeta_1,\tau_i),f(\zeta_2,\tau_i),\cdots,f(\zeta_N,\tau_i)]^T$

Similar expressions are obtained for derivatives of the other functions $\theta_{m+1}(\eta,\xi)$, $\phi_{m+1}(\eta,\xi)$, $\varphi_{m+1}(\eta,\xi)$, and $\chi_{m+1}(\eta,\xi)$ with respect to η and ξ. Applying the pseudo-spectral method in both η and ξ gives

$$
A^{(1)}\mathbf{F}_i + \gamma_{5,i}^{(1)}\sum_{j=0}^{M}\mathbf{d}_{i,j}\mathbf{D}\mathbf{F}_j + \gamma_{6,i}^{(1)}\sum_{j=0}^{M}\mathbf{d}_{i,j}\mathbf{F}_j = \mathbf{R}_{1,i} \tag{2.29}
$$

$$
A^{(2)}\mathbf{\Theta}_i + \gamma_{3,i}^{(2)}\sum_{j=0}^{M}\mathbf{d}_{i,j}\mathbf{D}\mathbf{\Theta}_j = \mathbf{R}_{2,i} \tag{2.30}
$$

$$A^{(3)}\mathbf{\Phi}_i + \gamma_{3,i}^{(3)} \sum_{j=0}^{M} \mathbf{d}_{i,j}\mathbf{D}\mathbf{\Phi}_j = \mathbf{R}_{3,i} \tag{2.31}$$

$$A^{(4)}\varphi_i + \gamma_{3,i}^{(4)} \sum_{j=0}^{M} \mathbf{d}_{i,j}\mathbf{D}\varphi_j = \mathbf{R}_{4,i} \tag{2.32}$$

$$A^{(5)}\chi_r + \gamma_{4,i}^{(5)} \sum_{j=0}^{M} \mathbf{d}_{i,j}\mathbf{D}\chi_j = \mathbf{R}_{5,i} \tag{2.33}$$

where

$$\begin{aligned}
A^{(1)} &= \gamma_{1,i}^{(1)}\mathbf{D}^3 + \gamma_{2,i}^{(1)}\mathbf{D}^2 + \gamma_{3,i}^{(1)}\mathbf{D} + \gamma_{4,i}^{(1)}\mathbf{I},\\
A^{(2)} &= \gamma_{1,i}^{(2)}\mathbf{D}^2 + \gamma_{2,i}^{(2)}\mathbf{D},\\
A^{(3)} &= \gamma_{1,i}^{(3)}\mathbf{D}^2 + \gamma_{2,i}^{(3)}\mathbf{D},\\
A^{(4)} &= \gamma_{1,i}^{(4)}\mathbf{D}^2 + \gamma_{2,i}^{(4)}\mathbf{D},\\
A^{(5)} &= \gamma_{1,i}^{(5)}\mathbf{D}^2 + \gamma_{2,i}^{(5)}\mathbf{D} + \gamma_{3,i}^{(5)}\mathbf{I},\\
\gamma_{k,i}^{(1)} &= diag(a_{k,r}(\zeta_0,\tau_i), a_{k,r}(\zeta_1,\tau_i), a_{k,r}(\zeta_2,\tau_i), \cdots, a_{k,r}(\zeta_N,\tau_i)), k = 1,2,3,4,5,\\
\gamma_{k,i}^{(2)} &= diag(b_{k,r}(\zeta_0,\tau_i), b_{k,r}(\zeta_1,\tau_i), b_{k,r}(\zeta_2,\tau_i), \cdots, b_{k,r}(\zeta_N,\tau_i)), k = 1,2,3,\\
\gamma_{k,i}^{(3)} &= diag(c_{k,r}(\zeta_0,\tau_i), c_{k,r}(\zeta_1,\tau_i), c_{k,r}(\zeta_2,\tau_i), \cdots, c_{k,r}(\zeta_N,\tau_i)), k = 1,2,3,\\
\gamma_{k,i}^{(4)} &= diag(d_{k,r}(\zeta_0,\tau_i), d_{k,r}(\zeta_1,\tau_i), d_{k,r}(\zeta_2,\tau_i), \cdots, d_{k,r}(\zeta_N,\tau_i)), k = 1,2,3,\\
\gamma_{k,i}^{(5)} &= diag(e_{k,r}(\zeta_0,\tau_i), e_{k,r}(\zeta_1,\tau_i), e_{k,r}(\zeta_2,\tau_i), \cdots, e_{k,r}(\zeta_N,\tau_i)), k = 1,2,3,4,\\
\mathbf{R}_{k,i} &= diag(R_{k,r}(\zeta_0,\tau_i), R_{k,r}(\zeta_1,\tau_i), R_{k,r}(\zeta_2,\tau_i), \cdots, R_{k,r}(\zeta_N,\tau_i)), k = 1,2,3,4,5.
\end{aligned}$$

Here $diag(x_1, x_2, x_3, \cdots x_N)$ is the diagonal matrix of order $N \times N$ with $x_1, x_2, x_3, \cdots x_N$ as its diagonal elements and $\mathbf{I}$ is the identity matrix. The matrix form of equation (2.29) can be written as

$$\begin{bmatrix}
A_{0,0}^{(1)} & A_{0,1}^{(1)} & A_{0,2}^{(1)} & \cdots & A_{0,M}^{(1)}\\
A_{1,0}^{(1)} & A_{1,1}^{(1)} & A_{1,2}^{(1)} & \cdots & A_{1,M}^{(1)}\\
A_{2,0}^{(1)} & A_{2,1}^{(1)} & A_{2,2}^{(1)} & \cdots & A_{2,M}^{(1)}\\
\vdots & \vdots & \vdots & \ddots & \vdots\\
A_{M,0}^{(1)} & A_{M,1}^{(1)} & A_{M,2}^{(1)} & \cdots & A_{M,M}^{(1)}
\end{bmatrix}
\begin{bmatrix}
\mathbf{F}_0\\ \mathbf{F}_1\\ \mathbf{F}_2\\ \vdots\\ \mathbf{F}_M
\end{bmatrix}
=
\begin{bmatrix}
\mathbf{R}_{1,0}\\ \mathbf{R}_{1,1}\\ \mathbf{R}_{1,2}\\ \vdots\\ \mathbf{R}_{1,M}
\end{bmatrix} \tag{2.34}$$

where

$$\begin{aligned}
A_{i,j}^{(1)} &= A^{(1)} + \gamma_{5,i}^{(1)}\mathbf{d}_{i,i}\mathbf{D} + \gamma_{6,i}^{(1)}\mathbf{d}_{i,i}\mathbf{I}, \quad for \quad i = j;\\
A_{i,j}^{(1)} &= \gamma_{5,i}^{(1)}\mathbf{d}_{i,j}\mathbf{D} + \gamma_{6,i}^{(1)}\mathbf{d}_{i,j}\mathbf{I}, \quad for \quad i \neq j
\end{aligned} \tag{2.35}$$

The matrix form of Eq.(2.30) is

$$\begin{bmatrix} A^{(2)}_{0,0} & A^{(2)}_{0,1} & A^{(2)}_{0,2} & \cdots & A^{(2)}_{0,M} \\ A^{(2)}_{1,0} & A^{(2)}_{1,1} & A^{(2)}_{1,2} & \cdots & A^{(2)}_{1,M} \\ A^{(2)}_{2,0} & A^{(2)}_{2,1} & A^{(2)}_{2,2} & \cdots & A^{(2)}_{2,M} \\ \vdots & \vdots & \vdots & \ddots & \vdots \\ A^{(2)}_{M,0} & A^{(2)}_{M,1} & A^{(2)}_{M,2} & \cdots & A^{(2)}_{M,M} \end{bmatrix} \begin{bmatrix} \mathbf{\Theta}_0 \\ \mathbf{\Theta}_1 \\ \mathbf{\Theta}_2 \\ \vdots \\ \mathbf{\Theta}_M \end{bmatrix} = \begin{bmatrix} \mathbf{R}_{2,0} \\ \mathbf{R}_{2,1} \\ \mathbf{R}_{2,2} \\ \vdots \\ \mathbf{R}_{2,M} \end{bmatrix} \tag{2.36}$$

where

$$\begin{aligned} A^{(2)}_{i,j} &= A^{(2)} + \gamma^{(2)}_{3,i}\mathbf{d}, \quad for \quad i = j; \\ A^{(2)}_{i,j} &= \gamma^{(2)}_{3,i}\mathbf{d}, \quad for \quad i \neq j \end{aligned} \tag{2.37}$$

In a similar manner, we can write the matrix form of the equations (2.31) to (2.33). The approximate solutions are obtained by solving these matrix equations, iteratively, with the help of suitable initial approximation.

2.4 Computational Results and Discussion

In this study, attention is given to analyze the computational results of the non-dimensional skin friction coefficient Cf_ξ, Nusselt number Nu_ξ, Sherwood number Sh_ξ, nanoparticle Sherwood number NSh_ξ, and density number of motile microorganism Q_ξ graphically. The effect of the parameters on the non-dimensional quantities velocity $f(\xi,\eta)$, temperature $\theta(\xi,\eta)$, Nanoparticle concentration $\phi(\xi,\eta)$, fluid concentration $\varphi(\xi,\eta)$ and density of motile microorganisms $\chi(\xi,\eta)$ are not presented for conciseness. The influence of angle of inclination A, amplitude of the wavy surface α, bioconvection Peclet number Pe, nanoparticle Lewis number Ln, bioconvection Schmidt number Sc, Brownian motion parameter N_b, regular double diffusive buoyancy Ratio N_c, modified Dufour number N_d, nanofluid buoyancy ratio N_r, Thermophoresis parameter N_t, bioconvection Rayleigh number R_b, Soret number S_r and microorganism slip parameter $\delta\chi$ on the physical quantities Cf_ξ, Nu_ξ, Sh_ξ, NSh_ξ, and Q_ξ graphically.is presented through Figs. 2.2 - 2.7.

To check the convergence, the code written to solve 2.11 - 2.15 along with the boundary conditions 2.16 using the bivariate pseudo-spectral local linearisation method (BPSLLM) is executed for skin friction coefficient and heat transfer rate by changing the number of collocation points N and M in both η and ξ directions as $N = 20, 40, 50, 60, 80$ and $M =$

$20, 40, 50, 60, 80$ and in each case we found very good agreement between them and can be observed from Table 2.1. The same tendency is witnessed by changing the values of parameters. Hence, a grid size of 50×50 is adopted to be satisfactory for the convergence criterion of 10^{-6}.

Table 2.1: Convergence of $f''(\xi, 0)$ and $\theta(\xi, 0)$ by BPSLLM for Pr = 2, $Pe = 2$, $Le = 5$, $Sc = 0.5$, $Sr = 0.5$, $Nb = 0.5$, $Nb = 0.5$, $Nt = 0.1$, $Nr = 0.3$, $Rb = 0.5$, $Nc = 0.3$, $Ln = 5$, $\alpha = 0.01$, $A = \pi/4$

Number of grid points in η direction	Number of grid points in ξ direction	$f''(\xi, 0)$	$\theta(\xi, 0)$
20	20	4.406218	-0.178631
20	30	4.406177	-0.178455
30	20	4.431318	-0.178471
30	30	4.431313	-0.178303
40	30	4.431470	-0.178309
40	40	4.431470	-0.178275
50	40	4.431468	-0.178275
50	50	4.431468	-0.178278
60	40	4.431468	-0.178275
70	60	4.431468	-0.178291
80	60	4.431468	-0.178291
90	60	4.431468	-0.178291

To validate the accuracy of the method, the code developed is verified by comparing the present numerical results of skin friction coefficient and rate of heat transfer coefficient with the published results of Hossain *et al.* [46] for different values of Prandtl number Pr by taking angle of inclination $A = \pi/2$, amplitude of the wavy surface $\alpha = 0.001$, and considering the parameters Pe, Ln, Le, Sc, N_b, approximately zero and ignoring N_c, N_d, N_r, N_t, R_b, S_r and $\delta\chi$. The computed results are presented in the Table 2.2. It is evident from the Table 2.2 that the present results are in good agreement with the results of Hossain *et al.* [46].

All the numerical computations are carried out by assigning $Le = 5$, $Ln = 5$, $Pe = 2$, Pr = 2, $Sc = 0.5$, $N_b = 0.5$, $N_c = 0.3$, $N_d = 0.5$, $N_r = 0.3$, $N_t = 0.1$, $R_b = 0.5$, $S_r = 0.5$, $\alpha = 0.01$, and $\delta\chi = 0.01$ unless otherwise mentioned.

The influence of bioconvection Peclet number Pe and Rayleigh number R_b on skinfriction coefficient Cf_ξ, Nusselt number Nu_ξ, Sherwood number Sh_ξ, nanoparticle Sherwood number NSh_ξ, and density number of motile microorganism Q_ξ is demonstrated in Figure 2.2. It is noticed that from Fig. 2.2(a) to 2.2(e) the enhancement of bioconvection Peclet number Pe enhances Cf_ξ, Nu_ξ, Sh_ξ, NSh_ξ, and Q_ξ. Pe helps to intensify the speed of the microorgan-

Table 2.2: Comparative analysis for the values of skin friction coefficient $f''(x,0)$ and heat transfer coefficient $-\theta'(x,0)$ by the present method for $\alpha = 0.001$, $A = \pi/2$, $Pe = 10^{-5}$, $Ln = 10^{-5}$, $Le = 10^{-5}$, $Sc = 10^{-5}$, $N_b = 10^{-5}$, $S_r = N_d = N_t = N_r = R_b = N_c = \delta\chi = 0.0$ with the results of Hossain *et al.* [46]

	$f''(x,0)$		$-\theta'(x,0)$	
Pr	Present	Ref.[46]	Present	Ref. [46]
1. 0	0.908118	0.908	0.401454	0.401
10.0	0.591434	0.591	0.825327	0.825
25.0	0.485327	0.485	1.067486	1.066
50.0	0.417273	0.485	1.288404	1.066
100.0	0.352136	0.352	1.542391	1.542

isms in the fluid and so the density number of the microorganisms is enhanced at the wavy surface. An enhancement in bioconvection Rayleigh number results in the reduction of Cf_ξ, Nu_ξ, Sh_ξ, and NSh_ξ, as depicted in Figs. 2.2(a) -2.2(d). It is detected from Fig. 2.2(e) that Q_ξ is declining with a rise in the bioconvection Rayleigh number.

Figure 2.3 presents the effect of the inclination angle A and amplitude α on skin friction coefficient Cf_ξ, Nusselt number Nu_ξ, Sherwood number Sh_ξ, nanoparticle Sherwood number NSh_ξ, and density number of motile microorganism Q_ξ. It is clear from figures 2.3(a) to 2.3(e), that Cf_ξ, Nu_ξ, Sh_ξ, NSh_ξ and Q_ξ are increasing with the rise in the value of A. It is perceived from Fig. 2.3(a) that the impact of wavy surface amplitude is not much significant. On the close observation of graph 2.3(a), it is noticed that the coefficient of skin friction is decreasing with an increase in α. As there is an increment in amplitude, it is found that Nu_ξ, Sh_ξ, and NSh_ξ, are decreasing first and then increasing during one period. This trend is witnessed at regular intervals over ξ. It is remarkable to observe that Q_ξ is increasing first and then decreasing over one period with growth in α as depicted in 2.3(e). Here also, the variations are observed periodically.

The variation of the Cf_ξ, Nu_ξ, Sh_ξ, NSh_ξ and Q_ξ for diverse values of double-diffusive buoyancy ratio N_c and nanofluid buoyancy ratio N_r is demonstrated in Fig. 2.4. It is illustrated from this figure that a rise in the double-diffusive buoyancy ratio results in an increase in Cf_ξ, Nu_ξ, Sh_ξ, NSh_ξ and Q_ξ. Whereas the reverse trend is observed for the nanofluid buoyancy ratio.

Figure 2.5 illustrates the influence of bioconvection Schmidt number Sc and nanoparticle Lewis number Ln on Cf_ξ, Nu_ξ, Sh_ξ, NSh_ξ and Q_ξ. It is observed from Fig. 2.5(a) - 2.5(e) that Cf_ξ, Nu_ξ, Sh_ξ, NSh_ξ and Q_ξ are rising with the rise in Sc. Cf_ξ, Nu_ξ, NSh_ξ and Q_ξ are decreasing with a raise in nanoparticle Lewis number except for the Sherwood number. The

Sherwood number is increasing for an increase in nanoparticle Lewis number as displayed in Fig. 2.5(c).

The effect of Soret number S_r and modified Dufour number N_d on Cf_ξ, Nu_ξ, Sh_ξ, NSh_ξ and Q_ξ are depicted in figure (2.6). It is found from the figures 2.6(a), and 2.6(c) - 2.6(e) that, Cf_ξ, Sh_ξ, NSh_ξ and Q_ξ are increasing with an increase in both S_r and N_d. A rise in the values of S_r and N_d results in the decrease of Nu_ξ, as displayed in figure 2.6(b).

The variation of on Cf_ξ, Nu_ξ, Sh_ξ, NSh_ξ and Q_ξ with the microorganism slip parameter is portrayed in figure 2.7. It is perceived from Fig. 2.7(a) that, the effect of the microorganism slip parameter on the skin-friction coefficient is very small. Though, the skin friction coefficient is increasing slightly with a rise in $\delta\chi$. As and when there is an escalation in the parameter $\delta\chi$, it is observed from Fig. 2.7(a) - 2.7(e) that the Cf_ξ, Nu_ξ, Sh_ξ, NSh_ξ and Q_ξ are increasing.

2.5 Conclusions

In this chapter, an analysis is presented to study the double diffusion effect on the bioconvection past a slanted sinusoidal surface in a nanofluid encompassing motile microorganisms. The nonlinear equations are linearized utilizing local linearization procedure and the resultant system is solved by a bivariate pseudo-spectral collocation method. The following are some important observations:

- The coefficient of skin-friction improves with the rise in the parameters Pe, A, N_c, Sc, S_r, N_d and $\delta\chi$.
- Increase in Pe, A, N_c, Sc, $\delta\chi$, intensify the Nu_ξ.
- For all parameters, except for the nanoparticle Lewis number, the Sherwood number for concentration and nanoparticles either increase or decrease simultaneously.
- The skin-friction, Nusselt number, Sherwood number, and NSh_ξ are reducing initially and then rising over one period with an intensification in α, whereas an opposite behaviour is perceived for the density number of motile microorganisms.
- The density number of motile microbe reduces for an increase in R_b, N_r, Ln.

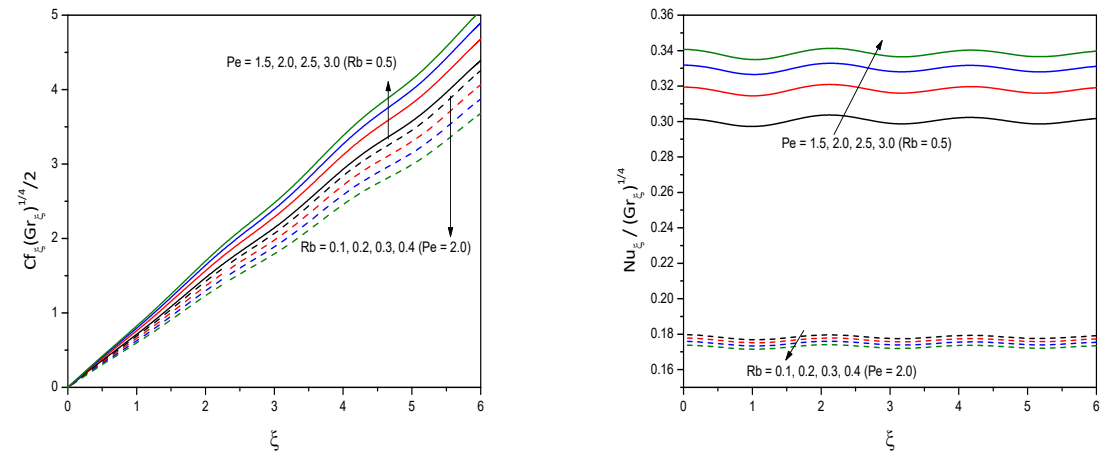

(a) (b)

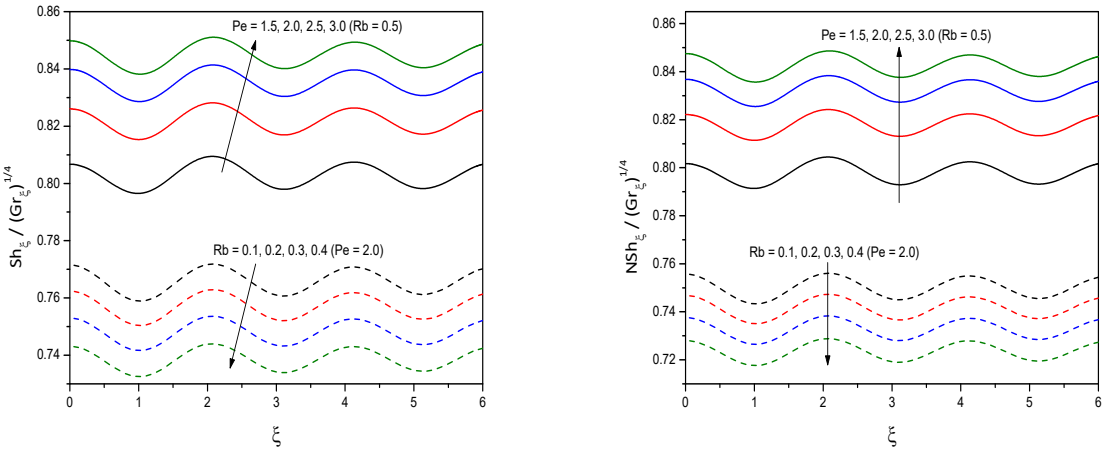

(c) (d)

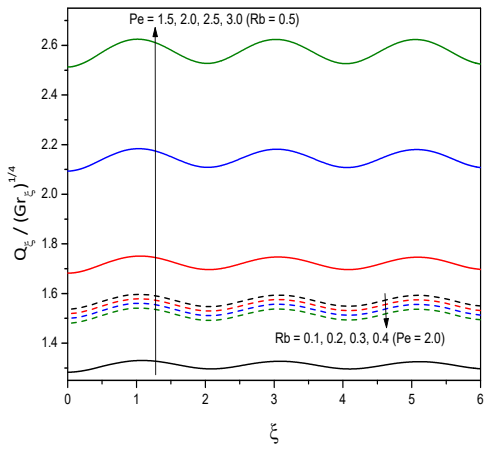

(e)

Figure 2.2: "Effect of the bioconvection Peclet number Pe and bioconvection Rayleigh number R_b on the profiles of (a) $Cf_\xi(Gr_\xi^{1/4})/2$ (b) $\frac{Nu_\xi}{Gr_\xi^{1/4}}$ (c) $\frac{Sh_\xi}{Gr_\xi^{1/4}}$, (d) $\frac{NSh_\xi}{Gr_\xi^{1/4}}$ (e) $\frac{Q_\xi}{Gr_\xi^{1/4}}$".

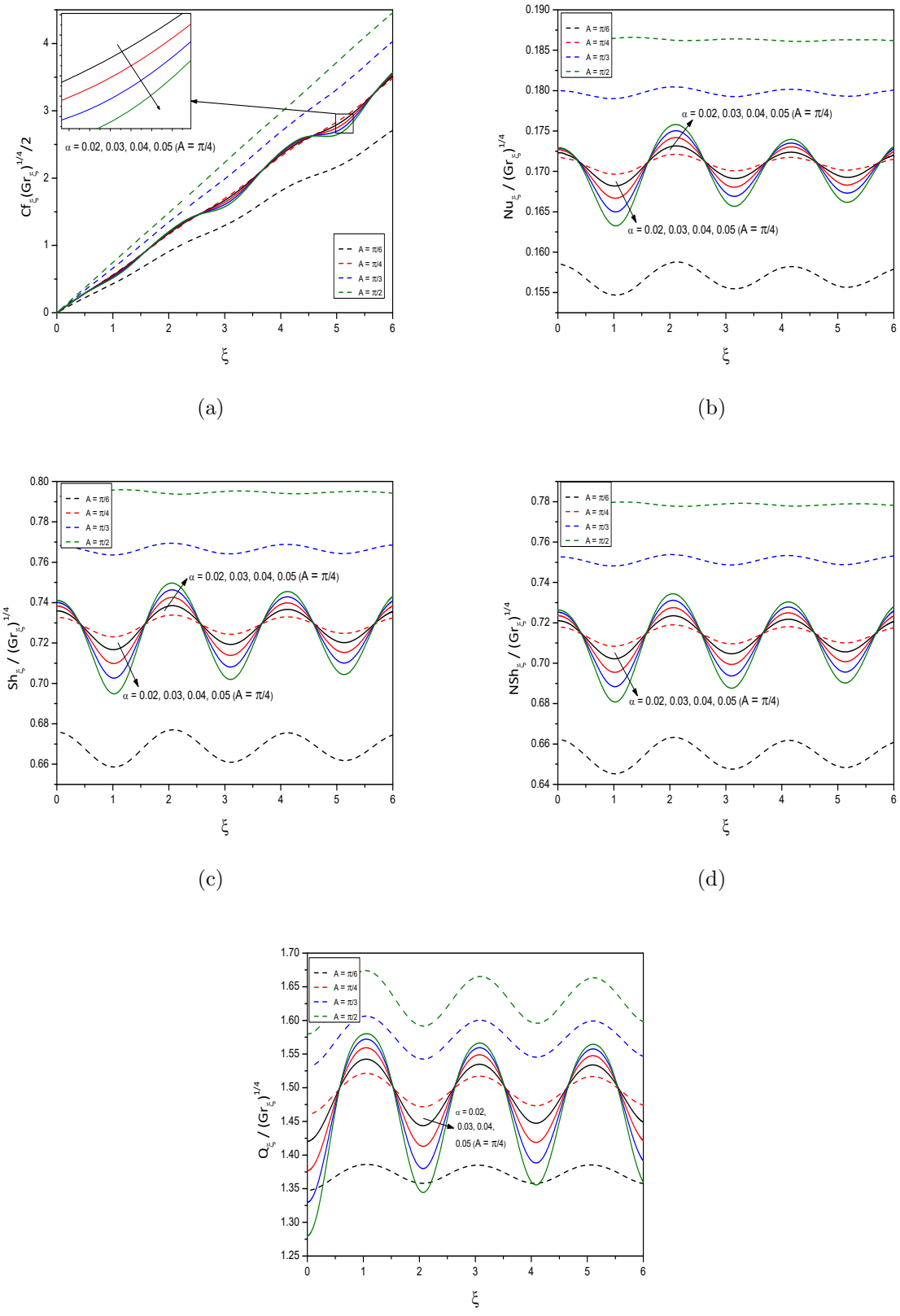

Figure 2.3: "Effect of the inclination angle (A) and amplitude of the wavy surface α on the profiles of (a) $Cf_\xi(Gr_\xi^{1/4})/2$ (b) $\frac{Nu_\xi}{Gr_\xi^{1/4}}$ (c) $\frac{Sh_\xi}{Gr_\xi^{1/4}}$, (d) $\frac{NSh_\xi}{Gr_\xi^{1/4}}$ (e) $\frac{Q_\xi}{Gr_\xi^{1/4}}$".

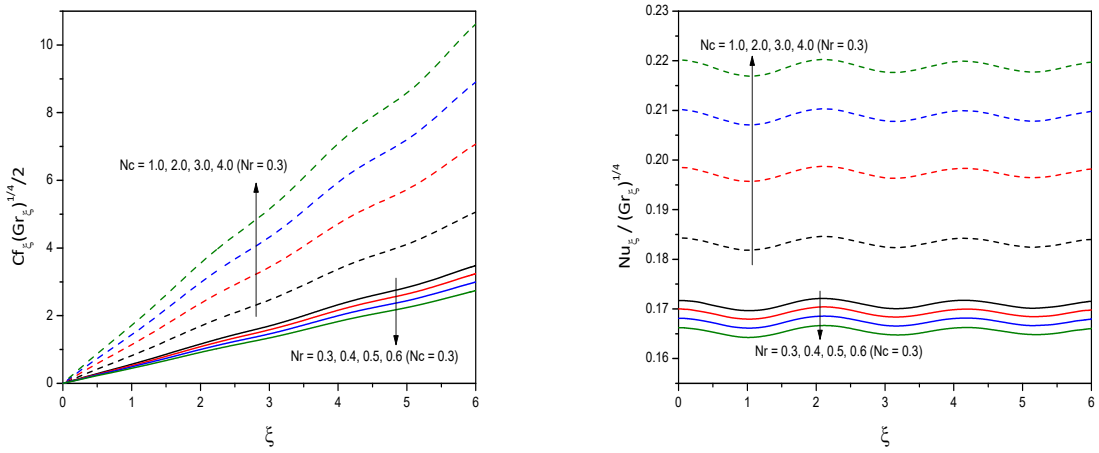

(a) (b)

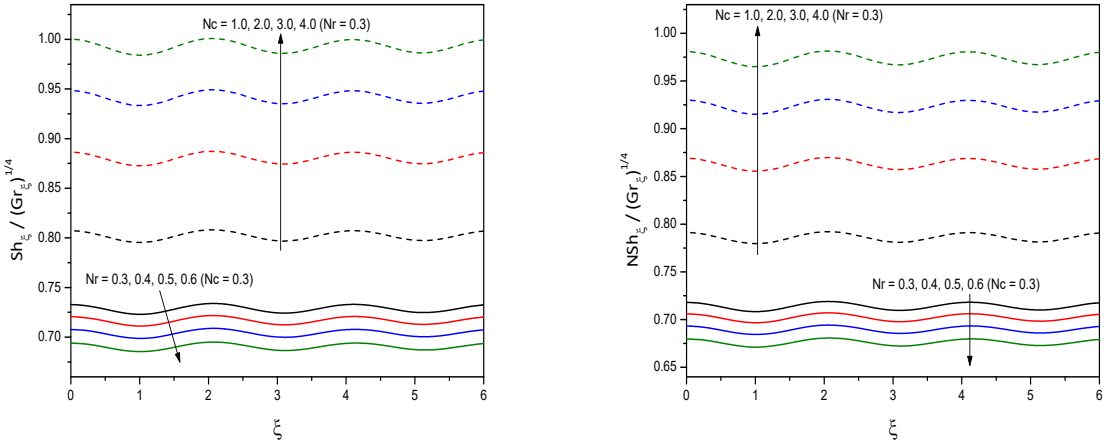

(c) (d)

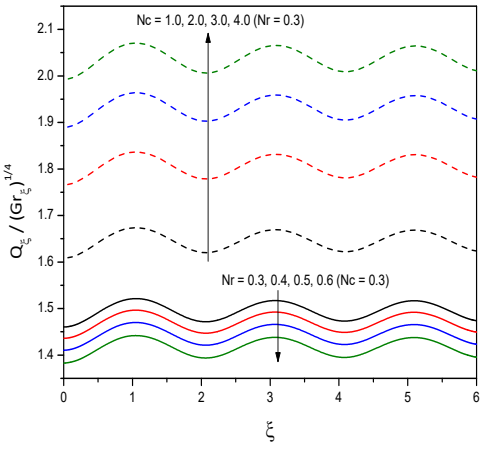

(e)

Figure 2.4: "Effect of the regular double diffusive buoyancy ratio N_c and nanofluid buoyancy ratio N_r on the profiles of (a) $Cf_\xi(Gr_\xi^{1/4})/2$ (b) $\frac{Nu_\xi}{Gr_\xi^{1/4}}$ (c) $\frac{Sh_\xi}{Gr_\xi^{1/4}}$, (d) $\frac{NSh_\xi}{Gr_\xi^{1/4}}$ (e) $\frac{Q_\xi}{Gr_\xi^{1/4}}$".

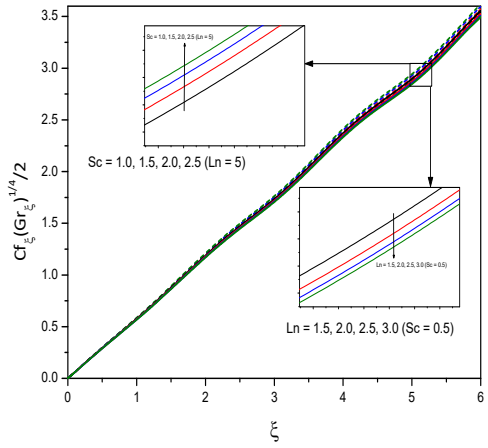

(a)

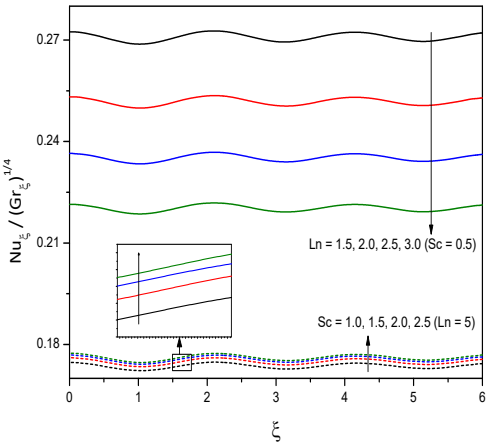

(b)

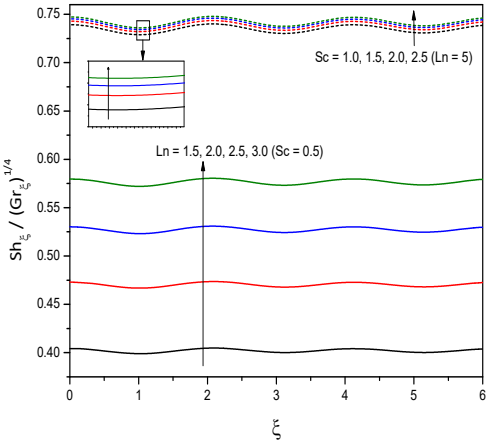

(c)

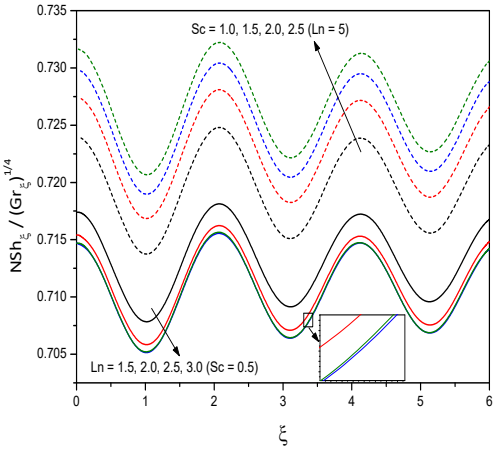

(d)

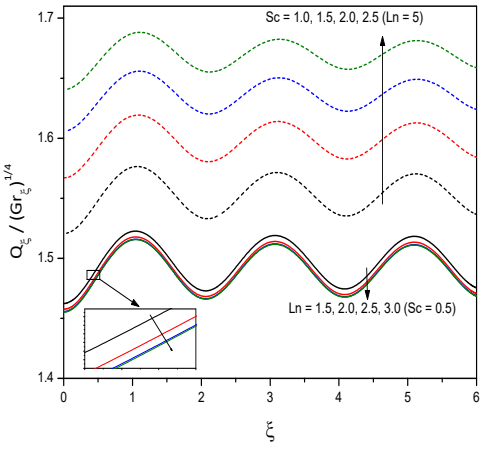

(e)

Figure 2.5: "Effect of the bioconvection Schmidt number Sc and nanoparticle Lewis number Ln on the profiles of (a) $Cf_\xi(Gr_\xi^{1/4})/2$ (b) $\frac{Nu_\xi}{Gr_\xi^{1/4}}$ (c) $\frac{Sh_\xi}{Gr_\xi^{1/4}}$, (d) $\frac{NSh_\xi}{Gr_\xi^{1/4}}$ (e) $\frac{Q_\xi}{Gr_\xi^{1/4}}$".

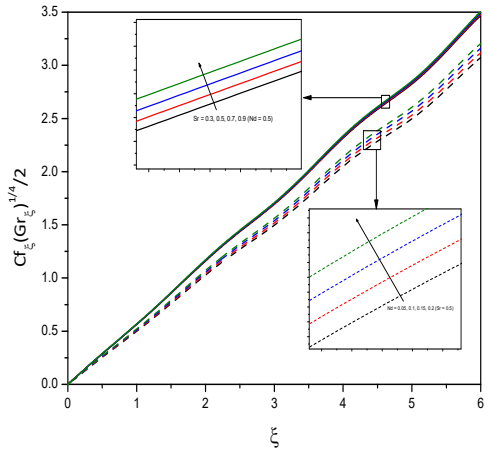

(a)

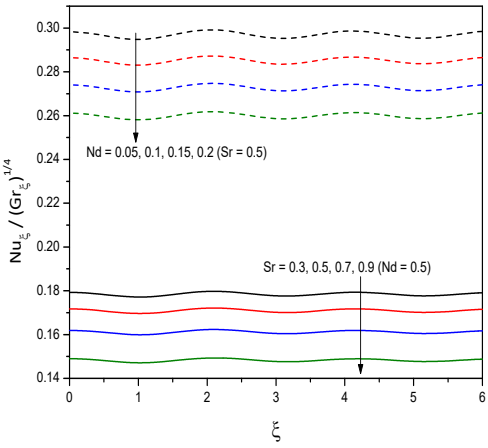

(b)

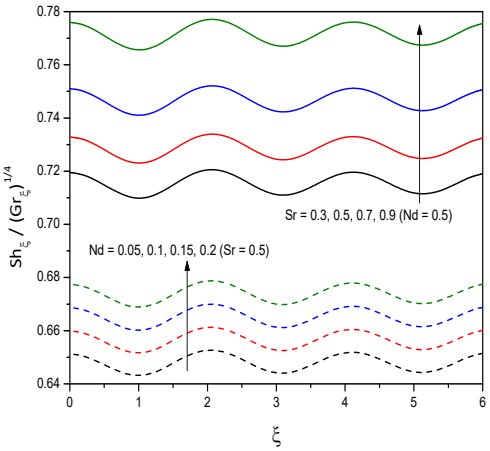

(c)

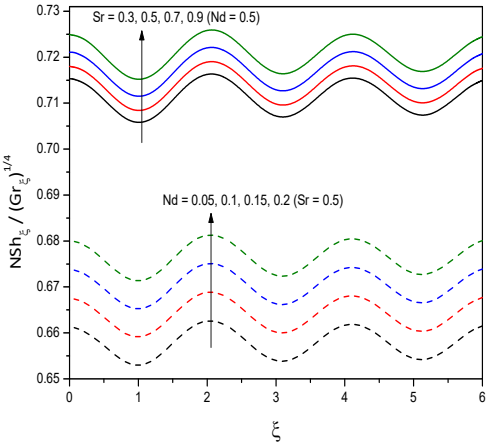

(d)

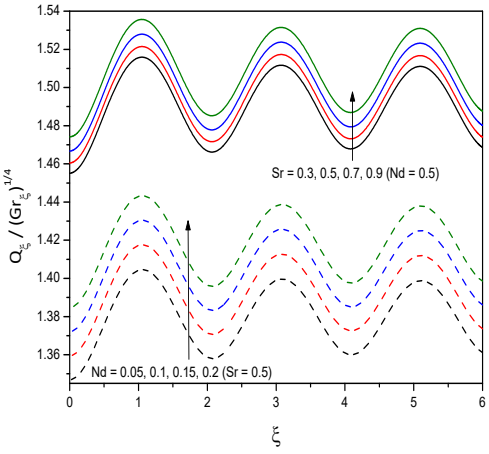

(e)

Figure 2.6: "Effect of the modified Dufour number N_d and Soret number S_r the profiles of (a) $Cf_\xi(Gr_\xi^{1/4})/2$ (b) $\frac{Nu_\xi}{Gr_\xi^{1/4}}$ (c) $\frac{Sh_\xi}{Gr_\xi^{1/4}}$, (d) $\frac{NSh_\xi}{Gr_\xi^{1/4}}$ (e) $\frac{Q_\xi}{Gr_\xi^{1/4}}$".

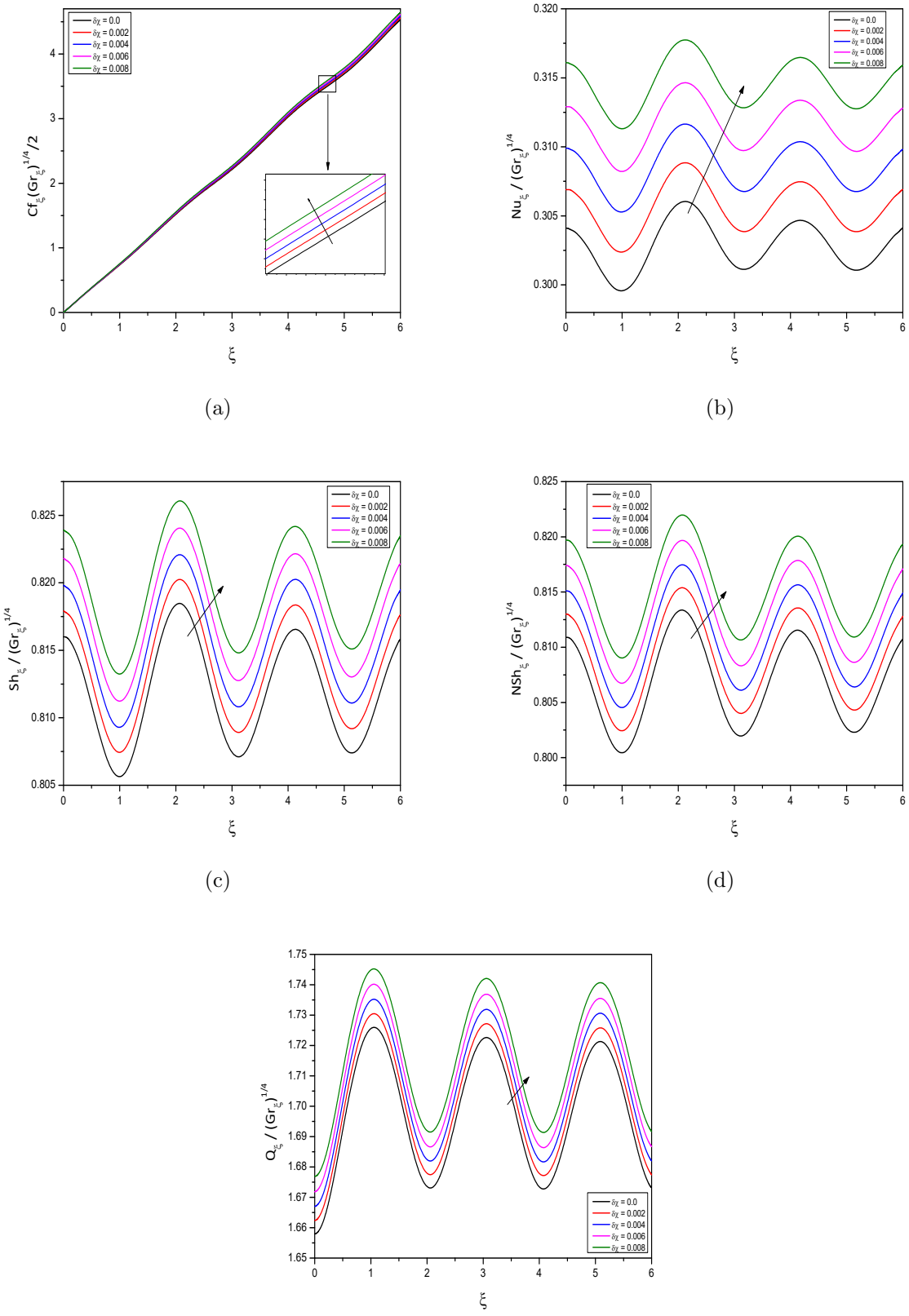

Figure 2.7: "Effect of the microorganism slip parameter $\delta\chi$ on the profiles of (a) $Cf_\xi(Gr_\xi^{1/4})/2$ (b) $\frac{Nu_\xi}{Gr_\xi^{1/4}}$ (c) $\frac{Sh_\xi}{Gr_\xi^{1/4}}$, (d) $\frac{NSh_\xi}{Gr_\xi^{1/4}}$ (e) $\frac{Q_\xi}{Gr_\xi^{1/4}}$".

Chapter 3

Thermal Radiation and Double Diffusion Effects on Bioconvection Flow of a Nanofluid Past an Inclined Wavy Surface. [1]

3.1 Introduction

The study of the effects of thermal radiation on convective heat and mass transfer processes has gained great importance in view of its applications in nuclear power plants, steel rolling, gas turbines, design fins, and various propulsion devices for missiles, aircraft, space vehicles, and satellites. The radiation within these systems is generally the consequence of discharge by hot walls and operational fluid. Hayat [43] discussed the effects of nonlinear thermal radiation, inclined magnetic field, and heat source/sink on the flow of nanofluid. Javed *et al.* [54] investigated the radiation effect on hydromagnetic flow along a vertical impermeable wavy texture heated with uniform flux. Khan *et al.* [59] analysed the impact of gyrotactic microorganisms and nonlinear thermal radiation on the Magneto-Burgers nanofluid. Siddiqa *et al.* [111] discussed the impact of thermal radiation on the natural convection along a wavy surface. Srinivasacharya and Vijay Kumar [119] investigated the effect of radiation on natural convection over an inclined wavy surface embedded in a non-Darcy porous medium saturated with a nanofluid.

[1] Published in "**Thermal Science and Engineering Progress"**, 22 (2021): 100830

Several investigators, to mention a few, D'Alessio *et al.* [30], Cheng [25], Bhat [16] have analyzed the convective heat/mass from an inclined wavy surface. Cheng [24] investigated the double-diffusive natural convection along an inclined wavy surface in a porous medium. Narayana *et al.* [87] analyzed the double-diffusive convection over a horizontal wavy surface in a porous medium with uniform heating and salting. Ibrahim and Marin [1] obtained an analytical solution of thermoelastic interaction in a half-space by pulsed laser heating.

In this chapter, we investigate the influence of thermal radiation and gyrotactic microorganisms on double-diffusive convection past an inclined wavy surface immersed in a nanofluid. The governing equations are linearized using the local linearization method and the resulting equations are solved using the bivariate pseudo-spectral method(BPSLLM). The effects of various parameters governing the flow and geometry on the rate of heat transfer, mass transfer, nanoparticle mass transfer, and density number of the microorganism are discussed in detail.

3.2 Mathematical Formulation

Consider the flow of a nanofluid containing motile microorganisms along a semi-infinite inclined wavy surface. The coordinate system and physical model are as depicted in Fig. 2.1. In addition to the assumptions made in Chapter 2, here we assume that the wavy surface is maintained at a uniform and constant heat, mass, nanoparticle volume fraction, and density of motile microorganism fluxes q_w, q_m, q_{np} and q_n respectively. The fluid is considered to be a grey, emitting/absorbing radiation, but non-scattering medium, and the radiative heat flux is defined by Rosseland approximation [115].

The equations governing the flow are [24, 90, 64, 19]

$$\frac{\partial U}{\partial X}+\frac{\partial V}{\partial Y}=0, \tag{3.1}$$

$$\rho_{f\infty}\left(U\frac{\partial U}{\partial X}+V\frac{\partial U}{\partial Y}\right)=-\frac{\partial P}{\partial X}+\mu\left(\frac{\partial^2 U}{\partial X^2}+\frac{\partial^2 U}{\partial Y^2}\right)+[(1-\Phi_\infty)\beta_T\rho_{f\infty}(T-T_\infty) \tag{3.2}$$
$$+(1-\Phi_\infty)\beta_C\rho_{f\infty}(C-C_\infty)-(\rho_p-\rho_{f\infty})(\Phi-\Phi_\infty)-\beta_M(\rho_m-\rho_{f\infty})(M-M_\infty)]\,g\sin A,$$

$$\rho_{f\infty}\left(U\frac{\partial V}{\partial X}+V\frac{\partial V}{\partial Y}\right)=-\frac{\partial P}{\partial Y}+\mu\left(\frac{\partial^2 V}{\partial X^2}+\frac{\partial^2 V}{\partial Y^2}\right)+[(1-\Phi_\infty)\beta_T\rho_{f\infty}(T-T_\infty)\tag{3.3}$$
$$+(1-\Phi_\infty)\beta_C\rho_{f\infty}(C-C_\infty)-(\rho_p-\rho_{f\infty})(\Phi-\Phi_\infty)-\beta_M(\rho_m-\rho_{f\infty})(M-M_\infty)]\,g\cos A,$$

$$U\frac{\partial T}{\partial X}+V\frac{\partial T}{\partial Y}=\alpha_m\left(\frac{\partial^2 T}{\partial X^2}+\frac{\partial^2 T}{\partial Y^2}\right)+\gamma\left\{D_B\left(\frac{\partial\Phi}{\partial X}\frac{\partial T}{\partial X}+\frac{\partial\Phi}{\partial Y}\frac{\partial T}{\partial Y}\right)\right.\tag{3.4}$$
$$\left.+\frac{D_T}{T_\infty}\left[\left(\frac{\partial T}{\partial X}\right)^2+\left(\frac{\partial T}{\partial Y}\right)^2\right]\right\}+D_{TC}\left(\frac{\partial^2 C}{\partial X^2}+\frac{\partial^2 C}{\partial Y^2}\right)+\frac{16\sigma_2 T_\infty^3}{3K_e}\left(\frac{\partial^2 T}{\partial X^2}+\frac{\partial^2 T}{\partial Y^2}\right)$$

$$U\frac{\partial\Phi}{\partial X}+V\frac{\partial\Phi}{\partial Y}=D_B\left(\frac{\partial^2\Phi}{\partial X^2}+\frac{\partial^2\Phi}{\partial Y^2}\right)+\frac{D_T}{T_\infty}\left(\frac{\partial^2 T}{\partial X^2}+\frac{\partial^2 T}{\partial Y^2}\right),\tag{3.5}$$

$$U\frac{\partial C}{\partial X}+V\frac{\partial C}{\partial Y}=D_S\left(\frac{\partial^2 C}{\partial X^2}+\frac{\partial^2 C}{\partial Y^2}\right)+D_{CT}\left(\frac{\partial^2 T}{\partial X^2}+\frac{\partial^2 T}{\partial Y^2}\right),\tag{3.6}$$

$$U\frac{\partial M}{\partial X}+V\frac{\partial M}{\partial Y}+\frac{\partial}{\partial X}\left(M\widetilde{V}\right)+\frac{\partial}{\partial Y}\left(M\widetilde{V}\right)=D_n\left(\frac{\partial^2 M}{\partial X^2}+\frac{\partial^2 M}{\partial Y^2}\right),\tag{3.7}$$

where K_e is the mean absorption coefficient, σ_2 is the Stefan Boltzman constant. The average swimming velocity vector of microorganism is $\widetilde{V}=\dfrac{q_n D_B b_c w_c}{q_{np} D_n M_\infty}\dfrac{\partial\Phi}{\partial Y}$, All other quantities are defined in Chapter 2.

The corresponding boundary conditions are :

$$\left.\begin{aligned} &U=V=0,\ q_w=-k(\hat{n}.\nabla T),\ q_{np}=-D_B(\hat{n}.\nabla\Phi),\ q_m=-D_S(\hat{n}.\nabla C),\\ &\qquad\qquad q_n=-D_n(\hat{n}.\nabla M)\quad \text{at } Y=Y_w=\sigma(X).\\ &U\to 0,\ T\to T_\infty,\ \Phi\to\Phi_\infty,\ C\to C_\infty,\ M\to M_\infty \text{ as } Y\to\infty\ . \end{aligned}\right\}\tag{3.8}$$

where $\hat{n}$ is the unit normal to the wavy surface. The irregular wavy surface is transformed to a flat surface, by the following transformations ([131])

$$\left.\begin{aligned} &\xi=\frac{X}{L},\quad \eta=\frac{Y-\sigma}{L\xi^{\frac{1}{5}}}Gr^{\frac{1}{5}},\quad \psi=\frac{\mu Gr^{\frac{2}{5}}\xi^{\frac{4}{5}}}{\rho_{f\infty}}f(\xi,\eta),\quad p=\frac{L^2}{\rho_{f\infty}\nu^2}Gr^{-\frac{4}{5}}P,\\ &T-T_\infty=\frac{q_w L}{k}Gr^{-1/5}\xi^{1/5}\theta(\xi,\eta),\quad \Phi-\Phi_\infty=\frac{q_{np}L}{D_B}Gr^{-1/5}\xi^{1/5}\phi(\xi,\eta),\\ &C-C_\infty=\frac{q_m L}{D_S}Gr^{-1/5}\xi^{1/5}\varphi(\xi,\eta),\quad M-M_\infty=\frac{q_n L}{D_n}Gr^{-1/5}\xi^{1/5}\chi(\xi,\eta). \end{aligned}\right\}\tag{3.9}$$

where $Gr=\dfrac{(1-\Phi_\infty)\,g\beta_T q_w L^4}{k\nu^2}$ is the Grashof number and ψ is the stream function given in

2.10.

Substituting Eq. (3.9) into the Eqs. (3.2) to (3.8), we get

$$\left(1+\sigma_\xi^2\right) f''' + \frac{4}{5} f f'' - \left[\frac{3}{5} + \frac{\xi\sigma_\xi\sigma_{\xi\xi}}{1+\sigma_\xi^2}\right](f')^2 + \frac{(\theta + N_c\varphi - N_r\phi - R_b\chi)}{(1+{\sigma_\xi}^2)}(\sin A + \sigma_\xi \cos A) = \xi\left[f'\frac{\partial f'}{\partial \xi} - \frac{\partial f}{\partial \xi} f''\right] \tag{3.10}$$

$$\frac{\left(1+\sigma_\xi^2\right)}{\Pr}\left[\theta'' + N_b\xi^{\frac{1}{5}}\phi'\theta' + N_t\xi^{\frac{1}{5}}(\theta')^2 + N_d\varphi'' + \frac{4R_d\Pr}{3}\theta''\right] + \frac{1}{5}(4f\theta' - f'\theta) = \xi\left[f'\frac{\partial\theta}{\partial\xi} - \theta'\frac{\partial f}{\partial\xi}\right], \tag{3.11}$$

$$\frac{\left(1+\sigma_\xi^2\right)}{Le}\left[\phi'' + \frac{N_t}{N_b}\theta''\right] + \frac{1}{5}(4f\phi' - f'\phi) = \xi\left[f'\frac{\partial\phi}{\partial\xi} - \phi'\frac{\partial f}{\partial\xi}\right], \tag{3.12}$$

$$\frac{\left(1+\sigma_\xi^2\right)}{Ln}\left[\varphi'' + S_r\theta''\right] + \frac{1}{5}(4f\varphi' - f'\varphi) = \xi\left[f'\frac{\partial\varphi}{\partial\xi} - \varphi'\frac{\partial f}{\partial\xi}\right], \tag{3.13}$$

$$\frac{\left(1+\sigma_\xi^2\right)}{Sc}\chi'' - \frac{Pe}{Sc}(1-\sigma_\xi)\phi'' + \frac{1}{5}(4f\chi' - f'\chi) = \xi\left[f'\frac{\partial\chi}{\partial\xi} - \chi'\frac{\partial f}{\partial\xi}\right], \tag{3.14}$$

and

$$\left.\begin{aligned} &f'(\xi,\eta) = 0, \quad f(\xi,\eta) = -\frac{5}{4}\xi\frac{\partial f}{\partial\xi}, \quad \theta'(\xi,\eta) = -\frac{1}{\sqrt{1+\sigma_\xi^2}}, \\ &\phi'(\xi,\eta) = -\frac{1}{\sqrt{1+\sigma_\xi^2}}, \ \varphi'(\xi,\eta) = -\frac{1}{\sqrt{1+\sigma_\xi^2}}, \ \chi'(\xi,\eta) = -\frac{1}{\sqrt{1+\sigma_\xi^2}} \text{ at } \eta = 0. \\ &f'(\xi,\eta) = \theta(\xi,\eta) = \phi(\xi,\eta) = \varphi(\xi,\eta) = \chi(\xi,\eta) = 0 \text{ as } \eta\to\infty. \end{aligned}\right\} \tag{3.15}$$

The parameters Brownian motion parameter N_b, regular double diffusive buoyancy ratio N_c, modified Dufour number N_d, nanofluid buoyancy ratio N_r, thermophoresis parameter N_t, bioconvection Rayleigh number R_b, Soret number S_r and radiation parameter R_d are defined by

$$\left.\begin{aligned} &N_b = \frac{\gamma q_{np}}{\alpha_m}, \quad R_b = \frac{\gamma(\rho_m - \rho_{f\infty})q_n k}{(1-\Phi_\infty)\beta_T\rho_{f\infty}q_w D_n}, \quad N_c = \frac{\beta_C}{\beta_T}\frac{q_m k}{q_w D_S}, \\ &N_d = \frac{D_{TC}q_m k}{D_S q_w \alpha_m}, \quad N_r = \frac{(\rho_p - \rho_{f\infty})q_{np}k}{(1-\Phi_\infty)\beta_T\rho_{f\infty}q_w D_B}, \quad N_t = \frac{\gamma D_T q_w}{\alpha_m T_\infty k}, \\ &S_r = \frac{D_{CT}q_w}{k q_m}, \quad R_d = \frac{4\sigma_2 T_\infty^3}{K_e\alpha_m}. \end{aligned}\right\} \tag{3.16}$$

The remaining parameters are already defined in Chapter 2.

The heat, mass, nanoparticle mass flux and motile microorganism density flux can be obtained from

$$q_w = -k_m(\hat{n}\cdot\nabla T), \quad q_m = -D_S(\hat{n}\cdot\nabla C),$$
$$q_{np} = -D_B(\hat{n}\cdot\nabla\phi), \quad q_n = -D_n(\hat{n}\cdot\nabla M).$$

The non dimensional Nusselt number Nu_ξ, Sherwood number Sh_ξ, nanoparticle Sherwood number NSh_ξ and motile microorganism density number Q_ξ are given by :

$$\frac{Nu_\xi}{Gr_\xi^{1/5}} = \frac{1}{\theta(\xi,0)}, \qquad \frac{Sh_\xi}{Gr_\xi^{1/5}} = \frac{1}{\varphi(\xi,0)},$$
$$\frac{NSh_\xi}{Gr_\xi^{1/5}} = \frac{1}{\phi(\xi,0)}, \qquad \frac{Q_\xi}{Gr_\xi^{1/5}} = \frac{1}{\chi(\xi,0)}\ . \tag{3.17}$$

3.3 Method of Solution

The system of differential equations (3.10) - (3.14) along with the boundary conditions (3.15) are solved using the bivariate pseudo-spectral local linearisation method (BPSLLM) [67, 82].

On applying the procedure explained in Chapter 2 to the equations (3.10) - (3.14), we get the following system of linear differential equations.

$$a_{1,m}f'''_{m+1} + a_{2,m}f''_{m+1} + a_{3,m}f'_{m+1} + a_{4,m}f_{m+1} + a_{5,m}\frac{\partial f'_{m+1}}{\partial\xi} + a_{6,m}\frac{\partial f_{m+1}}{\partial\xi} = R_{1,m}, \tag{3.18}$$

$$b_{1,m}\theta''_{m+1} + b_{2,m}\theta'_{m+1} + b_{3,m}\theta_{m+1} + b_{4,m}\frac{\partial\theta_{m+1}}{\partial\xi} = R_{2,m}, \tag{3.19}$$

$$c_{1,m}\phi''_{m+1} + c_{2,m}\phi'_{m+1} + c_{m,r}\phi_{m+1} + c_{4,m}\frac{\partial\phi_{m+1}}{\partial\xi} = R_{3,m}, \tag{3.20}$$

$$d_{1,m}\varphi''_{m+1} + d_{2,m}\varphi'_{m+1} + d_{3,m}\varphi_{m+1} + d_{4,m}\frac{\partial\varphi_{m+1}}{\partial\xi} = R_{4,m}, \tag{3.21}$$

$$e_{1,m}\chi''_{m+1} + e_{2,m}\chi'_{m+1} + e_{3,m}\chi_{m+1} + e_{4,m}\frac{\partial\chi_{m+1}}{\partial\xi} = R_{5,m}. \tag{3.22}$$

The coefficients are :

$$a_{1,m} = 1+\sigma_\xi^2, \quad a_{2,m} = \frac{4}{5}f_m + \xi\frac{\partial f_m}{\partial\xi}, \quad a_{3,m} = -\left[\frac{3}{5} + \frac{\xi\sigma_\xi\sigma_{\xi\xi}}{1+\sigma_\xi^2}\right]2f'_m - \xi\frac{\partial f'_m}{\partial\xi},$$

$$a_{4,m} = \frac{4}{5} f''_m, \quad a_{5,m} = -\xi f'_m, \quad a_{6,m} = \xi f''_m,$$

$$R_{1,m} = \xi f''_m \frac{\partial f_m}{\partial \xi} - \xi f'_m \frac{\partial f'_m}{\partial \xi} - \left[\frac{3}{5} + \frac{\xi \sigma_\xi \sigma_{\xi\xi}}{1+\sigma_\xi^2}\right] (f'_m)^2 + \frac{4}{5} f_m f''_m \\ \frac{(\theta_m + N_c\, \varphi_m - N_r \phi_m - R_b \chi_m)}{(1+{\sigma_\xi}^2)} \left(\sin A + \sigma_\xi \cos A\right),$$

$$b_{1,m} = \left(1+{\sigma_\xi}^2\right)\left(\frac{1}{\mathrm{Pr}} + \frac{4R_d}{3}\right),$$

$$b_{2,m} = \frac{1+\sigma_\xi^2}{\mathrm{Pr}} \xi^{1/5} N_b \phi'_m + \frac{1+\sigma_\xi^2}{\mathrm{Pr}} 2 N_t \xi^{1/5} \theta'_m + \frac{4}{5} f_{m+1} + \xi \frac{\partial f_{m+1}}{\partial \xi},$$

$$b_{3,m} = -\frac{1}{5} f'_{m+1}, \quad b_{4,m} = -\xi f'_{m+1}, \quad R_{2,m} = \frac{1+\sigma_\xi^2}{\mathrm{Pr}} \left[\xi^{1/5} N_t {\theta'_m}^2 - N_d \varphi''_m\right],$$

$$c_{1,m} = \frac{1+\sigma_\xi^2}{Le}, \quad c_{2,m} = \frac{4}{5} f_{m+1} + \xi \frac{\partial f_{m+1}}{\partial \xi}, \quad c_{3,m} = -\frac{1}{5} f'_{m+1}, \quad c_{4,m} = -\xi f'_{m+1},$$

$$R_{3,m} = -\frac{1+\sigma_\xi^2}{Le} \frac{N_t}{N_b} \theta''_{m+1}, \quad d_{1,m} = \frac{1+\sigma_\xi^2}{Ln}, \quad d_{2,m} = \frac{4}{5} f_{m+1} + \xi \frac{\partial f_{m+1}}{\partial \xi},$$

$$d_{3,m} = -\frac{1}{5} f'_{m+1}, \quad d_{4,m} = -\xi f'_{m+1}, \quad R_{4,m} = -\left(1+{\sigma_\xi}^2\right) \frac{S_r}{Ln} \theta''_{m+1},$$

$$e_{1,m} = \frac{1+\sigma_\xi^2}{Sc}, \quad e_{2,m} = \frac{4}{5} f_{m+1} + \xi \frac{\partial f_{m+1}}{\partial \xi}, \quad e_{3,m} = -\frac{1}{5} f'_{m+1},$$

$$e_{4,m} = -\xi f'_{m+1}, \quad R_{5,m} = (1-\sigma_\xi) \frac{Pe}{Sc} \phi''_{m+1}.$$

The corresponding boundary conditions are :

$$\left.\begin{aligned} & f'_{m+1}(\xi,0) = 0\,, \quad f_{m+1}(\xi,0) = -\frac{5}{4} \xi \frac{\partial f}{\partial \xi}, \\ & \theta'_{m+1}(\xi,0) = \phi'_{m+1}(\xi,0) = \varphi'_{m+1}(\xi,0) = \chi'_{m+1}(\xi,0) = -\frac{1}{\sqrt{1+\sigma_\xi^2}}, \\ & f'_{m+1}(\xi,\infty) = \theta_{m+1}(\xi,\infty) = \phi_{m+1}(\xi,\infty) = \varphi_{m+1}(\xi,\infty) = \chi_{m+1}(\xi,\infty) = 0. \end{aligned}\right\} \quad (3.23)$$

As explained in Chapter 2, applying Chebyshev pseudo spectral method in both ξ and η directions on the system of linearized equations (3.18) to (3.22), we get

$$A^{(1)}\mathbf{F}_i + \gamma_{5,i}^{(1)} \sum_{j=0}^{M} \mathbf{d}_{i,j}\mathbf{D}\mathbf{F}_j + \gamma_{6,i}^{(1)} \sum_{j=0}^{M} \mathbf{d}_{i,j}\mathbf{F}_j = \mathbf{R}_{1,i}, \tag{3.24}$$

$$A^{(2)}\mathbf{\Theta}_i + \gamma_{4,i}^{(2)} \sum_{j=0}^{M} \mathbf{d}_{i,j}\mathbf{\Theta}_j = \mathbf{R}_{2,i}, \tag{3.25}$$

$$A^{(3)}\mathbf{\Phi}_i + \gamma_{4,i}^{(3)} \sum_{j=0}^{M} \mathbf{d}_{i,j}\mathbf{\Phi}_j = \mathbf{R}_{3,i}, \tag{3.26}$$

$$A^{(4)}\varphi_i + \gamma_{4,i}^{(4)} \sum_{j=0}^{M} \mathbf{d}_{i,j}\varphi_j = \mathbf{R}_{4,i}, \tag{3.27}$$

$$A^{(5)}\chi_i + \gamma_{4,i}^{(5)} \sum_{j=0}^{M} \mathbf{d}_{i,j}\chi_j = \mathbf{R}_{5,i}, \tag{3.28}$$

where

$$\begin{aligned}
A^{(1)} &= \gamma_{1,i}^{(1)}\mathbf{D}^3 + \gamma_{2,i}^{(1)}\mathbf{D}^2 + \gamma_{3,i}^{(1)}\mathbf{D} + \gamma_{4,i}^{(1)}\mathbf{I} \\
A^{(2)} &= \gamma_{1,i}^{(2)}\mathbf{D}^2 + \gamma_{2,i}^{(2)}\mathbf{D} + \gamma_{3,i}^{(2)}\mathbf{I} \\
A^{(3)} &= \gamma_{1,i}^{(3)}\mathbf{D}^2 + \gamma_{2,i}^{(3)}\mathbf{D} + \gamma_{3,i}^{(3)}\mathbf{I} \\
A^{(4)} &= \gamma_{1,i}^{(4)}\mathbf{D}^2 + \gamma_{2,i}^{(4)}\mathbf{D} + \gamma_{3,i}^{(4)}\mathbf{I} \\
A^{(5)} &= \gamma_{1,i}^{(5)}\mathbf{D}^2 + \gamma_{2,i}^{(5)}\mathbf{D} + \gamma_{3,i}^{(5)}\mathbf{I}\,.
\end{aligned}$$

Here $\gamma_{k,i}^{(1)}$, $\gamma_{k,i}^{(2)}$, $\gamma_{k,i}^{(3)}$, $\gamma_{k,i}^{(4)}$, $\gamma_{k,i}^{(5)}$ and $\mathbf{R}_{k,i}$ are N^{th} order diagonal matrices with diagonal elements as, $a_{k,m}(\zeta_r, \tau_i)$, $b_{k,m}(\zeta_r, \tau_i)$, $c_{k,m}(\zeta_r, \tau_i)$, $d_{k,m}(\zeta_r, \tau_i)$, $e_{k,m}(\zeta_r, \tau_i)$ and $R_{k,m}(\zeta_r, \tau_i)$ for $r = 1, 2, 3, \cdots N$ respectively and $\mathbf{I}$ refers the identity matrix.

The matrix form of equation (3.24) can be written as :

$$\begin{bmatrix}
A_{0,0}^{(1)} & A_{0,1}^{(1)} & A_{0,2}^{(1)} & \cdots & A_{0,M}^{(1)} \\
A_{1,0}^{(1)} & A_{1,1}^{(1)} & A_{1,2}^{(1)} & \cdots & A_{1,M}^{(1)} \\
A_{2,0}^{(1)} & A_{2,1}^{(1)} & A_{2,2}^{(1)} & \cdots & A_{2,M}^{(1)} \\
\vdots & \vdots & \vdots & \ddots & \vdots \\
A_{M,0}^{(1)} & A_{M,1}^{(1)} & A_{M,2}^{(1)} & \cdots & A_{M,M}^{(1)}
\end{bmatrix}
\begin{bmatrix}
\mathbf{F}_0 \\ \mathbf{F}_1 \\ \mathbf{F}_2 \\ \vdots \\ \mathbf{F}_M
\end{bmatrix}
=
\begin{bmatrix}
\mathbf{R}_{1,0} \\ \mathbf{R}_{1,1} \\ \mathbf{R}_{1,2} \\ \vdots \\ \mathbf{R}_{1,M}
\end{bmatrix}, \tag{3.29}$$

where

$$A^{(1)}_{i,j} = A^{(1)} + \gamma^{(1)}_{5,i}\mathbf{d}_{i,i}\mathbf{D} + \gamma^{(1)}_{6,i}\mathbf{d}_{i,i}\mathbf{I}, \quad for \quad i = j;$$
$$A^{(1)}_{i,j} = \gamma^{(1)}_{5,i}\mathbf{d}_{i,j}\mathbf{D} + \gamma^{(1)}_{6,i}\mathbf{d}_{i,j}\mathbf{I}, \quad for \quad i \neq j \ . \tag{3.30}$$

In a similar manner, we can write the matrix form of the equations (3.25) to (3.28). Solving these matrix equations, we obtain the approximate solutions by choosing appropriate initial approximation.

3.4 Computational Results and Discussion

The bivariate pseudo-spectral local linearisation method (BPSLLM) is used to solve the equations (3.10) - (3.14) along with the boundary conditions (3.15). As in the previous chapter, to check the grid independence, the code developed in MATLAB is executed for heat and mass transfer rates by changing the number of collocation points N and M in both η and ξ directions i.e. by taking $N = 20, 40, 50, 60, 80$ and $M = 20, 40, 50, 60, 80$. In each case, we found a very good agreement between them. The same tendency is witnessed by changing the values of the parameters. Hence, a grid size of 50×50 is adopted to be satisfactory for the convergence criterion of 10^{-6}.

The double diffusive convection of a Nanofluid past an inclined wavy surface is governed by several parameters A, α, Pe, Ln, Sc, N_b, N_c, N_d, N_r, N_t, R_b, S_r and Rd. The values of the other parameters are fixed as $Pr = 2$, $Le = 5$, $Ln = 5$, $N_b = 0.5$, $N_r = 0.3$ and $N_t = 0.1$. The choice of values for N_r, N_t and N_b is based on those values utilized by Nield and Kuznetsov [88] for the case with the isothermal wall boundary condition and the other values are in the limit of physical requirements of the problem model. Further, the effect of governing parameters on the non-dimensional velocity components, temperature, concentration, nanoparticle volume fraction, and motile microorganisms are not presented for the sake of brevity.

The variation of rate of heat transfer, mass transfer, nanoparticle mass transfer, and motile microorganisms transfer with radiation parameter R_d is depicted in Fig.3.1. It is found from the figure 3.1(a) that, the heat transfer rate is decreasing as R_d is increasing. The radiative energy is proportional to the fourth power of absolute temperature and inversely proportional to emissivity on the surface. Hence, R_d modifies the temperature even for quite small values of emissivity. The surface roughness causes weaker temperature gradients

and reduces the extent of the temperature gradients. The mass transfer, nanoparticle mass transfer, and density number of motile microorganisms are increasing with an increase in the radiation parameter.

Figure 3.2 provides the influence of the angle of inclination A on the local Nusselt number, local Sherwood number, nanoparticle Sherwood number, and density number of motile microorganisms. It is clear from this figure that the rate of transfer of heat, mass, nanoparticle mass and motile microorganisms mass across the boundary are increasing with an increase in inclination angle. Hence, the transfer rate of all the physical quantities is more for the vertical surface compared to the horizontal surface.

The influence of amplitude of the wavy surface α on heat transfer rate, mass transfer rate, nanoparticle mass transfer rate, and density number of motile microorganisms is presented in Fig.3.3. It is seen from Figs.3.3(a) to 3.3(d) that the heat transfer rate, mass transfer rate, nanoparticle mass transfer are increasing first and then decreasing as there is an increment in amplitude over one period. This change is observed periodically over ξ. It is interesting to note that the rate of motile microorganisms is decreasing first and then increasing with an increase in the amplitude of the wavy surface as depicted in Fig. 3.3(d).

Figure 3.4 shows the effect of bioconvection Peclet number Pe on $Nu_\xi/Gr_\xi^{1/5}$, $Sh_\xi/Gr_\xi^{1/5}$, $NSh_\xi/Gr_\xi^{1/5}$, and $Q_\xi/Gr_\xi^{1/5}$. It is noticed that an increase in the bioconvection Peclet number causes a rise in the local Nusselt number, local Sherwood number, nanoparticle Sherwood number, and density number of motile microorganisms. Enhancing the bioconvection Peclet number results in an increase of movement of microorganisms along with the concentration of gradients as the bioconvection Peclet number assists to enhance the speed of the microorganisms in the fluid. Hence, an increase of Pe, i.e., an increase of particles movements causes the rise of all the dimensionless physical quantities under consideration.

The impact of bioconvection Rayleigh number R_b in the profiles of local Nusselt number, local Sherwood number, nanoparticle Sherwood number and density number of motile microorganisms is depicted in Fig.3.5. It is noticed that the enhancement of bioconvection Rayleigh number results in a reduction in the local heat transfer rate, mass transfer rate, nanoparticle mass transfer rate, and density of motile microorganisms. The reason for this is the movement of the nanoparticles present in the base fluid. These nanoparticles move arbitrarily in the fluid and eventually the temperature of the fluid increases. Due to this heat transport at the surface reduces

Figure 3.6 presents the effect of bioconvection Schmidt number Sc on $Nu_\xi/Gr_\xi^{1/5}$, $Sh_\xi/Gr_\xi^{1/5}$, $NSh_\xi/Gr_\xi^{1/5}$, and $Q_\xi/Gr_\xi^{1/5}$. It is observed from figures 3.6(a) - 3.6(d) that all the dimen-

sionless physical quantities are increasing with a rise in the bioconvection Schmidt number.

The variation of local Nusselt number, local Sherwood number, nanoparticle Sherwood number, and density number of motile microorganisms for different values of double-diffusive buoyancy ratio N_c is displayed in Fig.3.7. This figure reveals that an increase in the double-diffusive buoyancy ratio increases local heat transfer rate, mass transfer rate, nanoparticle mass transfer rate, and motile microorganisms density rate.

The effect of modified Dufour number N_d on the $Nu_\xi/Gr_\xi^{1/5}$, $Sh_\xi/Gr_\xi^{1/5}$, $NSh_\xi/Gr_\xi^{1/5}$, and $Q_\xi/Gr_\xi^{1/5}$ is depicted in Fig. 3.8. It is seen from Fig.3.8(a) that, the local heat transfer rate is decreasing with an increase in the values of N_d. The local mass transfer rate, nanoparticle mass transfer rate, and motile microorganisms rate are increasing with an increase in modified Dufour number as depicted in Fig. 3.8(b) - 3.8(d). The Dufour number signifies the influence of the solutal gradients on the thermal energy flux in the flow. Hence, an enhance in the Dufour number results in an increase in the temperature and a drop in the concentration.

The influence of Soret number S_r on the local heat transfer rate, mass transfer rate, nanoparticle mass transfer rate, and density number of motile microorganisms is portrayed in Fig. 3.9. It is found in Figs. 3.9(c) and 3.9(d) that, the nanoparticle mass transfer and density number of motile microorganisms are increasing with an increase in Soret number. The effect of the Soret number on the heat transfer rate is very less. A slight increase in heat transfer rate at the beginning and then minor decrease as ξ increases is noticed for increasing values of the Soret number as shown in the enlarged part of the Fig. 3.9(a). The mass transfer rate decreases in the beginning and changes its behaviour as ξ increases with an increase in Soret number as depicted in 3.9(b). Soret number is the ratio of a temperature difference to the concentration. Hence, the increase in the Soret number stands for an increase in the temperature difference and precipitous gradient.

3.5 Conclusions

In the present chapter, a theoretical analysis is made on the effect of thermal radiation on free convection double diffusion of a nanofluid past an inclined wavy surface in the presence of gyrotactic microorganisms. The nonlinear governing equations along with the boundary conditions are solved using a Bivariate pseudo-spectral local linearization method together with the Chebyshev collocation method. Important observations are itemized below:

- Increase in Pe, A, N_c, Sc results in increase of heat transfer rate.
- The mass transfer rate and nanoparticle mass transfer rate either increase or decrease simultaneously for all parameters except for Le, Ln, and S_r.
- The influence of α on heat transfer rate, mass transfer rate, nanoparticle mass transfer rate, and density of motile organisms is both increasing and decreasing.
- The density of motile microorganism falls for a raise in R_d, Sr, A, Pe.

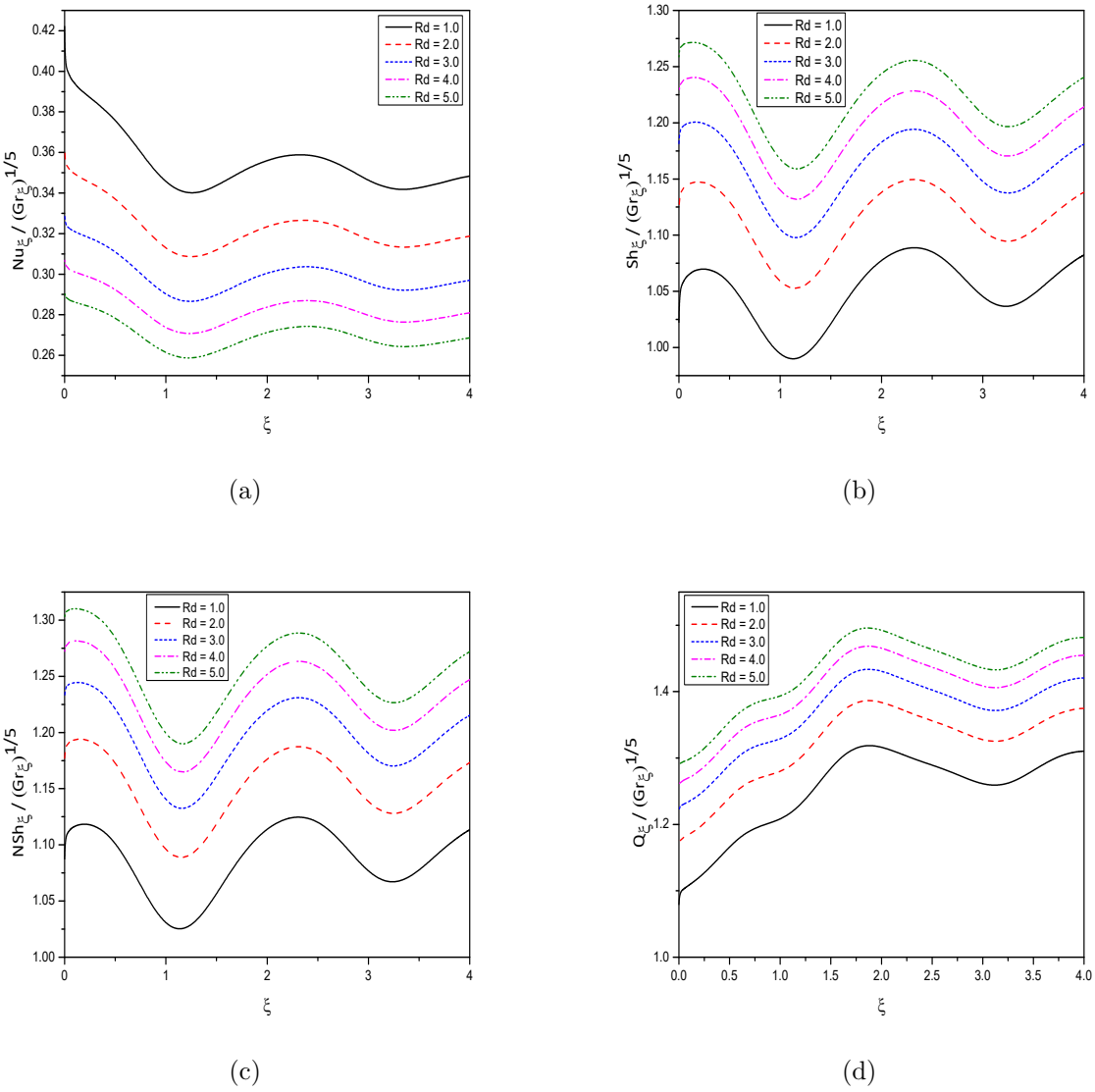

Figure 3.1: "Effect of the Radiation parameter R_d on the profiles of (a) $\frac{Nu_\xi}{Gr_\xi^{1/5}}$ (b) $\frac{Sh_\xi}{Gr_\xi^{1/5}}$ (c) $\frac{NSh_\xi}{Gr_\xi^{1/5}}$ (d) $\frac{Q_\xi}{Gr_\xi^{1/5}}$".

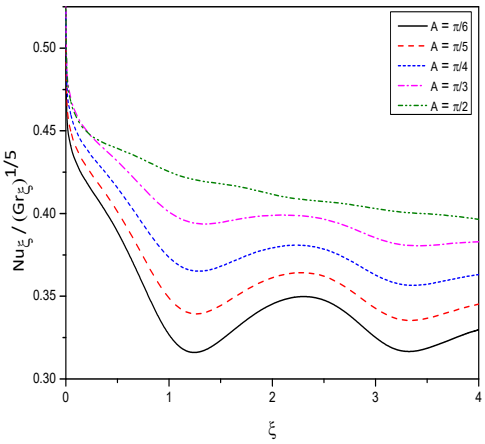

(a)

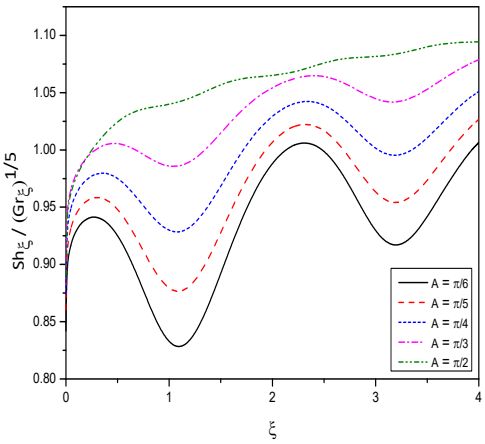

(b)

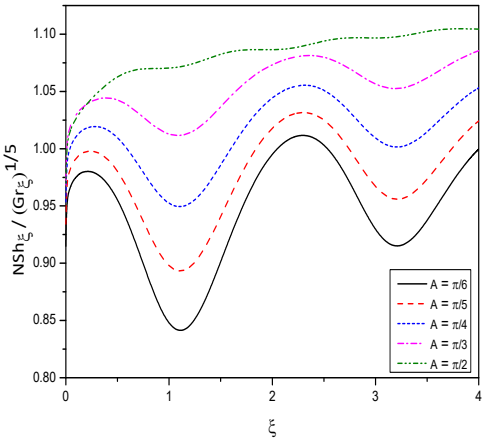

(c)

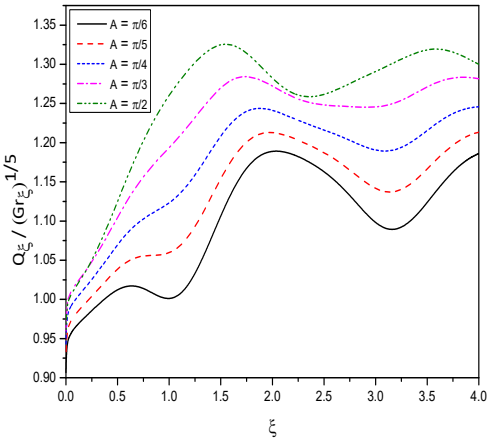

(d)

Figure 3.2: "Effect of the inclination angle A on the profiles of (a) $\frac{Nu_\xi}{Gr_\xi^{1/5}}$ (b) $\frac{Sh_\xi}{Gr_\xi^{1/5}}$ (c) $\frac{NSh_\xi}{Gr_\xi^{1/5}}$ (d) $\frac{Q_\xi}{Gr_\xi^{1/5}}$".

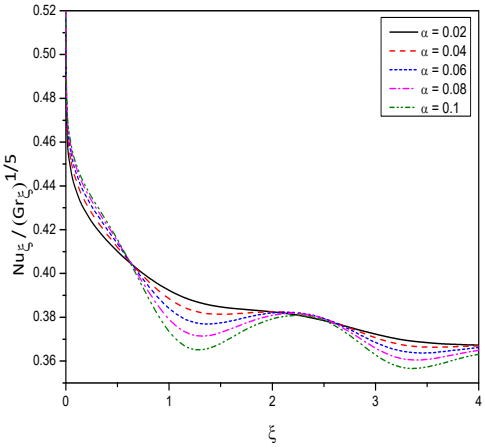

(a)

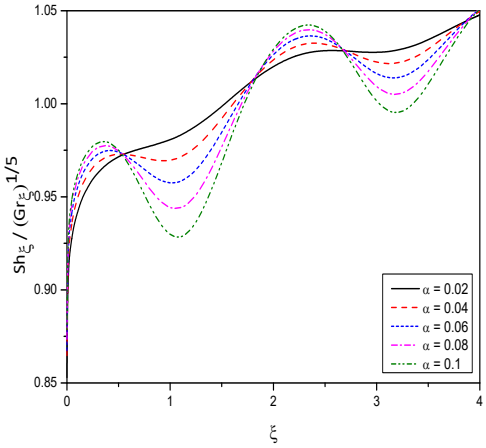

(b)

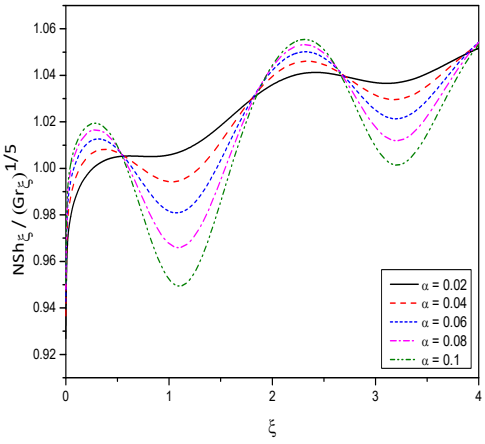

(c)

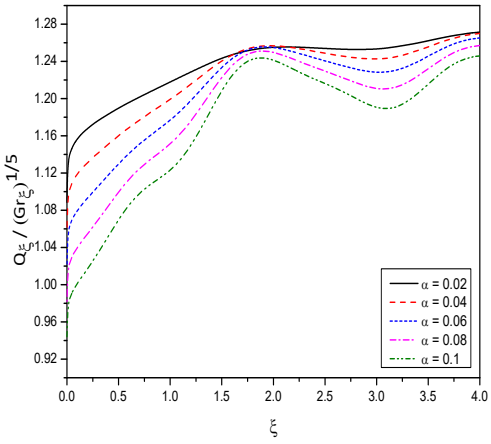

(d)

Figure 3.3: "Effect of the amplitude of the wavy surface α on the profiles of (a) $\frac{Nu_\xi}{Gr_\xi^{1/5}}$ (b) $\frac{Sh_\xi}{Gr_\xi^{1/5}}$ (c) $\frac{NSh_\xi}{Gr_\xi^{1/5}}$ (d) $\frac{Q_\xi}{Gr_\xi^{1/5}}$".

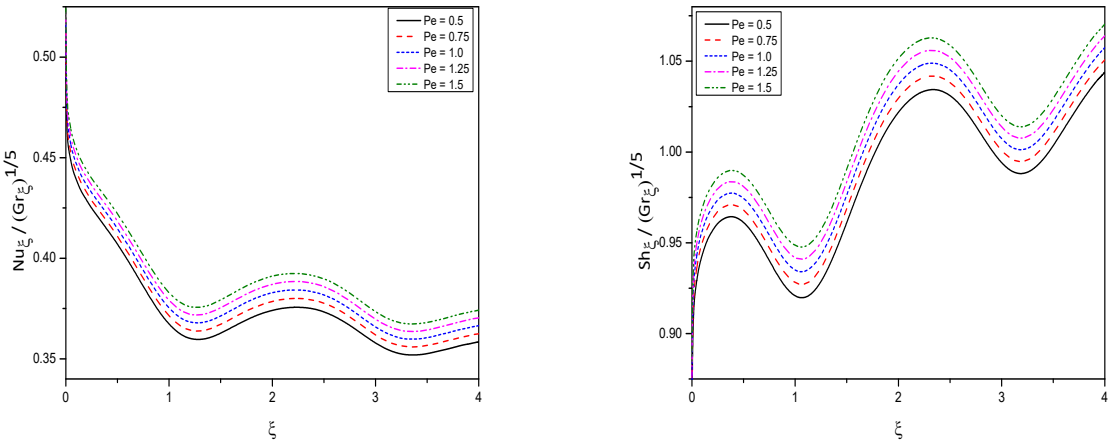

(a) (b)

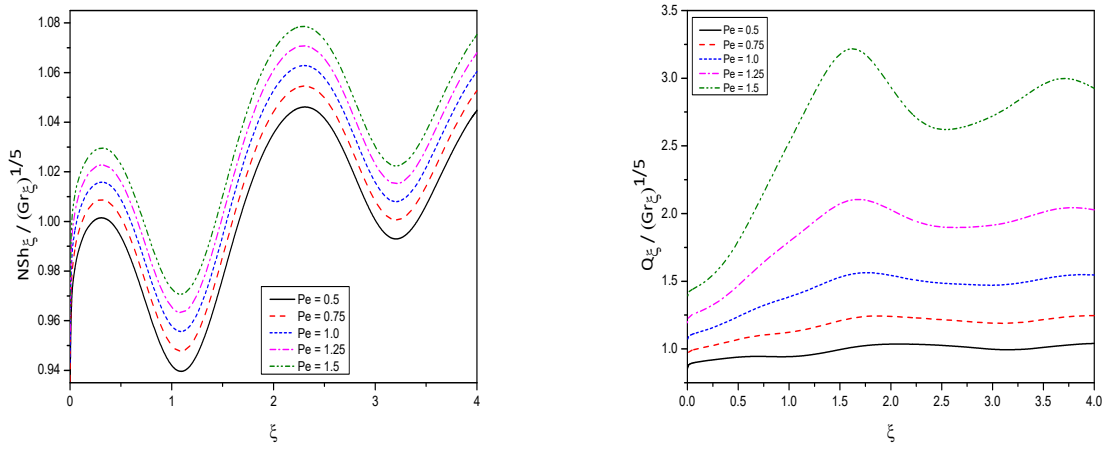

(c) (d)

Figure 3.4: "Effect of the bioconvection Peclet number Pe on the profiles of (a) $\frac{Nu_\xi}{Gr_\xi^{1/5}}$ (b) $\frac{Sh_\xi}{Gr_\xi^{1/5}}$ (c) $\frac{NSh_\xi}{Gr_\xi^{1/5}}$ (d) $\frac{Q_\xi}{Gr_\xi^{1/5}}$".

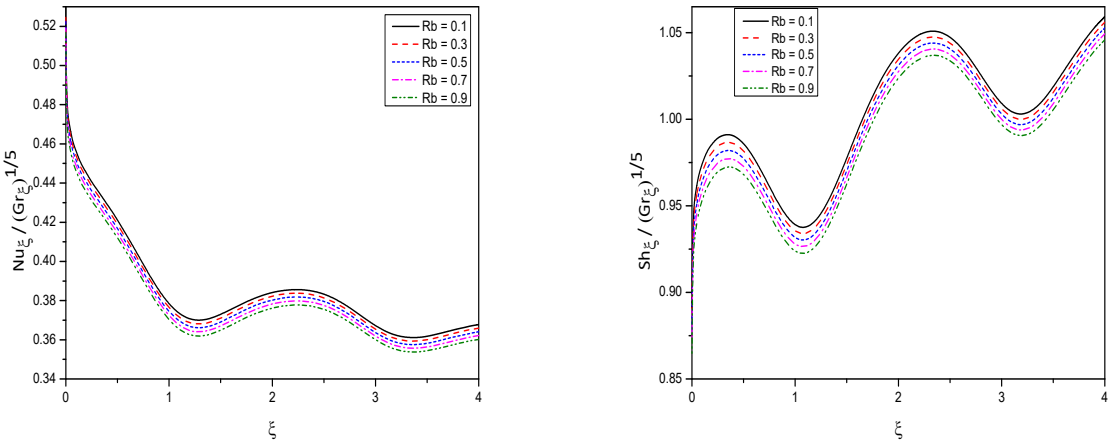

(a) (b)

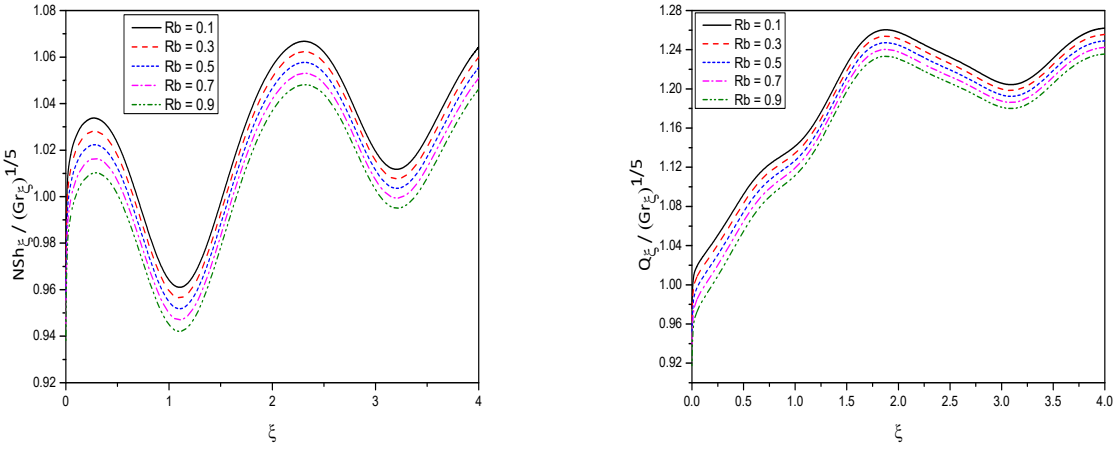

(c) (d)

Figure 3.5: "Effect of the bioconvection Rayleigh number R_b on the profiles of (a) $\frac{Nu_\xi}{Gr_\xi^{1/5}}$ (b) $\frac{Sh_\xi}{Gr_\xi^{1/5}}$ (c) $\frac{NSh_\xi}{Gr_\xi^{1/5}}$ (d) $\frac{Q_\xi}{Gr_\xi^{1/5}}$".

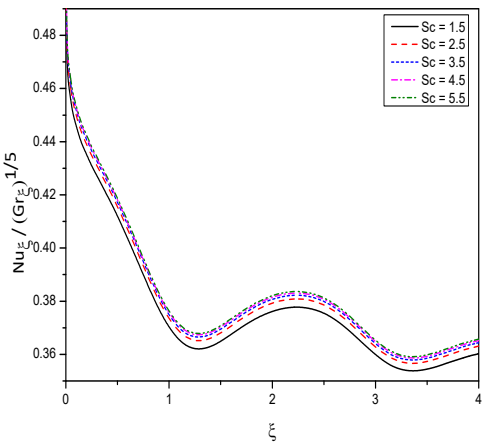

(a)

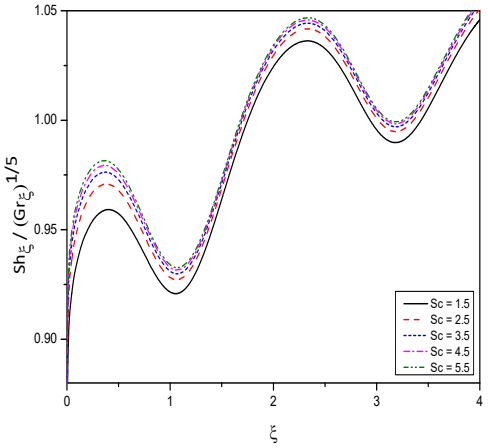

(b)

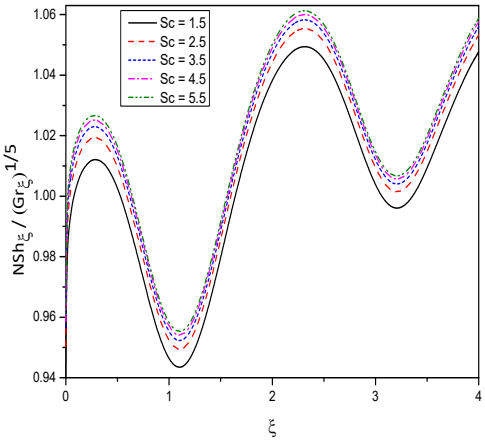

(c)

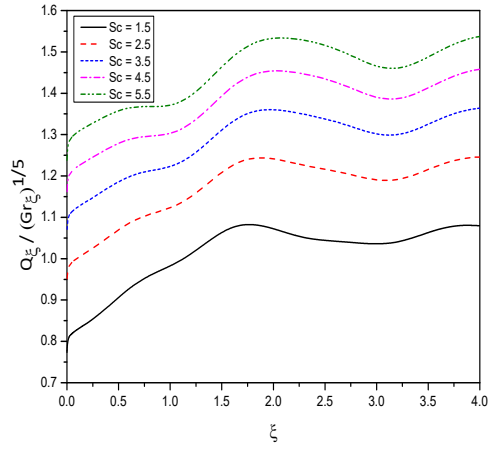

(d)

Figure 3.6: "Effect of the bioconvection Schmidt number Sc on the profiles of (a) $\frac{Nu_\xi}{Gr_\xi^{1/5}}$ (b) $\frac{Sh_\xi}{Gr_\xi^{1/5}}$ (c) $\frac{NSh_\xi}{Gr_\xi^{1/5}}$ (d) $\frac{Q_\xi}{Gr_\xi^{1/5}}$".

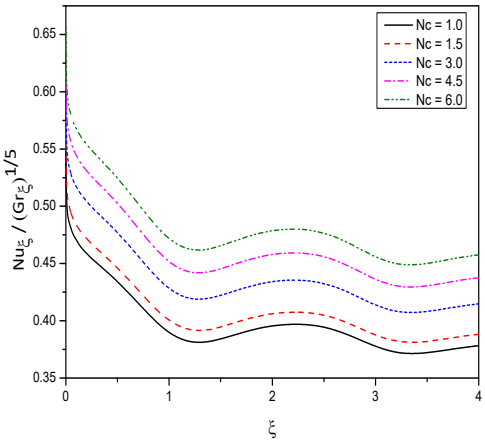

(a)

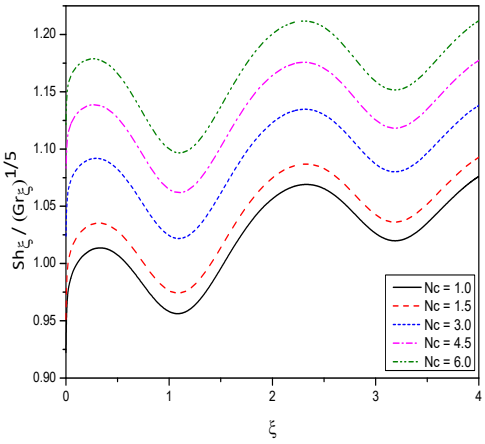

(b)

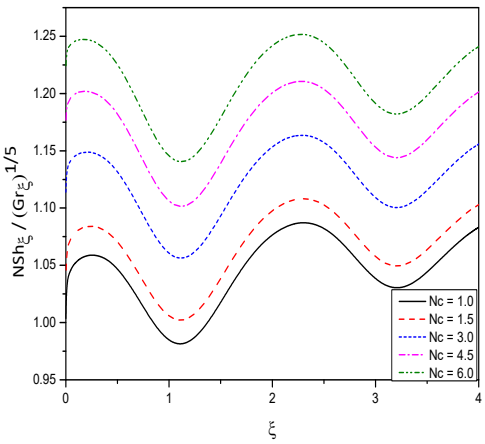

(c)

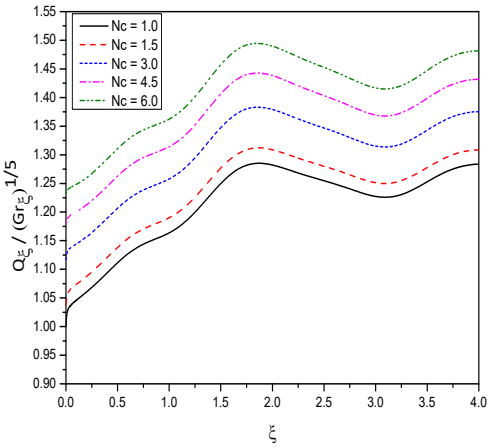

(d)

Figure 3.7: "Effect of the regular double diffusive buoyancy ratio N_c on the profiles of (a) $\frac{Nu_\xi}{Gr_\xi^{1/5}}$ (b) $\frac{Sh_\xi}{Gr_\xi^{1/5}}$ (c) $\frac{NSh_\xi}{Gr_\xi^{1/5}}$ (d) $\frac{Q_\xi}{Gr_\xi^{1/5}}$".

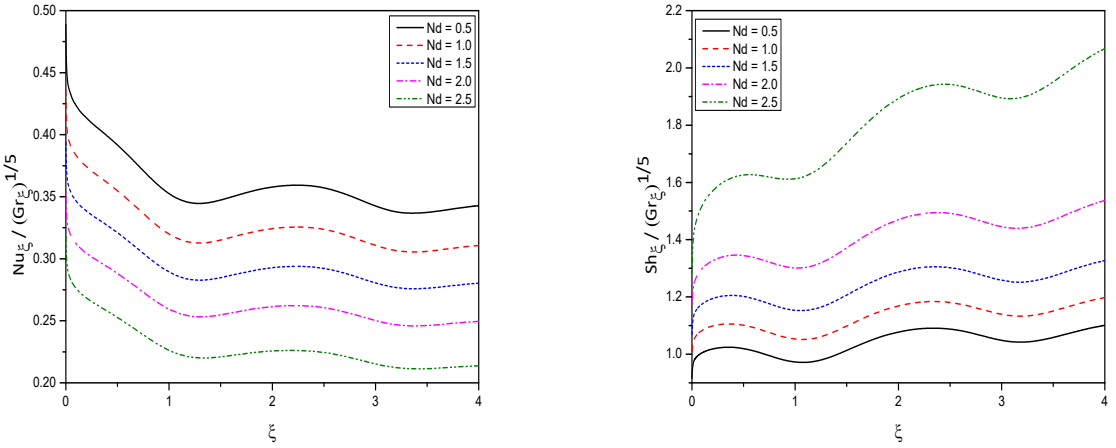

(a) (b)

(c) (d)

Figure 3.8: "Effect of the modified Dufour number N_d on the profiles of (a) $\frac{Nu_\xi}{Gr_\xi^{1/5}}$ (b) $\frac{Sh_\xi}{Gr_\xi^{1/5}}$ (c) $\frac{NSh_\xi}{Gr_\xi^{1/5}}$ (d) $\frac{Q_\xi}{Gr_\xi^{1/5}}$".

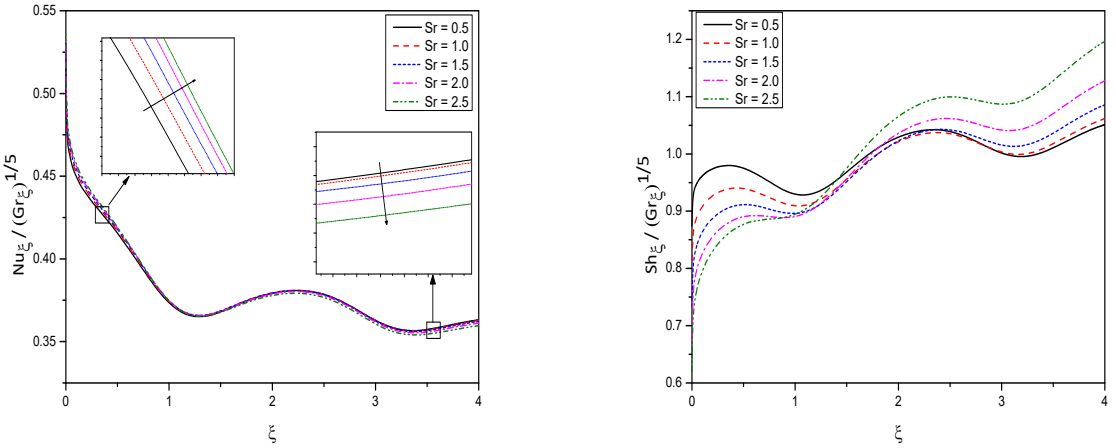

(a)

(b)

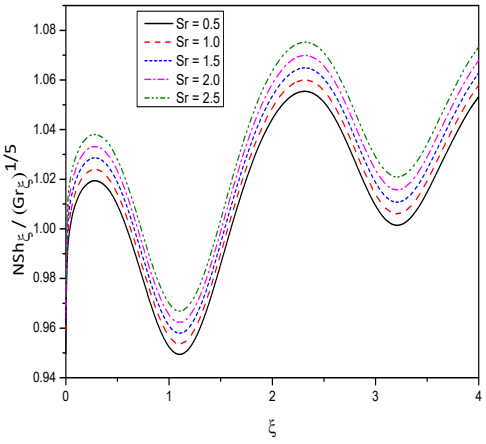

(c)

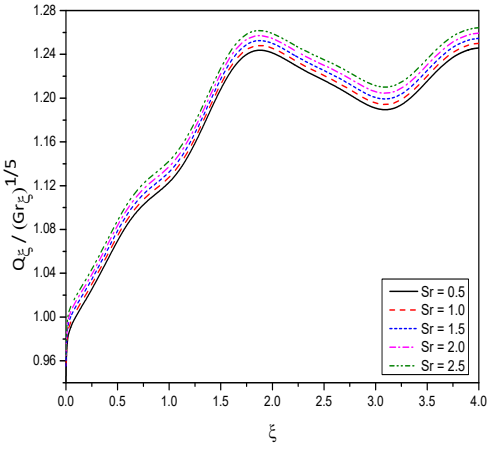

(d)

Figure 3.9: "Effect of the Soret number S_r on the profiles of (a) $\frac{Nu_\xi}{Gr_\xi^{1/5}}$ (b) $\frac{Sh_\xi}{Gr_\xi^{1/5}}$ (c) $\frac{NSh_\xi}{Gr_\xi^{1/5}}$ (d) $\frac{Q_\xi}{Gr_\xi^{1/5}}$".

Chapter 4

Mixed Bioconvection of a Nanofluid Past an Inclined Wavy Surface [1]

4.1 Introduction

The mixed convection over an inclined plate has been attracting researchers due to its industrial and technological applications like electroplating, ash or scrubber waste treatment, chemical processing of heavy metals, etc. Several investigators have analyzed the convective heat/mass along inclined surfaces Bhat [16] analyzed the stability of the flow of adulterated fluid over an inclined slip plane. Goyal and Bhargava [39] numerically studied the transient convective flow of a nanofluid over an inclined plate with a magnetic effect. Rafique *et al.* [95] scrutinized the effect of Soret and Dufour on a Casson nanofluid flow over an inclined elongating surface. Barik *et al.* [13] studied numerically the MHD characteristics of nanofluid past an inclined elongating sheet.

In this chapter, the mixed bioconvection of a nanofluid past an inclined wavy surface is considered. The solution for the governing equations is attained employing the bivariate pseudo-spectral local linearization method (BPSLLM). The effect of different fluid and geometry parameters on the rate of heat transfer, rate of nanoparticle mass transfer, and density number of the microorganism are evaluated and presented through graphs.

[1] Published in "**Heat Transfer"**, Early View, 2021, DOI: 10.1002htj.22291

4.2 Mathematical Formulation

Consider the steady and incompressible flow of a nanofluid containing motile microorganisms along a semi-infinite inclined wavy surface. The coordinate system and physical model are as depicted in Fig. 2.1. The flow is assumed to be mixed convective.

By implementing Oberbeck-Boussinesq approximation, the equations governing the flow are

$$\frac{\partial U}{\partial X}+\frac{\partial V}{\partial Y}=0 \tag{4.1}$$

$$\rho_{f\infty}\left(U\frac{\partial U}{\partial X}+V\frac{\partial U}{\partial Y}\right)=-\frac{\partial P}{\partial X}+\mu\left(\frac{\partial^2 U}{\partial X^2}+\frac{\partial^2 U}{\partial Y^2}\right)+[(1-\Phi_\infty)\beta_T\rho_{f\infty}(T-T_\infty) - (\rho_p-\rho_{f\infty})(\Phi-\Phi_\infty)-\beta_M(\rho_m-\rho_{f\infty})(M-M_\infty)]\,g\sin A \tag{4.2}$$

$$\rho_{f\infty}\left(U\frac{\partial V}{\partial X}+V\frac{\partial V}{\partial Y}\right)=-\frac{\partial P}{\partial Y}+\mu\left(\frac{\partial^2 V}{\partial X^2}+\frac{\partial^2 V}{\partial Y^2}\right)+[(1-\Phi_\infty)\beta_T\rho_{f\infty}(T-T_\infty) - (\rho_p-\rho_{f\infty})(\Phi-\Phi_\infty)-\beta_M(\rho_m-\rho_{f\infty})(M-M_\infty)]\,g\cos A \tag{4.3}$$

$$U\frac{\partial T}{\partial X}+V\frac{\partial T}{\partial Y}=\alpha_m\left(\frac{\partial^2 T}{\partial X^2}+\frac{\partial^2 T}{\partial Y^2}\right)+\gamma\left\{D_B\left(\frac{\partial\Phi}{\partial X}\frac{\partial T}{\partial X}+\frac{\partial\Phi}{\partial Y}\frac{\partial T}{\partial Y}\right) + \frac{D_T}{T_\infty}\left[\left(\frac{\partial T}{\partial X}\right)^2+\left(\frac{\partial T}{\partial Y}\right)^2\right]\right\} \tag{4.4}$$

$$U\frac{\partial\Phi}{\partial X}+V\frac{\partial\Phi}{\partial Y}=D_B\left(\frac{\partial^2\Phi}{\partial X^2}+\frac{\partial^2\Phi}{\partial Y^2}\right)+\frac{D_T}{T_\infty}\left(\frac{\partial^2 T}{\partial X^2}+\frac{\partial^2 T}{\partial Y^2}\right) \tag{4.5}$$

$$U\frac{\partial M}{\partial X}+V\frac{\partial M}{\partial Y}+\frac{\partial}{\partial X}\left(M\widetilde{V}\right)+\frac{\partial}{\partial Y}\left(M\widetilde{V}\right)=D_n\left(\frac{\partial^2 M}{\partial X^2}+\frac{\partial^2 M}{\partial Y^2}\right) \tag{4.6}$$

where The average swimming velocity vector of microbes is $\widetilde{V}=\dfrac{q_n D_B b_c w_c}{q_{np} D_n M_\infty}\dfrac{\partial\Phi}{\partial Y}$. All other quantities are defined in Chapter 2.

The conditions on the boundary are :

$$\left.\begin{array}{l} U=0,\ V=0,\ q_w=-k(\hat{n}.\nabla T),\ q_{np}=-D_B(\hat{n}.\nabla\Phi),\ q_n=-D_n(\hat{n}.\nabla M)\,\text{at}\,Y=\sigma(X) \\ U\to U_\infty,\ T\to T_\infty,\ \Phi\to\Phi_\infty,\ M\to M_\infty\ \text{as}\ Y\to\infty \end{array}\right\} \tag{4.7}$$

where $\hat{n}$ is the unit normal to the surface.

The following transformations are applied to convert the irregular wavy surface to a flat surface [131]

$$\left.\begin{aligned}
&\xi = \frac{X}{L}, \quad \eta = \frac{Y-\sigma}{L\xi^{\frac{1}{2}}}\sqrt{Re}, \quad f(\xi,\eta) = \frac{\psi\sqrt{Re}}{LU_\infty\sqrt{\xi}} \quad p = \frac{P}{\rho_{f\infty}U_\infty^2},\\
&T - T_\infty = \frac{q_w L}{k} Re^{-1/2}\xi^{1/2}\theta(\xi,\eta), \quad \Phi - \Phi_\infty = \frac{q_{np}L}{D_B}\mathrm{Re}^{-1/2}\xi^{1/2}\phi(\xi,\eta),\\
&M - M_\infty = \frac{q_n L}{D_n}\mathrm{Re}^{-1/2}\xi^{1/2}\chi(\xi,\eta),
\end{aligned}\right\} \tag{4.8}$$

where $Re = \dfrac{U_\infty L}{\nu}$ is the Reynolds number and ψ is the stream function defined in 2.10 of Chapter2.

Using Eq. (4.8) in the governing equations (4.1) to (4.6) and invoking the boundary layer approximation, we get the following dimensionless form.

$$\left(1+\sigma_\xi^2\right) f''' + \frac{1}{2}ff'' - \frac{\xi\sigma_\xi\sigma_{\xi\xi}}{\left(1+\sigma_\xi^2\right)}(f')^2 + \frac{Ri\left(\theta - N_r\phi - R_b\chi\right)\xi^{\frac{3}{2}}}{(1+{\sigma_\xi}^2)}\left(\sin A + \sigma_\xi\cos A\right) = \xi\left[f'\frac{\partial f'}{\partial\xi} - \frac{\partial f}{\partial\xi}f''\right] \tag{4.9}$$

$$\frac{\left(1+\sigma_\xi^2\right)}{\mathrm{Pr}}\left[\theta'' + N_b\xi^{\frac{1}{2}}\phi'\theta' + N_t\xi^{\frac{1}{2}}(\theta')^2\right] + \frac{1}{2}\left(f\theta' - f'\theta\right) = \xi\left[f'\frac{\partial\theta}{\partial\xi} - \theta'\frac{\partial f}{\partial\xi}\right] \tag{4.10}$$

$$\frac{\left(1+\sigma_\xi^2\right)}{Le}\left[\phi'' + \frac{N_t}{N_b}\theta''\right] + \frac{1}{2}\left(f\phi' - f'\phi\right) = \xi\left[f'\frac{\partial\phi}{\partial\xi} - \phi'\frac{\partial f}{\partial\xi}\right] \tag{4.11}$$

$$\frac{\left(1+\sigma_\xi^2\right)}{Sc}\chi'' - \frac{Pe}{Sc}\left(1-\sigma_\xi\right)\phi'' + \frac{1}{2}\left(f\chi' - f'\chi\right) = \xi\left[f'\frac{\partial\chi}{\partial\xi} - \chi'\frac{\partial f}{\partial\xi}\right] \tag{4.12}$$

and

$$\left.\begin{aligned}
&f'(\xi,0) = 0, \quad f(\xi,0) = -2\xi\left.\frac{\partial f}{\partial\xi}\right|_{(\xi,0)}, \quad \theta'(\xi,0) = -\frac{1}{\sqrt{1+\sigma_\xi^2}},\\
&\phi'(\xi,0) = -\frac{1}{\sqrt{1+\sigma_\xi^2}}, \quad \chi'(\xi,0) = -\frac{1}{\sqrt{1+\sigma_\xi^2}}\\
&f'(\xi,\infty) = 1,\ \theta(\xi,\infty) = 0,\ \phi(\xi,\infty) = 0,\ \chi(\xi,\infty) = 0
\end{aligned}\right\} \tag{4.13}$$

The parameters Pr, Pe, Le, Sc, N_b, N_r, N_t, R_b, are same as in 3.16 of Chapter 3 and the mixed convection parameter Ri is defined as $Ri = \dfrac{Gr}{Re^{5/2}}$.

The non-dimensional form of skin friction, Nusselt number, nanoparticle Sherwood num-

ber, and the density number of motile microbe. are given by

$$\frac{1}{2}(Cf_\xi)(Re_\xi^{1/2}) = \sqrt{1+\sigma_\xi^2}f''(\xi,0), \qquad \frac{Nu_\xi}{Re_\xi^{1/2}} = \frac{1}{\theta(\xi,0)},$$
$$\frac{NSh_\xi}{Re_\xi^{1/2}} = \frac{1}{\phi(\xi,0)}, \qquad \frac{Q_\xi}{Re_\xi^{1/2}} = \frac{1}{\chi(\xi,0)}, \tag{4.14}$$

4.3 Method of Solution

The set of non-similar Equations (4.9) - (4.12) with (4.13) are solved using the bivariate pseudo-spectral local linearization method (BPSLLM) as explained in Chapter 2.

On applying this procedure to the equations (4.9) - (4.12), we obtain the following set of linear differential equations.

$$a_{1,m}f'''_{m+1} + a_{2,m}f''_{m+1} + a_{3,m}f'_{m+1} + a_{4,m}f_{m+1} + a_{5,m}\frac{\partial f'_{m+1}}{\partial\xi} + a_{6,m}\frac{\partial f_{m+1}}{\partial\xi} = R_{1,m} \tag{4.15}$$

$$b_{1,m}\theta''_{m+1} + b_{2,m}\theta'_{m+1} + b_{3,m}\theta_{m+1} + b_{4,m}\frac{\partial\theta_{m+1}}{\partial\xi} = R_{2,m} \tag{4.16}$$

$$c_{1,m}\phi''_{m+1} + c_{2,m}\phi'_{m+1} + c_{3,m}\phi_{m+1} + c_{4,m}\frac{\partial\phi_{m+1}}{\partial\xi} = R_{3,m} \tag{4.17}$$

$$d_{1,m}\chi''_{m+1} + d_{2,m}\chi'_{m+1} + d_{3,m}\chi_{m+1} + d_{4,m}\frac{\partial\chi_{m+1}}{\partial\xi} = R_{4,m} \tag{4.18}$$

where the coefficients are

$$a_{1,m} = 1+\sigma_\xi^2, \quad a_{2,m} = \frac{1}{2}f_m + \xi\frac{\partial f_m}{\partial\xi}, \quad a_{3,m} = -\left[\frac{\xi\sigma_\xi\sigma_{\xi\xi}}{1+\sigma_\xi^2}\right]2f'_m - \xi\frac{\partial f'_m}{\partial\xi}$$

$$a_{4,m} = \frac{1}{2}f''_m \quad a_{5,m} = -\xi f'_m \quad a_{6,m} = \xi f''_m$$

$$R_{1,m} = \xi f''_m\frac{\partial f_m}{\partial\xi} - \frac{\xi\sigma_\xi\sigma_{\xi\xi}}{1+\sigma_\xi^2}(f'_m)^2 + \frac{1}{2}f_m f''_m - \xi f'_m\frac{\partial f'_m}{\partial\xi}$$
$$-\frac{Ri\,(\theta_m - N_r\,\phi_m - R_b\,\chi_m)\,\xi^{3/2}}{(1+{\sigma_\xi}^2)}\,(\sin A + \sigma_\xi\cos A)$$

$$b_{1,m} = \frac{(1+{\sigma_\xi}^2)}{\mathrm{Pr}},\ b_{2,m} = \frac{1+\sigma_\xi^2}{\mathrm{Pr}}\xi^{1/2}N_b\phi'_m + \frac{1+\sigma_\xi^2}{\mathrm{Pr}}2N_t\xi^{1/2}\theta'_m + \frac{1}{2}f_{m+1} + \xi\frac{\partial f_{m+1}}{\partial\xi},$$

$$b_{3,m} = -\frac{1}{2}f'_{m+1}, \quad b_{4,m} = -\xi f'_{m+1}, \quad R_{2,m} = \frac{1+\sigma_\xi^2}{\mathrm{Pr}}\xi^{1/2}N_t(\theta'_m)^2,$$

$$c_{1,m} = \frac{1+\sigma_\xi^2}{Le}, \quad c_{2,m} = \frac{1}{2}f_{m+1} + \xi\frac{\partial f_{m+1}}{\partial \xi}, \quad c_{3,m} = -\frac{1}{2}f'_{m+1}, \quad c_{4,m} = -\xi f'_{m+1},$$

$$R_{3,m} = -\frac{1+\sigma_\xi^2}{Le}\frac{N_t}{N_b}\theta''_{m+1}, \quad d_{1,m} = \frac{1+\sigma_\xi^2}{Sc}, \quad d_{2,m} = \frac{1}{2}f_{m+1} + \xi\frac{\partial f_{m+1}}{\partial \xi},$$

$$d_{3,m} = -\frac{1}{2}f'_{m+1}, \quad d_{4,m} = -\xi f'_{m+1}, \quad R_{4,m} = (1-\sigma_\xi)\frac{Pe}{Sc}\phi''_{m+1}.$$

The corresponding boundary conditions are

$$\left.\begin{aligned} &f'_{m+1}(\xi,0) = 0\,, \quad f_{m+1}(\xi,0) = -2\xi\left.\frac{\partial f}{\partial \xi}\right|_{(\xi,0)}, \quad \theta'_{m+1}(\xi,0) = -\frac{1}{\sqrt{1+\sigma_\xi^2}}, \\ &\phi'_{m+1}(\xi,0) = -\frac{1}{\sqrt{1+\sigma_\xi^2}}, \quad \chi'_{m+1}(\xi,0) = -\frac{1}{\sqrt{1+\sigma_\xi^2}} \\ &f'_{m+1}(\xi,\infty) = 1, \quad \theta_{m+1}(\xi,\infty) = 0, \quad \phi_{m+1}(\xi,\infty) = 0, \quad \chi_{m+1}(\xi,\infty) = 0 \end{aligned}\right\} \tag{4.19}$$

Applying the pseudo-spectral method in both η and ξ gives, which was explained in Chapter 2, we get

$$A^{(1)}\mathbf{F}_i + \gamma_{5,i}^{(1)}\sum_{j=0}^{M}\mathbf{d}_{i,j}\mathbf{D}\mathbf{F}_j + \gamma_{6,i}^{(1)}\sum_{j=0}^{M}\mathbf{d}_{i,j}\mathbf{F}_j = \mathbf{R}_{1,i} \tag{4.20}$$

$$A^{(2)}\mathbf{\Theta}_i + \gamma_{4,i}^{(2)}\sum_{j=0}^{M}\mathbf{d}_{i,j}\mathbf{\Theta}_j = \mathbf{R}_{2,i} \tag{4.21}$$

$$A^{(3)}\mathbf{\Phi}_i + \gamma_{4,i}^{(3)}\sum_{j=0}^{M}\mathbf{d}_{i,j}\mathbf{\Phi}_j = \mathbf{R}_{3,i} \tag{4.22}$$

$$A^{(4)}\chi_i + \gamma_{4,i}^{(4)}\sum_{j=0}^{M}\mathbf{d}_{i,j}\chi_j = \mathbf{R}_{4,i} \tag{4.23}$$

where

$$A^{(1)} = \gamma_{1,i}^{(1)}\mathbf{D}^3 + \gamma_{2,i}^{(1)}\mathbf{D}^2 + \gamma_{3,i}^{(1)}\mathbf{D} + \gamma_{4,i}^{(1)}\mathbf{I},$$
$$A^{(2)} = \gamma_{1,i}^{(2)}\mathbf{D}^2 + \gamma_{2,i}^{(2)}\mathbf{D} + \gamma_{3,i}^{(2)}\mathbf{I},$$
$$A^{(3)} = \gamma_{1,i}^{(3)}\mathbf{D}^2 + \gamma_{2,i}^{(3)}\mathbf{D} + \gamma_{3,i}^{(3)}\mathbf{I},$$
$$A^{(4)} = \gamma_{1,i}^{(4)}\mathbf{D}^2 + \gamma_{2,i}^{(4)}\mathbf{D} + \gamma_{3,i}^{(4)}\mathbf{I}$$

Here $\gamma_{k,i}^{(1)}$, $\gamma_{k,i}^{(2)}$, $\gamma_{k,i}^{(3)}$, $\gamma_{k,i}^{(4)}$ and $\mathbf{R}_{k,i}$ are N^{th} order diagonal matrices with diagonal elements as, $a_{k,m}(\zeta_r, \tau_i)$, $b_{k,m}(\zeta_r, \tau_i)$, $c_{k,m}(\zeta_r, \tau_i)$, $d_{k,m}(\zeta_r, \tau_i)$ and $R_{k,m}(\zeta_r, \tau_i)$ for $r = 1, 2, 3, \cdots N$ respectively and $\mathbf{I}$ refers the identity matrix.

The matrix form of equation (4.20) can be written as

$$\begin{bmatrix} A_{0,0}^{(1)} & A_{0,1}^{(1)} & A_{0,2}^{(1)} & \cdots & A_{0,M}^{(1)} \\ A_{1,0}^{(1)} & A_{1,1}^{(1)} & A_{1,2}^{(1)} & \cdots & A_{1,M}^{(1)} \\ A_{2,0}^{(1)} & A_{2,1}^{(1)} & A_{2,2}^{(1)} & \cdots & A_{2,M}^{(1)} \\ \vdots & \vdots & \vdots & \vdots & \vdots \\ A_{M,0}^{(1)} & A_{M,1}^{(1)} & A_{M,2}^{(1)} & \cdots & A_{M,M}^{(1)} \end{bmatrix} \begin{bmatrix} \mathbf{F}_0 \\ \mathbf{F}_1 \\ \mathbf{F}_2 \\ \vdots \\ \mathbf{F}_M \end{bmatrix} = \begin{bmatrix} \mathbf{R}_{1,0} \\ \mathbf{R}_{1,1} \\ \mathbf{R}_{1,2} \\ \vdots \\ \mathbf{R}_{1,M} \end{bmatrix} \tag{4.24}$$

where

$$A_{i,j}^{(1)} = A^{(1)} + \gamma_{5,i}^{(1)}\mathbf{d}_{i,i}\mathbf{D} + \gamma_{6,i}^{(1)}\mathbf{d}_{i,i}\mathbf{I}, \quad for \quad i = j;$$
$$A_{i,j}^{(1)} = \gamma_{5,i}^{(1)}\mathbf{d}_{i,j}\mathbf{D} + \gamma_{6,i}^{(1)}\mathbf{d}_{i,j}\mathbf{I}, \quad for \quad i \neq j \tag{4.25}$$

In a similar manner, we can write the matrix form of the equations (4.21) to (4.23). The approximate solutions are obtained by solving these matrix equations, iteratively, with the help of suitable initial approximation.

4.4 Computational Results and Discussions

To check the convergence, the code developed for the bivariate pseudo-spectral local linearization method (BPSLLM) in MATLAB is executed for $f''(\xi, 0)$ and $\theta(\xi, 0)$ by changing the number of collocation points N and M in both η and ξ directions and the results obtained are presented in Table 4.1 for randomly selected values for various parameters. It is apparent from this table that the least stable eigenvalue attain convergence criterion of 10^{-7} for N =

51 and M = 51. There is no change in the results with an increase of N and M. The same tendency is witnessed for other values of parameters. Hence, N = 51 and M = 51 is adopted to implement the numerical calculations.

To confirm the correctness of the method, the code developed is verified by comparing our computational results $\sqrt{Re_\xi}Cf_\xi$ with the published results of Cebeci and Bradshaw [21], Yih [132], Chamkha *et al.* [22] and $Nu_\xi/\sqrt{Re_\xi}$ with the published results of Lin and Lin [66] for diverse values of Prandtl number Pr by taking the angle of inclination $A = \pi/2$ and ignoring the parameters α, Pe, Le, Sc, N_b, N_r, N_t, and R_b, The computed results are presented in Table 4.2 and Table 4.3 and the comparisons are found to be in very good agreement.

Table 4.1: Convergence of $f''(\xi, 0)$ and $\theta(\xi, 0)$ by BPSLLM for Pr = 2, $Pe = 0.75$, $Le = 5$, $Sc = 2.5$, $Ri = 1.0$, $Nb = 0.5$, $Nt = 0.1$, $Nr = 0.3$, $Rb = 0.6$, $\alpha = 0.1$, $\xi = 1$, $A = \pi/6$

Number of grid points in η direction	Number of grid points in ξ direction	$f''(\xi, 0)$	$\theta(\xi, 0)$
20	20	0.5456057	2.0609942
30	20	0.5456099	2.0609948
30	30	0.5456108	2.0609966
40	30	0.5456108	2.0609966
40	40	0.5456111	2.0609971
50	40	0.5456111	2.0609971
50	50	0.5456111	2.0609972
60	50	0.5456111	2.0609972
60	60	0.5456111	2.0609972
80	60	0.5456111	2.0609972

Table 4.2: Comparative analysis for the values of $\sqrt{Re_\xi}Cf_\xi$ by the present method for $\alpha = 0.0$, $A = \pi/2$, $Pe = 10^{-5}$, $Le = 10^{-5}$, $Sc = 10^{-5}$, $N_b = 10^{-5}$, $N_t = N_r = R_b = 0.0$ with the results of Cebeci and Bradshaw [21], Yih [132], Chamkha *et al.* [22]

Cebeci and Bradshaw [21]	Yih [132]	Chamkha *et al.* [22]	Present
0.33206	0.332057	0.332206	0.332066

In this study, special attention is given to analyze the effect of inclination angle A, amplitude α, mixed convection parameter Ri, bioconvection Peclet number Pe, bioconvection Rayleigh number R_b and bioconvection Schmidt number Sc on the coefficient of skin friction $\sqrt{Re_\xi}Cf_\xi$, Nusselt number $Nu_\xi/\sqrt{Re_\xi}$, nanoparticle Sherwood number $NSh_\xi/\sqrt{Re_\xi}$ and density number of motile microbes $Q_\xi/\sqrt{Re_\xi}$. The other parameter values are fixed as Pr = 2, $Le = 5$, $Nb = 0.5$, $Nr = 0.3$ and $Nt = 0.1$.

Table 4.3: Comparative analysis for the values of $Nu_\xi/\sqrt{Re_\xi}$ by the present method for $\alpha = 0.0$, $A = \pi/2$, $Pe = 10^{-5}$, $Le = 10^{-5}$, $Sc = 10^{-5}$, $N_b = 10^{-5}$, $N_t = N_r = R_b = 0.0$ with the results of Lin and Lin [66]

Pr	Lin and Lin [66]	Present
0.01	0.0775587	0.0775601
0.1	0.200655	0.2006412
1	0.458971	0.4589723
10	0.997888	0.9978392
100	2.15196	2.1522064

Figure 4.1 provides the effect of the inclination angle A on the skin friction coefficient, local Nusselt number, nanoparticle Sherwood number, and density number of motile microorganisms It is noticed from Figs. 4.1(a) to 4.1(d) that the coefficient of skin friction, the rate of transfer of heat, nanoparticle mass, and concentration of motile microorganisms across the boundary are increasing with the rise in the inclination angle. Hence, the transfer rate of all the physical quantities is more for the vertical surface compared to the horizontal surface.

The variation of the coefficient of skin friction, heat exchange rate, nanoparticle mass transmission rate, and density number of motile microbes the amplitude α is presented in Fig. 4.2. It is seen from Figs. 4.2(a) to 4.2(c) that the heat transfer rate, nanoparticle mass transfer are increasing first and then decreasing as there is an increment in amplitude over one period. This change is observed periodically over ξ. It is interesting to note that the rate of motile microorganisms is decreasing first and then increasing with an increase in the amplitude of the wavy surface as depicted in Fig. 4.2(d).

The effect of mixed convection parameter Ri on the skin friction, heat transfer rate, motile microorganism density number, and nanoparticle mass transfer rate is portrayed graphically in Fig. 4.3. Forced convection is the dominant mode of transport of heat when $Ri \to 0$, whereas free convection, is the dominant mode when $Ri \to \infty$. The coefficient of skin friction, local Nusselt number, Local nanoparticle Sherwood number, and density number of microorganisms are less for forced convection and more for free convection. There is a decrease of coefficient of skin friction, local Nusselt number, Local nanoparticle Sherwood number, and Density number of microorganisms with ξ for forced convection, whereas an increase in the physical quantities is observed for free convection. It is observed that the coefficient of skin friction, Nusselt number, nanoparticle Sherwood number, and rate of transfer of density of motile microorganisms are increasing with a rise in the mixed convection

parameter.

Figure 4.4 shows the effect of bioconvection Peclet number Pe on the coefficient of skin friction, local Nusselt number, nanoparticle Sherwood number, and density number of motile microorganisms. It is witnessed from Figs. 4.4(a) to 4.4(d) that the enhancement in Pe causes a rise in the profiles of the coefficient of skin friction, local Nusselt number, nanoparticle Sherwood number, and density number of motile microorganisms. Increasing values of the bioconvection Peclet number enhances the movement of microbes along with the concentration of gradients. Hence, an increase of Pe, i.e., an increase of microorganism movements cause the rise of all dimensionless parameters under consideration.

The impact of bioconvection Rayleigh number R_b in the profiles of local Nusselt number, nanoparticle Sherwood number, and density number of motile microorganisms is depicted in Fig. 4.5. It is noticed from Figs. 4.5(a) - 4.5(d) that an increase in bioconvection Rayleigh number reduces the skin friction, heat transfer rate, motile microorganism density number, and nanoparticle mass transfer rate. The possible interpretation of $R_b = 0$ is the absence of microorganisms from the expression of R_b. Hence, the presence of microorganisms reduces all the physical quantities under consideration. The movement of the nanoparticles present in the base fluid is the explanation for this. These nanoparticles move in the fluid arbitrarily, and the fluid temperature gradually rises.

Figure 4.6 elucidates the influence of bioconvection Schmidt number Sc on the coefficient of skin friction, Nusselt number, nanoparticle Sherwood number, and rate of transfer of density of motile microorganisms. It is observed from Figs. 4.6(a) - 4.6(d) that all the physical quantities are increasing with a rise in bioconvection Schmidt number.

The effect of Nb on the skin friction, heat transfer rate, motile microorganism density number, and nanoparticle mass transfer rate is presented in Fig. 4.7. It is noticed from Figs. 4.7(a), 4.7(c), 4.7(d) that, the coefficient of skin friction, nanoparticle Sherwood number and rate of transfer of density of motile microorganisms are increasing with an increase in Nb. A rise in the values of the Nb results in the fall of the Nusselt number, as portrayed in Fig. 4.7(b).

The influence of thermophoresis parameter on the local heat transfer rate, nanoparticle mass transfer rate and density number of motile microorganisms is portrayed in Fig. 4.8. It is noticed from Fig. 4.8(b) that, a rise in the thermophoresis parameter reduces the rate of heat transfer. Whereas the $\sqrt{Re_\xi}Cf_\xi$, $NSh_\xi/\sqrt{Re_\xi}$, and $Q_\xi/\sqrt{Re_\xi}$ are increasing for intensification in the values of the thermophoresis parameter as presented in the Figs. 4.8(a), 4.8(c) and 4.8(d).

4.5 Conclusions

In the present chapter, the nanofluid flow past an inclined wavy surface in the existence of gyrotactic microbes is studied. The solution of the governing equations is attained using a bivariate pseudo-spectral local linearization technique followed by the Chebyshev collocation method. The following are the important observations:

- The skin friction coefficient, heat transfer rate, and nanoparticle mass transfer rate, and density of motile microorganisms are more for the vertical surface compared to the horizontal surface.
- An increase in the boiconvection Peclet number and bioconvection Schmidt number enhances the skin friction coefficient, heat transfer rate and nanoparticle mass transfer rate, and density of motile microorganisms. A reverse trend is noticed for the influence of bioconvection Rayleigh number.
- The coefficient of skin friction, Nusselt number, nanoparticle Sherwood number, and rate of transfer of density of motile microorganisms are increasing with a rise in the mixed convection parameter.
- The influence of Brownian motion and thermophoresis parameters is to increase the coefficient of skin friction, nanoparticle mass transfer rate, and density of motile organisms.

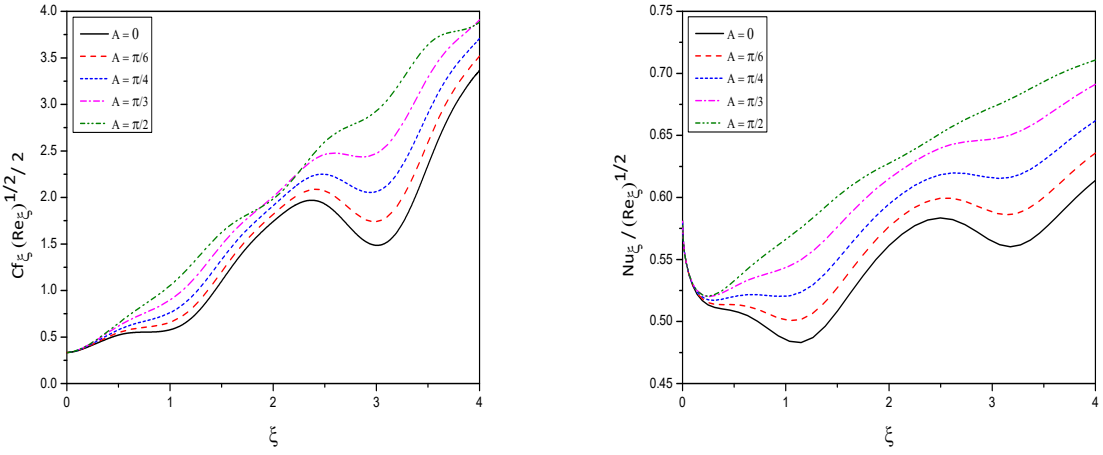

(a)

(b)

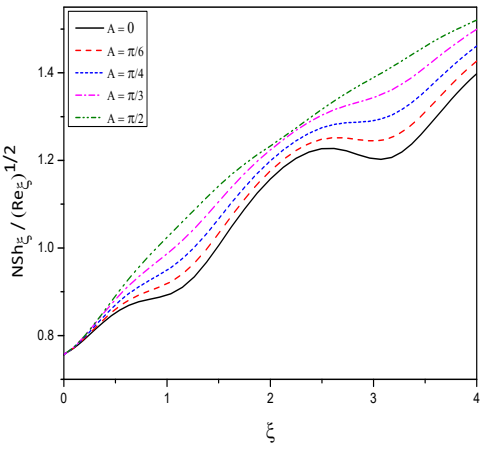

(c)

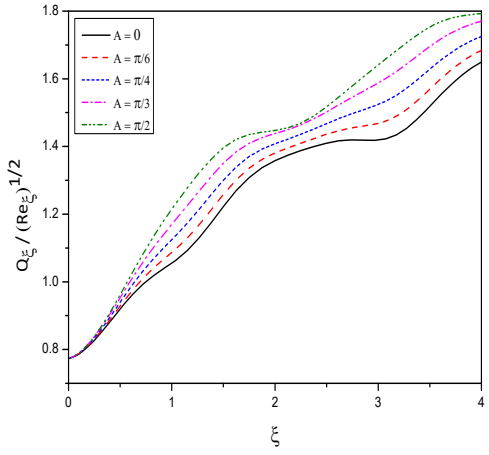

(d)

Figure 4.1: "Effect of the angle of inclination A on the profiles of (a) $Cf_\xi(Re_\xi^{1/2})/2$ (b) $\frac{Nu_\xi}{Re_\xi^{1/2}}$ (c) $\frac{NSh_\xi}{Re_\xi^{1/2}}$ (d) $\frac{Q_\xi}{Re_\xi^{1/2}}$".

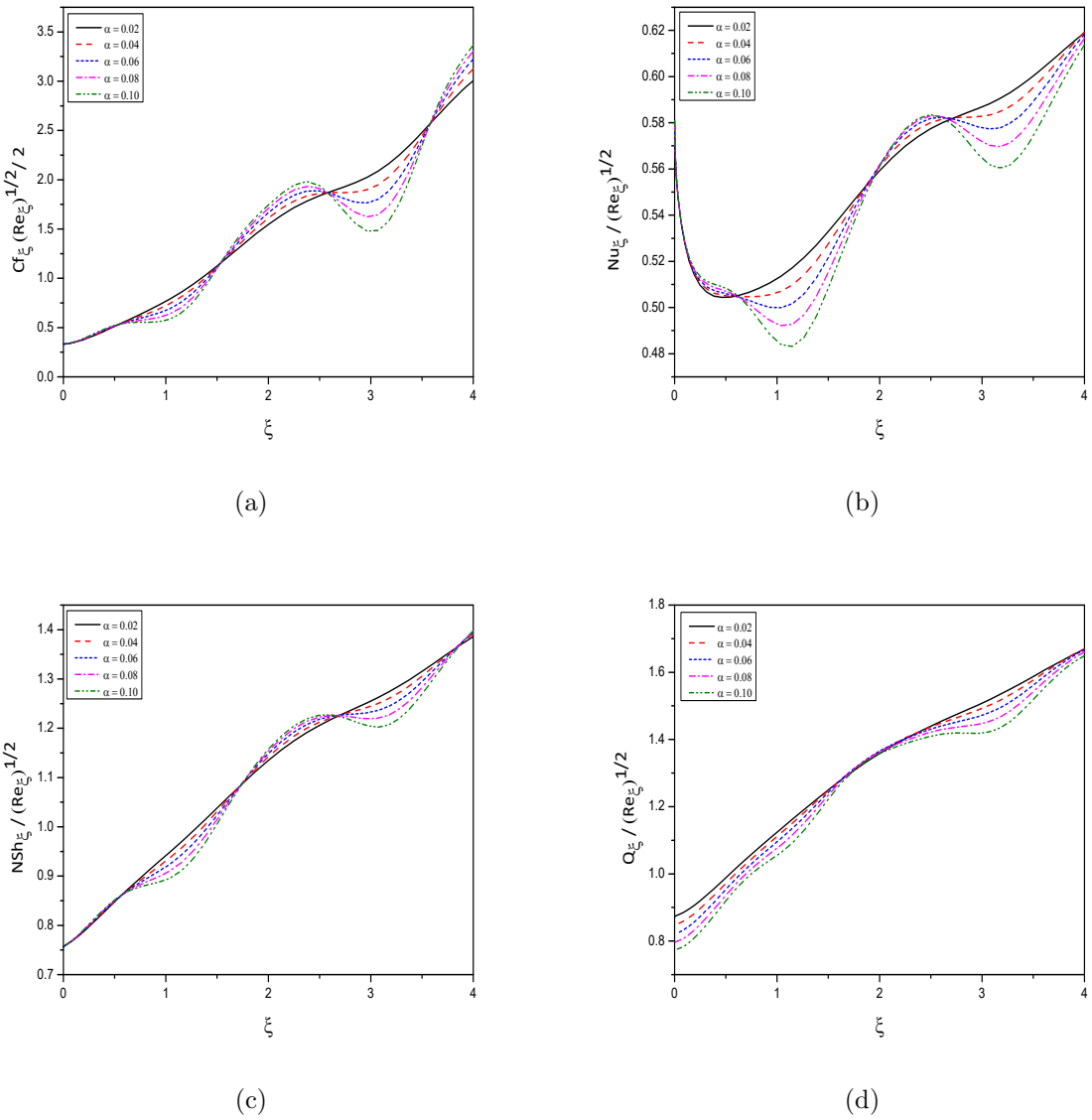

Figure 4.2: "Effect of the amplitude of the wavy surface α on the profiles of (a) $Cf_\xi(Re_\xi^{1/2})/2$ (b) $\frac{Nu_\xi}{Re_\xi^{1/2}}$ (c) $\frac{NSh_\xi}{Re_\xi^{1/2}}$ (d) $\frac{Q_\xi}{Re_\xi^{1/2}}$".

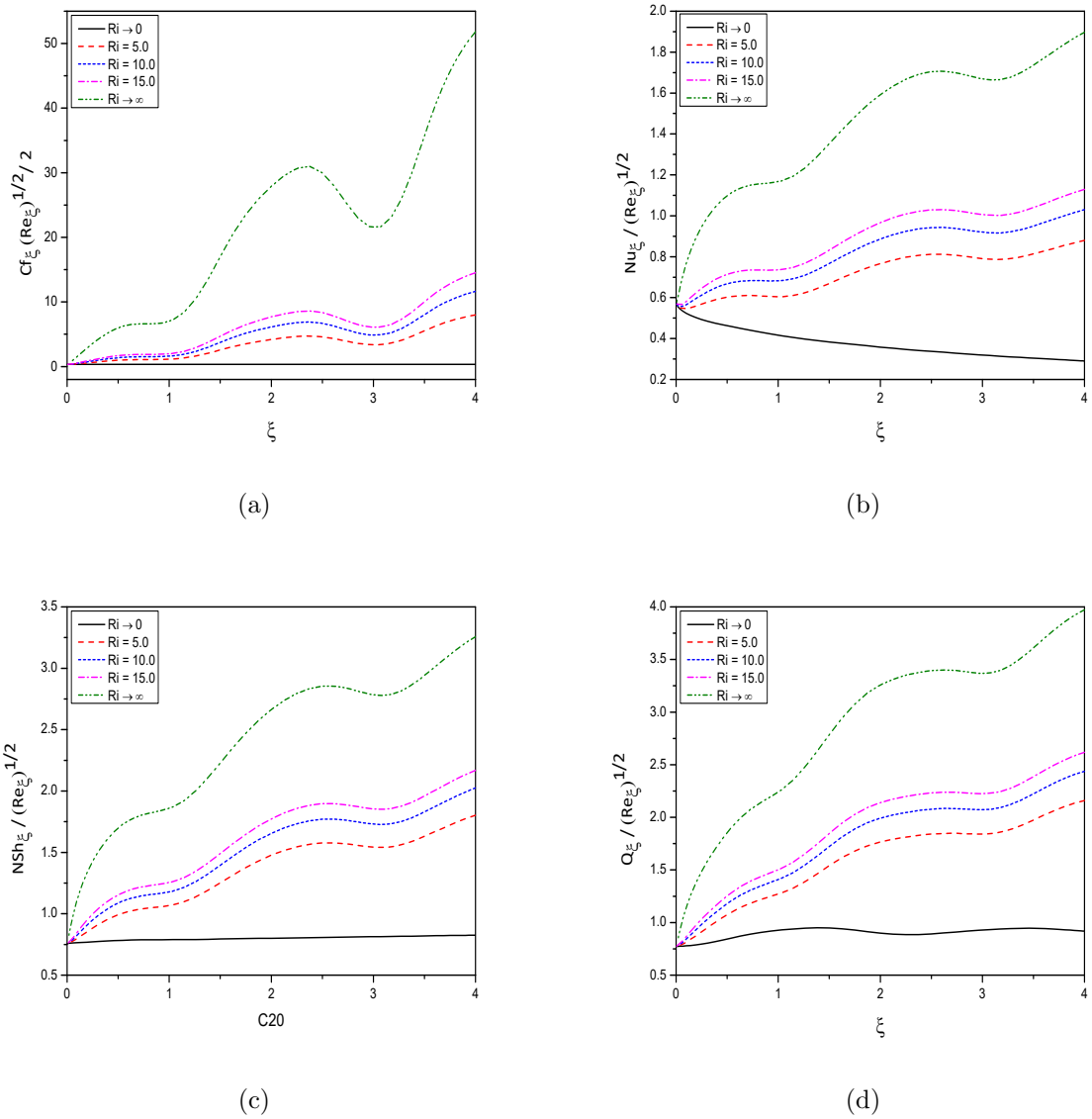

Figure 4.3: "Effect of the mixed convection parameter Ri on the profiles of (a) $Cf_\xi(Re_\xi^{1/2})/2$ (b) $\frac{Nu_\xi}{Re_\xi^{1/2}}$ (c) $\frac{NSh_\xi}{Re_\xi^{1/2}}$ (d) $\frac{Q_\xi}{Re_\xi^{1/2}}$".

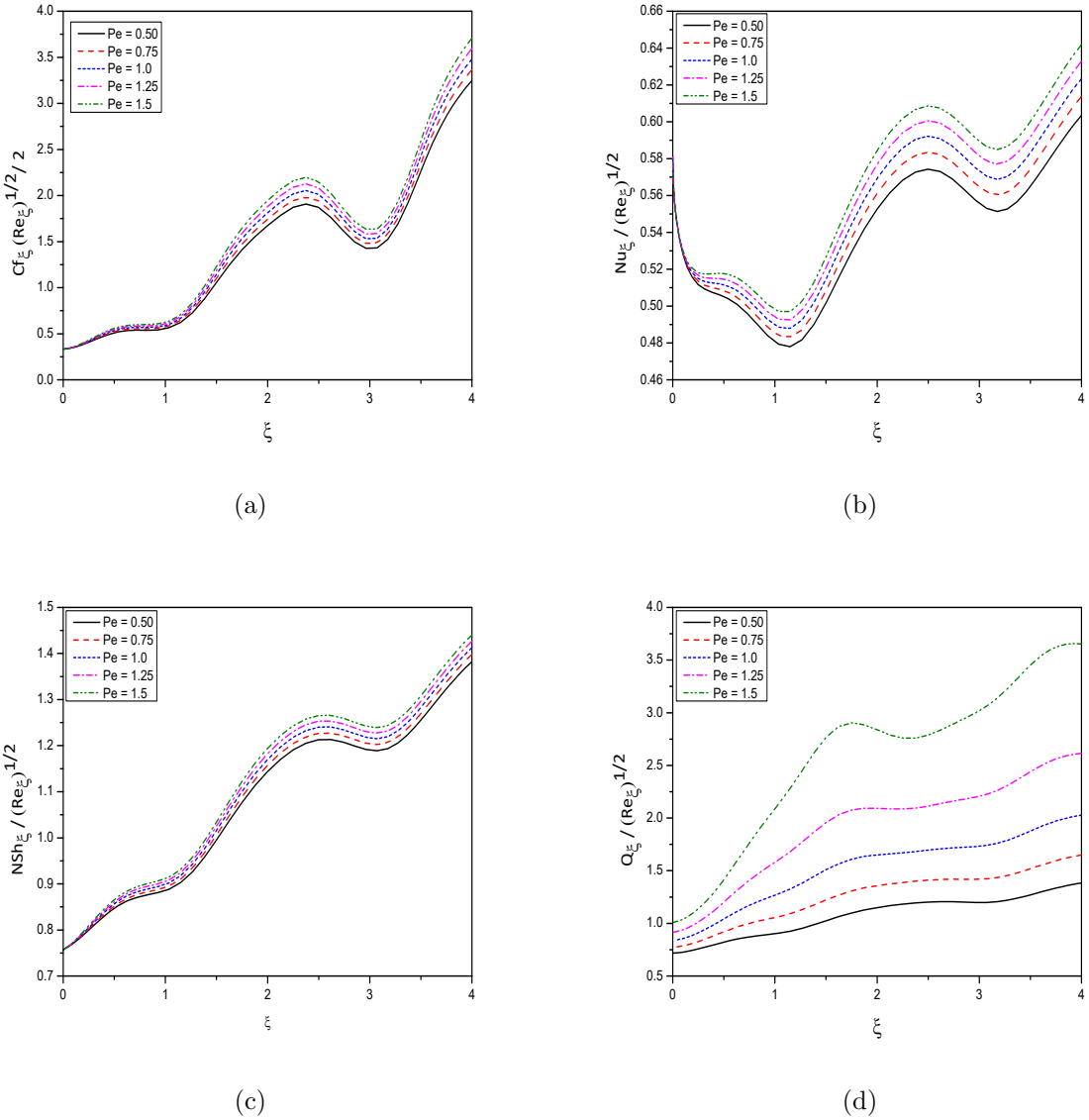

Figure 4.4: "Effect of the bioconvection Peclet number Pe on the profiles of (a) $Cf_\xi(Re_\xi^{1/2})/2$ (b) $\frac{Nu_\xi}{Re_\xi^{1/2}}$ (c) $\frac{NSh_\xi}{Re_\xi^{1/2}}$ (d) $\frac{Q_\xi}{Re_\xi^{1/2}}$".

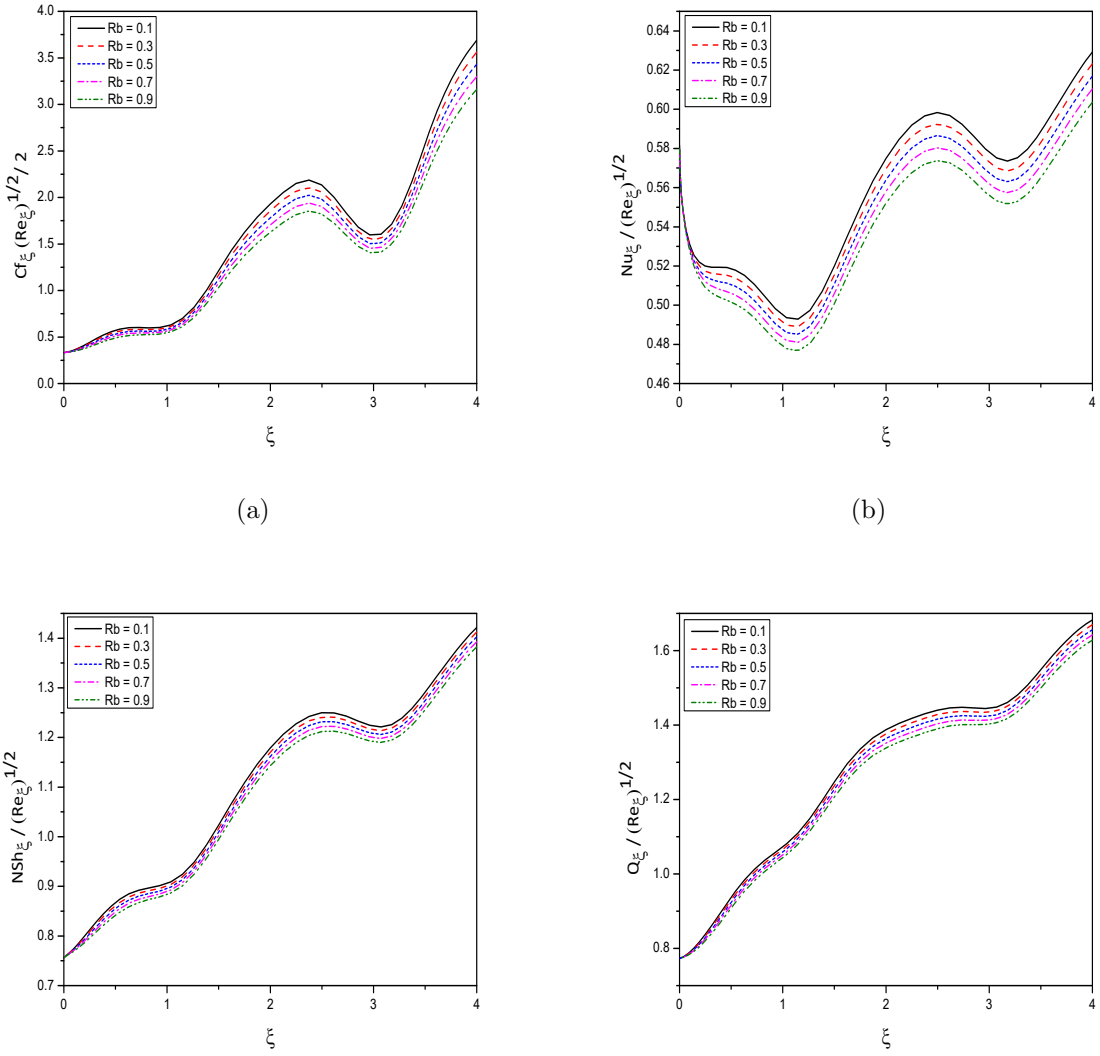

(a) (b)

(c) (d)

Figure 4.5: "Effect of the bioconvection Rayleigh number R_b on the profiles of (a) $Cf_\xi(Re_\xi^{1/2})/2$ (b) $\frac{Nu_\xi}{Re_\xi^{1/2}}$ (c) $\frac{NSh_\xi}{Re_\xi^{1/2}}$ (d) $\frac{Q_\xi}{Re_\xi^{1/2}}$".

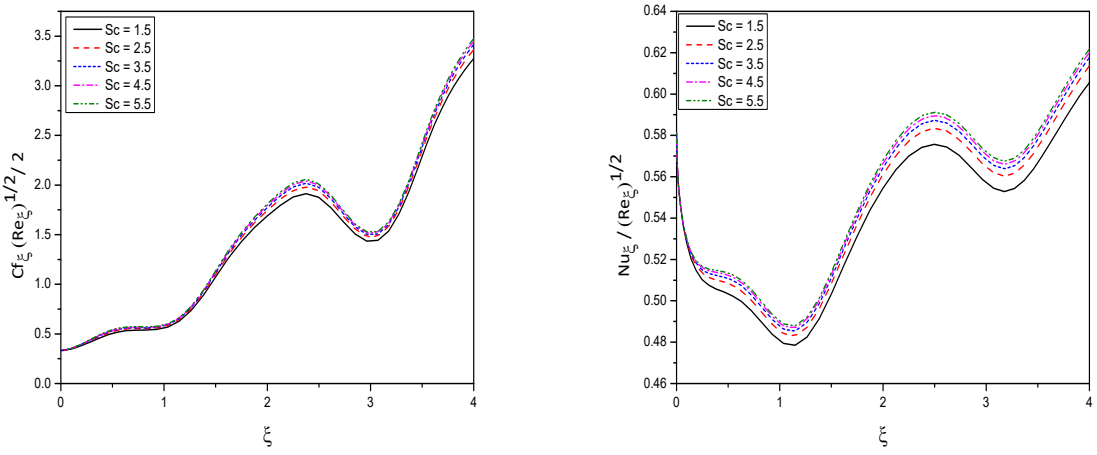

(a)

(b)

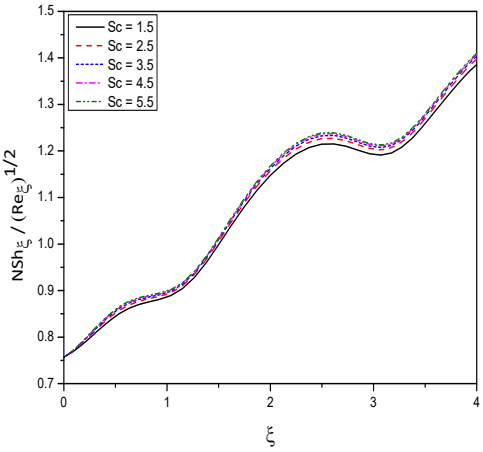

(c)

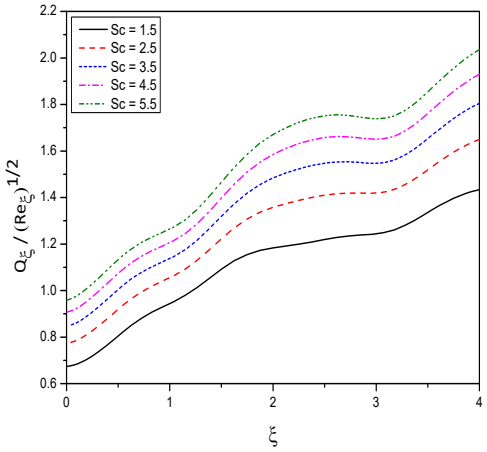

(d)

Figure 4.6: "Effect of the bioconvection Schmidt number Sc on the profiles of (a) $Cf_\xi(Re_\xi^{1/2})/2$ (b) $\frac{Nu_\xi}{Re_\xi^{1/2}}$ (c) $\frac{NSh_\xi}{Re_\xi^{1/2}}$ (d) $\frac{Q_\xi}{Re_\xi^{1/2}}$".

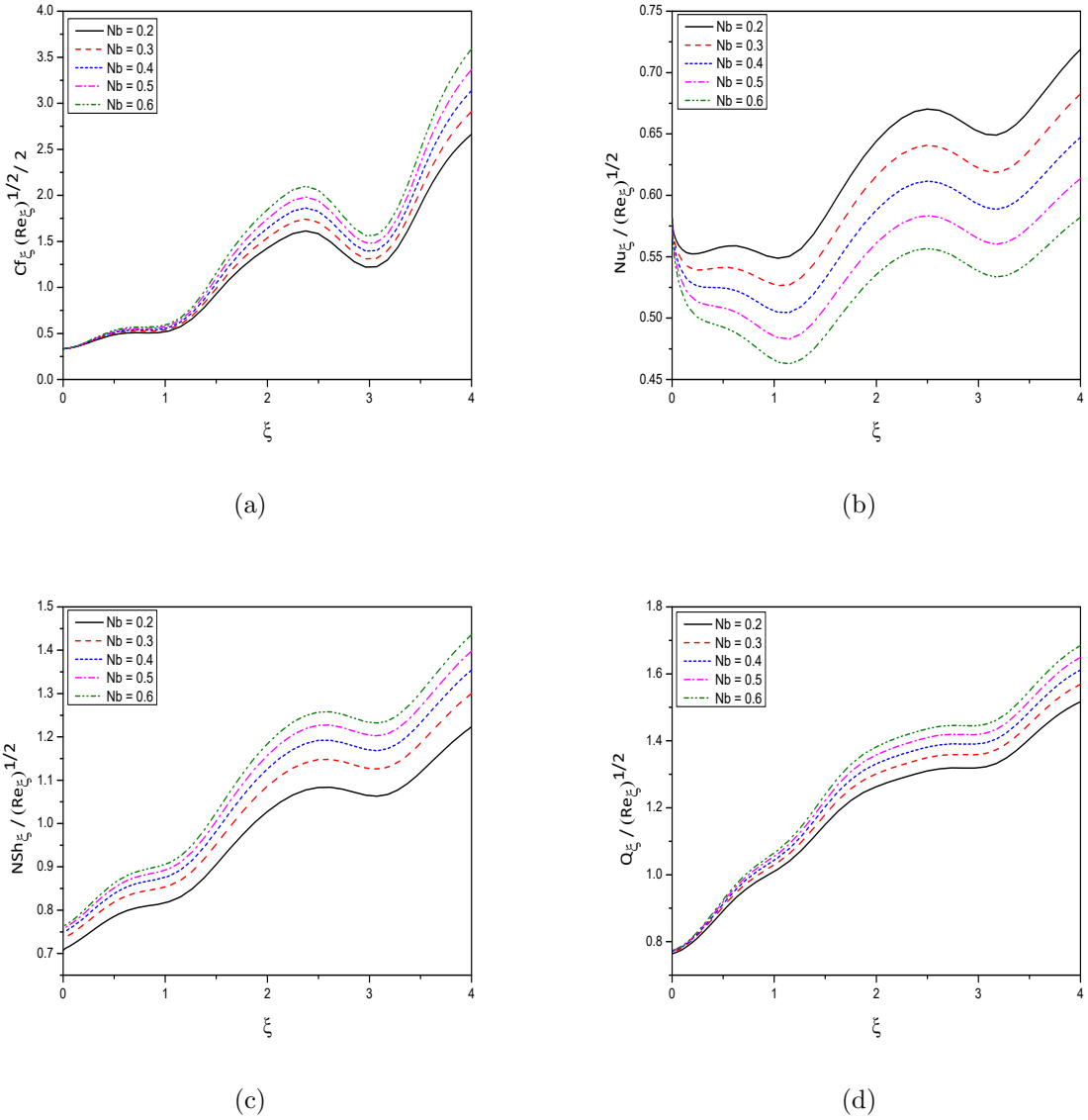

Figure 4.7: "Effect of the Brownian motion parameter N_b on the profiles of (a) $Cf_\xi(Re_\xi^{1/2})/2$ (b) $\frac{Nu_\xi}{Re_\xi^{1/2}}$ (c) $\frac{NSh_\xi}{Re_\xi^{1/2}}$ (d) $\frac{Q_\xi}{Re_\xi^{1/2}}$".

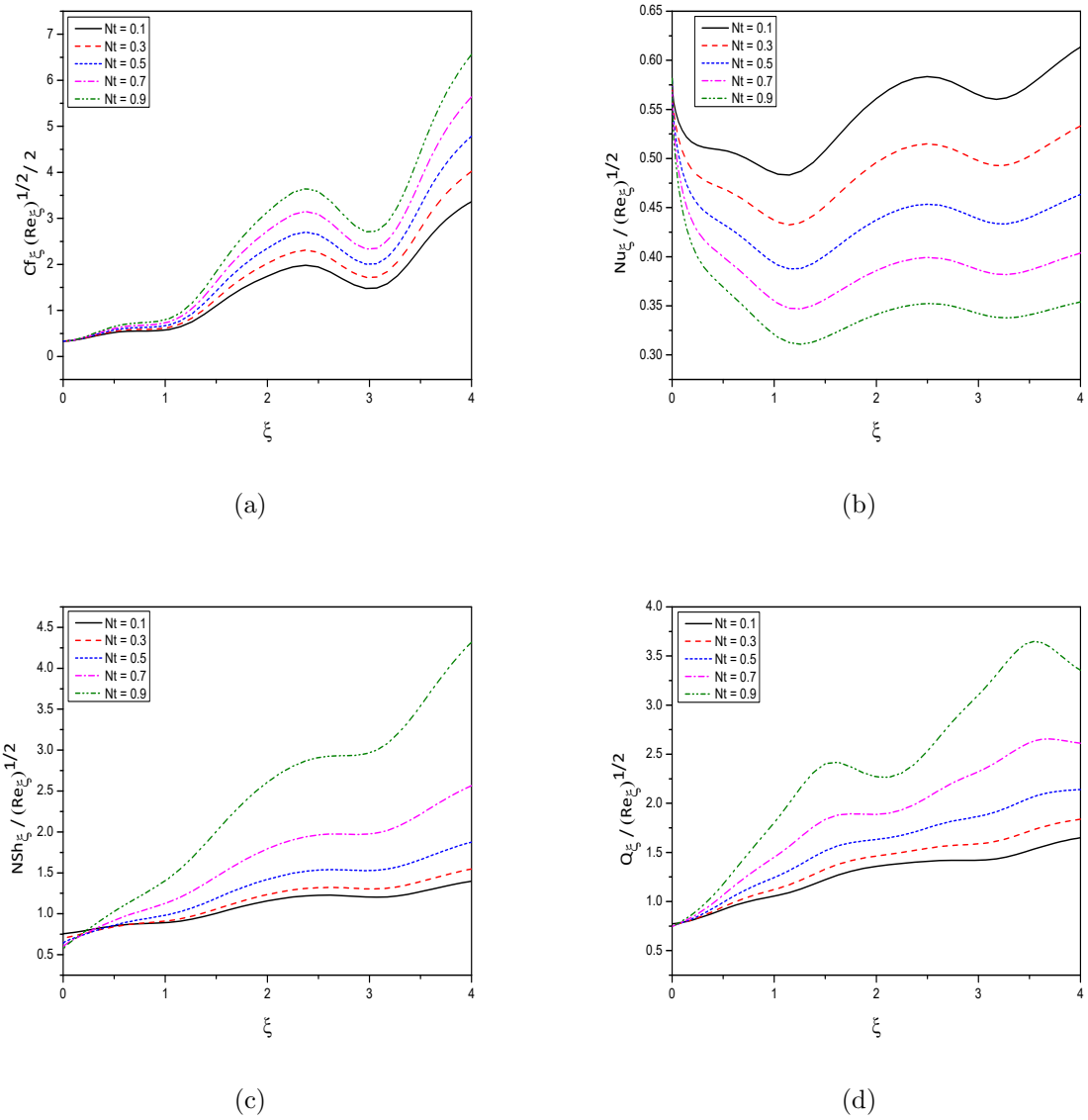

Figure 4.8: "Effect of the thermophoresis parameter N_t on the profiles of (a) $Cf_\xi(Re_\xi^{1/2})/2$ (b) $\frac{Nu_\xi}{Re_\xi^{1/2}}$ (c) $\frac{NSh_\xi}{Re_\xi^{1/2}}$ (d) $\frac{Q_\xi}{Re_\xi^{1/2}}$".

Chapter 5

Mixed Bioconvection of a Nanofluid Past an Inclined Wavy Surface in the presence of Magnetic Field [1]

5.1 Introduction

The magnetic field effect on the heat transfer characteristics and fluid flow behaviour of nanofluids has captured attention due to its several applications in different areas such as Medicine, Physics, and Engineering. In particular, the applications are in the files of solar technology, electronic device/microchip cooling, fusion reactors, nuclear reactor, crystal growth, geothermal energy extraction, polymer sheet, metal casting, food processing, manufacturing filaments, and wind up roller, and so on. The phenomenon of mixed convection in the presence of a magnetic field has also received a lot of attention [80, 27]. In contrast to traditional heat transfer fluids, the suspension of nanoparticles in a base-fluid exhibits meritorious heat transfer properties of the nanofluid and thus amplifies the heat transfer characteristics.

This chapter deals with the study of mixed convection of a nanofluid past an inclined wavy surface in the presence of gyrotactic microorganisms and magnetic fields. Bivariate pseudo-spectral local linearisation (BPSLLM) approach is used to solve the partial differential equations, which govern the flow. The influence of pertinent parameters on the Nusselt number, nanoparticle Sherwood number, and density number of the microbes are presented.

[1] Communicated to "**Pramana Journal of Physics**"

5.2 Mathematical Formulation

Consider the flow of a nanofluid containing motile microorganisms along a semi-infinite inclined wavy surface. The physical model of the problem is given in Fig. 2.1. All the assumptions considered are the same as in Chapter 2. The equations governing the flow are

$$\frac{\partial U}{\partial X}+\frac{\partial V}{\partial Y}=0 \tag{5.1}$$

$$\rho_{f\infty}\left(U\frac{\partial U}{\partial X}+V\frac{\partial U}{\partial Y}\right)=-\frac{\partial P}{\partial X}+\mu\left(\frac{\partial^2 U}{\partial X^2}+\frac{\partial^2 U}{\partial Y^2}\right)+[(1-\Phi_\infty)\beta_T\rho_{f\infty}(T-T_\infty) - (\rho_p-\rho_{f\infty})(\Phi-\Phi_\infty)-\beta_M(\rho_m-\rho_{f\infty})M]\,g\sin A-\sigma_f B_0^2(U-U_\infty) \tag{5.2}$$

$$\rho_{f\infty}\left(U\frac{\partial V}{\partial X}+V\frac{\partial V}{\partial Y}\right)=-\frac{\partial P}{\partial Y}+\mu\left(\frac{\partial^2 V}{\partial X^2}+\frac{\partial^2 V}{\partial Y^2}\right)+[(1-\Phi_\infty)\beta_T\rho_{f\infty}(T-T_\infty) - (\rho_p-\rho_{f\infty})(\Phi-\Phi_\infty)-\beta_M(\rho_m-\rho_{f\infty})M]\,g\cos A \tag{5.3}$$

$$U\frac{\partial T}{\partial X}+V\frac{\partial T}{\partial Y}=\alpha_m\left(\frac{\partial^2 T}{\partial X^2}+\frac{\partial^2 T}{\partial Y^2}\right)+\gamma\left\{D_B\left(\frac{\partial\Phi}{\partial X}\frac{\partial T}{\partial X}+\frac{\partial\Phi}{\partial Y}\frac{\partial T}{\partial Y}\right)+\frac{D_T}{T_\infty}\left[\left(\frac{\partial T}{\partial X}\right)^2+\left(\frac{\partial T}{\partial Y}\right)^2\right]\right\}+\frac{\mu}{\rho_{f\infty}C_{pf}}\left\{2\left[\left(\frac{\partial U}{\partial X}\right)^2+\left(\frac{\partial V}{\partial Y}\right)^2\right]+\left(\frac{\partial U}{\partial Y}+\frac{\partial V}{\partial X}\right)^2\right\} +\frac{\sigma_f B_0^2}{\rho_{f\infty}C_{pf}}(U-U_\infty)^2 \tag{5.4}$$

$$U\frac{\partial\Phi}{\partial X}+V\frac{\partial\Phi}{\partial Y}=D_B\left(\frac{\partial^2\Phi}{\partial X^2}+\frac{\partial^2\Phi}{\partial Y^2}\right)+\frac{D_T}{T_\infty}\left(\frac{\partial^2 T}{\partial X^2}+\frac{\partial^2 T}{\partial Y^2}\right) \tag{5.5}$$

$$U\frac{\partial M}{\partial X}+V\frac{\partial M}{\partial Y}+\frac{\partial}{\partial X}\left(M\widetilde{V}\right)+\frac{\partial}{\partial Y}\left(M\widetilde{V}\right)=D_n\left(\frac{\partial^2 M}{\partial X^2}+\frac{\partial^2 M}{\partial Y^2}\right) \tag{5.6}$$

where σ_f, C_{pf} are the electrical conductivity, the specific heat of the fluid and B_0^2 is Magnetic field strength. The average swimming velocity of the microorganisms' is $\widetilde{V}=\dfrac{b_c w_c}{\Phi_w-\Phi_\infty}\dfrac{\partial\Phi}{\partial Y}$. All other quantities are defined in the previous chapters.

The boundary conditions are :

$$\left.\begin{array}{l} U=0,\ V=0,\ T=T_w,\ \Phi=\Phi_w,\ M=M_w \quad \text{at} \quad Y=\sigma(X) \\ U\to U_\infty,\ T\to T_\infty,\ \Phi\to\Phi_\infty,\ M\to M_\infty \quad \text{as} \quad Y\to\infty \end{array}\right\} \tag{5.7}$$

The wavy surface is converted to a plane surface using the following non-dimensional transformations [131]

$$\left.\begin{aligned} &\xi = \frac{X}{L}, \quad \eta = \frac{Y-\sigma}{L\xi^{\frac{1}{2}}}\sqrt{Re}, \quad \psi = \frac{LU_\infty \xi^{\frac{1}{2}} f(\xi,\eta)}{\sqrt{Re}}, \quad p = \frac{P}{\rho_{f\infty}U_\infty^2}, \\ &\theta(\xi,\eta) = \frac{T-T_\infty}{T_w-T_\infty}, \quad \phi(\xi,\eta) = \frac{\Phi-\Phi_\infty}{\Phi_w-\Phi_\infty}, \quad \chi(\xi,\eta) = \frac{M}{M_w}, \end{aligned}\right\} \tag{5.8}$$

where

$$Gr = \frac{(1-\Phi_\infty)\, g\beta_T\,(T_w-T_\infty)\, L^3}{\nu^2} \quad and \quad Re = \frac{U_\infty L}{\nu}$$

are the Grashof number and Reynolds number. Here ψ is the stream function defined in 2.10 of Chapter2.

Substituting (5.8) in the equations (5.1) to (5.6), and by invoking the boundary layer approximation, we get the following non-dimensional equations.

$$\left(1+\sigma_\xi^2\right) f''' + \frac{1}{2} f f'' - \frac{\xi\sigma_\xi\sigma_{\xi\xi}}{\left(1+\sigma_\xi^2\right)}(f')^2 + \frac{Ri\,(\theta - N_r\phi - R_b\chi)\,\xi}{(1+{\sigma_\xi}^2)}\,(\sin A + \sigma_\xi \cos A) - \frac{Ha^2\xi(f'-1)}{(1+{\sigma_\xi}^2)} = \xi\left[f'\frac{\partial f'}{\partial \xi} - \frac{\partial f}{\partial \xi}f''\right] \tag{5.9}$$

$$\frac{\left(1+\sigma_\xi^2\right)}{\Pr}\left[\theta'' + N_b\phi'\theta' + N_t(\theta')^2\right] + \frac{1}{2}f\theta' + \left(1+\sigma_\xi^2\right)(f'')^2\, Ec + J_0\,(f'-1)^2\,\xi = \xi\left[f'\frac{\partial\theta}{\partial\xi} - \theta'\frac{\partial f}{\partial\xi}\right] \tag{5.10}$$

$$\frac{\left(1+\sigma_\xi^2\right)}{Le}\left[\phi'' + \frac{N_t}{N_b}\theta''\right] + \frac{1}{2}f\phi' = \xi\left[f'\frac{\partial\phi}{\partial\xi} - \phi'\frac{\partial f}{\partial\xi}\right] \tag{5.11}$$

$$\frac{\left(1+\sigma_\xi^2\right)}{Sc}\chi'' - \frac{Pe}{Sc}\,(1-\sigma_\xi)\,(\chi\phi'' + \chi'\phi') + \frac{1}{2}f\chi' = \xi\left[f'\frac{\partial\chi}{\partial\xi} - \chi'\frac{\partial f}{\partial\xi}\right] \tag{5.12}$$

and

$$\left.\begin{aligned} &f'(\xi,0) = 0, \quad f(\xi,0) = -2\xi\left.\frac{\partial f}{\partial\xi}\right|_{(\xi,0)}, \quad \theta(\xi,0) = 1, \quad \phi(\xi,0) = 1, \quad \chi(\xi,0) = 1 \\ &f'(\xi,\infty) = 1, \quad \theta(\xi,\infty) = 0, \quad \phi(\xi,\infty) = 0, \quad \chi(\xi,\infty) = \delta\chi \end{aligned}\right\} \tag{5.13}$$

The parameters Pr, Pe, Le, Sc, N_b, N_r, N_t, R_b are same as in 2.17 of Chapter 2 and mixed convection parameter Ri, Eckert number Ec, magnetic induction number Ha, Joule heating

parameter J_0 are defined by

$$Ri = \frac{Gr}{Re^2}, \quad Ec = \frac{U_\infty^2}{C_{pf}\left(T_w - T_\infty\right)}, \quad Ha^2 = \frac{\sigma_f B_0^2 L}{\rho_{f\infty} U_\infty}, \quad J_0 = EcHa^2 = \frac{\sigma_f B_0^2 L U_\infty}{C_{pf}\left(T_w - T_\infty\right)\rho_{f\infty}}.$$

The quantities Nusselt number, nanoparticle Sherwood number, and motile microorganism density number are studied and their non-dimensional forms are given by

$$\frac{Nu_\xi}{Re_\xi^{1/2}} = -\sqrt{1+\sigma_\xi^2}\,\theta'(\xi,0), \ \frac{NSh_\xi}{Re_\xi^{1/2}} = -\sqrt{1+\sigma_\xi^2}\,\phi'(\xi,0), \ \frac{Q_\xi}{Re_\xi^{1/2}} = -\sqrt{1+\sigma_\xi^2}\,\chi'(\xi,0) \quad (5.14)$$

5.3 Method of Solution

The set of equations (5.9) - (5.12) with (5.13) are solved using BPSLLM [82]. By using this approach, an iteration scheme is obtained by linearizing the non-linear component of single differential equations about a single dependent variable at a time as explained earlier Chapter 2.

On implementing this technique to equations (5.9) - (5.12), we obtain

$$a_{1,m} f'''_{m+1} + a_{2,m} f''_{m+1} + a_{3,m} f'_{m+1} + a_{4,m} f_{m+1} + a_{5,m}\frac{\partial f'_{m+1}}{\partial \xi} + a_{6,m}\frac{\partial f_{m+1}}{\partial \xi} = R_{1,m} \quad (5.15)$$

$$b_{1,m}\theta''_{m+1} + b_{2,m}\theta'_{m+1} + b_{3,m}\theta_{m+1} + b_{4,m}\frac{\partial \theta_{m+1}}{\partial \xi} = R_{2,m} \quad (5.16)$$

$$c_{1,m}\phi''_{m+1} + c_{2,m}\phi'_{m+1} + c_{3,m}\phi_{m+1} + c_{4,m}\frac{\partial \phi_{m+1}}{\partial \xi} = R_{3,m} \quad (5.17)$$

$$d_{1,m}\chi''_{m+1} + d_{2,m}\chi'_{m+1} + d_{3,m}\chi_{m+1} + d_{4,m}\frac{\partial \chi_{m+1}}{\partial \xi} = R_{4,m} \quad (5.18)$$

where the coefficients are

$$a_{1,m} = 1+\sigma_\xi^2, \quad a_{2,m} = \frac{1}{2}f_m + \xi\frac{\partial f_m}{\partial \xi}, \quad a_{3,m} = -\left[\frac{\xi\sigma_\xi\sigma_{\xi\xi}}{1+\sigma_\xi^2}\right]2f'_m - \xi\frac{\partial f'_m}{\partial \xi} - \frac{Ha^2\xi}{(1+{\sigma_\xi}^2)},$$

$$a_{4,m} = \frac{1}{2}f''_m, \quad a_{5,m} = -\xi f'_m, \quad a_{6,m} = \xi f''_m,$$

$$R_{1,m} = \xi f''_m \frac{\partial f_m}{\partial \xi} - \frac{\xi \sigma_\xi \sigma_{\xi\xi}}{1+\sigma_\xi^2}(f'_m)^2 + \frac{1}{2} f_m f''_m - \xi f'_m \frac{\partial f'_m}{\partial \xi},$$
$$- \frac{Ri\,(\theta_m - N_r\,\phi_m - R_b\,\chi_m)\,\xi}{(1+{\sigma_\xi}^2)}\,(\sin A + \sigma_\xi \cos A) - \frac{Ha^2 \xi}{(1+{\sigma_\xi}^2)}$$

$$b_{1,m} = \frac{(1+{\sigma_\xi}^2)}{\mathrm{Pr}}, \quad b_{2,m} = \frac{1+\sigma_\xi^2}{\mathrm{Pr}} N_b \phi'_m + \frac{1+\sigma_\xi^2}{\mathrm{Pr}} 2 N_t \theta'_m + \frac{1}{2} f_{m+1} + \xi \frac{\partial f_{m+1}}{\partial \xi}, \quad b_{3,m} = 0,$$

$$b_{4,m} = -\xi f'_{m+1}, \quad R_{2,m} = \frac{1+\sigma_\xi^2}{\mathrm{Pr}} N_t (\theta'_m)^2 - \left(1+\sigma_\xi^2\right) Ec \left(f''_{m+1}\right)^2 - J_0 \xi \left(f'_{m+1} - 1\right)^2,$$

$$c_{1,m} = \frac{1+\sigma_\xi^2}{Le}, \quad c_{2,m} = \frac{1}{2} f_{m+1} + \xi \frac{\partial f_{m+1}}{\partial \xi}, \quad c_{3,m} = 0, \quad c_{4,m} = -\xi f'_{m+1},$$

$$R_{3,m} = -\frac{1+\sigma_\xi^2}{Le} \frac{N_t}{N_b} \theta''_{m+1}, \; d_{1,m} = \frac{1+\sigma_\xi^2}{Sc}, \; d_{2,m} = \frac{1}{2} f_{m+1} + \xi \frac{\partial f_{m+1}}{\partial \xi} - (1-\sigma_\xi) \frac{Pe}{Sc} \phi'_{m+1},$$

$$d_{3,m} = -\,(1-\sigma_\xi) \frac{Pe}{Sc} \phi''_{m+1}, \quad d_{4,m} = -\xi f'_{m+1}, \quad R_{4,m} = 0.$$

and the boundary conditions (5.13) reduce to

$$\left.\begin{array}{l} f'_{m+1}(\xi,0) = 0\,, \quad f_{m+1}(\xi,0) = -2\xi \left.\dfrac{\partial f}{\partial \xi}\right|_{(\xi,0)}, \quad \theta_{m+1}(\xi,0) = 1, \\ \phi_{m+1}(\xi,0) = 1\,, \quad \chi_{m+1}(\xi,0) = 1 \\ f'_{m+1}(\xi,\infty) = 1, \quad \theta_{m+1}(\xi,\infty) = 0, \quad \phi_{m+1}(\xi,\infty) = 0, \quad \chi_{m+1}(\xi,\infty) = \delta\chi \end{array}\right\} \tag{5.19}$$

Applying psuedo-spectral method in both η and ξ on equations (5.15) to (5.18), we get

$$A^{(1)}\mathbf{F}_i + \gamma^{(1)}_{5,i} \sum_{j=0}^{M} \mathbf{d}_{i,j} \mathbf{D}\mathbf{F}_j + \gamma^{(1)}_{6,i} \sum_{j=0}^{M} \mathbf{d}_{i,j} \mathbf{F}_j = \mathbf{R}_{1,i} \tag{5.20}$$

$$A^{(2)}\mathbf{\Theta}_i + \gamma^{(2)}_{4,i} \sum_{j=0}^{M} \mathbf{d}_{i,j} \mathbf{\Theta}_j = \mathbf{R}_{2,i} \tag{5.21}$$

$$A^{(3)}\mathbf{\Phi}_i + \gamma^{(3)}_{4,i} \sum_{j=0}^{M} \mathbf{d}_{i,j} \mathbf{\Phi}_j = \mathbf{R}_{3,i} \tag{5.22}$$

$$A^{(4)}\chi_i + \gamma^{(4)}_{4,i} \sum_{j=0}^{M} \mathbf{d}_{i,j} \chi_j = \mathbf{R}_{4,i} \tag{5.23}$$

where

$$A^{(1)} = \gamma_{1,i}^{(1)}\mathbf{D}^3 + \gamma_{2,i}^{(1)}\mathbf{D}^2 + \gamma_{3,i}^{(1)}\mathbf{D} + \gamma_{4,i}^{(1)}\mathbf{I},$$
$$A^{(2)} = \gamma_{1,i}^{(2)}\mathbf{D}^2 + \gamma_{2,i}^{(2)}\mathbf{D} + \gamma_{3,i}^{(2)}\mathbf{I},$$
$$A^{(3)} = \gamma_{1,i}^{(3)}\mathbf{D}^2 + \gamma_{2,i}^{(3)}\mathbf{D} + \gamma_{3,i}^{(3)}\mathbf{I},$$
$$A^{(4)} = \gamma_{1,i}^{(4)}\mathbf{D}^2 + \gamma_{2,i}^{(4)}\mathbf{D} + \gamma_{3,i}^{(4)}\mathbf{I}$$

Here $\gamma_{k,i}^{(1)}$, $\gamma_{k,i}^{(2)}$, $\gamma_{k,i}^{(3)}$, $\gamma_{k,i}^{(4)}$ and $\mathbf{R}_{k,i}$ are N^{th} order diagonal matrices with diagonal elements as, $a_{k,m}(\zeta_r, \tau_i)$, $b_{k,m}(\zeta_r, \tau_i)$, $c_{k,m}(\zeta_r, \tau_i)$, $d_{k,m}(\zeta_r, \tau_i)$ and $R_{k,m}(\zeta_r, \tau_i)$ for $r = 1, 2, 3, \cdots N$ respectively and $\mathbf{I}$ refers the identity matrix.

Equation (5.20) in the form of matrix is

$$\begin{bmatrix} A_{0,0}^{(1)} & A_{0,1}^{(1)} & A_{0,2}^{(1)} & \cdots & A_{0,M}^{(1)} \\ A_{1,0}^{(1)} & A_{1,1}^{(1)} & A_{1,2}^{(1)} & \cdots & A_{1,M}^{(1)} \\ A_{2,0}^{(1)} & A_{2,1}^{(1)} & A_{2,2}^{(1)} & \cdots & A_{2,M}^{(1)} \\ \vdots & \vdots & \vdots & \vdots & \vdots \\ A_{M,0}^{(1)} & A_{M,1}^{(1)} & A_{M,2}^{(1)} & \cdots & A_{M,M}^{(1)} \end{bmatrix} \begin{bmatrix} \mathbf{F}_0 \\ \mathbf{F}_1 \\ \mathbf{F}_2 \\ \vdots \\ \mathbf{F}_M \end{bmatrix} = \begin{bmatrix} \mathbf{R}_{1,0} \\ \mathbf{R}_{1,1} \\ \mathbf{R}_{1,2} \\ \vdots \\ \mathbf{R}_{1,M} \end{bmatrix} \tag{5.24}$$

where

$$A_{i,j}^{(1)} = A^{(1)} + \gamma_{5,i}^{(1)}\mathbf{d}_{i,i}\mathbf{D} + \gamma_{6,i}^{(1)}\mathbf{d}_{i,i}\mathbf{I}, \quad for \quad i = j;$$
$$A_{i,j}^{(1)} = \gamma_{5,i}^{(1)}\mathbf{d}_{i,j}\mathbf{D} + \gamma_{6,i}^{(1)}\mathbf{d}_{i,j}\mathbf{I}, \quad for \quad i \neq j \tag{5.25}$$

Similarly, (5.21) to (5.23) can also be written in the form of matrix equations. We solve these equations, iteratively, using suitable initial approximation.

5.4 Computational Results and Discussion

Here, concentration is to examine the effect of inclination angle A, amplitude α, Eckert number Ec, magnetic induction parameter Ha, Joule heating parameter J_o, mixed convection parameter Ri on Nusselt number $Nu_\xi/(Re_\xi)^{\frac{1}{2}}$, nanoparticle Sherwood number $NSh_\xi/(Re_\xi)^{\frac{1}{2}}$ and density number of motile microorganisms' $Q_\xi/(Re_\xi)^{\frac{1}{2}}$.

Figure 5.1 provides the effect of the angle of the wavy surface A on required parameters. It is clear from the figures 5.1(b) and 5.1(c) that, $NSh_\xi/(Re_\xi)^{\frac{1}{2}}$ and $Q_\xi/(Re_\xi)^{\frac{1}{2}}$ are increasing

rapidly against the increase in angle A. But $Nu_\xi/(Re_\xi)^{\frac{1}{2}}$, is increasing in the first half of the channel and decreasing in the second half, against the increase in angle A. This can be observed in 5.1(a). Hence we can say that the inclinations of the surface also play an important role in varying the local heat parameter, nanoparticle mass transfer, and density of motile microorganisms.

The parameters $Nu_\xi/(Re_\xi)^{\frac{1}{2}}$, $NSh_\xi/(Re_\xi)^{\frac{1}{2}}$ and $Q_\xi/(Re_\xi)^{\frac{1}{2}}$ behave typically with respect amplitude of the wavy surface α, which we can observe in figures 5.2(a) to 5.2(c). As there is an increment in amplitude, we found both increasing and decreasing nature in the profiles based on the parameter ξ. The profiles of $Nu_\xi/(Re_\xi)^{\frac{1}{2}}$, $NSh_\xi/(Re_\xi)^{\frac{1}{2}}$ and $Q_\xi/(Re_\xi)^{\frac{1}{2}}$ are found to be increasing and decreasing nature for an increase in α. Also we found overall raise in $NSh_\xi/(Re_\xi)^{\frac{1}{2}}$ and $Q_\xi/(Re_\xi)^{\frac{1}{2}}$ and overall fall in $Nu_\xi/(Re_\xi)^{\frac{1}{2}}$, when we move across the channel from left to right. This concludes in general that, increasing the wave amplitude roughens the surface more.

The effect of Eckert number Ec on $Nu_\xi/(Re_\xi)^{\frac{1}{2}}$, $NSh_\xi/(Re_\xi)^{\frac{1}{2}}$ and $Q_\xi/(Re_\xi)^{\frac{1}{2}}$ is spotted in figure 5.3. It is found from the figures 5.3(b) - 5.3(c) that, the parameters $NSh_\xi/(Re_\xi)^{\frac{1}{2}}$ and $Q_\xi/(Re_\xi)^{\frac{1}{2}}$ are increasing with an increase in Ec and an raise in the values of Ec results in the decrease of $Nu_\xi/(Re_\xi)^{\frac{1}{2}}$ as depicted in figure 5.3(a).

The variation of $Nu_\xi/(Re_\xi)^{\frac{1}{2}}$, $NSh_\xi/(Re_\xi)^{\frac{1}{2}}$ and $Q_\xi/(Re_\xi)^{\frac{1}{2}}$ for different values of magnetic induction Ha is displayed in figure 5.4. The figures 5.4(b) and 5.4(c) shows that increase in the values of magnetic induction results in an increase in $NSh_\xi/(Re_\xi)^{\frac{1}{2}}$ and $Q_\xi/(Re_\xi)^{\frac{1}{2}}$. But, when there is a raise in the values of magnetic induction, $Nu_\xi/(Re_\xi)^{\frac{1}{2}}$ falls down as observed in Fig. 5.4(a).

The influence of Joule heating parameter J_o is represented in figures 5.5(a) - 5.5(c). It is observed that the amplification of Joule heating parameter concludes in shrinkage of dimensionless parameter given by $Nu_\xi/(Re_\xi)^{\frac{1}{2}}$ and raise in $NSh_\xi/(Re_\xi)^{\frac{1}{2}}$, $Q_\xi/(Re_\xi)^{\frac{1}{2}}$.

The effect of mixed convection parameter Ri on $Nu_\xi/(Re_\xi)^{\frac{1}{2}}$, $NSh_\xi/(Re_\xi)^{\frac{1}{2}}$ and $Q_\xi/(Re_\xi)^{\frac{1}{2}}$ is depicted graphically in figure 5.6. It is found that, the parameter $Nu_\xi/(Re_\xi)^{\frac{1}{2}}$ is decreasing for a raise in mixed convection parameter Ri. It is observed that the parameters $NSh_\xi/(Re_\xi)^{\frac{1}{2}}$, $Q_\xi/(Re_\xi)^{\frac{1}{2}}$ are rising in anticipation of a rise in the mixed convection parameter Ri

5.5 Conclusions

In this chapter, a theoretical model for mixed convection of a nanofluid past an inclined wavy surface in the presence of gyrotactic microorganisms and the magnetic field is presented. The bivariate pseudo-spectral local linearization method along with the Chebyshev collocation method is used to solve the nonlinear ordinary differential equations with given boundary conditions. The following are the key findings:

- An increase in the wave amplitude α gives overall raise in nanoparticle mass transfer rate $NSh_\xi/(Re_\xi)^{\frac{1}{2}}$ and density of motile microorganisms $Q_\xi/(Re_\xi)^{\frac{1}{2}}$.
- The nanoparticle mass transfer rate $NSh_\xi/(Re_\xi)^{\frac{1}{2}}$ and the density of motile microorganisms $Q_\xi/(Re_\xi)^{\frac{1}{2}}$ are increasing, for all parameters under consideration.
- The effect of Eckert number decreases the local heat parameter $Nu_\xi/(Re_\xi)^{\frac{1}{2}}$ and increases $NSh_\xi/(Re_\xi)^{\frac{1}{2}}$, $Q_\xi/(Re_\xi)^{\frac{1}{2}}$.
- A decrease in heat transfer rate $Nu_\xi/(Re_\xi)^{\frac{1}{2}}$ is observed for an increase in magnetic induction.
- The Joule heating parameter influences for a raise in $NSh_\xi/(Re_\xi)^{\frac{1}{2}}$, $Q_\xi/(Re_\xi)^{\frac{1}{2}}$ and fall in $Nu_\xi/(Re_\xi)^{\frac{1}{2}}$.

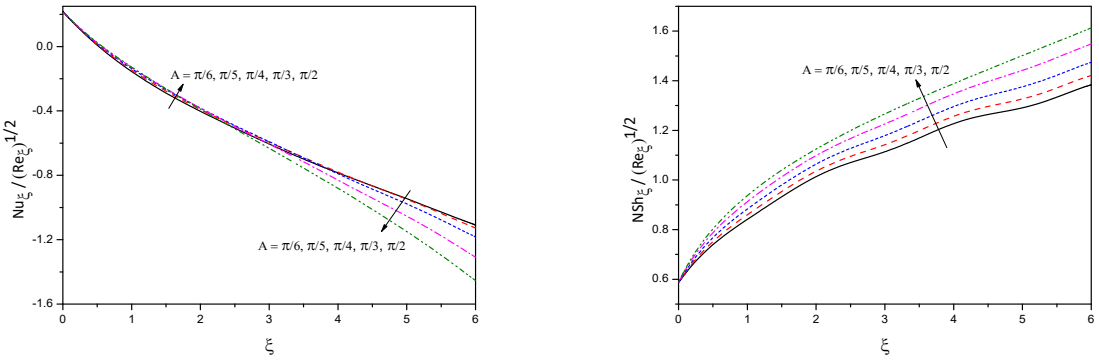

(a)

(b)

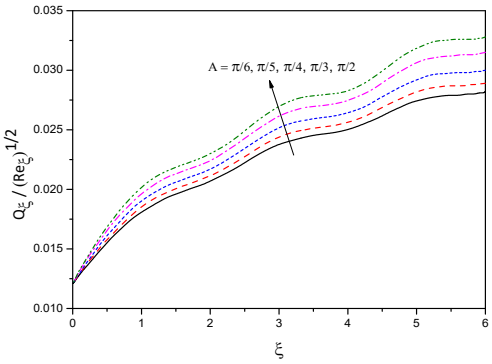

(c)

Figure 5.1: "Effect of the angle of inclination A on the profiles of (a) $\frac{Nu_\xi}{Re_\xi^{1/2}}$ (b) $\frac{NSh_\xi}{Re_\xi^{1/2}}$ (c) $\frac{Q_\xi}{Re_\xi^{1/2}}$".

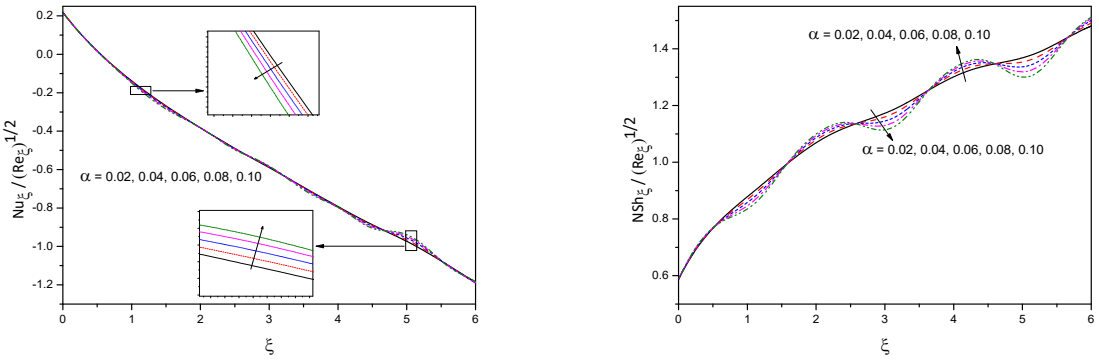

(a)

(b)

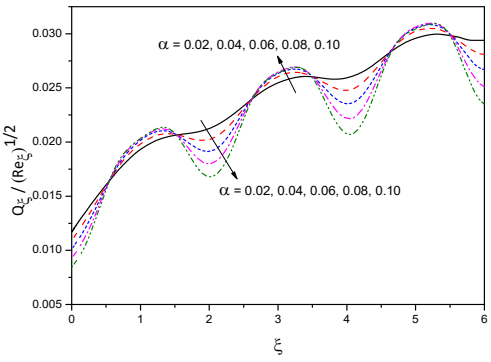

(c)

Figure 5.2: "Effect of the amplitude of the wavy surface α on the profiles of (a) $\frac{Nu_\xi}{Re_\xi^{1/2}}$ (b) $\frac{NSh_\xi}{Re_\xi^{1/2}}$ (c) $\frac{Q_\xi}{Re_\xi^{1/2}}$".

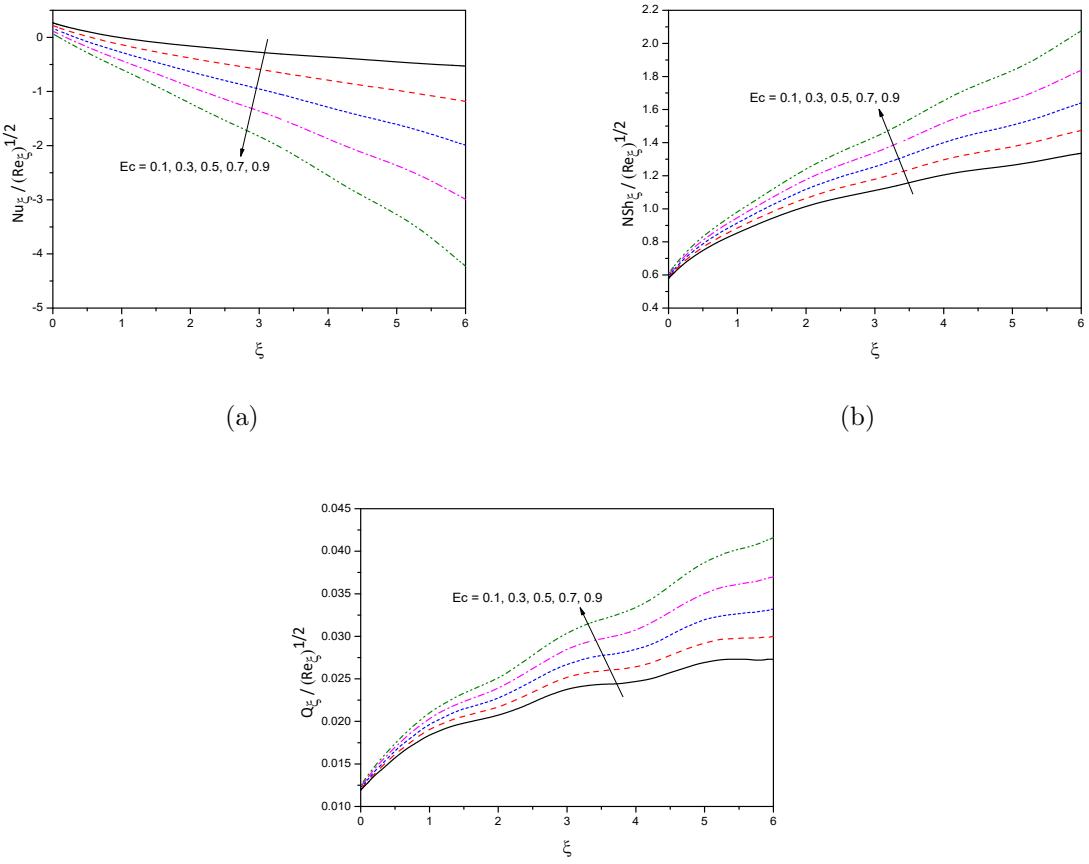

(a) (b)

(c)

Figure 5.3: "Effect of the Eckert number Ec on the profiles of (a) $\frac{Nu_\xi}{Re_\xi^{1/2}}$ (b) $\frac{NSh_\xi}{Re_\xi^{1/2}}$ (c) $\frac{Q_\xi}{Re_\xi^{1/2}}$".

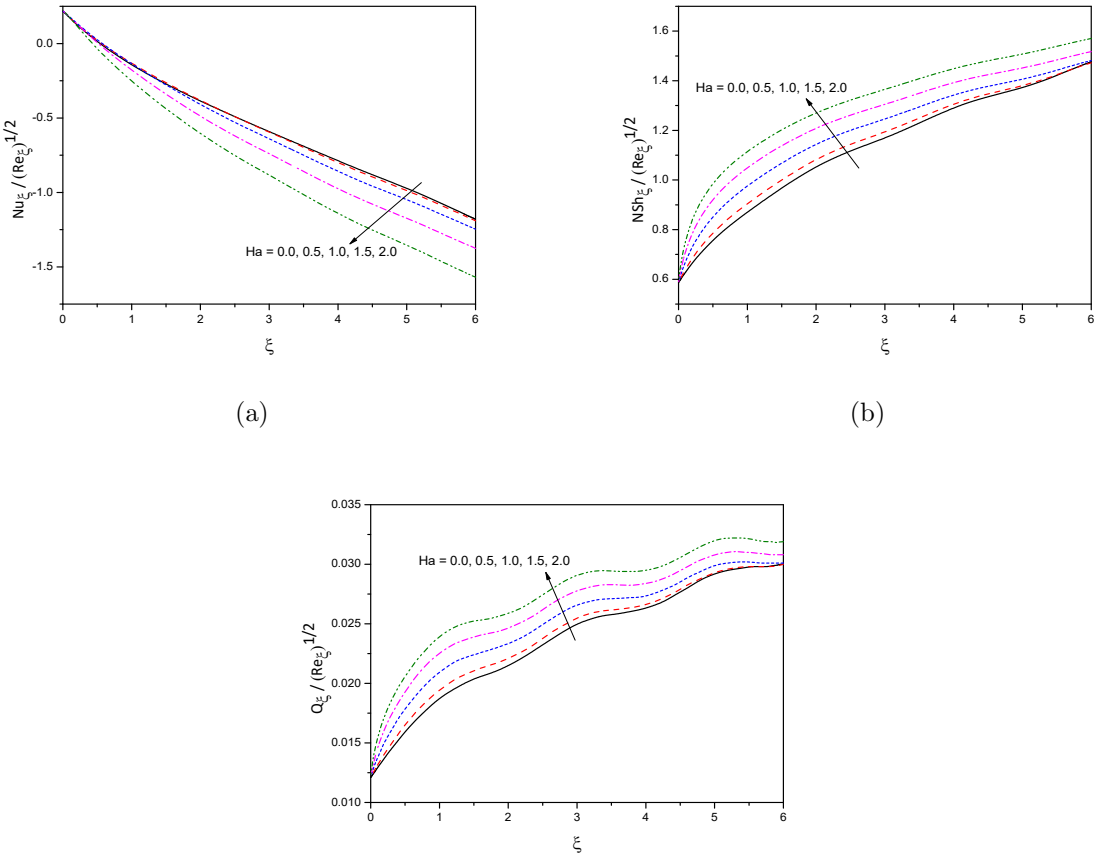

Figure 5.4: "Effect of the magnetic induction parameter Ha on the profiles of (a) $\frac{Nu_\xi}{Re_\xi^{1/2}}$ (b) $\frac{NSh_\xi}{Re_\xi^{1/2}}$ (c) $\frac{Q_\xi}{Re_\xi^{1/2}}$".

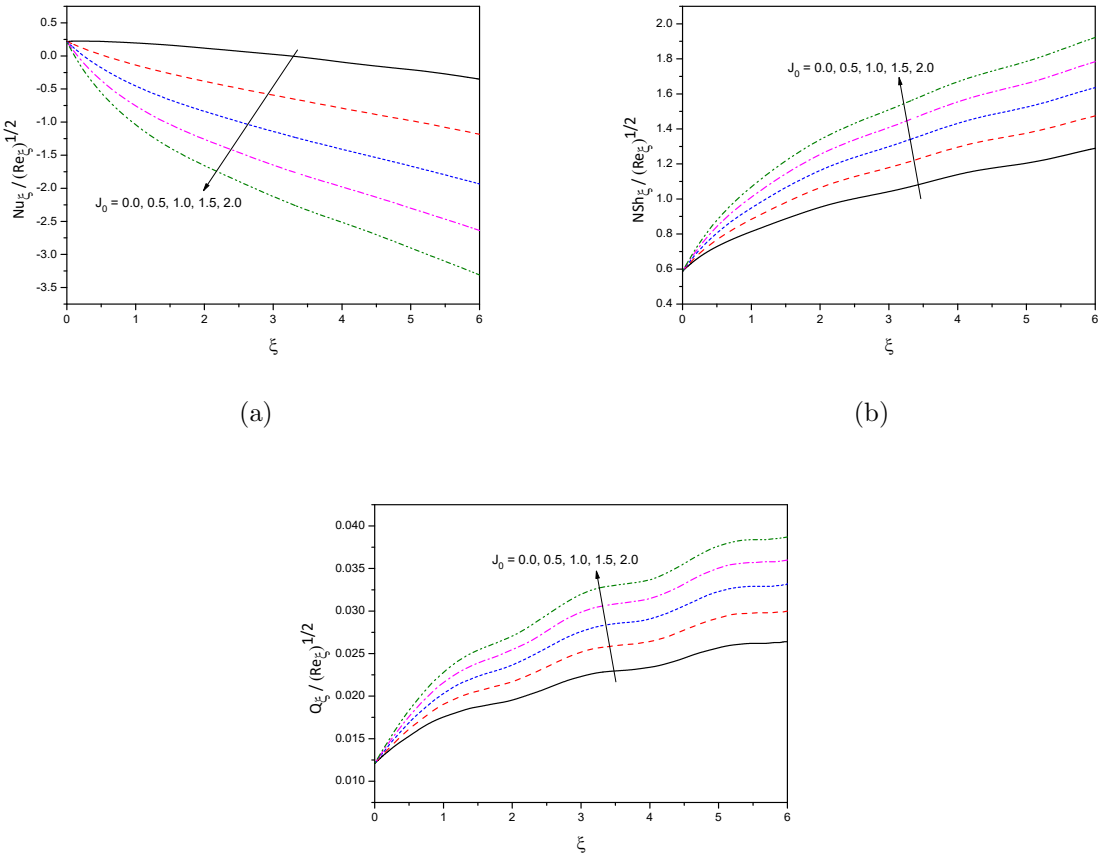

Figure 5.5: "Effect of the Joule heating parameter J_0 on the profiles of (a) $\frac{Nu_\xi}{Re_\xi^{1/2}}$ (b) $\frac{NSh_\xi}{Re_\xi^{1/2}}$ (c) $\frac{Q_\xi}{Re_\xi^{1/2}}$".

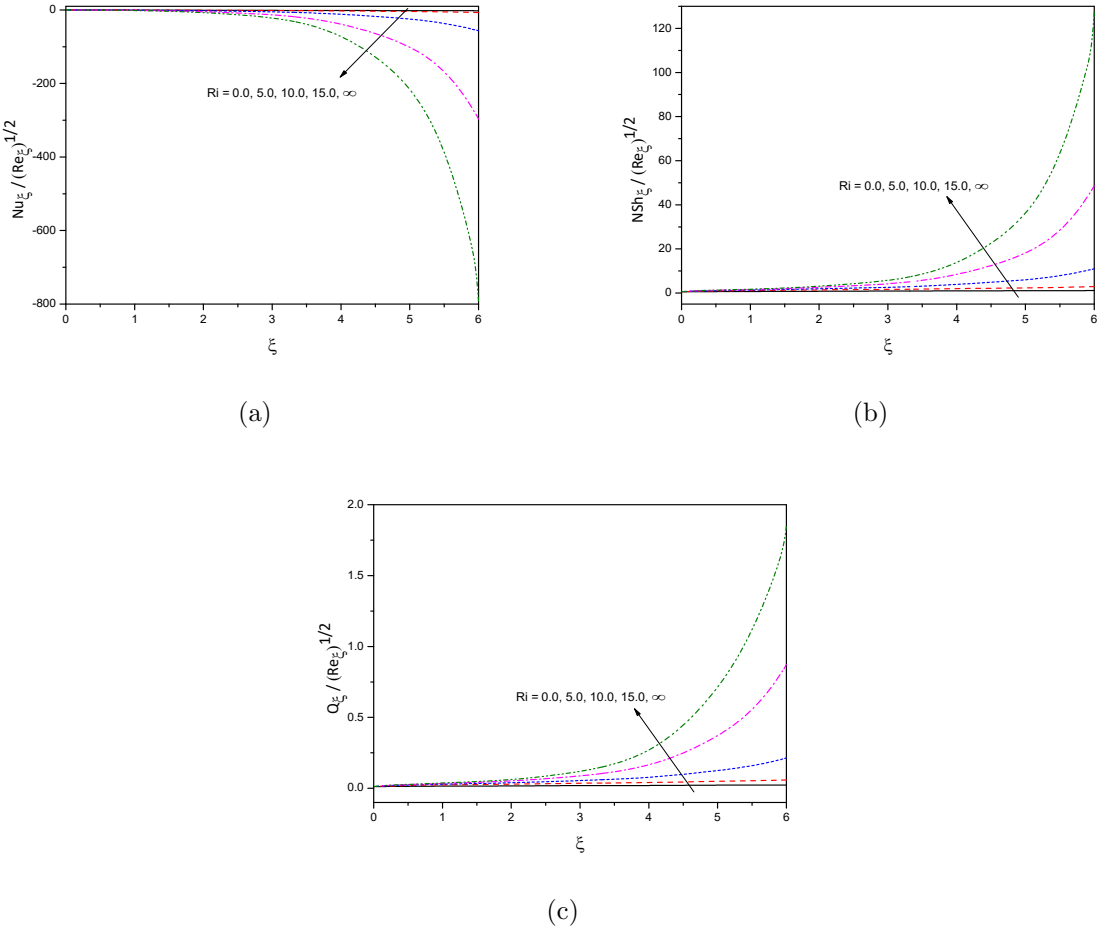

(a) (b)

(c)

Figure 5.6: "Effect of the mixed convection parameter Ri on the profiles of (a) $\frac{Nu_\xi}{Re_\xi^{1/2}}$ (b) $\frac{NSh_\xi}{Re_\xi^{1/2}}$ (c) $\frac{Q_\xi}{Re_\xi^{1/2}}$".

Chapter 6

Effect of variable properties on the Bioconvection in the Flow of Nanofluid over an Inclined Wavy Surface [1]

6.1 Introduction

The characteristics of fluids, such as viscosity and thermal conductivity, are well known to change with temperature. The intensification in temperature speeds up the transport phenomena by decreasing viscosity all over the thermal boundary layer, which influences the rate of heat and mass transfer. Heydari and Shokouhmand [45] studied the variable fluid properties along with nanoparticles through micro-annulus on nanofluid flow and heat transfer. Hayat *et al.* [44] discussed the influence of changeable thermal conductivity on the mixed convective flow past a cylinder in a viscoelastic nanofluid in the presence of heat source/sink. Nanofluid bioconvection with variable thermophysical properties was studied by Siddiqa *et al.* [15] for the geometry of uniformly heated vertical cone. Animasaun *et al.* [9] investigated the effect of radiation along with variable thermal conductivity and viscosity on the free convective over a moving porous vertical semi-infinite plate. Srinivasacharya *et al.* [116] examined the consequence of thermophoresis and variable fluid properties on the convection over a sinusoidal surface in a porous medium. Mjankwi *et al. et al.* [77] examined the unsteady

[1] Communicated to "**Computational Thermal Sciences**"

magnetohydrodynamics flow of a nanofluid in the presence of chemical reaction and thermal radiation over an inclined stretching sheet with variable fluid properties. The study of Viscosity depending on the temperature of magnetohydrodynamics nanofluid flow past porous plate has been done by Shahid *et al.* [106]. Hussain *et al.* [48] discussed variable viscosity, thermal conductivity effect on the slip flow, and heat transfer of nanofluids over a porous plate. Nandal and Bhargava [85] discussed convectively heated inclined plate in a nanofluid for variable fluid properties and magnetic field. Several researchers [105, 10, 68, 107, 6] also discussed temperature-dependent viscosity and temperature-dependent thermal conductivity for different geometries and in different conditions in nanofluids. Amirsom *et al.* [7] studied the impact of melting, dissipation, and magnetic field on the nanofluid bioconvection with variable thermophysical properties and second-order slip. Natural convection with heat transfer improvement and variable viscosity using hybrid nanofluids was discussed by Manjunatha *et al.* [69]. Haddad *et al.* [41] analyzed the significance of Brownian motion and thermophoresis effects in nanofluid heat transfer enrichment.

In this chapter, we considered the effect of variable properties on the bioconvection in a nanofluid flow past an inclined wavy surface. The influence of pertinent parameters on the Nusselt number, nanoparticle Sherwood number, and density number of the microbes are examined.

6.2 Mathematical Formulation

Consider the incompressible, steady, and laminar flow of a nanofluid consisting of motile microorganisms over an inclined wavy surface. The physical model and coordinate system are shown in Fig. 2.1

The equations governing the flow [90, 19] considered are

$$\frac{\partial U}{\partial X}+\frac{\partial V}{\partial Y}=0 \tag{6.1}$$

$$\rho_{f\infty}\left(U\frac{\partial U}{\partial X}+V\frac{\partial U}{\partial Y}\right)=-\frac{\partial P}{\partial X}+2\frac{\partial}{\partial X}\left(\mu(T)\frac{\partial U}{\partial X}\right)+2\frac{\partial}{\partial Y}\left(\mu(T)\left[\frac{\partial U}{\partial Y}+\frac{\partial V}{\partial X}\right]\right)$$
$$+\left[\left(1-\Phi_{\infty}\right)\beta_T\rho_{f\infty}\left(T-T_{\infty}\right)-\left(\rho_p-\rho_{f\infty}\right)\left(\Phi-\Phi_{\infty}\right)-\beta_M(\rho_m-\rho_{f\infty})M\right]gSinA \tag{6.2}$$

$$\rho_{f\infty}\left(U\frac{\partial V}{\partial X}+V\frac{\partial V}{\partial Y}\right)=-\frac{\partial P}{\partial Y}+2\frac{\partial}{\partial X}\left(\mu(T)\left[\frac{\partial U}{\partial Y}+\frac{\partial V}{\partial X}\right]\right)+2\frac{\partial}{\partial Y}\left(\mu(T)\frac{\partial V}{\partial Y}\right)$$
$$+\left[(1-\Phi_\infty)\,\beta_T\rho_{f\infty}\,(T-T_\infty)-(\rho_p-\rho_{f\infty})\,(\Phi-\Phi_\infty)-\beta_M(\rho_m-\rho_{f\infty})M\right]gCosA \quad (6.3)$$

$$(\rho c)_f\left(U\frac{\partial T}{\partial X}+V\frac{\partial T}{\partial Y}\right)=\frac{\partial}{\partial X}\left(k(T)\frac{\partial T}{\partial X}\right)+\frac{\partial}{\partial Y}\left(k(T)\frac{\partial T}{\partial Y}\right)$$
$$+(\rho c)_p\left\{D_B\left(\frac{\partial\Phi}{\partial X}\frac{\partial T}{\partial X}+\frac{\partial\Phi}{\partial Y}\frac{\partial T}{\partial Y}\right)+\frac{D_T}{T_\infty}\left[\left(\frac{\partial T}{\partial X}\right)^2+\left(\frac{\partial T}{\partial Y}\right)^2\right]\right\} \quad (6.4)$$

$$U\frac{\partial\Phi}{\partial X}+V\frac{\partial\Phi}{\partial Y}=D_B\left(\frac{\partial^2\Phi}{\partial X^2}+\frac{\partial^2\Phi}{\partial Y^2}\right)+\frac{D_T}{T_\infty}\left(\frac{\partial^2 T}{\partial X^2}+\frac{\partial^2 T}{\partial Y^2}\right) \quad (6.5)$$

$$U\frac{\partial M}{\partial X}+V\frac{\partial M}{\partial Y}+\frac{\partial}{\partial X}\left(M\widetilde{V}\right)+\frac{\partial}{\partial Y}\left(M\widetilde{V}\right)=D_n\left(\frac{\partial^2 M}{\partial X^2}+\frac{\partial^2 M}{\partial Y^2}\right) \quad (6.6)$$

Here, the average swimming velocity of microorganism is $\widetilde{V}=\dfrac{b_c w_c}{\Phi_w-\Phi_\infty}\dfrac{\partial\Phi}{\partial Y}$. The viscosity μ, the thermal conductivity k are considered as linear functions of temperature [14] given by

$$\mu(T)=\mu_\infty\left[1+A(T_w-T)\right] \qquad \text{and} \qquad k(T)=k_0\left[1+B(T-T_\infty)\right] \quad (6.7)$$

where μ_∞ is the absolute viscosity of the fluid, k_0 is the thermal conductivity and A and B are constants. All other quantities are defined in previous Chapters.

The associated conditions on the boundary are :

$$\left.\begin{array}{l} U=0,\ V=0,\ T=T_w,\ \Phi=\Phi_w,\ M=M_w \text{ at } Y=\sigma(X) \\ U\to 0,\ T\to T_\infty,\ \Phi\to\Phi_\infty,\ M\to M_\infty \text{ as } Y\to\infty \end{array}\right\} \quad (6.8)$$

The irregular wavy surface is converted to a plane surface using the following transformations [131]

$$\left.\begin{array}{l} \xi=\dfrac{X}{L},\quad \eta=\dfrac{Y-\sigma}{L\xi^{\frac{1}{4}}}Gr^{\frac{1}{4}},\quad \psi=\dfrac{\mu_\infty Gr^{\frac{1}{2}}\xi^{\frac{3}{4}}}{\rho_{f\infty}}f(\xi,\eta),\quad p=\dfrac{PL^2Gr^{-1}}{\rho_{f\infty}\nu^2}, \\ \theta(\xi,\eta)=\dfrac{T-T_\infty}{T_w-T_\infty},\quad \phi(\xi,\eta)=\dfrac{\Phi-\Phi_\infty}{\Phi_w-\Phi_\infty},\quad \chi(\xi,\eta)=\dfrac{M}{M_w} \end{array}\right\} \quad (6.9)$$

where

$$Gr=\frac{(1-\Phi_\infty)\,g\beta_T\,(T_w-T_\infty)\,L^3}{\nu^2}$$

is the Grashof number. Here the stream function ψ is same as in 2.10 of Chapter2.

The non-dimensional form of Eq. (6.7) is

$$\mu(\theta) = \mu_\infty \left[1 + \epsilon(1-\theta)\right] \qquad \text{and} \qquad k(\theta) = k_0 \left[1 + \beta\theta\right] \tag{6.10}$$

where $\epsilon = A(T_w - T_\infty)$ and $\beta = B(T_w - T_\infty)$ are the temperature dependent viscosity and thermal conductivity parameters.

Substituting Eq. (6.9) in the governing equations (6.1) to (6.6) and invoking the boundary layer approximation, we get,

$$\begin{aligned}\left(1+\sigma_\xi^2\right)\left([1+\epsilon(1-\theta)]f''' - \epsilon\theta' f''\right) + \frac{3}{4}ff'' - \left[\frac{1}{2} + \frac{\xi\sigma_\xi\sigma_{\xi\xi}}{\left(1+\sigma_\xi^2\right)}\right](f')^2 \\ + \frac{(\theta - N_r\phi - R_b\chi)}{\left(1+\sigma_\xi^2\right)}\left(\sin A + \sigma_\xi \cos A\right) = \xi\left[f'\frac{\partial f'}{\partial \xi} - \frac{\partial f}{\partial \xi}f''\right]\end{aligned} \tag{6.11}$$

$$\frac{\left(1+\sigma_\xi^2\right)}{\mathrm{Pr}}\left[(1+\beta\theta)\theta'' + \beta(\theta')^2 + N_b\phi'\theta' + N_t(\theta')^2\right] + \frac{3}{4}f\theta' = \xi\left[f'\frac{\partial\theta}{\partial\xi} - \theta'\frac{\partial f}{\partial\xi}\right] \tag{6.12}$$

$$\frac{\left(1+\sigma_\xi^2\right)}{Le}\left[\phi'' + \frac{N_t}{N_b}\theta''\right] + \frac{3}{4}f\phi' = \xi\left[f'\frac{\partial\phi}{\partial\xi} - \phi'\frac{\partial f}{\partial\xi}\right] \tag{6.13}$$

$$\frac{\left(1+\sigma_\xi^2\right)}{Sc}\chi'' - \frac{Pe}{Sc}\left(1-\sigma_\xi\right)\left(\chi\phi'' + \chi'\phi'\right) + \frac{3}{4}f\chi' = \xi\left[f'\frac{\partial\chi}{\partial\xi} - \chi'\frac{\partial f}{\partial\xi}\right] \tag{6.14}$$

and

$$\left.\begin{aligned} &f'(\xi,0) = 0, \quad f(\,\xi,\,0) = -\frac{4}{3}\xi\left.\frac{\partial f}{\partial\xi}\right|_{(\,\xi,0)}, \quad \theta\,(\,\xi,\,0) = \ \phi\,(\,\xi,\,0) = \ \chi\,(\,\xi,\,0) = 1 \\ &f'\,(\,\xi,\,\infty) = 0, \quad \theta\,(\,\xi,\,\infty) = 0, \quad \phi\,(\,\xi,\,\infty) = 0, \quad \chi\,(\,\xi,\,\infty) = \delta\chi \end{aligned}\right\} \tag{6.15}$$

The parameters Pr, Pe, Sc, Le, N_b, N_r, N_t, R_b are same as in 2.17 of Chapter 2.

The non-dimensional form of the coefficient of skin friction, Nusselt number, nanoparticle mass transfer rate, and density number of motile microbe are given in 2.19 of Chapter 2.

6.3 Method of Solution

The set of equations (6.11) - (6.15) is solved using the BPSLLM [82]. By using this approach, an iteration scheme is obtained by linearizing the non-linear component of single differential equations about a single dependent variable at a time, as we saw in chapter 2.

On implementing this technique to equations (6.11) - (6.14), we obtain

$$a_{1,m}f'''_{m+1} + a_{2,m}f''_{m+1} + a_{3,m}f'_{m+1} + a_{4,m}f_{m+1} + a_{5,m}\frac{\partial f'_{m+1}}{\partial \xi} + a_{6,m}\frac{\partial f_{m+1}}{\partial \xi} = R_{1,m} \tag{6.16}$$

$$b_{1,m}\theta''_{m+1} + b_{2,m}\theta'_{m+1} + b_{3,m}\theta_{m+1} + b_{4,m}\frac{\partial \theta_{m+1}}{\partial \xi} = R_{2,m} \tag{6.17}$$

$$c_{1,m}\phi''_{m+1} + c_{2,m}\phi'_{m+1} + c_{3,m}\frac{\partial \phi_{m+1}}{\partial \xi} = R_{3,m} \tag{6.18}$$

$$d_{1,m}\chi''_{m+1} + d_{2,m}\chi'_{m+1} + d_{3,m}\chi_{m+1} + d_{4,m}\frac{\partial \chi_{m+1}}{\partial \xi} = R_{4,m} \tag{6.19}$$

where the coefficients are

$$a_{1,m} = [1+\epsilon(1-\theta_m)]\left(1+\sigma_\xi^2\right), \quad a_{2,m} = -\epsilon\left(1+\sigma_\xi^2\right)\theta'_m + \frac{3}{4}f_m + \xi\frac{\partial f_m}{\partial \xi},$$

$$a_{3,m} = -2\left[\frac{1}{2} + \frac{\xi\sigma_\xi\sigma_{\xi\xi}}{1+\sigma_\xi^2}\right]f'_m - \xi\frac{\partial f'_m}{\partial \xi}, \quad a_{4,m} = \frac{3}{4}f''_m, \quad a_{5,m} = -\xi f'_r, \quad a_{6,m} = \xi f''_r,$$

$$R_{1,m} = \xi f''_m\frac{\partial f_m}{\partial \xi} - \left[\frac{1}{2} + \frac{\xi\sigma_\xi\sigma_{\xi\xi}}{1+\sigma_\xi^2}\right](f'_m)^2 + \frac{3}{4}f_m f''_m - \xi f'_m\frac{\partial f'_m}{\partial \xi}$$
$$-\frac{(\theta_m - N_r\,\phi_m - R_b\,\chi_m)}{(1+{\sigma_\xi}^2)}(\sin A + \sigma_\xi \cos A)$$

$$b_{1,m} = \frac{(1+\beta\theta_m)\,(1+{\sigma_\xi}^2)}{\mathrm{Pr}}, \quad b_{2,m} = \frac{(1+\sigma_\xi^2)}{\mathrm{Pr}}N_b\phi'_m + \frac{2(1+\sigma_\xi^2)(\beta+N_t)}{\mathrm{Pr}}\theta'_m + \frac{3}{4}f_{m+1} + \xi\frac{\partial f_{m+1}}{\partial \xi},$$

$$b_{3,m} = \frac{\beta(1+\sigma_\xi^2)}{\mathrm{Pr}}\theta''_r, \quad b_{4,m} = -\xi f'_{m+1},$$

$$R_{2,m} = \frac{(1+\sigma_\xi^2)(\beta+N_t)}{\mathrm{Pr}}(\theta'_m)^2 + \frac{\beta(1+\sigma_\xi^2)}{Pr}\theta''_m\theta_m$$

$$c_{1,m} = \frac{1+\sigma_\xi^2}{Le}, \quad c_{2,m} = \frac{3}{4}f_{m+1} + \xi\frac{\partial f_{m+1}}{\partial \xi}, \quad c_{3,m} = -\xi f'_{m+1},$$

$$R_{3,m} = -\frac{(1+\sigma_\xi^2)}{Le}\frac{N_t}{N_b}\theta''_{m+1},$$

$$d_{1,m} = \frac{1+\sigma_\xi^2}{Sc}, \quad d_{2,m} = \frac{3}{4}f_{m+1} + \xi\frac{\partial f_{m+1}}{\partial \xi} - (1-\sigma_\xi)\frac{Pe}{Sc}\phi'_{m+1},$$

$$d_{3,m} = -(1-\sigma_\xi)\frac{Pe}{Sc}\phi''_{m+1}, \quad d_{4,m} = -\xi f'_{m+1}, \quad R_{4,m} = 0$$

The conditions on the boundary are

$$\left.\begin{array}{l} f'_{m+1}(\xi,0)=0\,, \quad f_{m+1}(\xi,0)=-\dfrac{4}{3}\xi\left.\dfrac{\partial f}{\partial \xi}\right|_{(\xi,0)}, \quad \theta_{m+1}(\xi,0)=1, \\ \phi_{m+1}(\xi,0)=1\,, \quad \chi_{m+1}(\xi,0)=1 \\ f'_{m+1}(\xi,\infty)=0, \quad \theta_{m+1}(\xi,\infty)=0, \quad \phi_{m+1}(\xi,\infty)=0, \quad \chi_{m+1}(\xi,\infty)=\delta\chi \end{array}\right\} \tag{6.20}$$

The set of linearized equations (6.16) to (6.19) is solved by applying bivariate Chebyshev spectral collocation method [20]. Implementing this method in both η and ξ directions, we get

$$A^{(1)}\mathbf{F}_i+\gamma^{(1)}_{5,i}\sum_{j=0}^{M}\mathbf{d}_{i,j}\mathbf{D}\mathbf{F}_j+\gamma^{(1)}_{6,i}\sum_{j=0}^{M}\mathbf{d}_{i,j}\mathbf{F}_j=\mathbf{R}_{1,i} \tag{6.21}$$

$$A^{(2)}\mathbf{\Theta}_i+\gamma^{(2)}_{4,i}\sum_{j=0}^{M}\mathbf{d}_{i,j}\mathbf{\Theta}_j=\mathbf{R}_{2,i} \tag{6.22}$$

$$A^{(3)}\mathbf{\Phi}_i+\gamma^{(3)}_{3,i}\sum_{j=0}^{M}\mathbf{d}_{i,j}\mathbf{\Phi}_j=\mathbf{R}_{3,i} \tag{6.23}$$

$$A^{(4)}\chi_i+\gamma^{(4)}_{4,i}\sum_{j=0}^{M}\mathbf{d}_{i,j}\chi_j=\mathbf{R}_{4,i} \tag{6.24}$$

where

$$\begin{aligned} A^{(1)}&=\gamma^{(1)}_{1,i}\mathbf{D}^3+\gamma^{(1)}_{2,i}\mathbf{D}^2+\gamma^{(1)}_{3,i}\mathbf{D}+\gamma^{(1)}_{4,i}\mathbf{I}, \\ A^{(2)}&=\gamma^{(2)}_{1,i}\mathbf{D}^2+\gamma^{(2)}_{2,i}\mathbf{D}+\gamma^{(2)}_{3,i}\mathbf{I}, \\ A^{(3)}&=\gamma^{(3)}_{1,i}\mathbf{D}^2+\gamma^{(3)}_{2,i}\mathbf{D}, \\ A^{(4)}&=\gamma^{(4)}_{1,i}\mathbf{D}^2+\gamma^{(4)}_{2,i}\mathbf{D}+\gamma^{(4)}_{3,i}\mathbf{I} \end{aligned}$$

Here $\gamma^{(1)}_{k,i}$, $\gamma^{(2)}_{k,i}$, $\gamma^{(3)}_{k,i}$, $\gamma^{(4)}_{k,i}$ and $\mathbf{R}_{k,i}$ are N^{th} order diagonal matrices with diagonal elements as, $a_{k,m}(\zeta_r,\tau_i)$, $b_{k,m}(\zeta_r,\tau_i)$, $c_{k,m}(\zeta_r,\tau_i)$, $d_{k,m}(\zeta_r,\tau_i)$ and $R_{k,m}(\zeta_r,\tau_i)$ for $r=1,2,3,\cdots N$ respectively and $\mathbf{I}$ refers the identity matrix.

The equation (6.21) written in matrix form as

$$\begin{bmatrix} A^{(1)}_{0,0} & A^{(1)}_{0,1} & A^{(1)}_{0,2} & \cdots & A^{(1)}_{0,M} \\ A^{(1)}_{1,0} & A^{(1)}_{1,1} & A^{(1)}_{1,2} & \cdots & A^{(1)}_{1,M} \\ A^{(1)}_{2,0} & A^{(1)}_{2,1} & A^{(1)}_{2,2} & \cdots & A^{(1)}_{2,M} \\ \vdots & \vdots & \vdots & \cdots & \vdots \\ A^{(1)}_{M,0} & A^{(1)}_{M,1} & A^{(1)}_{M,2} & \cdots & A^{(1)}_{M,M} \end{bmatrix} \begin{bmatrix} \mathbf{F}_0 \\ \mathbf{F}_1 \\ \mathbf{F}_2 \\ \vdots \\ \mathbf{F}_M \end{bmatrix} = \begin{bmatrix} \mathbf{R}_{1,0} \\ \mathbf{R}_{1,1} \\ \mathbf{R}_{1,2} \\ \vdots \\ \mathbf{R}_{1,M} \end{bmatrix} \tag{6.25}$$

where

$$\begin{aligned} A^{(1)}_{i,j} &= A^{(1)} + \gamma^{(1)}_{5,r}\mathbf{d}_{i,i}\mathbf{D} + \gamma^{(1)}_{6,r}\mathbf{d}_{i,i}\mathbf{I},\ \ for\ i = j; \\ A^{(1)}_{i,j} &= \gamma^{(1)}_{5,r}\mathbf{d}_{i,j}\mathbf{D} + \gamma^{(1)}_{6,r}\mathbf{d}_{i,j}\mathbf{I},\ \ for\ i \neq j \end{aligned} \tag{6.26}$$

In a similar manner, the equations (6.22) to (6.24) can be written in matrix form. Solving these matrix equations, iteratively, we obtain the solution to (6.11) - (6.15).

6.4 Computational Results and Discussion

To validate the method accuracy, the code developed is tested by comparing the existing numerical values of the coefficients of skin friction and rate of heat transfer with the published results of Hossain *et al.* [46] for diverse values of Prandtl number Pr by taking inclination angle $A = \pi/2$, the wavy surface amplitude $\alpha = 0.01$, and ignoring the parameters Pe, Le, Sc, N_b, N_r, N_t, R_b, β, ϵ and $\delta\chi$. The computed results are demonstrated in Table 6.1. It is perceived from Table 6.1 that our results are matching with the results of Hossain *et al.* [46].

Table 6.1: Comparative analysis for the values of $f''(x,0)$ and $-\theta'(x,0)$ by the present method for $Pe = 10^{-5}$, $Le = 10^{-5}$, $Sc = 10^{-5}$, $N_b = 10^{-5}$, $N_t = 0.0$, $N_r = 0.0$, $R_b = 0.0$, $\alpha = 0.01$, $A = \pi/2$, $\delta\chi = 0.0$, $\beta = 0.0$, $\epsilon = 0.0$ with the results of Hossain *et al.* [46]

$f''(x,0)$			$-\theta'(x,0)$	
Pr	Present	Hossain *et al.* [46]	Present	Hossain *et al.* [46]
1. 0	0.907109	0.908	0.400750	0.401
10.0	0.591821	0.591	0.825911	0.825
25.0	0.486460	0.485	1.067343	1.066
50.0	0.416407	0.485	1.287233	1.066
100.0	0.354761	0.352	1.546196	1.542

The focus of this investigation is to analyse the effect of bioconvection Peclet number Pe, bioconvection Rayleigh number Rb, inclination angle A, amplitude of the wavy surface α, Browninan motion parameter N_b, Thermophoresis parameter N_t, bioconvection Schmidt number Sc, variable viscosity parameter ϵ, variable thermal conductivity parameter β, on coefficient of skin friction $Cf_\xi(Gr_\xi)^{\frac{1}{4}}$, Nusselt number $Nu_\xi/(Gr_\xi)^{\frac{1}{4}}$, nanoparticle Sherwood number $NSh_\xi/(Gr_\xi)^{\frac{1}{4}}$ and density number of motile microbes $Q_\xi/(Gr_\xi)^{\frac{1}{4}}$. All the Numerical computations are carried out by assigning $Pr = 10.0$, $Pe = 2.0$, $Le = 5.0$, $A = \pi/4$, $N_b = 0.05$, $N_r = 0.03$, $N_t = 0.01$, $R_b = 0.05$, $Sc = 2.0$, $\alpha = 0.01$, $\delta\chi = 0.01$, $\beta = 0.1$, and $\epsilon = 0.1$ unless otherwise mentioned.

The variation of non-dimensional skin friction coefficient, local Nusselt number, nanoparticle Sherwood number, and density number of motile microorganisms for distinct values of bioconvection Peclet number Pe is displayed in Fig. 6.1. An increase in the bioconvection Peclet number increases all the physical quantities under consideration as shown in the graphs. The bioconvection Peclet number is the ratio of the characteristic velocity due to gyrotactic swimming to a characteristic velocity due to random diffusive swimming. Since the microorganisms are heavier than water, their up-swimming creates unstable density stratification. Pe helps to intensify the speed of the microorganisms in the fluid and so the density number of the microorganisms is enhanced at the wavy surface.

The impact of R_b, bioconvection Rayleigh number on the coefficient of skin friction, local heat transfer rate, local nanoparticle mass transfer rate and local motile microorganism density number is presented in Figs. 6.2(a) - 6.2(d). It is noticed that, as the bioconvection Rayleigh number rises, the physical quantities $Cf_\xi(Gr_\xi)^{\frac{1}{4}}$, $Nu_\xi/(Gr_\xi)^{\frac{1}{4}}$, $NSh_\xi/(Gr_\xi)^{\frac{1}{4}}$ and $Q_\xi/(Gr_\xi)^{\frac{1}{4}}$ decrease. The movement of the nanoparticles present in the base fluid is the explanation for this. These nanoparticles moves in the fluid arbitrarily, and the fluid temperature gradually rises.

Figure 6.3 presents the effect of the angle of the inclination A on $Cf_\xi(Gr_\xi)^{\frac{1}{4}}$, $Nu_\xi/(Gr_\xi)^{\frac{1}{4}}$, $NSh_\xi/(Gr_\xi)^{\frac{1}{4}}$ and $Q_\xi/(Gr_\xi)^{\frac{1}{4}}$. The skin friction coefficient, local Nusselt number, nanoparticle Sherwood number and density number of motile microorganism are increasing as the inclination angle A increase. As a result, on a vertical wavy surface, all physical quantities are greater than on a horizontal wavy surface.

Figure 6.4 presents the variation of the coefficient of skin friction, local heat transfer rate, local nanoparticle mass transfer rate, and local motile microorganism density number for the amplitude of the wavy surface α. As ξ rises, it is discovered that the profiles have both an increasing and decreasing nature. For an increase in α, the profiles of $Cf_\xi(Gr_\xi)^{\frac{1}{4}}$,

$Nu_\xi/(Gr_\xi)^{\frac{1}{4}}$, $NSh_\xi/(Gr_\xi)^{\frac{1}{4}}$ and $Q_\xi/(Gr_\xi)^{\frac{1}{4}}$ are found to be increasing.

The effect of N_b, Brownian motion parameter, on the skin friction coefficient, local Nusselt number, nanoparticle Sherwood number and density number of motile microorganism is depicted in figure 6.5. It is noticed from the figures 6.5(a), 6.5(c), 6.5(d) that, $Cf_\xi(Gr_\xi)^{\frac{1}{4}}$, $NSh_\xi/(Gr_\xi)^{\frac{1}{4}}$ and $Q_\xi/(Gr_\xi)^{\frac{1}{4}}$ are increasing with increase in Brownian motion parameter. This is because, when the Browninan motion increases, there is a raise in the thermal boundary layer thickness, therefore results for the reduced nanoparticle concentration. An improvement in the values of the Brownian motion parameter results in the decrease of $Nu_\xi/(Gr_\xi)^{\frac{1}{4}}$ as shown in figure 6.5(b).

The impact of the thermophoresis parameter N_t, which can be perceived in figures 6.6(a) to 6.6(d). One can identify from these figures that, for a rise in the thermophoresis parameter, the physical quantities $Cf_\xi(Gr_\xi)^{\frac{1}{4}}$, $Nu_\xi/(Gr_\xi)^{\frac{1}{4}}$, $NSh_\xi/(Gr_\xi)^{\frac{1}{4}}$ and $Q_\xi/(Gr_\xi)^{\frac{1}{4}}$ are decreasing.

Figure 6.7 represents the effect of the bioconvection Schmidt number Sc, on the coefficient of skin friction, local heat transfer rate, local nanoparticle mass transfer rate, and local motile microorganism density number. It is observed from figures 6.7(a) to 6.7(d), that the physical quantities rise, for a rise in bioconvection Schmidt number. Physically this is because the bioconvection Schmidt number rises, the viscous diffusion rate enhances which in turn decreases the dimensionless velocity and consequently increases the density number of the microorganisms.

Figure 6.8 demonstrates the effect of the variable viscosity parameter ϵ on the skin friction coefficient, local Nusselt number, nanoparticle Sherwood number, and density number of motile microorganisms. It is noticed that the effect variable viscosity parameter on the coefficient of skin friction is marginal. A close observation of Fig. 6.8(a) reveals that the skin friction coefficient is increasing with a rise in ϵ. Further, the profiles of local Nusselt number, nanoparticle Sherwood number, and density number of motile microorganisms are found to be decreasing with an increase in ϵ.

The influence of variable thermal conductivity parameter β on the coefficient of skin friction, local heat transfer rate, local nanoparticle mass transfer rate and local motile microorganism density number is demonstrated in figure 6.9. It is depicted that these quantities $Cf_\xi(Gr_\xi)^{\frac{1}{4}}$, $NSh_\xi/(Gr_\xi)^{\frac{1}{4}}$ and $Q_\xi/(Gr_\xi)^{\frac{1}{4}}$ are increasing for an increase in the thermal conductivity parameter β and the parameter $Nu_\xi/(Gr_\xi)^{\frac{1}{4}}$, is decreasing for an rise in the variable thermal conductivity parameter β.

The variation of physical quantities with the microorganism slip parameter $\delta\chi$ is depicted in figure 6.10. It is found that not much variation or tiny variation in the profiles of $Cf_\xi(Gr_\xi)^{\frac{1}{4}}$, $Nu_\xi/(Gr_\xi)^{\frac{1}{4}}$, $NSh_\xi/(Gr_\xi)^{\frac{1}{4}}$ is observed. An increase in the parameter $\delta\chi$, decreases the coefficient of skin friction, local heat transfer rate, local nanoparticle mass transfer rate and local motile microorganism density number.

6.5 Conclusions

In this chapter, an analysis is presented to study the nanofluid flow over an inclined sinusoidal surface with natural convection in the existence of gyrotactic microorganisms with variable properties. The nonlinear equations are linearized employing local linearization procedure and the resultant system is solved by a bivariate pseudo-spectral collocation method. Important observations are itemized below:

- An increase in the bioconvection Peclet number and bioconvection Schmidt number enhances the skin friction coefficient, heat transfer rate and nanoparticle mass transfer rate, and density of motile microorganisms. A reverse trend is noticed for the influence of bioconvection Rayleigh number.
- The influence of Brownian motion parameter is to increase and thermophoresis is to decrease the coefficient of skin friction, nanoparticle mass transfer rate, and density of motile organisms.
- The heat transfer rate, nanoparticle mass transfer rate, and motile microorganism density number are decreasing whereas the skin friction coefficient is not affected by an increase in the variable viscosity parameter.
- An increase in variable thermal conductivity parameter increases the skin friction coefficient, nanoparticle Sherwood number, and density number of motile microorganism whereas decreases the Nusselt number.

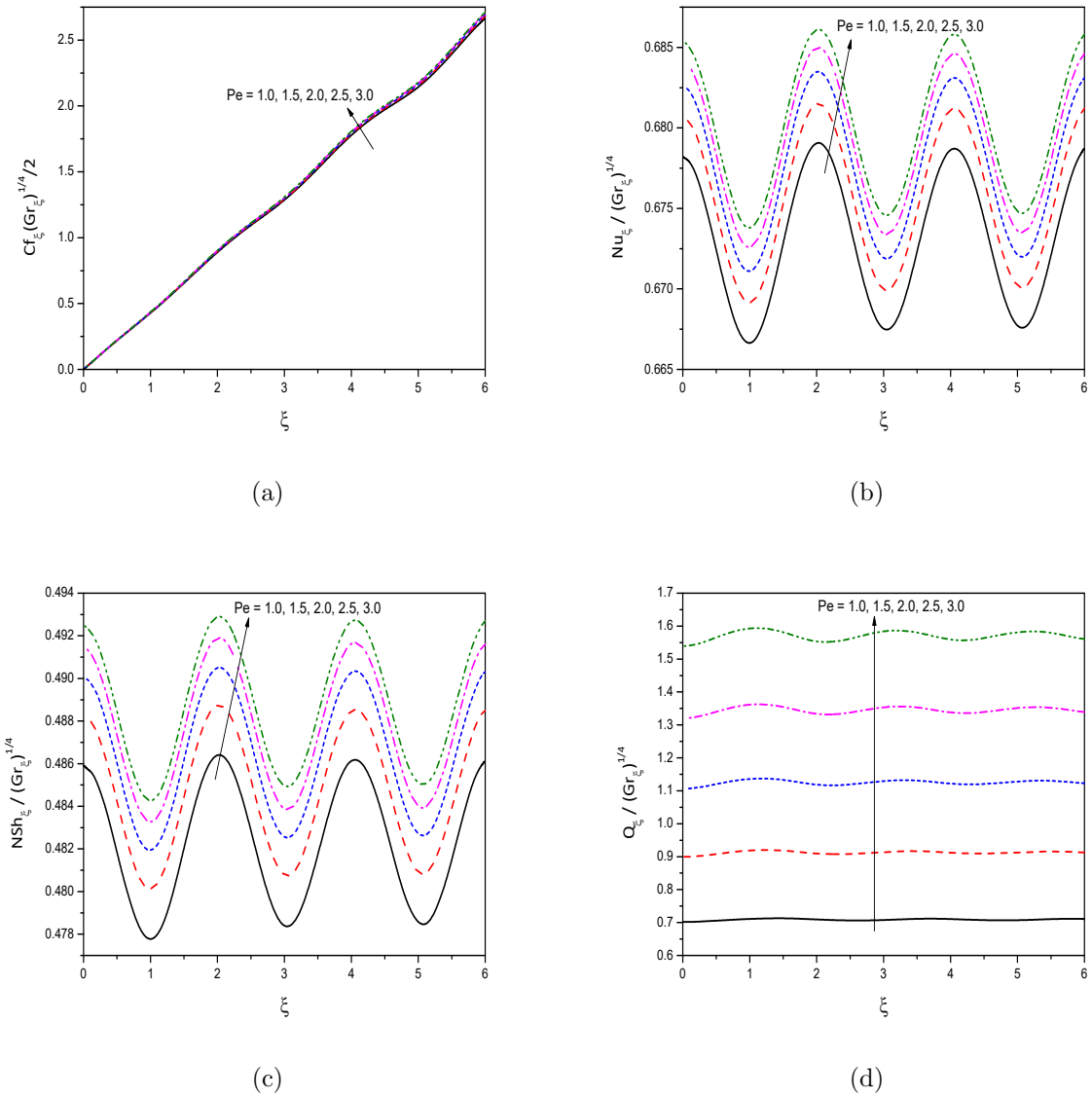

Figure 6.1: "Effect of the bioconvection Peclet number Pe on the profiles of (a) $Cf_\xi(Gr_\xi^{1/4})/2$ (b) $\frac{Nu_\xi}{Gr_\xi^{1/4}}$ (c) $\frac{NSh_\xi}{Gr_\xi^{1/4}}$ (d) $\frac{Q_\xi}{Gr_\xi^{1/4}}$".

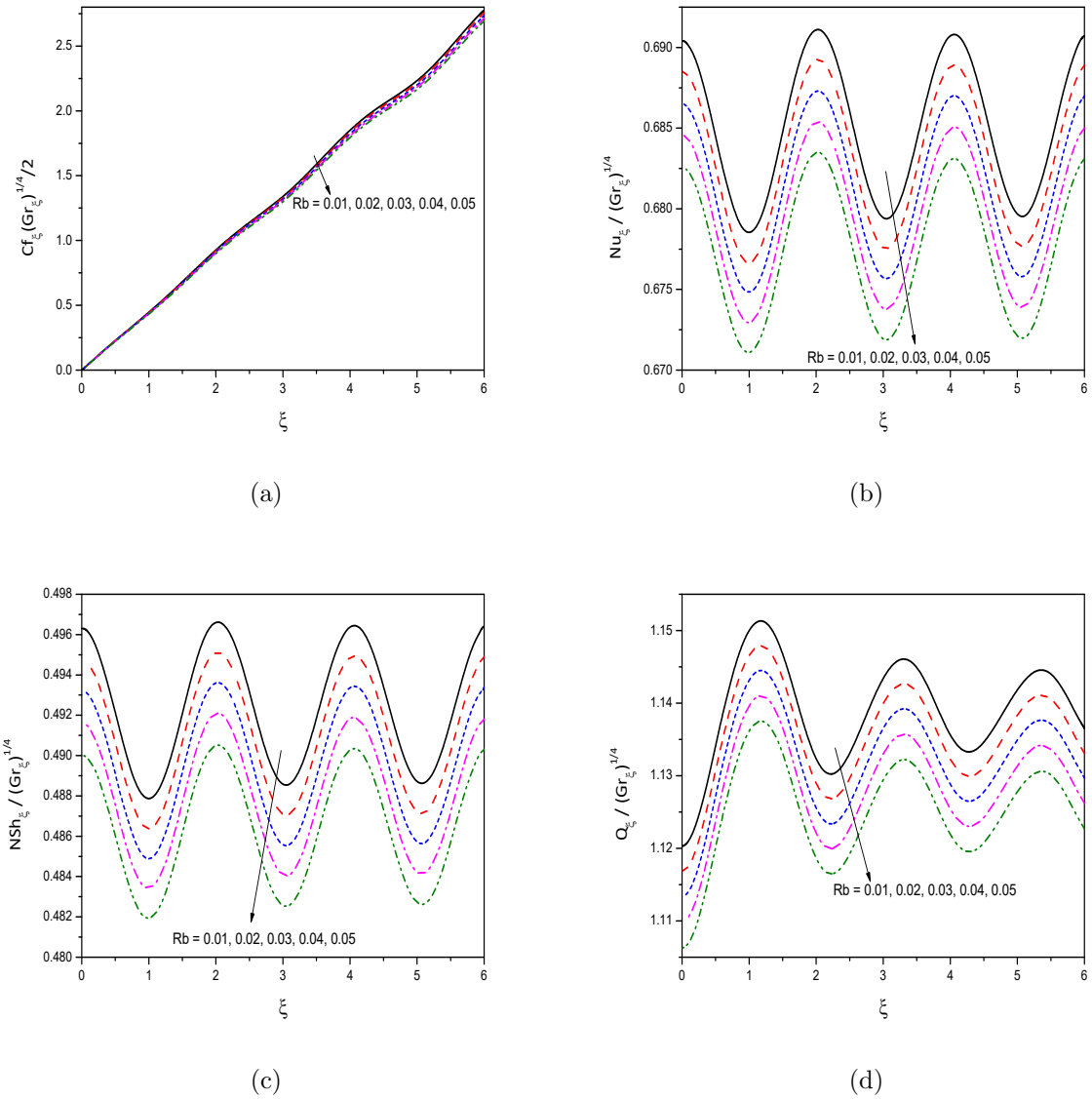

Figure 6.2: "Effect of the bioconvection Rayleigh number on the profiles of (a) $Cf_\xi(Gr_\xi^{1/4})/2$ (b) $\frac{Nu_\xi}{Gr_\xi^{1/4}}$ (c) $\frac{NSh_\xi}{Gr_\xi^{1/4}}$ (d) $\frac{Q_\xi}{Gr_\xi^{1/4}}$".

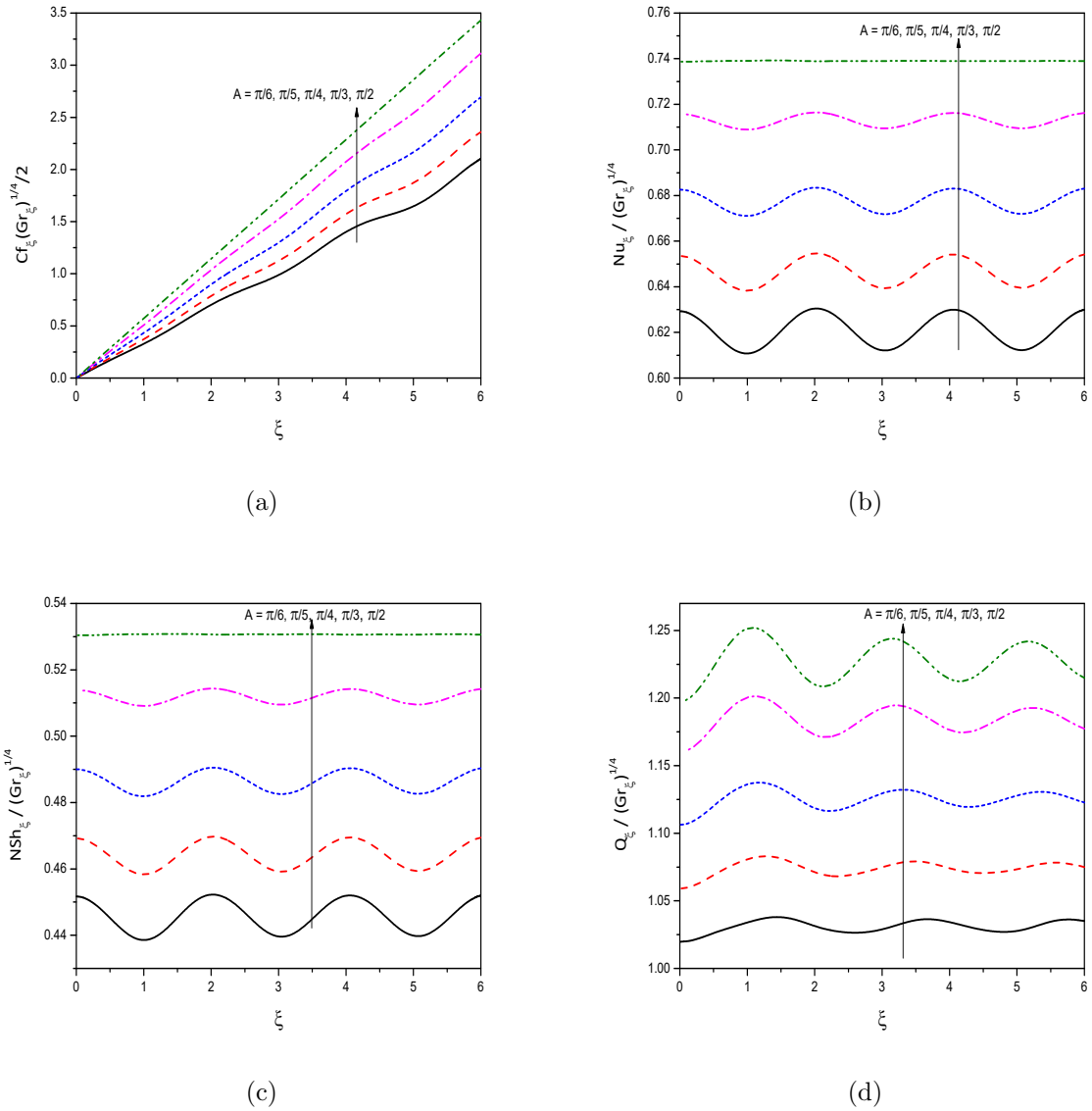

Figure 6.3: "Effect of angle of inclination A on the profiles of (a) $Cf_\xi(Gr_\xi^{1/4})/2$ (b) $\frac{Nu_\xi}{Gr_\xi^{1/4}}$ (c) $\frac{NSh_\xi}{Gr_\xi^{1/4}}$ (d) $\frac{Q_\xi}{Gr_\xi^{1/4}}$".

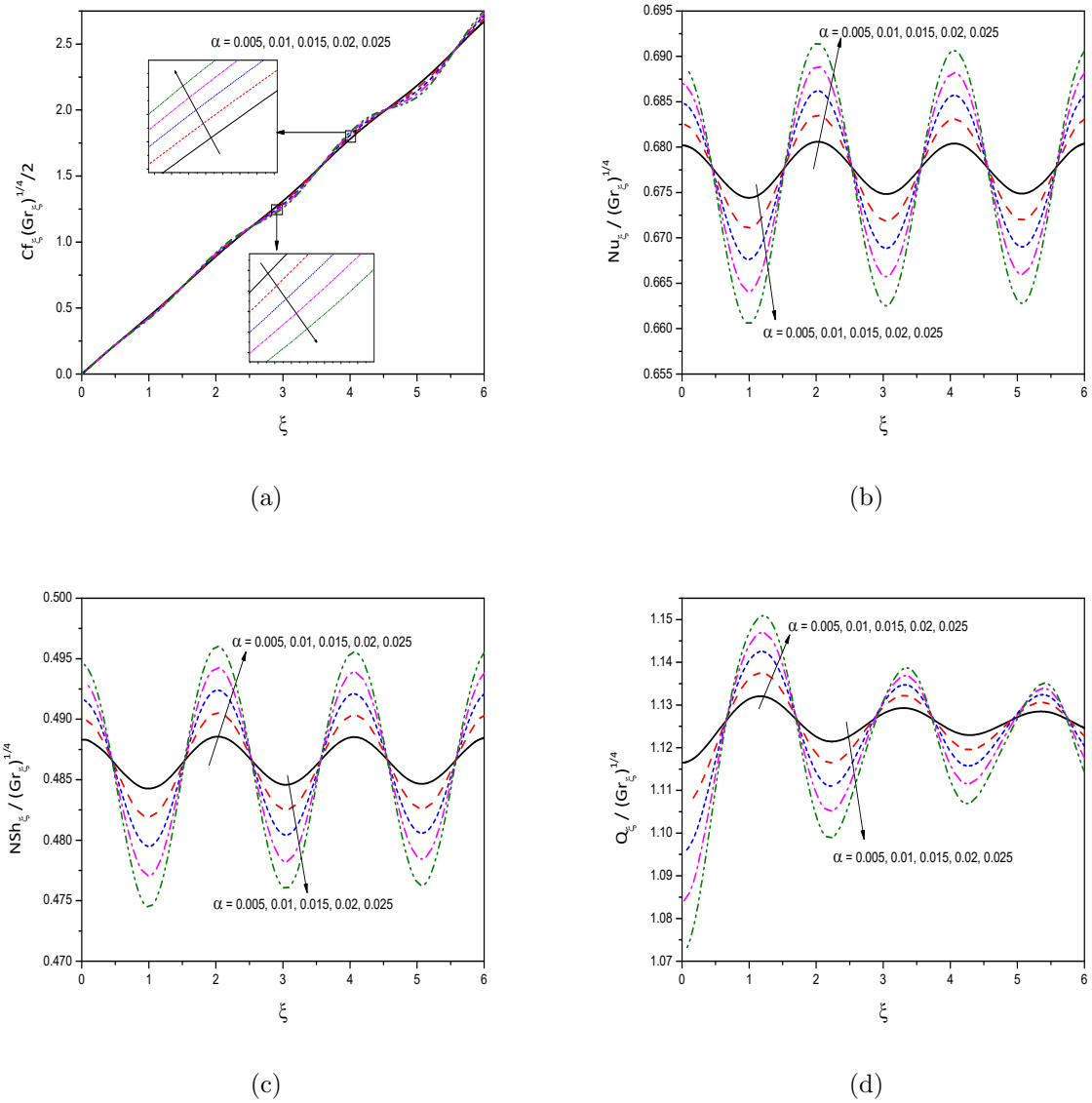

Figure 6.4: "Effect of the amplitude of the wavy surface α on the profiles of (a) $Cf_\xi(Gr_\xi^{1/4})/2$ (b) $\frac{Nu_\xi}{Gr_\xi^{1/4}}$ (c) $\frac{NSh_\xi}{Gr_\xi^{1/4}}$ (d) $\frac{Q_\xi}{Gr_\xi^{1/4}}$".

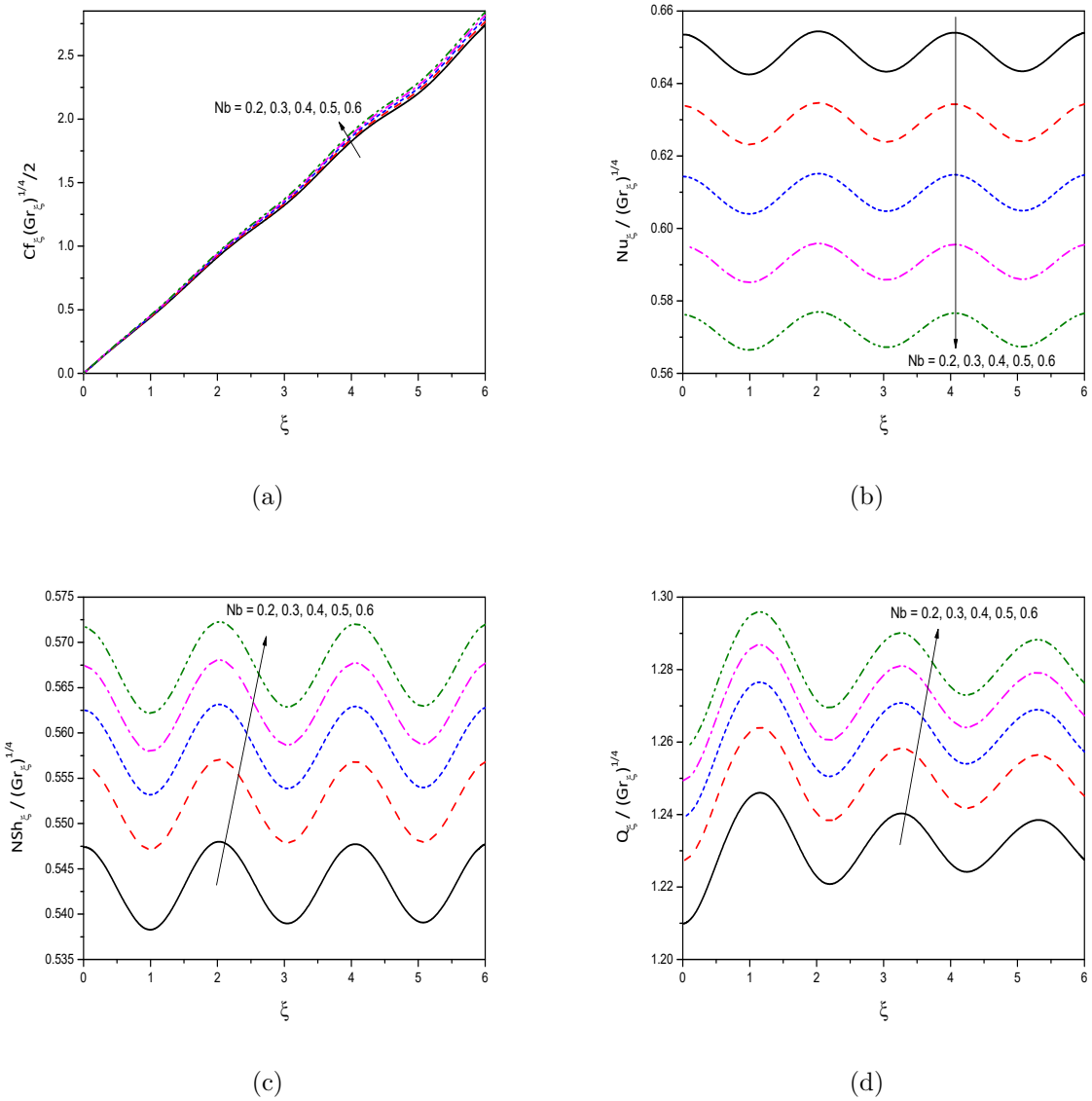

Figure 6.5: "Effect of the Brownian motion parameter N_b on the profiles of (a) $Cf_\xi(Gr_\xi^{1/4})/2$ (b) $\frac{Nu_\xi}{Gr_\xi^{1/4}}$ (c) $\frac{NSh_\xi}{Gr_\xi^{1/4}}$ (d) $\frac{Q_\xi}{Gr_\xi^{1/4}}$".

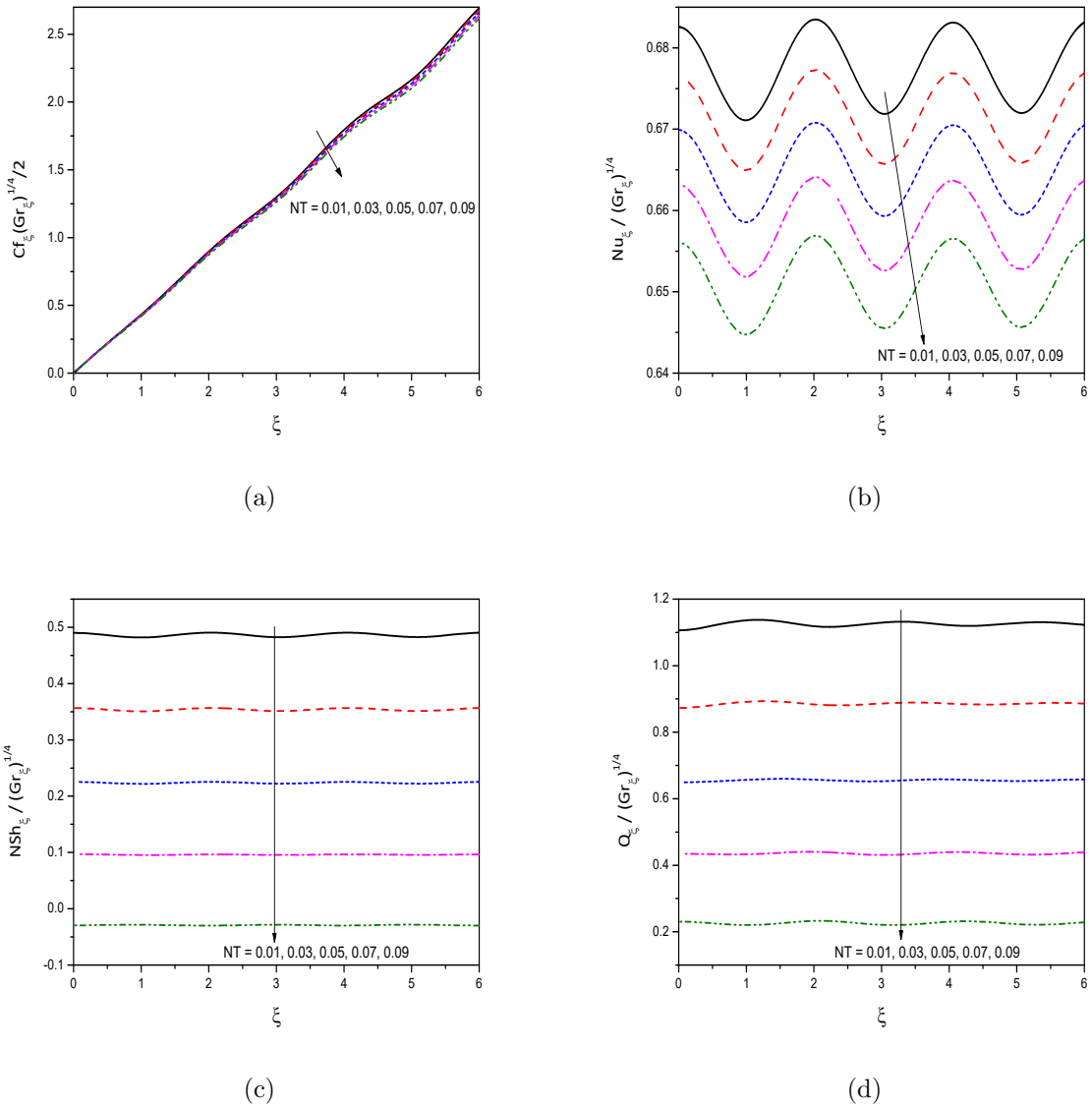

Figure 6.6: "Effect of the thermophoresis parameter N_t on the profiles of (a) $Cf_\xi(Gr_\xi^{1/4})/2$ (b) $\frac{Nu_\xi}{Gr_\xi^{1/4}}$ (c) $\frac{NSh_\xi}{Gr_\xi^{1/4}}$ (d) $\frac{Q_\xi}{Gr_\xi^{1/4}}$".

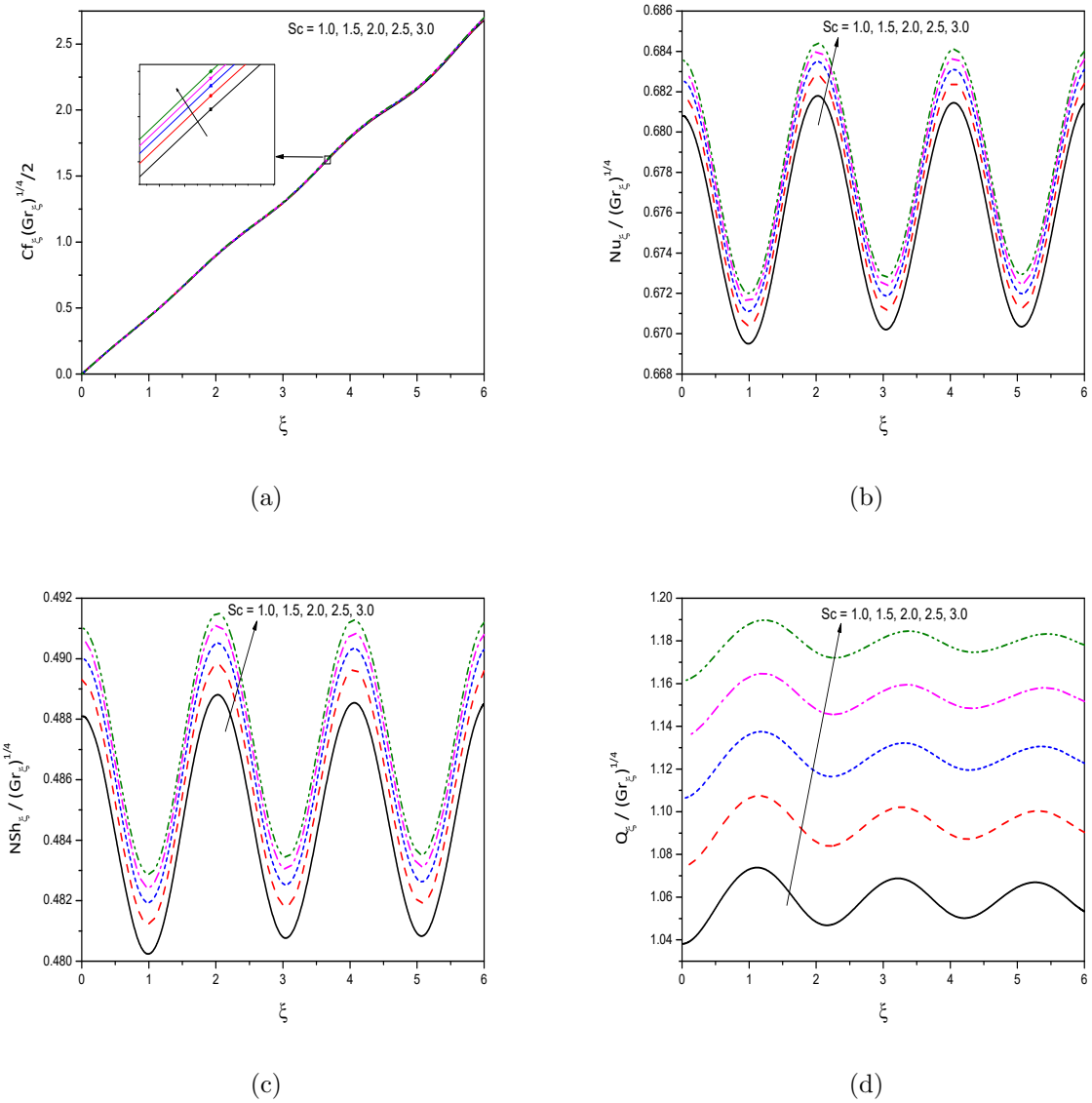

Figure 6.7: "Effect of the bioconvection Schmidt number Sc on the profiles of (a) $Cf_\xi(Gr_\xi^{1/4})/2$ (b) $\frac{Nu_\xi}{Gr_\xi^{1/4}}$ (c) $\frac{NSh_\xi}{Gr_\xi^{1/4}}$ (d) $\frac{Q_\xi}{Gr_\xi^{1/4}}$".

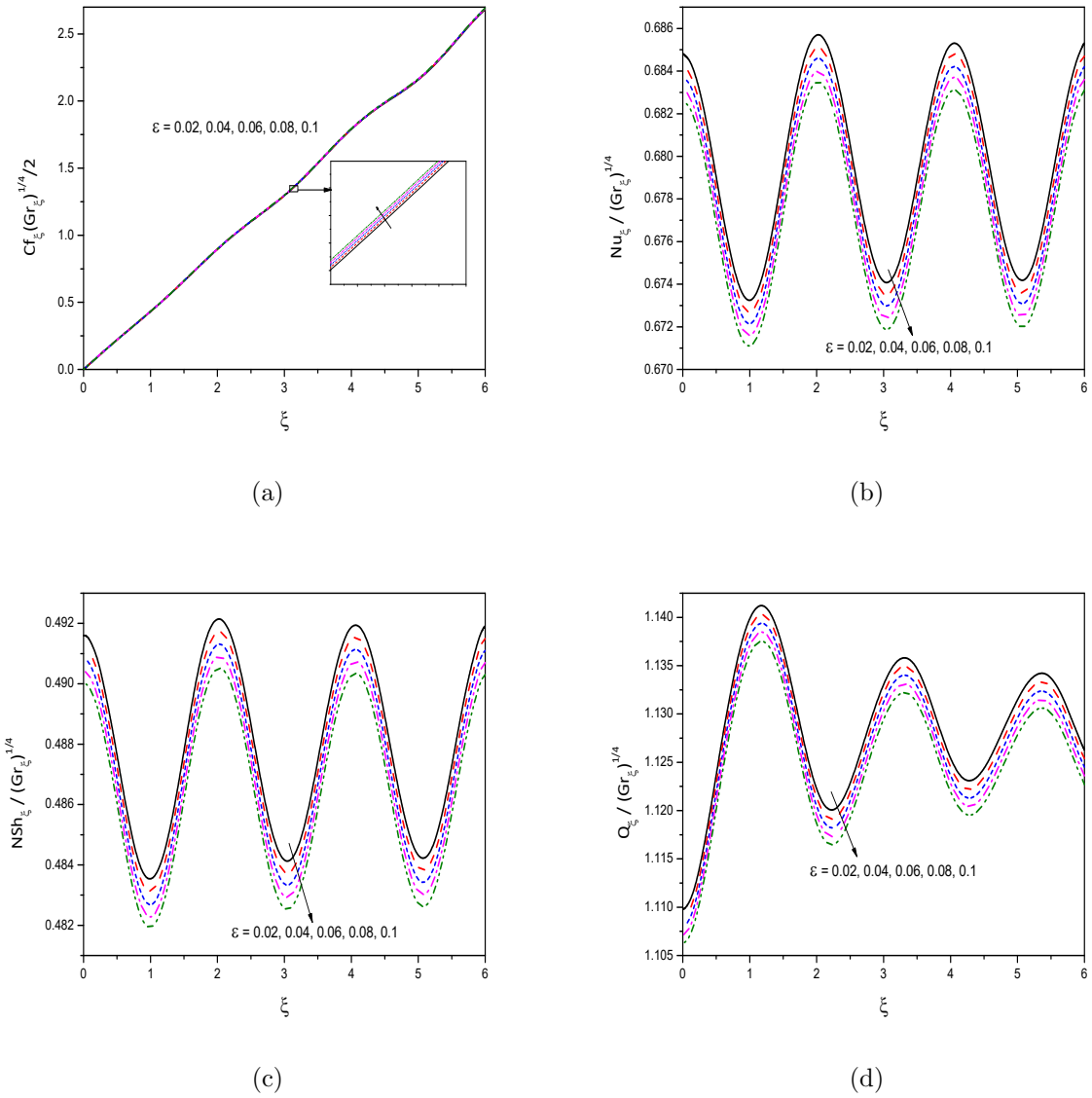

Figure 6.8: "Effect of the variable viscosity parameter ϵ on the profiles of (a) $Cf_\xi(Gr_\xi^{1/4})/2$ (b) $\frac{Nu_\xi}{Gr_\xi^{1/4}}$ (c) $\frac{NSh_\xi}{Gr_\xi^{1/4}}$ (d) $\frac{Q_\xi}{Gr_\xi^{1/4}}$".

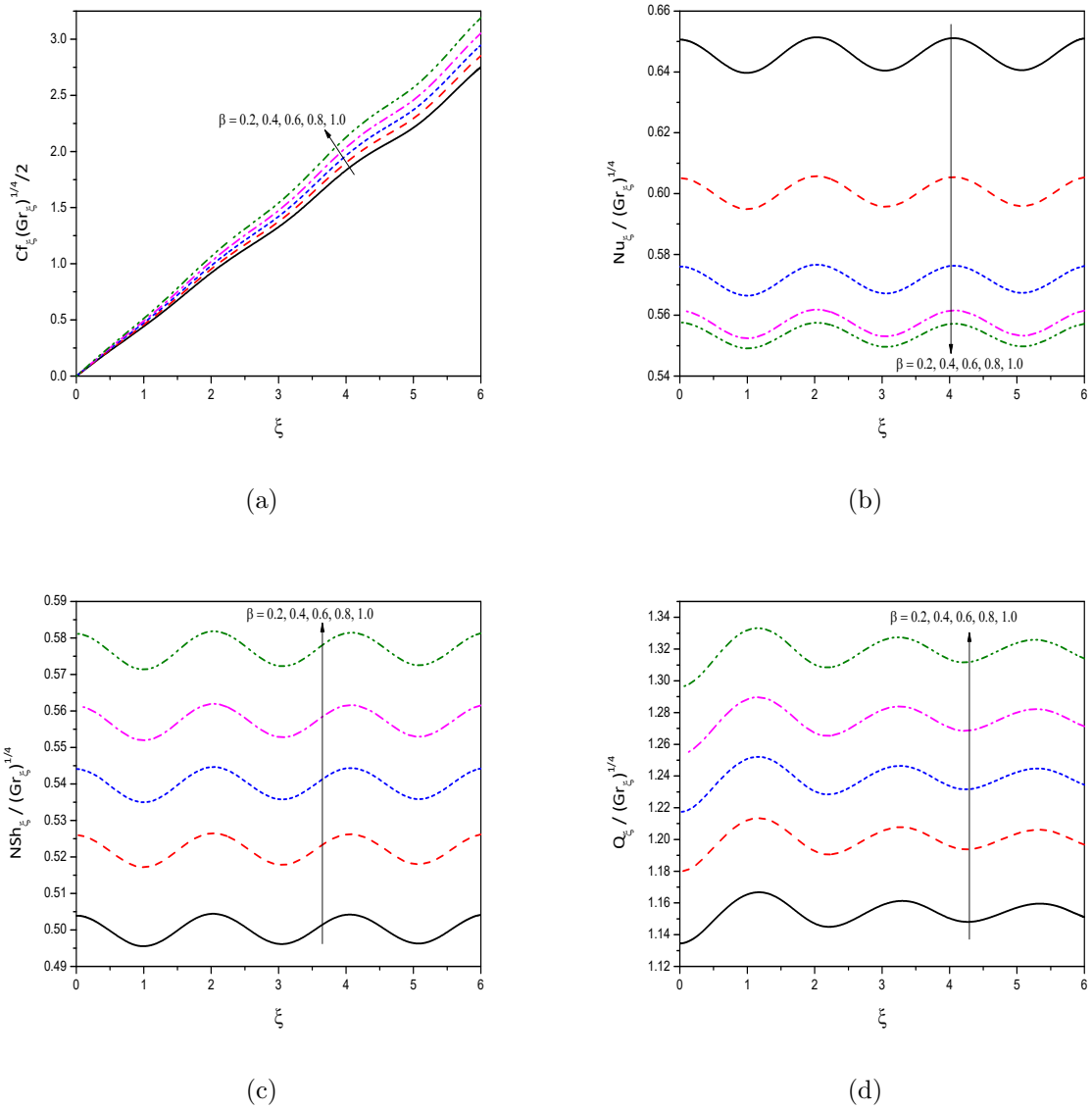

Figure 6.9: "Effect of the variable thermal conductivity parameter β on the profiles of (a) $Cf_\xi(Gr_\xi^{1/4})/2$ (b) $\frac{Nu_\xi}{Gr_\xi^{1/4}}$ (c) $\frac{NSh_\xi}{Gr_\xi^{1/4}}$ (d) $\frac{Q_\xi}{Gr_\xi^{1/4}}$".

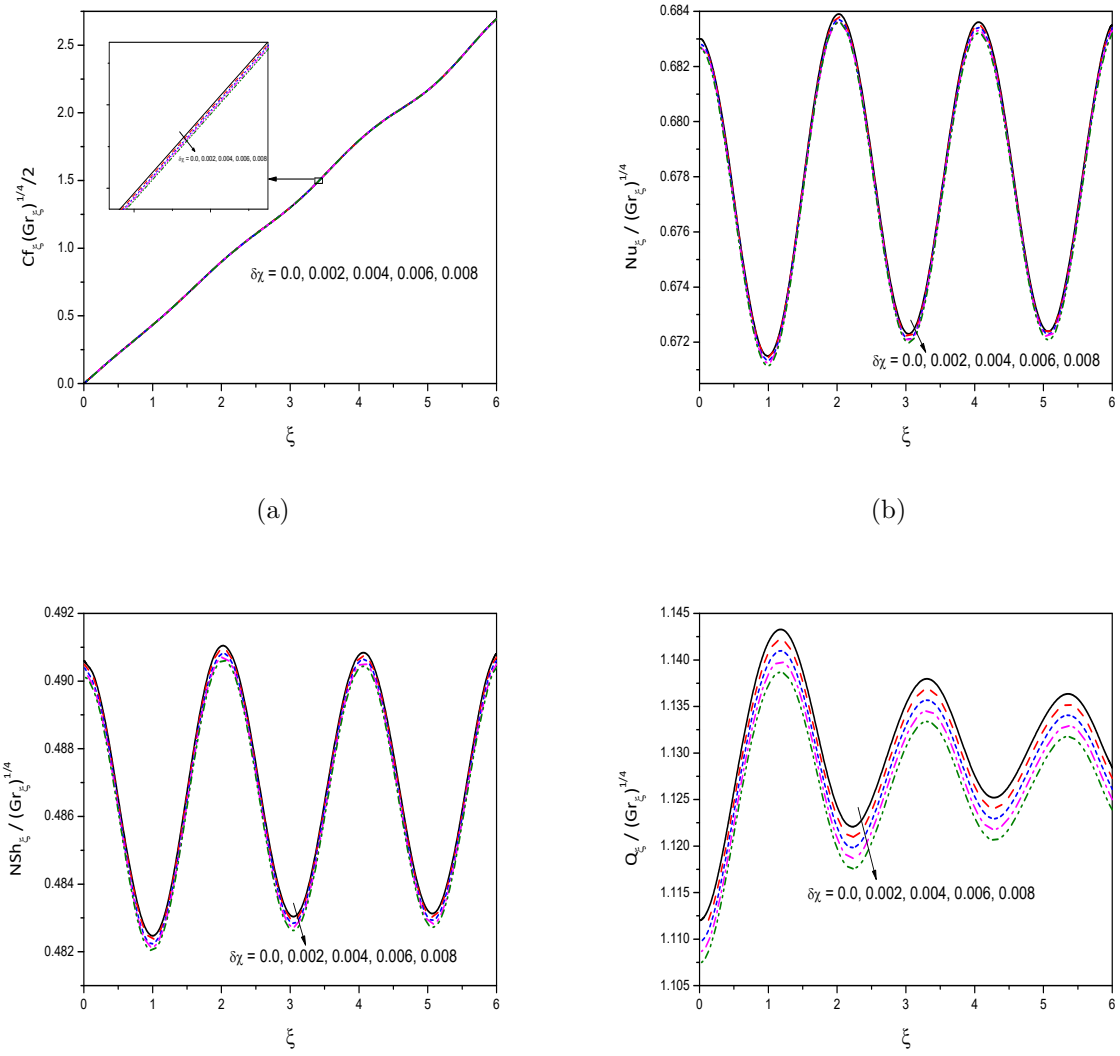

Figure 6.10: "Effect of the microorganism slip parameter $\delta\chi$ on the profiles of (a) $Cf_\xi(Gr_\xi^{1/4})/2$ (b) $\frac{Nu_\xi}{Gr_\xi^{1/4}}$ (c) $\frac{NSh_\xi}{Gr_\xi^{1/4}}$ (d) $\frac{Q_\xi}{Gr_\xi^{1/4}}$".

Chapter 7

Bioconvection of Nanofluid flow Past an Inclined Wavy Surface with Activation Energy [1]

7.1 Introduction

Several researchers included activation energy components in their models to study their effect on flow and heat transfer. Dhlamini *et al.* , [34] found that the activation energy increases the concentration of the chemical species in the boundary layer. Ijaz Khan *et al.* [50] reported that the activation energy parameter has a direct relation with the concentration of fluid. Ijaz [49] observed that the nanoparticle concentration is directly proportional to the chemical reaction with activation energy. Khan *et al.* [60] studied the natural bioconvective flow of Sisko nanofluid subject to gyrotactic microorganisms and activation energy. Ahmad *et al.* [3] studied activation energy and its effects on hybrid nanofluid in the presence of Hall and ion slip currents. Chu *et al.* [29] the significance of activation energy on the bioconvection and magnetohydrodynamic flow of non-Newtonian fluid using the Buongiorno model. Bhatti *et al.* [17] investigated the effect of activation energy on the flow of gyrotactic microorganisms in magnetized nanofluids past a porous plate. Sajid *et al.* [103] analysed the effect of activation energy on the Maxwell Darcy-Forchheimer nanofluid flow in the presence of nonlinear thermal radiation.

This chapter analyses the natural convection of nanofluid flow past an inclined wavy

[1] Communicated to "**International Journal of Engineering Systems Modelling and Simulation**"

surface in the presence of gyrotactic microorganisms with activation energy. The equations of the flow are non-dimensionalized and then solved using the bivariate pseudo-spectral local linearization method (BPSLLM). The influence of pertinent parameters on the heat transfer rate, nanoparticle mass transfer rate, and density number of the microbes are examined.

7.2 Mathematical Formulation

Consider an incompressible, steady, and laminar flow of a nanofluid containing motile microorganisms along an inclined wavy surface. The physical model and coordinate system are shown in Fig. 2.1. Here, in this chapter, the activation energy is incorporated into the model for its detailed study.

The equations governing the flow are

$$\frac{\partial U}{\partial X}+\frac{\partial V}{\partial Y}=0 \tag{7.1}$$

$$\rho_{f\infty}\left(U\frac{\partial U}{\partial X}+V\frac{\partial U}{\partial Y}\right)=-\frac{\partial P}{\partial X}+\mu\left(\frac{\partial^2 U}{\partial X^2}+\frac{\partial^2 U}{\partial Y^2}\right)+[(1-\Phi_\infty)\beta_T\rho_{f\infty}(T-T_\infty) - (\rho_p-\rho_{f\infty})(\Phi-\Phi_\infty)-\beta_M(\rho_m-\rho_{f\infty})M]\,g\sin A \tag{7.2}$$

$$\rho_{f\infty}\left(U\frac{\partial V}{\partial X}+V\frac{\partial V}{\partial Y}\right)=-\frac{\partial P}{\partial Y}+\mu\left(\frac{\partial^2 V}{\partial X^2}+\frac{\partial^2 V}{\partial Y^2}\right)+[(1-\Phi_\infty)\beta_T\rho_{f\infty}(T-T_\infty) - (\rho_p-\rho_{f\infty})(\Phi-\Phi_\infty)-\beta_M(\rho_m-\rho_{f\infty})M]\,g\cos A \tag{7.3}$$

$$U\frac{\partial T}{\partial X}+V\frac{\partial T}{\partial Y}=\alpha_m\left(\frac{\partial^2 T}{\partial X^2}+\frac{\partial^2 T}{\partial Y^2}\right)+\gamma\left\{D_B\left(\frac{\partial\Phi}{\partial X}\frac{\partial T}{\partial X}+\frac{\partial\Phi}{\partial Y}\frac{\partial T}{\partial Y}\right) + \frac{D_T}{T_\infty}\left[\left(\frac{\partial T}{\partial X}\right)^2+\left(\frac{\partial T}{\partial Y}\right)^2\right]\right\} \tag{7.4}$$

$$U\frac{\partial\Phi}{\partial X}+V\frac{\partial\Phi}{\partial Y}=D_B\left(\frac{\partial^2\Phi}{\partial X^2}+\frac{\partial^2\Phi}{\partial Y^2}\right)+\frac{D_T}{T_\infty}\left(\frac{\partial^2 T}{\partial X^2}+\frac{\partial^2 T}{\partial Y^2}\right) -k_0^2\,(\Phi-\Phi_\infty)\left(\frac{T}{T_\infty}\right)^n e^{-\frac{Ea}{\kappa T}} \tag{7.5}$$

$$U\frac{\partial M}{\partial X}+V\frac{\partial M}{\partial Y}+\frac{\partial}{\partial X}\left(M\widetilde{V}\right)+\frac{\partial}{\partial Y}\left(M\widetilde{V}\right)=D_n\left(\frac{\partial^2 M}{\partial X^2}+\frac{\partial^2 M}{\partial Y^2}\right) \tag{7.6}$$

where k_0^2 is the chemical reaction rate, κ is the Boltzman constant, and Ea is the co-effincient of activation energy. The whole expression $k_0^2\left(\Phi-\Phi_\infty\right)\left(\frac{T}{T_\infty}\right)^n e^{-\frac{Ea}{\kappa T}}$ is known as modified Arrhenius equation. The average swimming velocity vector of microorganism is $\widetilde{V}=\dfrac{b_c w_c}{\Phi_w-\Phi_\infty}\dfrac{\partial\Phi}{\partial Y}$. All other quantities are defined in Chapter 2.

The associated boundary conditions are :

$$\left.\begin{array}{l} U=0,\, V=0,\, T=T_w,\, \Phi=\Phi_w,\, M=M_w \,\text{at}\, Y=\sigma(X) \\ U\to 0,\; T\to T_\infty,\; \Phi\to\Phi_\infty,\; M\to M_\infty \,\text{as}\, Y\to\infty \end{array}\right\} \tag{7.7}$$

The irregular wavy surface is transformed to a flat surface, using the following transformations ([131])

$$\left.\begin{array}{l} \xi=\dfrac{X}{L},\quad \eta=\dfrac{Y-\sigma}{L\xi^{\frac{1}{4}}}Gr^{\frac{1}{4}},\quad \psi=\dfrac{\mu Gr^{\frac{1}{2}}\xi^{\frac{3}{4}}}{\rho_{f\infty}}f(\xi,\eta),\quad p=\dfrac{PL^2Gr^{-1}}{\rho_{f\infty}\nu^2}, \\ \theta(\xi,\eta)=\dfrac{T-T_\infty}{T_w-T_\infty},\quad \phi(\xi,\eta)=\dfrac{\Phi-\Phi_\infty}{\Phi_w-\Phi_\infty},\quad \chi(\xi,\eta)=\dfrac{M}{M_w} \end{array}\right\} \tag{7.8}$$

where

$$Gr=\frac{\left(1-\Phi_\infty\right)g\beta_T\left(T_w-T_\infty\right)L^3}{\nu^2}$$

is the Grashof number. Here the stream function ψ is same as in 2.10 of Chapter2.

Substituting Eq. (7.8) in the governing equations (7.1) to (7.6) and invoking the boundary layer approximation, we get the following non-dimensional equations.

$$\left(1+\sigma_\xi^2\right)f'''+\frac{3}{4}ff''-\left[\frac{1}{2}+\frac{\xi\sigma_\xi\sigma_{\xi\xi}}{\left(1+\sigma_\xi^2\right)}\right](f')^2 + \frac{(\theta-N_r\phi-R_b\chi)}{\left(1+\sigma_\xi^2\right)}\left(SinA+\sigma_\xi CosA\right)=\xi\left[f'\frac{\partial f'}{\partial\xi}-\frac{\partial f}{\partial\xi}f''\right] \tag{7.9}$$

$$\frac{\left(1+\sigma_\xi^2\right)}{\Pr}\left[\theta''+N_t(\theta')^2+N_b\phi'\theta'\right]+\frac{3}{4}f\theta'=\xi\left[f'\frac{\partial\theta}{\partial\xi}-\theta'\frac{\partial f}{\partial\xi}\right] \tag{7.10}$$

$$\frac{\left(1+\sigma_\xi^2\right)}{Le}\left[\phi''+\frac{N_t}{N_b}\theta''\right]+\frac{3}{4}f\phi'-\delta_1\phi\xi^{\frac{1}{2}}(1+\delta\theta)^n e^{-\frac{\varepsilon}{1+\delta\theta}}=\xi\left[f'\frac{\partial\phi}{\partial\xi}-\phi'\frac{\partial f}{\partial\xi}\right] \tag{7.11}$$

$$\frac{\left(1+\sigma_\xi^2\right)}{Sc}\chi''-\frac{Pe}{Sc}\left(1-\sigma_\xi\right)\left(\chi\phi''+\chi'\phi'\right)+\frac{3}{4}f\chi'=\xi\left[f'\frac{\partial\chi}{\partial\xi}-\chi'\frac{\partial f}{\partial\xi}\right] \tag{7.12}$$

and

$$\left.\begin{array}{l} f'(\xi,0)=0, \quad f(\xi,0)=-\frac{4}{3}\xi\left.\frac{\partial f}{\partial \xi}\right|_{(\xi,0)}, \quad \theta'(\xi,0)=\phi'(\xi,0)=\chi'(\xi,0)=1 \\ f'(\xi,\infty)=0, \quad \theta(\xi,\infty)=0, \quad \phi(\xi,\infty)=0, \quad \chi(\xi,\infty)=\frac{M_\infty}{M_w}=\delta\chi \end{array}\right\} \tag{7.13}$$

The parameters Pr, Pe, Le, Sc, N_b, N_r, N_t, R_b are same as in 2.17 of Chapter 2 and activation energy parameter E, temperature relative parameter δ, reaction rate parameter δ_1 are defined by

$$E=\frac{Ea}{\kappa T_\infty}, \quad \delta=\frac{T_w-T_\infty}{T_\infty}, \quad \delta_1=\frac{k_0^2L^2}{\nu}Gr^{-\frac{1}{2}} \tag{7.14}$$

The non-dimensional form of the coefficient of skin friction, Nusselt number, nanoparticle mass transfer rate, and density number of motile microbe are defined in 2.19 of Chapter 2.

7.3 Method of Solution

The set of equations (7.9) - (7.13) is solved using the BPSLLM [82]. On applying BPSLLM to all the equations (7.9) - (7.12), we get the following system of linear differential equations.

$$a_{1,m}f'''_{m+1}+a_{2,m}f''_{m+1}+a_{3,m}f'_{m+1}+a_{4,m}f_{m+1}+a_{5,m}\frac{\partial f'_{m+1}}{\partial \xi}+a_{6,m}\frac{\partial f_{m+1}}{\partial \xi}=R_{1,m} \tag{7.15}$$

$$b_{1,m}\theta''_{m+1}+b_{2,m}\theta'_{m+1}+b_{3,m}\frac{\partial \theta_{m+1}}{\partial \xi}=R_{2,m} \tag{7.16}$$

$$c_{1,m}\phi''_{m+1}+c_{2,m}\phi'_{m+1}+c_{3,m}\phi_{m+1}+c_{4,m}\frac{\partial \phi_{m+1}}{\partial \xi}=R_{3,m} \tag{7.17}$$

$$d_{1,m}\chi''_{m+1}+d_{2,m}\chi'_{m+1}+d_{3,m}\chi_{m+1}+d_{4,m}\frac{\partial \chi_{m+1}}{\partial \xi}=R_{4,m} \tag{7.18}$$

where the coefficients are

$$a_{1,m}=1+\sigma_\xi^2, \quad a_{2,m}=\frac{3}{4}f_m+\xi\frac{\partial f_m}{\partial \xi},$$

$$a_{3,m}=-2\left[\frac{1}{2}+\frac{\xi\sigma_\xi\sigma_{\xi\xi}}{1+\sigma_\xi^2}\right]f'_m-\xi\frac{\partial f'_m}{\partial \xi}, \quad a_{4,m}=\frac{3}{4}f''_m, \quad a_{5,m}=-\xi f'_r, \quad a_{6,m}=\xi f''_r$$

$$R_{1,m}=\xi f''_m\frac{\partial f_m}{\partial \xi}-\left[\frac{1}{2}+\frac{\xi\sigma_\xi\sigma_{\xi\xi}}{1+\sigma_\xi^2}\right](f'_m)^2+\frac{3}{4}f_mf''_m-\xi f'_m\frac{\partial f'_m}{\partial \xi}$$
$$-\frac{(\theta_m-N_r\phi_m-R_b\chi_m)}{\left(1+\sigma_\xi^2\right)}\left(SinA+\sigma_\xi CosA\right)$$

$$b_{1,m} = \frac{(1+{\sigma_\xi}^2)}{\mathrm{Pr}}, \quad b_{2,m} = \frac{(1+\sigma_\xi^2)}{\mathrm{Pr}} N_b \phi'_m + \frac{2(1+\sigma_\xi^2)}{\mathrm{Pr}} N_t \theta'_m + \frac{3}{4} f_{m+1} + \xi \frac{\partial f_{m+1}}{\partial \xi},$$

$$b_{3,m} = -\xi f'_{m+1}, \quad R_{2,m} = \frac{(1+\sigma_\xi^2) N_t}{\mathrm{Pr}} (\theta'_m)^2$$

$$c_{1,m} = \frac{1+\sigma_\xi^2}{Le}, \quad c_{2,m} = \frac{3}{4} f_{m+1} + \xi \frac{\partial f_{m+1}}{\partial \xi}, \quad c_{3,m} = \delta_1 \xi^{\frac{1}{2}} \left(1+\delta\theta_{m+1}\right)^n e^{\frac{-E}{1+\delta\theta_{m+1}}}$$

$$c_{4,m} = -\xi f'_{m+1}, \quad R_{3,m} = -\frac{(1+\sigma_\xi^2)}{Le} \frac{N_t}{N_b} \theta''_{m+1},$$

$$d_{1,m} = \frac{1+\sigma_\xi^2}{Sc}, \quad d_{2,m} = -\frac{Pe}{Sc}(1-\sigma_\xi)\phi'_{m+1} + \frac{3}{4} f_{m+1} + \xi \frac{\partial f_{m+1}}{\partial \xi},$$

$$d_{3,m} = -\frac{Pe}{Sc}(1-\sigma_\xi)\phi''_{m+1}, \quad d_{4,m} = -\xi f'_{m+1}, \quad R_{4,m} = 0.$$

The boundary conditions are

$$\left.\begin{array}{l} f'_{m+1}(\xi,0) = 0\,, \quad f_{m+1}(\xi,0) = -\dfrac{4}{3}\xi \left.\dfrac{\partial f}{\partial \xi}\right|_{(\xi,0)}, \quad \theta_{m+1}(\xi,0) = 1, \\ \phi_{m+1}(\xi,0) = 1\,, \quad \chi_{m+1}(\xi,0) = 1 \\ f'_{m+1}(\xi,\infty) = 0, \quad \theta_{m+1}(\xi,\infty) = 0, \quad \phi_{m+1}(\xi,\infty) = 0, \quad \chi_{m+1}(\xi,\infty) = \delta\chi \end{array}\right\} \tag{7.19}$$

Implementing bivariate Chebyshev spectral collocation method [20] to the set of linearized equations (7.15) to (7.18) in both η and ξ, we get

$$A^{(1)}\mathbf{F}_i + \gamma^{(1)}_{5,i} \sum_{j=0}^{M} \mathbf{d}_{i,j}\mathbf{D}\mathbf{F}_j + \gamma^{(1)}_{6,i} \sum_{j=0}^{M} \mathbf{d}_{i,j}\mathbf{F}_j = \mathbf{R}_{1,i} \tag{7.20}$$

$$A^{(2)}\mathbf{\Theta}_i + \gamma^{(2)}_{3,i} \sum_{j=0}^{M} \mathbf{d}_{i,j}\mathbf{\Theta}_j = \mathbf{R}_{2,i} \tag{7.21}$$

$$A^{(3)}\mathbf{\Phi}_i + \gamma^{(3)}_{4,i} \sum_{j=0}^{M} \mathbf{d}_{i,j}\mathbf{\Phi}_j = \mathbf{R}_{3,i} \tag{7.22}$$

$$A^{(4)}\chi_i + \gamma^{(4)}_{4,i} \sum_{j=0}^{M} \mathbf{d}_{i,j}\chi_j = \mathbf{R}_{4,i} \tag{7.23}$$

where

$$A^{(1)} = \gamma^{(1)}_{1,i}\mathbf{D}^3 + \gamma^{(1)}_{2,i}\mathbf{D}^2 + \gamma^{(1)}_{3,i}\mathbf{D} + \gamma^{(1)}_{4,i}\mathbf{I},$$
$$A^{(2)} = \gamma^{(2)}_{1,i}\mathbf{D}^2 + \gamma^{(2)}_{2,i}\mathbf{D},$$
$$A^{(3)} = \gamma^{(3)}_{1,i}\mathbf{D}^2 + \gamma^{(3)}_{2,i}\mathbf{D} + \gamma^{(3)}_{3,i}\mathbf{I},$$
$$A^{(4)} = \gamma^{(4)}_{1,i}\mathbf{D}^2 + \gamma^{(4)}_{2,i}\mathbf{D} + \gamma^{(4)}_{3,i}\mathbf{I}$$

Here $\gamma_{k,i}^{(1)}$, $\gamma_{k,i}^{(2)}$, $\gamma_{k,i}^{(3)}$, $\gamma_{k,i}^{(4)}$ and $\mathbf{R}_{k,i}$ are N^{th} order diagonal matrices with diagonal elements as, $a_{k,m}(\zeta_r, \tau_i)$, $b_{k,m}(\zeta_r, \tau_i)$, $c_{k,m}(\zeta_r, \tau_i)$, $d_{k,m}(\zeta_r, \tau_i)$ and $R_{k,m}(\zeta_r, \tau_i)$ for $r = 1, 2, 3, \cdots N$ respectively and $\mathbf{I}$ refers the identity matrix.

The equation (7.20) written in matrix form as

$$\begin{bmatrix} A_{0,0}^{(1)} & A_{0,1}^{(1)} & A_{0,2}^{(1)} & \cdots & A_{0,M}^{(1)} \\ A_{1,0}^{(1)} & A_{1,1}^{(1)} & A_{1,2}^{(1)} & \cdots & A_{1,M}^{(1)} \\ A_{2,0}^{(1)} & A_{2,1}^{(1)} & A_{2,2}^{(1)} & \cdots & A_{2,M}^{(1)} \\ \vdots & \vdots & \vdots & \cdots & \vdots \\ A_{M,0}^{(1)} & A_{M,1}^{(1)} & A_{M,2}^{(1)} & \cdots & A_{M,M}^{(1)} \end{bmatrix} \begin{bmatrix} \mathbf{F}_0 \\ \mathbf{F}_1 \\ \mathbf{F}_2 \\ \vdots \\ \mathbf{F}_M \end{bmatrix} = \begin{bmatrix} \mathbf{R}_{1,0} \\ \mathbf{R}_{1,1} \\ \mathbf{R}_{1,2} \\ \vdots \\ \mathbf{R}_{1,M} \end{bmatrix} \tag{7.24}$$

where

$$\begin{aligned} A_{i,j}^{(1)} &= A^{(1)} + \gamma_{5,r}^{(1)} \mathbf{d}_{i,i} \mathbf{D} + \gamma_{6,r}^{(1)} \mathbf{d}_{i,i} \mathbf{I}, \ for\ i = j; \\ A_{i,j}^{(1)} &= \gamma_{5,r}^{(1)} \mathbf{d}_{i,j} \mathbf{D} + \gamma_{6,r}^{(1)} \mathbf{d}_{i,j} \mathbf{I}, \ for\ i \neq j \end{aligned} \tag{7.25}$$

In a similar manner, the equations (7.21) to (7.23) can be written in matrix form. Solving these matrix equations, iteratively, we obtain the solution to (7.9) - (7.13).

The non-dimensional form of the parameters skin friction, Nusselt number, nanoparticle Sherwood number and density number of motile microbe are given in 4.14 of Chapter 4

7.4 Computational Results and Discussion

In the present study, we focus our discussion on analyzing the bioconvection Peclet number Pe, inclination angle effect A, amplitude α, bioconvection Schmidt number Sc, activation energy paramenter E, temperature relative parameter δ, reaction rate parameter δ_1, microorganism slip parameter $\delta\chi$, fitted rate constant n on the coeffient of skin friction $Cf_\xi (Gr_\xi)^{\frac{1}{4}}$, Nusselt number $Nu_\xi/(Gr_\xi)^{\frac{1}{4}}$, nanoparticle Sherwood number $NSh_\xi/(Gr_\xi)^{\frac{1}{4}}$ and density number of motile microbes $Q_\xi/(Gr_\xi)^{\frac{1}{4}}$. The values of the other parameters are fixed as $Pr = 10, Pe = 2, Le = 5, Sc = 2, N_b = 0.05, N_t = 0.01, N_r = 0.03, \alpha = 0.01, A = \pi/4, \delta\chi = 0.01, \delta = 0.1, \delta_1 = 0.1, E = 1, n = 2$ and $R_b = 0.1$ unless otherwise mentioned.

Figure 7.1 refers to the effects of bioconvection Peclet number Pe. It is found that Nusselt number, nanoparticle Sherwood number and density number of motile microbes are escalating for a raise in the bioconvection Peclet number Pe, Increase in Bio-convection

Peclet number results in increase of movement of particles along concentration of gradients (The bioconvection Peclet number helps to increase the speed of the microorganisms in respect of the fluid).

The effect of the angle of the wavy surface A on skin friction coefficient, Nusselt number, nanoparticle Sherwood number and density number of motile microbes is depicted in Fig. 7.2. The raise in the angle of inclination increases the coefficient of skin friction $Cf_\xi(Gr_\xi)^{\frac{1}{4}}$, Nusselt number $Nu_\xi/(Gr_\xi)^{\frac{1}{4}}$, nanoparticle Sherwood number $NSh_\xi/(Gr_\xi)^{\frac{1}{4}}$ and density number of motile microorganisms $Q_\xi/(Gr_\xi)^{\frac{1}{4}}$. As a result, the transfer rate of all physical quantities is greater for the vertical surface than for the horizontal surface.

Figure 7.3 elucidates the behaviour of $Cf_\xi(Gr_\xi)^{\frac{1}{4}}$, $Nu_\xi/(Gr_\xi)^{\frac{1}{4}}$, $NSh_\xi/(Gr_\xi)^{\frac{1}{4}}$, and $Q_\xi/(Gr_\xi)^{\frac{1}{4}}$ with amplitude of the wavy surface α. For an increase in α, it is found that both increasing and decreasing nature in the profiles. Also it is observed that overall raise in all these quantities.

The variation of $Cf_\xi(Gr_\xi)^{\frac{1}{4}}$, $Nu_\xi/(Gr_\xi)^{\frac{1}{4}}$, $NSh_\xi/(Gr_\xi)^{\frac{1}{4}}$, and $Q_\xi/(Gr_\xi)^{\frac{1}{4}}$ for different values of bioconvection Schmidt number Sc is presented in Fig. 7.4. It is noticed from this figure that increase in the value of Sc result in a increase in on all quantitites. The Schmidt number Sc describes the concentration layer's thickness in comparison to the momentum layer. A lower mass diffusivity is associated with a larger Schmidt number Sc. As a result, the presence of Sc in the motile microorganisms equation alters the microorganisms' dispersion regime significantly.

The effect of the activation parameter E on skin friction, Nusselt number, nanoparticle Sherwood number, and motile microbe density is shown in Figure 7.5. The energy activation parameter, in general, refers to the amount of energy used to stimulate atoms or molecules for chemical reactions. In a chemical reaction, there should be a significant number of atoms whose activation energy is less than or equal to translational energy. For increasing values of the parameter E, it is seen that solute layer thickness and concentration dispersion increase. It is examined that a greater value of the activation energy parameter E causes a decrease in the term $e^{-\frac{Ea}{\kappa\bar{T}}}$, resulting in parameter modification. This can be seen in figures 7.5(a) to 7.5(d).

Figure 7.6 depicts the effect of the temperature relative parameter δ on skin friction, Nusselt number, nanoparticle Sherwood number and motile microbe density. As the temperature relative parameter increases, the parameters $Cf_\xi(Gr_\xi)^{\frac{1}{4}}$, $Nu_\xi/(Gr_\xi)^{\frac{1}{4}}$, $NSh_\xi/(Gr_\xi)^{\frac{1}{4}}$, and $Q_\xi/(Gr_\xi)^{\frac{1}{4}}$ are decreasing.

Figure 7.7 shows the effect of reaction rate parameter δ_1, on $Cf_\xi(Gr_\xi)^{\frac{1}{4}}$, $Nu_\xi/(Gr_\xi)^{\frac{1}{4}}$, $NSh_\xi/(Gr_\xi)^{\frac{1}{4}}$, and $Q_\xi/(Gr_\xi)^{\frac{1}{4}}$. It is observed from figures 7.7(a) to 7.7(d), that the quantities are raising for a raise in reaction rate δ_1.

The influence of $\delta\chi$, microorganism slip parameter, is potrayed in figures 7.8(a) - 7.8(d). It is identified that the increase of microorganism slip parameter results in the diminution of all the dimensionless parameters $Cf_\xi(Gr_\xi)^{\frac{1}{4}}$, $Nu_\xi/(Gr_\xi)^{\frac{1}{4}}$, $NSh_\xi/(Gr_\xi)^{\frac{1}{4}}$, and $Q_\xi/(Gr_\xi)^{\frac{1}{4}}$.

Figure 7.9 shows the effect of fitted rate constant n, on $Cf_\xi(Gr_\xi)^{\frac{1}{4}}$, $Nu_\xi/(Gr_\xi)^{\frac{1}{4}}$, $NSh_\xi/(Gr_\xi)^{\frac{1}{4}}$, and $Q_\xi/(Gr_\xi)^{\frac{1}{4}}$. It is observed from figures 7.9(a) to 7.9(d), that the quantities are declining, for a raise in fitted rate constant n.

7.5 Conclusions

In this chapter, an analysis is presented to study the natural convection of nanofluid flow past an inclined wavy surface in the presence of gyrotactic microbes with activation energy. The nonlinear equations are linearized employing local linearization procedure and the resultant system is solved by a bivariate pseudo-spectral collocation method. Important observations are itemized below:

- The skin friction $Cf_\xi(Gr_\xi)^{\frac{1}{4}}$, nanoparticle Sherwood number $NSh_\xi/(Gr_\xi)^{\frac{1}{4}}$ and the density of motile microbes $Q_\xi/(Gr_\xi)^{\frac{1}{4}}$ escalates for a raise in bioconvection Peclet number, angle of inclination, bioconvection Schmidt number and activation energy parameter.
- An increase in bioconvection Peclet number, angle of inclination, bioconvection Schmidt number, and activation energy parameter results in an increase in heat transfer rate.
- Skin friction, Nusselt number, nanoparticle Sherwood number and density of motile microbes are declining for a raise in temperature relative parameter δ and reaction rate parameter δ_1
- Activation energy parameter E enriches the skin friction, Nusselt number, nanoparticle Sherwood number, and density of motile microorganisms.

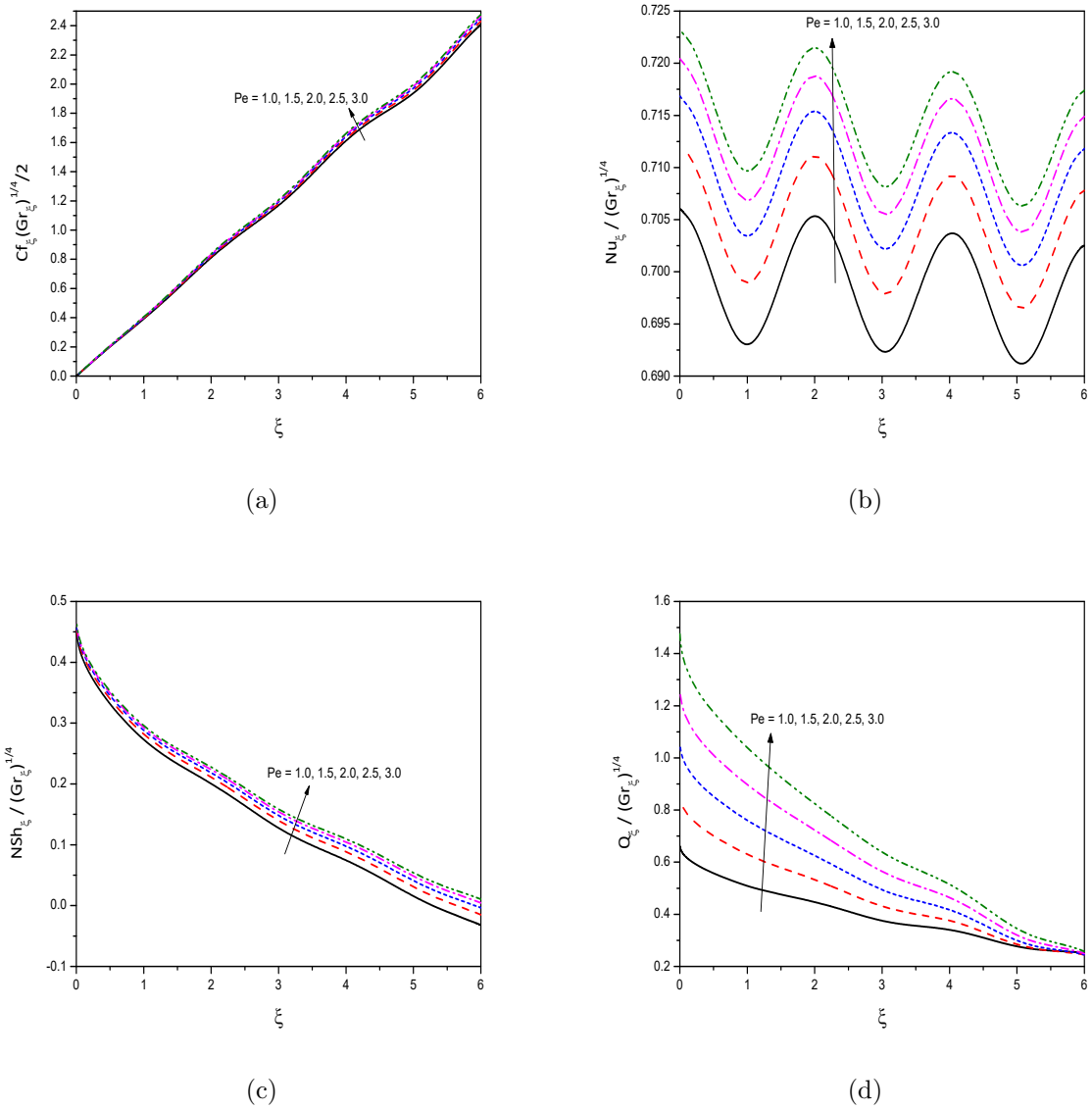

Figure 7.1: "Effect of the bioconvection Peclet number Pe on the profiles of (a) $Cf_\xi(Gr_\xi^{1/4})/2$ (b) $\frac{Nu_\xi}{Gr_\xi^{1/4}}$ (c) $\frac{NSh_\xi}{Gr_\xi^{1/4}}$ (d) $\frac{Q_\xi}{Gr_\xi^{1/4}}$".

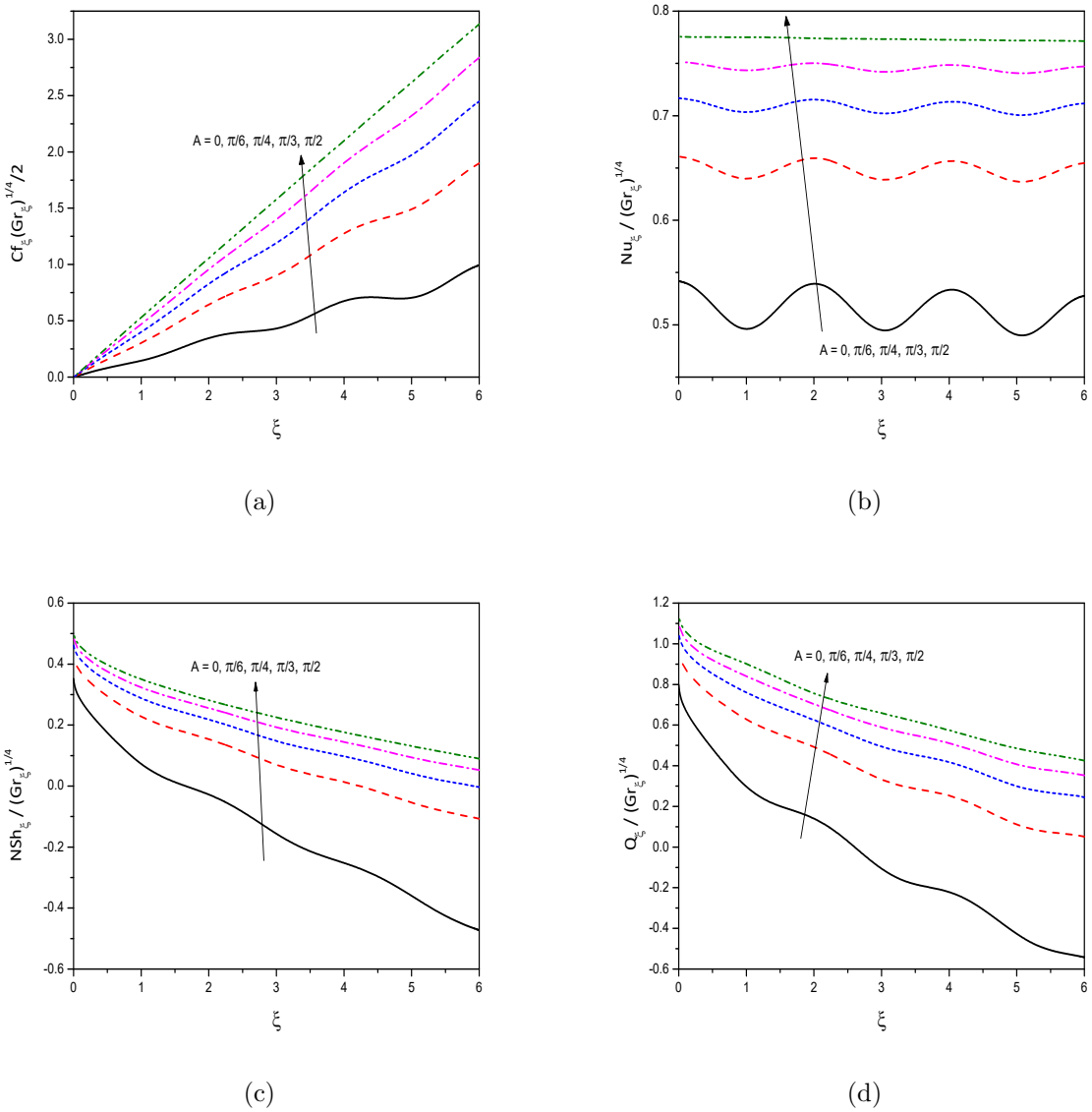

Figure 7.2: "Effect of the angle of inclination A on the profiles of (a) $Cf_\xi(Gr_\xi^{1/4})/2$ (b) $\frac{Nu_\xi}{Gr_\xi^{1/4}}$ (c) $\frac{NSh_\xi}{Gr_\xi^{1/4}}$ (d) $\frac{Q_\xi}{Gr_\xi^{1/4}}$".

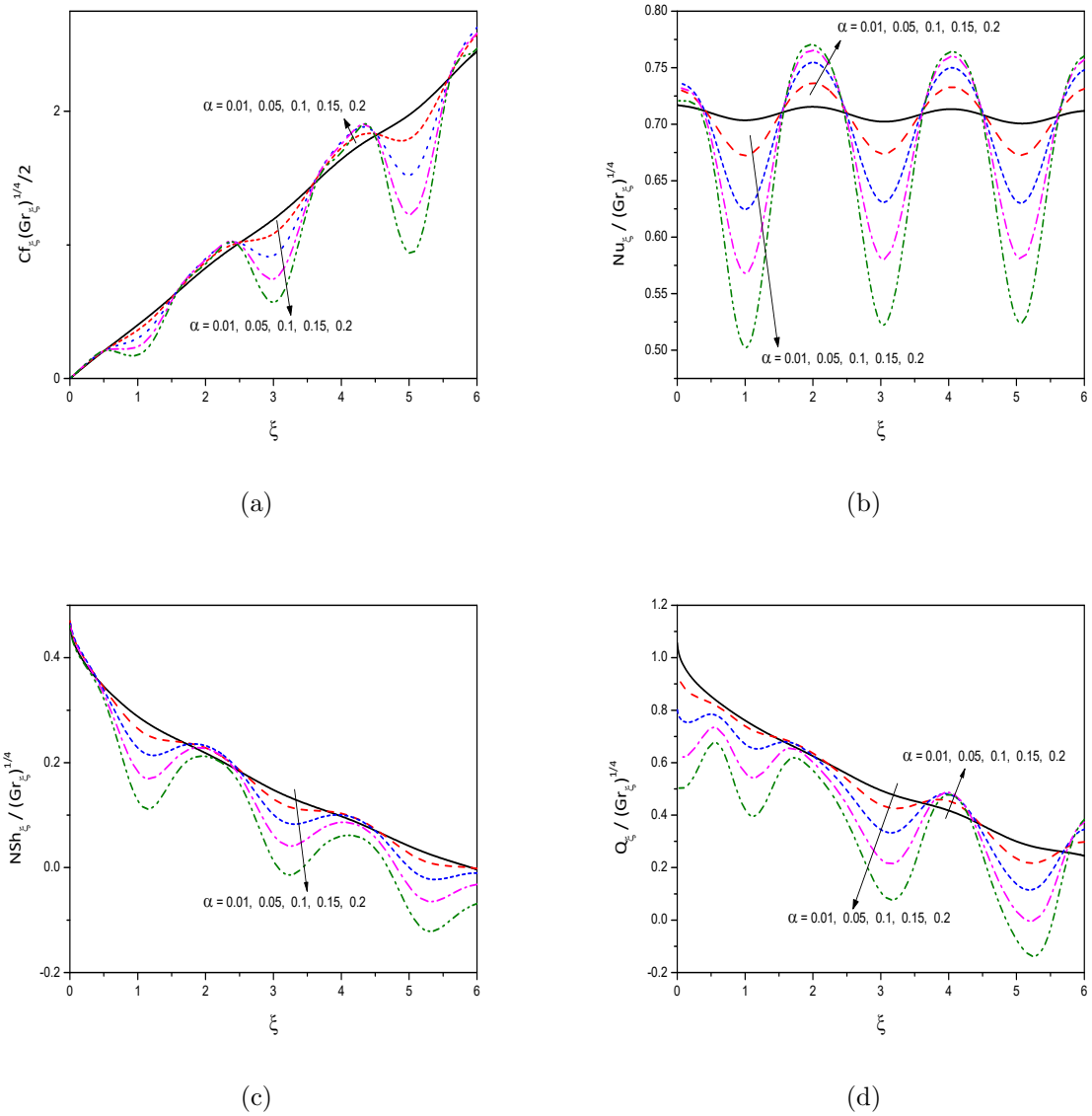

Figure 7.3: "Effect of the amplitude of the wavy surface α on the profiles of (a) $Cf_\xi(Gr_\xi^{1/4})/2$ (b) $\frac{Nu_\xi}{Gr_\xi^{1/4}}$ (c) $\frac{NSh_\xi}{Gr_\xi^{1/4}}$ (d) $\frac{Q_\xi}{Gr_\xi^{1/4}}$".

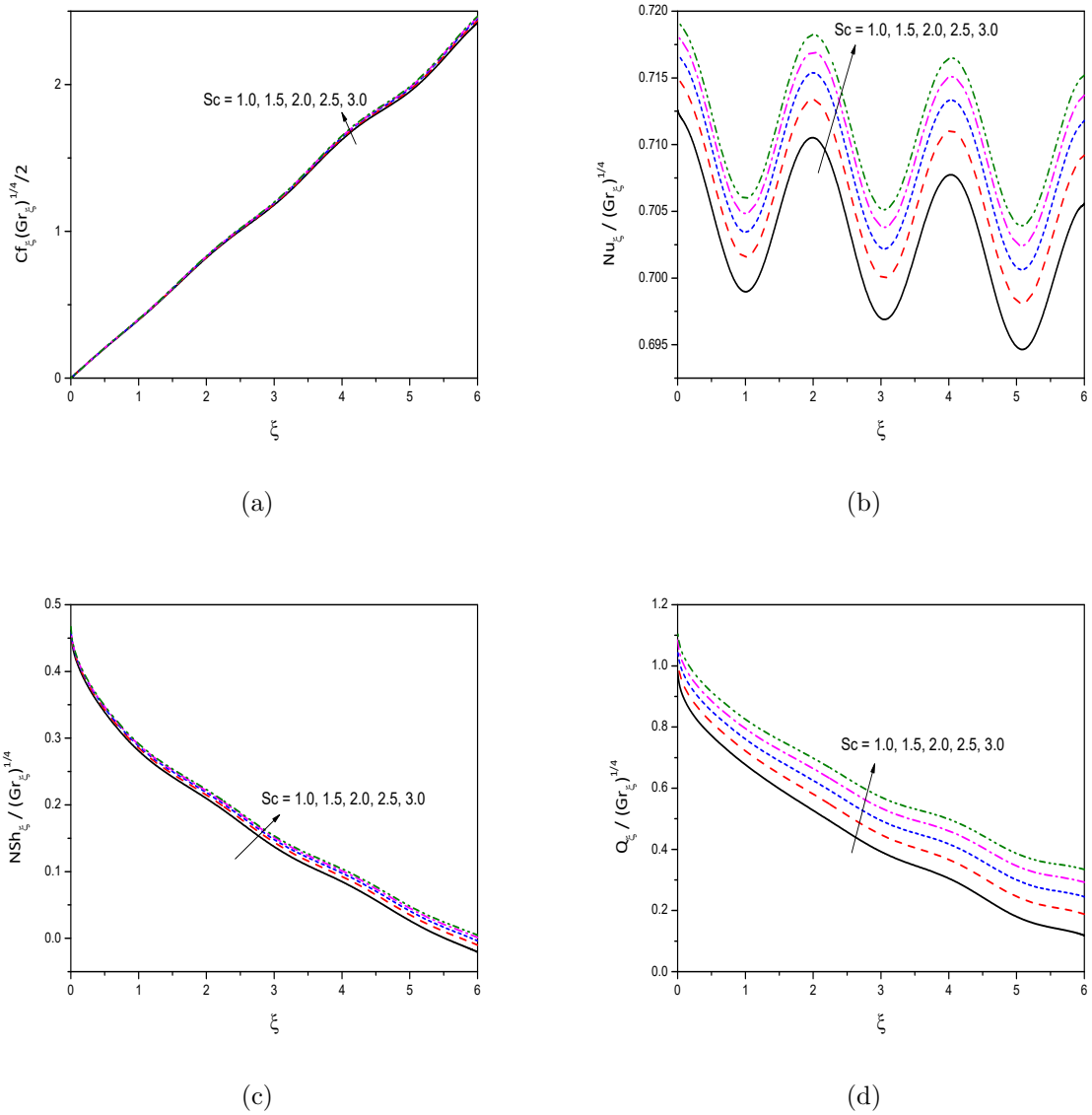

Figure 7.4: "Effect of the bioconvection Schmidt number Sc on the profiles of (a) $Cf_\xi(Gr_\xi^{1/4})/2$ (b) $\frac{Nu_\xi}{Gr_\xi^{1/4}}$ (c) $\frac{NSh_\xi}{Gr_\xi^{1/4}}$ (d) $\frac{Q_\xi}{Gr_\xi^{1/4}}$".

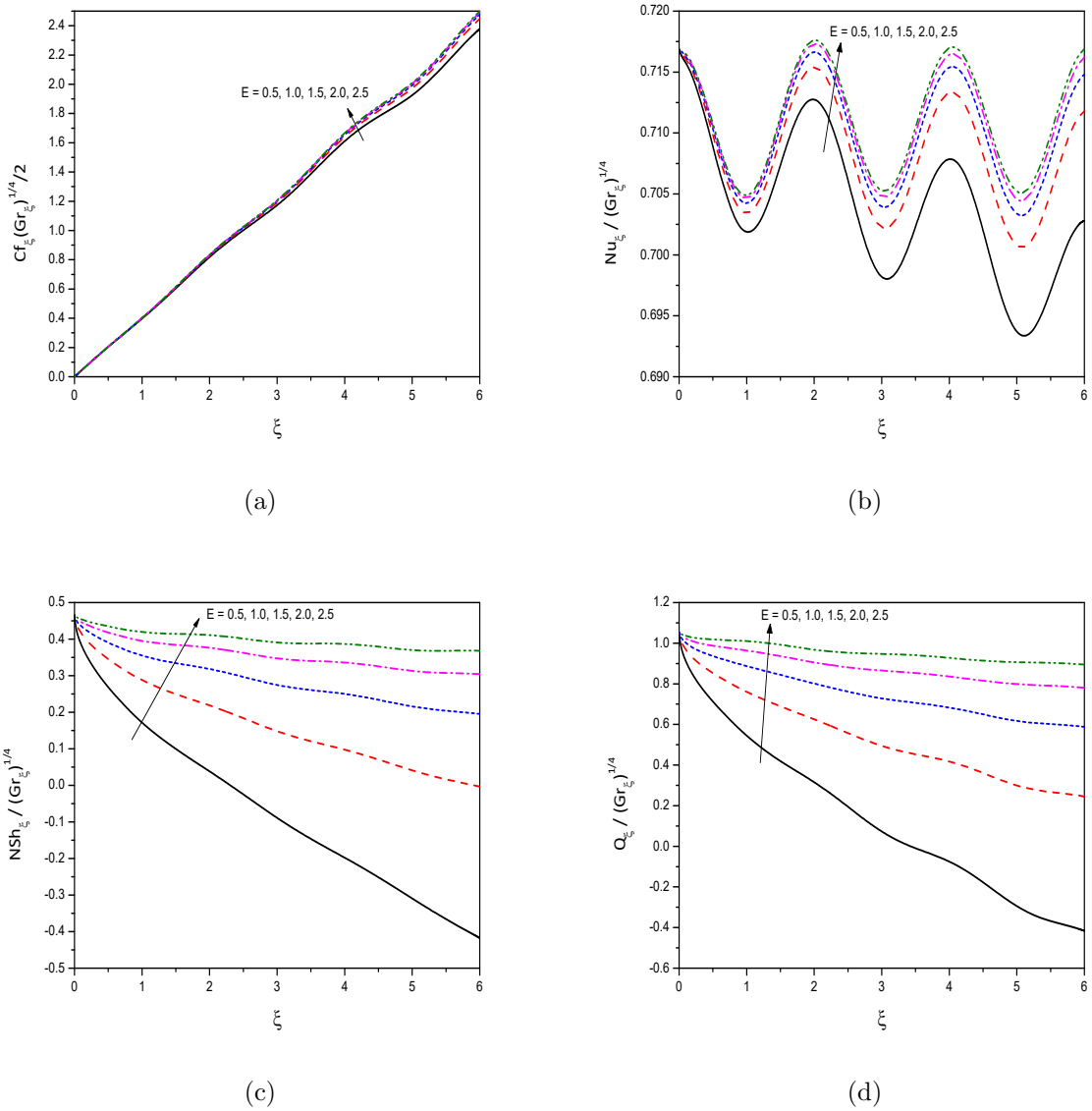

Figure 7.5: "Effect of the activation parameter E on the profiles of (a) $Cf_\xi(Gr_\xi^{1/4})/2$ (b) $\frac{Nu_\xi}{Gr_\xi^{1/4}}$ (c) $\frac{NSh_\xi}{Gr_\xi^{1/4}}$ (d) $\frac{Q_\xi}{Gr_\xi^{1/4}}$".

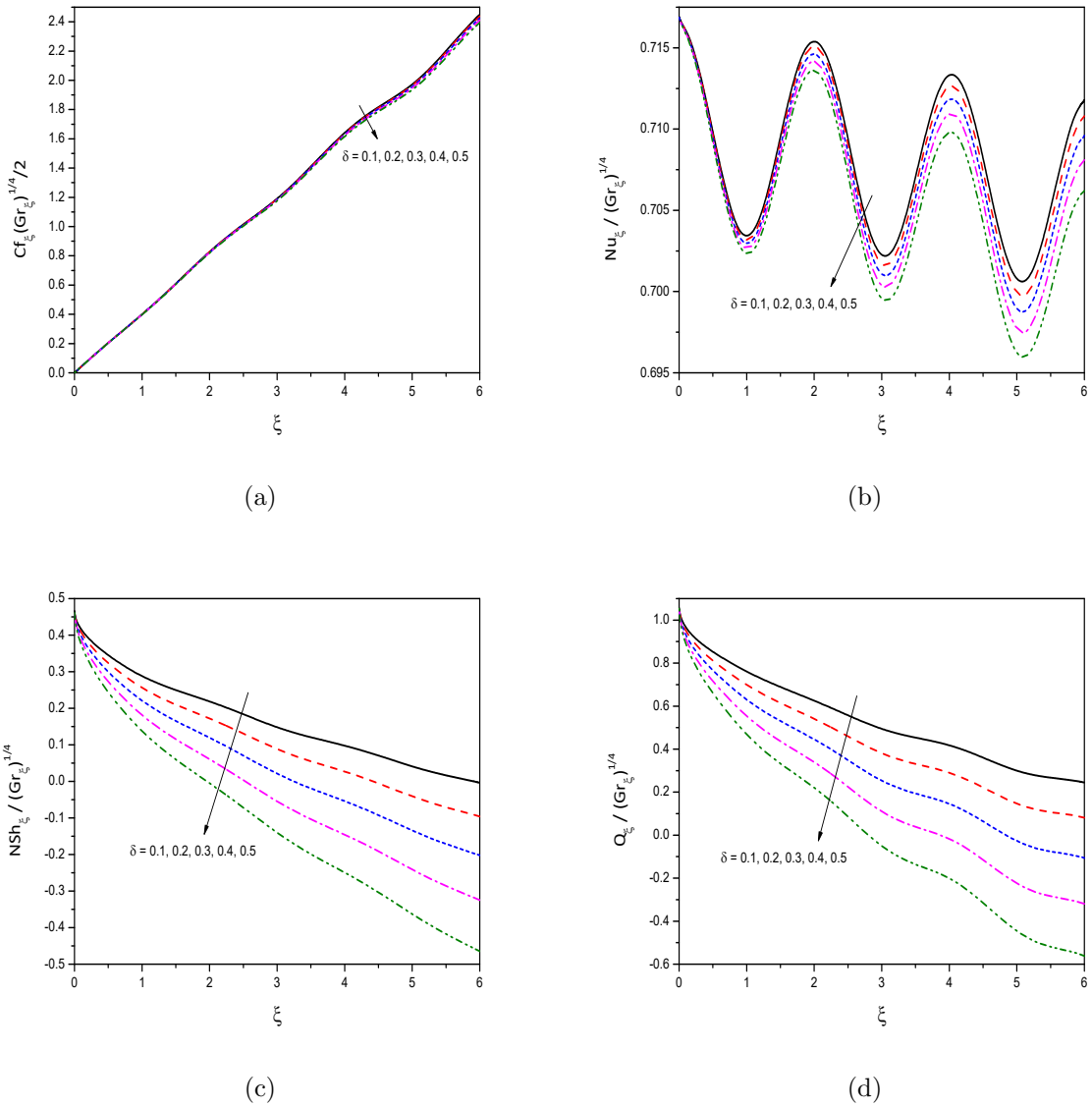

Figure 7.6: "Effect of the temperature relative parameter δ on the profiles of (a) $Cf_\xi(Gr_\xi^{1/4})/2$ (b) $\frac{Nu_\xi}{Gr_\xi^{1/4}}$ (c) $\frac{NSh_\xi}{Gr_\xi^{1/4}}$ (d) $\frac{Q_\xi}{Gr_\xi^{1/4}}$".

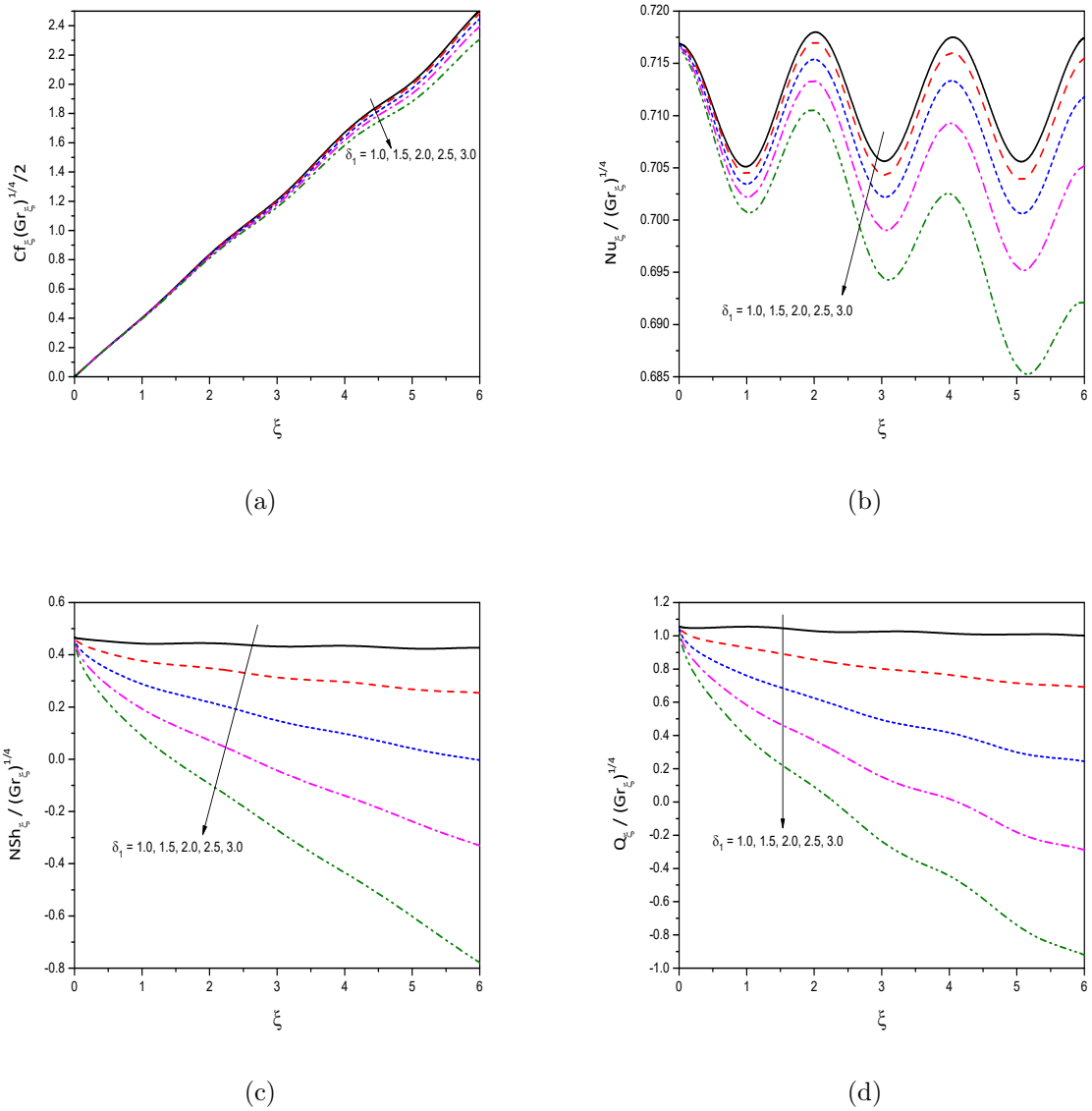

Figure 7.7: "Effect of the reaction rate parameter δ_1 on the profiles of (a) $Cf_\xi(Gr_\xi^{1/4})/2$ (b) $\frac{Nu_\xi}{Gr_\xi^{1/4}}$ (c) $\frac{NSh_\xi}{Gr_\xi^{1/4}}$ (d) $\frac{Q_\xi}{Gr_\xi^{1/4}}$".

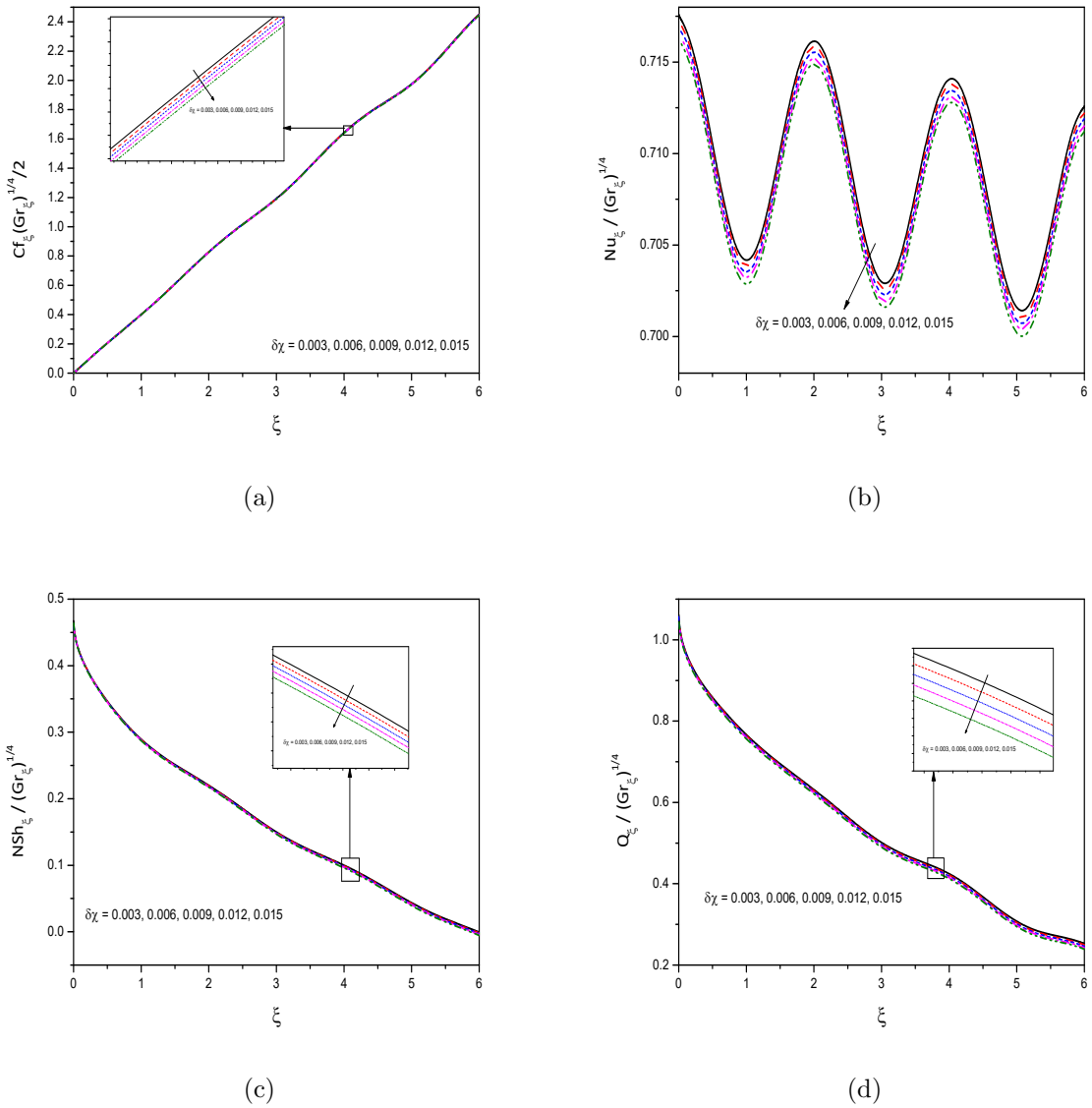

Figure 7.8: "Effect of the microorganism slip parameter $\delta\chi$ on the profiles of (a) $Cf_\xi(Gr_\xi^{1/4})/2$ (b) $\frac{Nu_\xi}{Gr_\xi^{1/4}}$ (c) $\frac{NSh_\xi}{Gr_\xi^{1/4}}$ (d) $\frac{Q_\xi}{Gr_\xi^{1/4}}$".

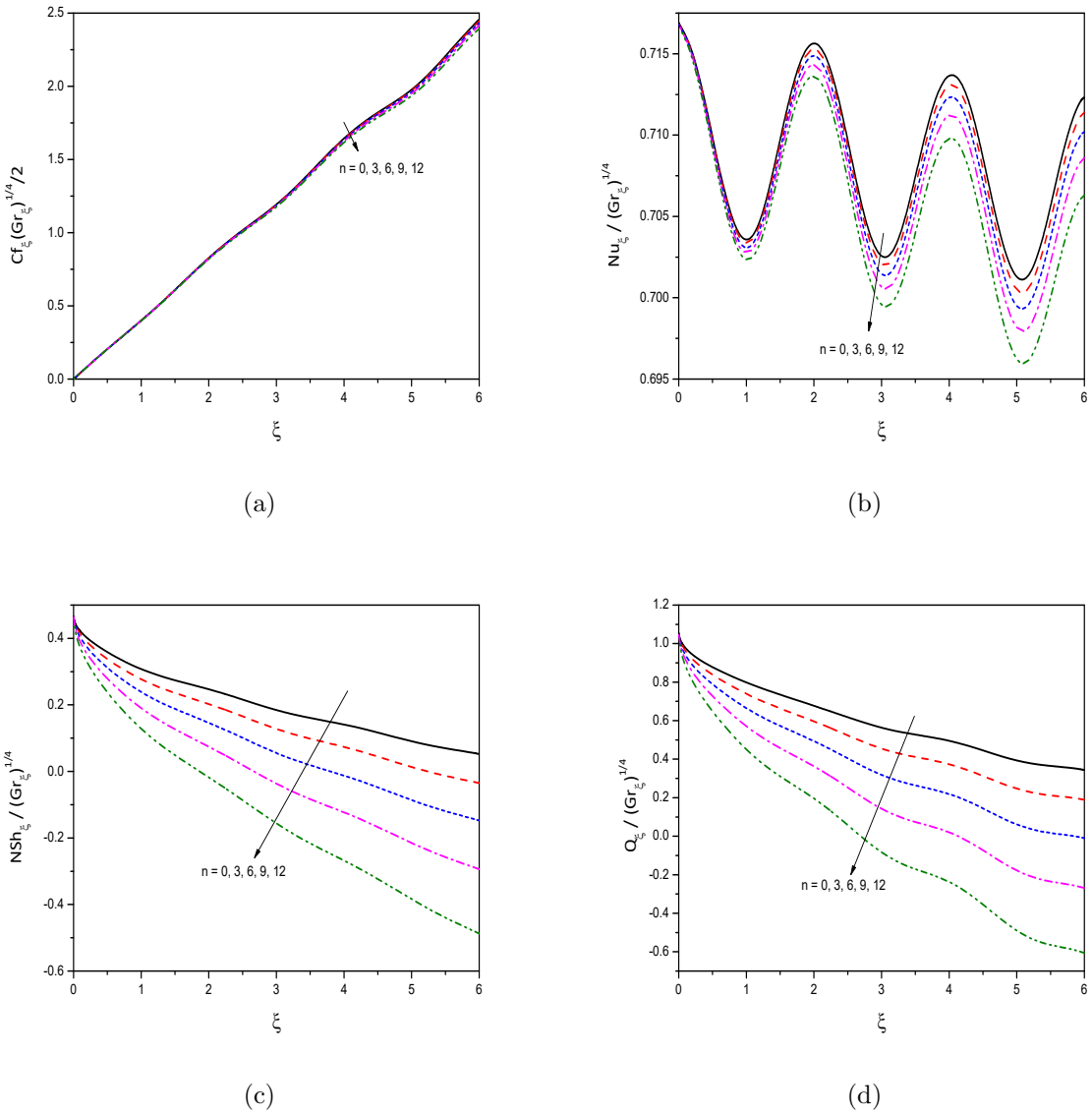

Figure 7.9: "Effect of the fitted rate constant n on the profiles of (a) $Cf_\xi(Gr_\xi^{1/4})/2$ (b) $\frac{Nu_\xi}{Gr_\xi^{1/4}}$ (c) $\frac{NSh_\xi}{Gr_\xi^{1/4}}$ (d) $\frac{Q_\xi}{Gr_\xi^{1/4}}$".

Chapter 8

Radiation effect on Mixed Bioconvection of a Nanofluid Past an Inclined Wavy Surface with Variable Properties [1]

8.1 Introduction

It is known that the viscosity of the fluid generally depends on pressure and temperature. However, less effect in fluid flow is observed with pressure. Therefore, viscosity is dependent on the temperature variation. Further, at high temperatures, the effect of radiation in space technology, space vehicle re-entry, nuclear engineering applications and other industrial areas are very significant. Hayat *et al.* [44] discussed the mixed convection flow of viscoelastic nanofluid due to a stretching cylinder with variable thermal conductivity and heat source/sink. Heydari and Shokouhmand [45] studied the effect of variable properties on the laminar forced convection Al_2O_3-water nanofluid flow and heat transfer through an annular microchannel. Bilal *et al.* [18] analyzed the MHD and thermal radiation of Williamson nanofluid flow with variable thermal conductivity over a stretching cylinder using numerical simulations. Mkhatshwa *et al.* [78] investigated the MHD bioconvective flow of Casson nanofluid past a vertical surface with variable thermophysical characteristics, chemical reaction, nonlinear radiation, Hall, and ion-slip currents. Azam *et al.* [12] presented a numerical

[1] Communicated to "**Journal of Applied Nonlinear Dynamics**"

simulation for variable thermal properties and heat source/sink in the flow of cross nanofluid over a moving cylinder. Ayele and Ibrahim [124] discussed hybrid nanofluids flow with mixed convection of MWCNTs - Al_2O_3/engine oil with variable viscosity and thermal conductivity over a spinning cone. Irfan [52] discussed the MHD nonlinear mixed convection Carreau nanofluid with variable conductivity subject to Buongiorno's theory along with the heat source/sink and chemical reaction. Irfan *et al.* [53] investigated the unsteady MHD flow of bio-nanofluid in a permeable medium taking thermal radiation and chemical reaction into account over a stretching sheet with variable thermophysical properties

In this chapter, the effect of radiation on the mixed convection of a nanofluid past an inclined wavy surface in the presence of gyrotactic microorganisms with variable properties is considered. The equations of the flow are non-dimensionalized and then solved using the bivariate pseudo-spectral local linearization method (BPSLLM). The influence of pertinent parameters on the heat transfer rate, nanoparticle mass transfer rate, and density number of the microbes are examined.

8.2 Mathematical formulation

Consider an incompressible, steady, and laminar flow of a nanofluid containing motile microorganisms along an inclined wavy surface. The wavy surface is inclined at an angle A ($0^o \leq A \leq 90^o$) for the horizontal line as depicted in Fig. 2.1. The equations governing the flow are

$$\frac{\partial U}{\partial X}+\frac{\partial V}{\partial Y}=0, \tag{8.1}$$

$$\rho_{f\infty}\left(U\frac{\partial U}{\partial X}+V\frac{\partial U}{\partial Y}\right)=-\frac{\partial P}{\partial X}+2\frac{\partial}{\partial X}\left(\mu(T)\frac{\partial U}{\partial X}\right)+2\frac{\partial}{\partial Y}\left(\mu(T)\left[\frac{\partial U}{\partial Y}+\frac{\partial V}{\partial X}\right]\right)$$
$$+\left[(1-\Phi_\infty)\,\beta_T\rho_{f\infty}\,(T-T_\infty)-(\rho_p-\rho_{f\infty})\,(\Phi-\Phi_\infty)-\beta_M(\rho_m-\rho_{f\infty})(M-M_\infty)\right]gSinA \tag{8.2}$$

$$\rho_{f\infty}\left(U\frac{\partial V}{\partial X}+V\frac{\partial V}{\partial Y}\right)=-\frac{\partial P}{\partial Y}+2\frac{\partial}{\partial X}\left(\mu(T)\left[\frac{\partial U}{\partial Y}+\frac{\partial V}{\partial X}\right]\right)+2\frac{\partial}{\partial Y}\left(\mu(T)\frac{\partial V}{\partial Y}\right)$$
$$+\left[(1-\Phi_\infty)\,\beta_T\rho_{f\infty}\,(T-T_\infty)-(\rho_p-\rho_{f\infty})\,(\Phi-\Phi_\infty)-\beta_M(\rho_m-\rho_{f\infty})(M-M_\infty)\right]gCosA \tag{8.3}$$

$$(\rho c)_f\left(U\frac{\partial T}{\partial X}+V\frac{\partial T}{\partial Y}\right)=\frac{\partial}{\partial X}\left(k(T)\frac{\partial T}{\partial X}\right)+\frac{\partial}{\partial Y}\left(k(T)\frac{\partial T}{\partial Y}\right)$$
$$+(\rho c)_p\left\{D_B\left(\frac{\partial \Phi}{\partial X}\frac{\partial T}{\partial X}+\frac{\partial \Phi}{\partial Y}\frac{\partial T}{\partial Y}\right)+\frac{D_T}{T_\infty}\left[\left(\frac{\partial T}{\partial X}\right)^2+\left(\frac{\partial T}{\partial Y}\right)^2\right]\right\}+\frac{16\sigma_2 T_\infty^3}{3K_e}\nabla^2 T \tag{8.4}$$

$$U\frac{\partial \Phi}{\partial X}+V\frac{\partial \Phi}{\partial Y}=D_B\left(\frac{\partial^2 \Phi}{\partial X^2}+\frac{\partial^2 \Phi}{\partial Y^2}\right)+\frac{D_T}{T_\infty}\left(\frac{\partial^2 T}{\partial X^2}+\frac{\partial^2 T}{\partial Y^2}\right), \tag{8.5}$$

$$U\frac{\partial M}{\partial X}+V\frac{\partial M}{\partial Y}+\frac{\partial}{\partial X}\left(M\widetilde{V}\right)+\frac{\partial}{\partial Y}\left(M\widetilde{V}\right)=D_n\nabla^2 M, \tag{8.6}$$

where K_e is the mean absorption coefficient, σ_2 is the Stefan Boltzman constant. The average swimming velocity vector of microorganism is $\widetilde{V}=\dfrac{q_n D_B b_c w_c}{q_{np} D_n M_\infty}\dfrac{\partial \Phi}{\partial Y}$.

The viscosity μ, the thermal conductivity k are considered as linear functions of temperature [14] given by

$$\mu(T)=\mu_\infty\left[1-b(T-T_\infty)\right] \qquad and \qquad k(T)=k_0\left[1+E(T-T_\infty)\right] \tag{8.7}$$

where μ_∞ is the absolute viscosity of the fluid, k_0 is the thermal conductivity at the wavy surface temperature, and b, E are constants. All other quantities are defined in previous Chapters.

The associated boundary conditions are :

$$\left.\begin{aligned} &U=0, \quad V=0, \quad q_w=-k(n.\nabla T), \quad q_{np}=-D_B(n.\nabla\Phi), \\ &\qquad\qquad\qquad\qquad q_n=-D_n(n.\nabla M) \quad \text{at} \quad Y=Y_w=\bar{\sigma}(X), \\ &U\to U_\infty, \quad T\to T_\infty, \quad \Phi\to\Phi_\infty, \quad M\to M_\infty \quad \text{as} \quad Y\to\infty \end{aligned}\right\} \tag{8.8}$$

The irregular wavy surface is transformed to a flat surface, using the following transformations ([131])

$$\left.\begin{aligned} &\xi=\frac{X}{L}, \quad \eta=\frac{Y-\sigma}{L\xi^{\frac{1}{2}}}\sqrt{Re}, \quad \psi=\frac{LU_\infty\xi^{\frac{1}{2}}f(\xi,\eta)}{\sqrt{Re}}, \quad p=\frac{P}{\rho_{f\infty}U_\infty^2}, \\ &T-T_\infty=\frac{q_w L}{k}Re^{-1/2}\xi^{1/2}\theta(\xi,\eta), \quad \Phi-\Phi_\infty=\frac{q_{np}L}{D_B}\mathrm{Re}^{-1/2}\xi^{1/2}\phi(\xi,\eta), \\ &M-M_\infty=\frac{q_n L}{D_n}\mathrm{Re}^{-1/2}\xi^{1/2}\chi(\xi,\eta), \quad \tilde{u}=\partial\psi/\partial y \ \ and \ \ \tilde{v}=-\partial\psi/\partial x \end{aligned}\right\} \tag{8.9}$$

where

$$Gr=\frac{(1-\Phi_\infty)\,g\beta_T q_w L^4}{k\nu^2} \quad and \quad Re=\frac{U_\infty L}{\nu}$$

are the Grashof number and Reynolds number respectively and the stream function ψ is same as in 2.10 of Chapter2.

The non-dimensional form of the terms in (8.7) can be written as

$$\mu(T) = \mu_\infty \left[1 - P_n \theta \xi^{\frac{1}{2}}\right] \qquad and \qquad k(T) = k_0 \left[1 + \beta \theta \xi^{\frac{1}{2}}\right] \tag{8.10}$$

where $P_n = \dfrac{bq_wL}{k} Re^{-\frac{1}{2}}$ is the temperature dependent viscous parameter known as Pearson number, $\beta = \dfrac{Eq_wL}{k} Re^{-\frac{1}{2}}$ is the temperature dependent thermal conductivity parameter.

Substituting Eq. (8.9) in the governing equations (8.1) to (8.6) and invoking the boundary layer approximation, we get the following non-dimensional form.

$$\begin{aligned}[1 - P_n\theta\xi^{\frac{1}{2}}]\left(1+\sigma_\xi^2\right) f''' + \frac{1}{2} f f'' - \frac{\xi\sigma_\xi\sigma_{\xi\xi}}{\left(1+\sigma_\xi^2\right)}\left(f'\right)^2 - P_n\left(1+\sigma_\xi^2\right)\xi^{\frac{1}{2}}\theta' f'' \\ + \frac{Ri\xi^{\frac{3}{2}}\left(\theta - N_r\phi - R_b\chi\right)}{\left(1+\sigma_\xi^2\right)}\left(SinA + \sigma_\xi CosA\right) = \xi\left[f'\frac{\partial f'}{\partial\xi} - \frac{\partial f}{\partial\xi} f''\right]\end{aligned} \tag{8.11}$$

$$\begin{aligned}\frac{\left(1+\sigma_\xi^2\right)}{\Pr}\left[(1+\beta\theta\xi^{\frac{1}{2}})\theta'' + \frac{4}{3}R_d\theta'' + \left(\beta + N_t\right)\xi^{\frac{1}{2}}(\theta')^2 + N_b\xi^{\frac{1}{2}}\phi'\theta'\right] \\ + \frac{1}{2}\left(f\theta' - f'\theta\right) = \xi\left[f'\frac{\partial\theta}{\partial\xi} - \theta'\frac{\partial f}{\partial\xi}\right]\end{aligned} \tag{8.12}$$

$$\frac{\left(1+\sigma_\xi^2\right)}{Le}\left[\phi'' + \frac{N_t}{N_b}\theta''\right] + \frac{1}{2}\left(f\phi' - f'\phi\right) = \xi\left[f'\frac{\partial\phi}{\partial\xi} - \phi'\frac{\partial f}{\partial\xi}\right] \tag{8.13}$$

$$\frac{\left(1+\sigma_\xi^2\right)}{Sc}\chi'' - \frac{Pe}{Sc}\left(1-\sigma_\xi\right)\phi'' + \frac{1}{2}\left(f\chi' - f'\chi\right) = \xi\left[f'\frac{\partial\chi}{\partial\xi} - \chi'\frac{\partial f}{\partial\xi}\right] \tag{8.14}$$

and

$$\left.\begin{aligned} &f'(\xi,0) = 0, \quad f(\xi,0) = -2\xi\left.\frac{\partial f}{\partial\xi}\right|_{(\xi,0)}, \quad \theta'(\xi,0) = -\frac{1}{\sqrt{1+\sigma_\xi^2}}, \\ &\phi'(\xi,0) = -\frac{1}{\sqrt{1+\sigma_\xi^2}}, \quad \chi'(\xi,0) = -\frac{1}{\sqrt{1+\sigma_\xi^2}} \\ &f'(\xi,\infty) = 1, \quad \theta(\xi,\infty) = 0, \quad \phi(\xi,\infty) = 0, \quad \chi(\xi,\infty) = 0 \end{aligned}\right\} \tag{8.15}$$

The parameters Pr, Pe, Le, Sc, N_b, N_r, N_t, R_b, R_d are same as in Chapter 3 and Chapter 4.

The non-dimensional form of the parameters coefficient of skin friction, Nusselt number, nanoparticle Sherwood number and density number of motile microbe are given in 4.14 of Chapter 4

8.3 Method of Solution

The set of equations (8.11) - (8.15) is solved using the BPSLLM [82]. By using this BPSLLM approach, an iteration scheme is obtained by linearizing the non-linear component of single differential equations about a single dependent variable at a time.

On implementing this technique to equations (8.11) - (8.14), we obtain

$$a_{1,m}f'''_{m+1} + a_{2,m}f''_{m+1} + a_{3,m}f'_{m+1} + a_{4,m}f_{m+1} + a_{5,m}\frac{\partial f'_{m+1}}{\partial \xi} + a_{6,m}\frac{\partial f_{m+1}}{\partial \xi} = R_{1,m} \tag{8.16}$$

$$b_{1,m}\theta''_{m+1} + b_{2,m}\theta'_{m+1} + b_{3,m}\theta_{m+1} + b_{4,m}\frac{\partial \theta_{m+1}}{\partial \xi} = R_{2,m} \tag{8.17}$$

$$c_{1,m}\phi''_{m+1} + c_{2,m}\phi'_{m+1} + c_{3,m}\phi_{m+1} + c_{4,m}\frac{\partial \phi_{m+1}}{\partial \xi} = R_{3,m} \tag{8.18}$$

$$d_{1,m}\chi''_{m+1} + d_{2,m}\chi'_{m+1} + d_{3,m}\chi_{m+1} + d_{4,m}\frac{\partial \chi_{m+1}}{\partial \xi} = R_{4,m} \tag{8.19}$$

where the coefficients are

$$a_{1,m} = \left[1 - P_n\theta_m\xi^{\frac{1}{2}}\right]\left(1+\sigma_\xi^2\right), \quad a_{2,m} = -P_n\left(1+\sigma_\xi^2\right)\xi^{\frac{1}{2}}\theta'_m + \frac{1}{2}f_m + \xi\frac{\partial f_m}{\partial \xi},$$

$$a_{3,m} = -2\left[\frac{\xi\sigma_\xi\sigma_{\xi\xi}}{1+\sigma_\xi^2}\right]f'_m - \xi\frac{\partial f'_m}{\partial \xi}, \quad a_{4,m} = \frac{1}{2}f''_m, \quad a_{5,m} = -\xi f'_r, \quad a_{6,m} = \xi f''_r$$

$$R_{1,m} = \xi f''_m\frac{\partial f_m}{\partial \xi} - \left[\frac{\xi\sigma_\xi\sigma_{\xi\xi}}{1+\sigma_\xi^2}\right](f'_m)^2 + \frac{1}{2}f_m f''_m - \xi f'_m\frac{\partial f'_m}{\partial \xi}$$
$$-\frac{Ri\xi^{\frac{3}{2}}\left(\theta_m - N_r\phi_m - R_b\chi_m\right)}{\left(1+\sigma_\xi^2\right)}\left(SinA + \sigma_\xi CosA\right)$$

$$b_{1,m} = \frac{\left(1+\beta\theta_m\xi^{\frac{1}{2}} + \frac{4}{3}R_d\right)\left(1+{\sigma_\xi}^2\right)}{\mathrm{Pr}},$$

$$b_{2,m} = \frac{(1+\sigma_\xi^2)}{\mathrm{Pr}}N_b\xi^{\frac{1}{2}}\phi'_m + \frac{2(1+\sigma_\xi^2)(\beta+N_t)\xi^{\frac{1}{2}}}{\mathrm{Pr}}\theta'_m + \frac{1}{2}f_{m+1} + \xi\frac{\partial f_{m+1}}{\partial \xi},$$

$$b_{3,m} = \frac{\beta(1+\sigma_\xi^2)\xi^{\frac{1}{2}}}{\mathrm{Pr}}\theta''_m - \frac{1}{2}f'_{m+1}, \quad b_{4,m} = -\xi f'_{m+1},$$

$$R_{2,m} = \frac{(1+\sigma_\xi^2)(\beta+N_t)\xi^{\frac{1}{2}}}{\mathrm{Pr}}(\theta'_m)^2 + \frac{\beta(1+\sigma_\xi^2)\xi^{\frac{1}{2}}}{Pr}\theta''_m\theta_m$$

$$c_{1,m} = \frac{1+\sigma_\xi^2}{Le}, \quad c_{2,m} = \frac{1}{2}f_{m+1} + \xi\frac{\partial f_{m+1}}{\partial \xi}, \quad c_{3,m} = -\frac{1}{2}f'_{m+1},$$

$$c_{4,m} = -\xi f'_{m+1}, \quad R_{3,m} = -\frac{(1+\sigma_\xi^2)}{Le}\frac{N_t}{N_b}\theta''_{m+1},$$
$$d_{1,m} = \frac{1+\sigma_\xi^2}{Sc}, \quad d_{2,m} = \frac{1}{2}f_{m+1} + \xi\frac{\partial f_{m+1}}{\partial \xi}$$
$$d_{3,m} = -\frac{1}{2}f''_{m+1}, \quad d_{4,m} = -\xi f'_{m+1}, \quad R_{4,m} = \frac{Pe}{Sc}(1-\sigma_\xi)\phi''_{m+1}$$

The boundary conditions are

$$\left.\begin{aligned} &f'_{m+1}(\xi,0) = 0\,, \quad f_{m+1}(\xi,0) = -2\xi\left.\frac{\partial f}{\partial \xi}\right|_{(\xi,0)}, \quad \theta'_{m+1}(\xi,0) = -\frac{1}{\sqrt{1+\sigma_\xi^2}}, \\ &\phi'_{m+1}(\xi,0) = -\frac{1}{\sqrt{1+\sigma_\xi^2}}\,, \quad \chi'_{m+1}(\xi,0) = -\frac{1}{\sqrt{1+\sigma_\xi^2}} \\ &f'_{m+1}(\xi,\infty) = 1, \quad \theta_{m+1}(\xi,\infty) = 0, \quad \phi_{m+1}(\xi,\infty) = 0, \quad \chi_{m+1}(\xi,\infty) = 0. \end{aligned}\right\} \tag{8.20}$$

Implementing the above method in both η and ξ, to the equations (8.16) to (8.19), we get

$$A^{(1)}\mathbf{F}_i + \gamma^{(1)}_{5,i}\sum_{j=0}^{M}\mathbf{d}_{i,j}\mathbf{D}\mathbf{F}_j + \gamma^{(1)}_{6,i}\sum_{j=0}^{M}\mathbf{d}_{i,j}\mathbf{F}_j = \mathbf{R}_{1,i} \tag{8.21}$$

$$A^{(2)}\mathbf{\Theta}_i + \gamma^{(2)}_{4,i}\sum_{j=0}^{M}\mathbf{d}_{i,j}\mathbf{\Theta}_j = \mathbf{R}_{2,i} \tag{8.22}$$

$$A^{(3)}\mathbf{\Phi}_i + \gamma^{(3)}_{3,i}\sum_{j=0}^{M}\mathbf{d}_{i,j}\mathbf{\Phi}_j = \mathbf{R}_{3,i} \tag{8.23}$$

$$A^{(4)}\chi_i + \gamma^{(4)}_{4,i}\sum_{j=0}^{M}\mathbf{d}_{i,j}\chi_j = \mathbf{R}_{4,i} \tag{8.24}$$

where

$$A^{(1)} = \gamma^{(1)}_{1,i}\mathbf{D}^3 + \gamma^{(1)}_{2,i}\mathbf{D}^2 + \gamma^{(1)}_{3,i}\mathbf{D} + \gamma^{(1)}_{4,i}\mathbf{I},$$
$$A^{(2)} = \gamma^{(2)}_{1,i}\mathbf{D}^2 + \gamma^{(2)}_{2,i}\mathbf{D} + \gamma^{(2)}_{3,i}\mathbf{I},$$
$$A^{(3)} = \gamma^{(3)}_{1,i}\mathbf{D}^2 + \gamma^{(3)}_{2,i}\mathbf{D} + \gamma^{(3)}_{3,i}\mathbf{I},$$
$$A^{(4)} = \gamma^{(4)}_{1,i}\mathbf{D}^2 + \gamma^{(4)}_{2,i}\mathbf{D} + \gamma^{(4)}_{3,i}\mathbf{I}$$

Here $\gamma^{(1)}_{k,i}$, $\gamma^{(2)}_{k,i}$, $\gamma^{(3)}_{k,i}$, $\gamma^{(4)}_{k,i}$ and $\mathbf{R}_{k,i}$ are N^{th} order diagonal matrices with diagonal elements as, $a_{k,m}(\zeta_r,\tau_i)$, $b_{k,m}(\zeta_r,\tau_i)$, $c_{k,m}(\zeta_r,\tau_i)$, $d_{k,m}(\zeta_r,\tau_i)$ and $R_{k,m}(\zeta_r,\tau_i)$ for $r = 1,2,3,\cdots N$ respec-

tively and **I** refers the identity matrix.

The equation (8.21) written in matrix form as

$$\begin{bmatrix} A^{(1)}_{0,0} & A^{(1)}_{0,1} & A^{(1)}_{0,2} & \cdots & A^{(1)}_{0,M} \\ A^{(1)}_{1,0} & A^{(1)}_{1,1} & A^{(1)}_{1,2} & \cdots & A^{(1)}_{1,M} \\ A^{(1)}_{2,0} & A^{(1)}_{2,1} & A^{(1)}_{2,2} & \cdots & A^{(1)}_{2,M} \\ \vdots & \vdots & \vdots & \cdots & \vdots \\ A^{(1)}_{M,0} & A^{(1)}_{M,1} & A^{(1)}_{M,2} & \cdots & A^{(1)}_{M,M} \end{bmatrix} \begin{bmatrix} \mathbf{F}_0 \\ \mathbf{F}_1 \\ \mathbf{F}_2 \\ \vdots \\ \mathbf{F}_M \end{bmatrix} = \begin{bmatrix} \mathbf{R}_{1,0} \\ \mathbf{R}_{1,1} \\ \mathbf{R}_{1,2} \\ \vdots \\ \mathbf{R}_{1,M} \end{bmatrix} \tag{8.25}$$

where

$$\begin{aligned} A^{(1)}_{i,j} &= A^{(1)} + \gamma^{(1)}_{5,r}\mathbf{d}_{i,i}\mathbf{D} + \gamma^{(1)}_{6,r}\mathbf{d}_{i,i}\mathbf{I},\ for\ i = j; \\ A^{(1)}_{i,j} &= \gamma^{(1)}_{5,r}\mathbf{d}_{i,j}\mathbf{D} + \gamma^{(1)}_{6,r}\mathbf{d}_{i,j}\mathbf{I},\ for\ i \neq j \end{aligned} \tag{8.26}$$

In a similar manner, the equations (8.22) to (8.24) can be written in matrix form. Solving these matrix equations, iteratively, we obtain the solution to (8.11) - (8.15).

8.4 Computational Results and Discussions

In the present study, we focus our discussion on analyzing the inclination angle effect A, amplitude α, mixed convection parameter Ri, bioconvection Peclet number Pe, bioconvection Schmidt number Sc, radiation parameter R_d, Pearson number P_n and temperature dependent thermal conductivity parameter β on the coefficient of skin friction $Cf_\xi\sqrt{Re_\xi}$, Nusselt number $Nu_\xi/\sqrt{Re_\xi}$, nanoparticle Sherwood number $NSh_\xi/\sqrt{Re_\xi}$ and density number of motile microbes $Q_\xi/\sqrt{Re_\xi}$. The values of the other parameters are fixed as $Pr = 2, Le = 5, N_b = 0.5, N_t = 0.1, N_r = 0.3$ and $R_b = 0.6$ unless otherwise mentioned.

Figure 8.1 refers to the effects of bioconvection Peclet number Pe on various physical parameters for given values of other required parameters in the discussion as mentioned above. It is found that the parameters are escalating for a raise in the bioconvection Peclet number Pe, i.e., a raise of particle movements cause the improvement of all dimensionless parameters under consideration. This is evident from the figures 8.1(a) to 8.1(d). The process of the bioconvection Peclet number is the ratio of gyrotactic swimming's characteristic velocity to a random diffusive swimming's characteristic velocity. Because microorganisms are heavier than water, their up-swimming causes an unstable density stratification. The

speed of the microorganisms in the fluid is increased by Pe, resulting in a higher density number of microorganisms at the wavy surface.

The variation $Cf_\xi\sqrt{Re_\xi}$, $Nu_\xi/\sqrt{Re_\xi}$, $NSh_\xi/\sqrt{Re_\xi}$ and $Q_\xi/\sqrt{Re_\xi}$ with bioconvection Schmidt number Sc on is presented in Figure 8.2. It is noticed from this fugure that $Cf_\xi\sqrt{Re_\xi}$, $Nu_\xi/\sqrt{Re_\xi}$, $NSh_\xi/\sqrt{Re_\xi}$ and $Q_\xi/\sqrt{Re_\xi}$ are increasing with an increase in the bioconvection Schmidt number Sc. Physically, this is because when the bioconvection Schmidt number grows, the viscous diffusion rate increases, lowering the dimensionless velocity and increasing the microbe density number.

Figure 8.3 delineates the effect of the angle of the wavy surface A on required parameters. The raise in the angle of inclination has positive effect on the coefficient of skin friction $Cf_\xi\sqrt{Re_\xi}$, Nusselt number $Nu_\xi/\sqrt{Re_\xi}$, nanoparticle Sherwood number $NSh_\xi/\sqrt{Re_\xi}$ and density number of motile microorganisms $Q_\xi/\sqrt{Re_\xi}$. As a result, the rate of transfer of all physical quantities is higher for vertical surfaces than for horizontal surfaces. This is clear from the figures 8.3(a), 8.3(b), 8.3(c) and 8.3(d).

Figure 8.4 elucidates the typical behaviour of $Cf_\xi\sqrt{Re_\xi}$, $Nu_\xi/\sqrt{Re_\xi}$, $NSh_\xi/\sqrt{Re_\xi}$ and $Q_\xi/\sqrt{Re_\xi}$ with respect to amplitude of the wavy surface α, which we can observe in figures 8.4(a) to 8.4(d). We found both increasing and decreasing nature in the profiles of the above said parameters for an increase in α. Also we found overall raise in all these parameters when we move across the channel from left to right.

The temperature-dependent thermal conductivity parameter β's effect on skin friction $Cf_\xi\sqrt{Re_\xi}$, heat transfer rate $Nu_\xi/\sqrt{Re_\xi}$, nanaoparticle mass tranfer rate $NSh_\xi/\sqrt{Re_\xi}$ and density of motile microorganisms $Q_\xi/\sqrt{Re_\xi}$ is portrayed in figure 8.5. It is found from the figures 8.5(a), 8.5(c) and 8.5(d) that, the parameters $Cf_\xi\sqrt{Re_\xi}$, $NSh_\xi/\sqrt{Re_\xi}$ and $Q_\xi/\sqrt{Re_\xi}$ are increasing with an increase in β. An increase in the values of the temperature dependent thermal conductivity parameter results in the decrease of $Nu_\xi/\sqrt{Re_\xi}$ as shown in figure 8.5(b). This is a consequence of the fact that the Nusselt number is inversely related to thermal conductivity.

The influence of Ri, mixed convection parameter, is portrayed in figures 8.6(a) - 8.6(d). It is identified that the increase of mixed convection parameter results in the enhancement of all the dimensionless parameters $Cf_\xi\sqrt{Re_\xi}$, $Nu_\xi/\sqrt{Re_\xi}$, $NSh_\xi/\sqrt{Re_\xi}$ and $Q_\xi/\sqrt{Re_\xi}$.

The variation of $Cf_\xi\sqrt{Re_\xi}$, $Nu_\xi/\sqrt{Re_\xi}$, $NSh_\xi/\sqrt{Re_\xi}$ and $Q_\xi/\sqrt{Re_\xi}$ for different values of radiation parameter R_d are displayed in figure 8.7. The figures 8.7(a), 8.7(c) and 8.7(d) shows that increasing the radiation parameter increases surface drag, nanoparticle mass

transfer, and motile microbe density. But it is found from the figure 8.7(b) that, the heat transfer rate is falling for a rise in radiation parameter. Surface emissivity is inversely proportional to the fourth power of absolute temperature, and radiant energy is proportional to the fourth power of absolute temperature. As a result, except for very low emissivity values, R_d changes the temperature. Surface roughness causes temperature gradients to be weaker and the extent of the gradients to be reduced.

Figure 8.8 shows the effect of P_n, Pearson number, on $Cf_\xi\sqrt{Re_\xi}$, $Nu_\xi/\sqrt{Re_\xi}$, $NSh_\xi/\sqrt{Re_\xi}$ and $Q_\xi/\sqrt{Re_\xi}$. It is observed from figures 8.8(a) to 8.8(d), that the parameters' values raise, for a raise in Pearson number.

8.5 Conclusions

In this chapter, an analysis is presented to study the nanofluid past an inclined wavy surface with mixed convection in the presence of gyrotactic microorganisms with variable properties and radiation effects. The nonlinear equations are linearized employing local linearization procedure and the resultant system is solved by a bivariate pseudo-spectral collocation method. Important observations are itemized below:

- An increase in the bioconvection Peclet number, bioconvection Schmidt number, mixed convection parameter, Pearson number, angle of inclination enhances the skin friction coefficient, heat transfer rate, nanoparticle mass transfer, and density of motile microorganisms.
- The influence of temperature-dependent thermal conductivity, radiation parameter enhances coefficient of skin friction, nanoparticle mass transfer rate, and density of motile microorganisms.
- The heat transfer rate decreases for an increase in temperature-dependent thermal conductivity, radiation parameter.
- The amplitude of the wavy surface behaves typically for skin friction. heat transfer rate, nanoparticle mass transfer rate, and density of microorganisms.

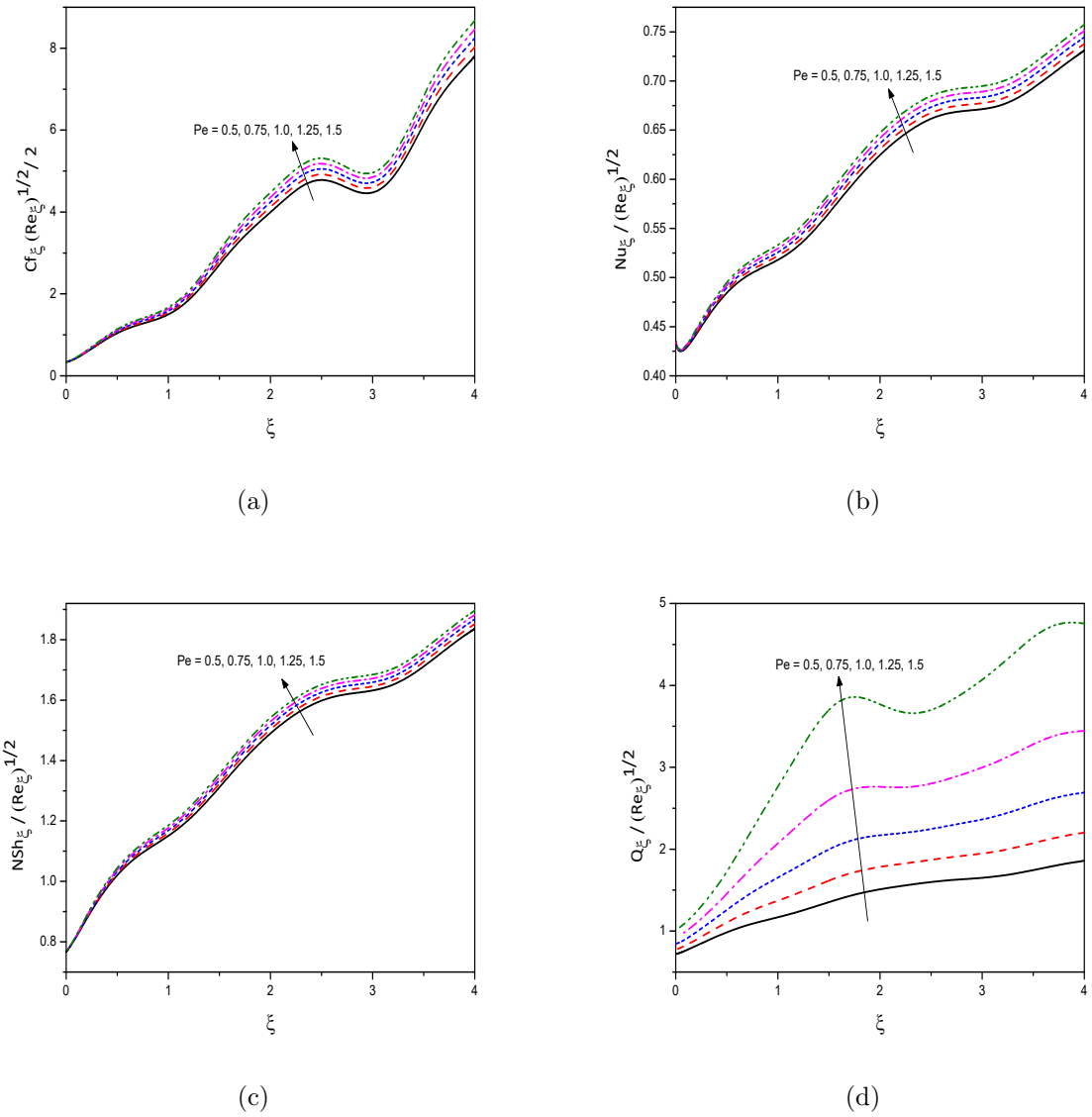

Figure 8.1: "Effect of the bioconvection Peclet number Pe on the profiles of (a) $Cf_\xi(Re_\xi^{1/2})/2$ (b) $\frac{Nu_\xi}{Re_\xi^{1/2}}$ (c) $\frac{NSh_\xi}{Re_\xi^{1/2}}$ (d) $\frac{Q_\xi}{Re_\xi^{1/2}}$".

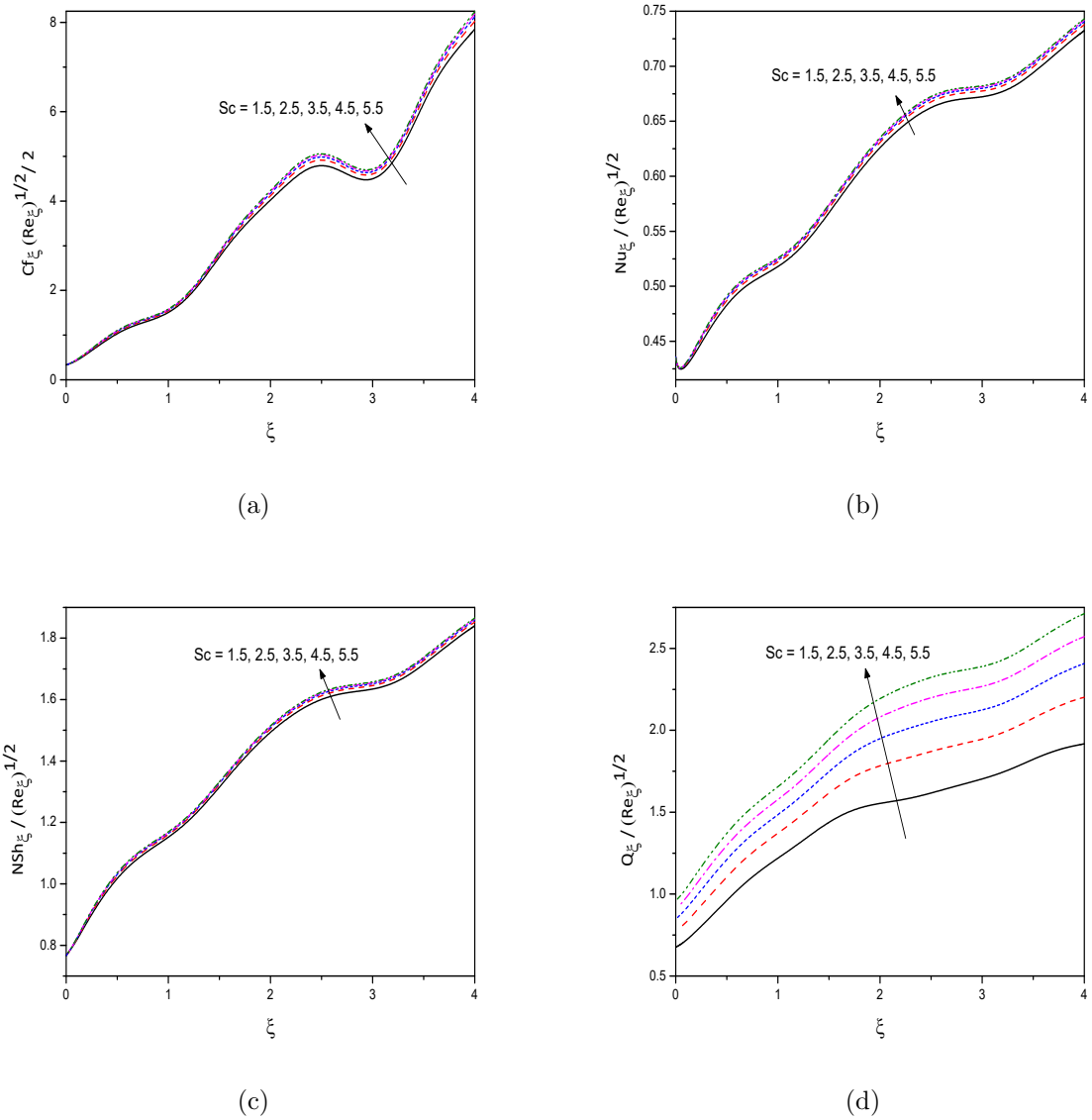

Figure 8.2: "Effect of the bioconvection Schmidt number Sc on the profiles of (a) $Cf_\xi(Re_\xi^{1/2})/2$ (b) $\frac{Nu_\xi}{Re_\xi^{1/2}}$ (c) $\frac{NSh_\xi}{Re_\xi^{1/2}}$ (d) $\frac{Q_\xi}{Re_\xi^{1/2}}$".

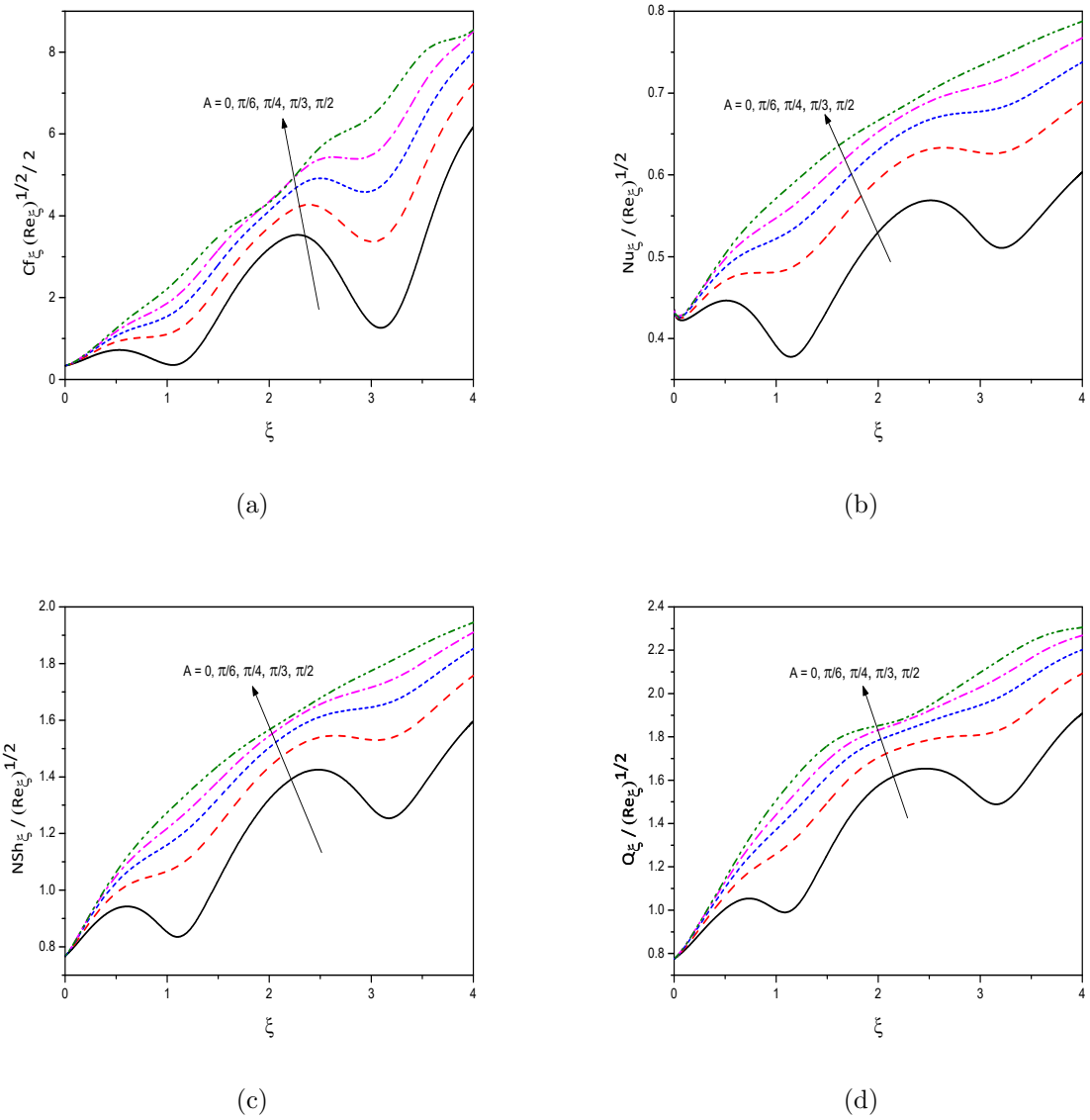

Figure 8.3: "Effect of the angle of inclination A on the profiles of (a) $Cf_\xi(Re_\xi^{1/2})/2$ (b) $\frac{Nu_\xi}{Re_\xi^{1/2}}$ (c) $\frac{NSh_\xi}{Re_\xi^{1/2}}$ (d) $\frac{Q_\xi}{Re_\xi^{1/2}}$".

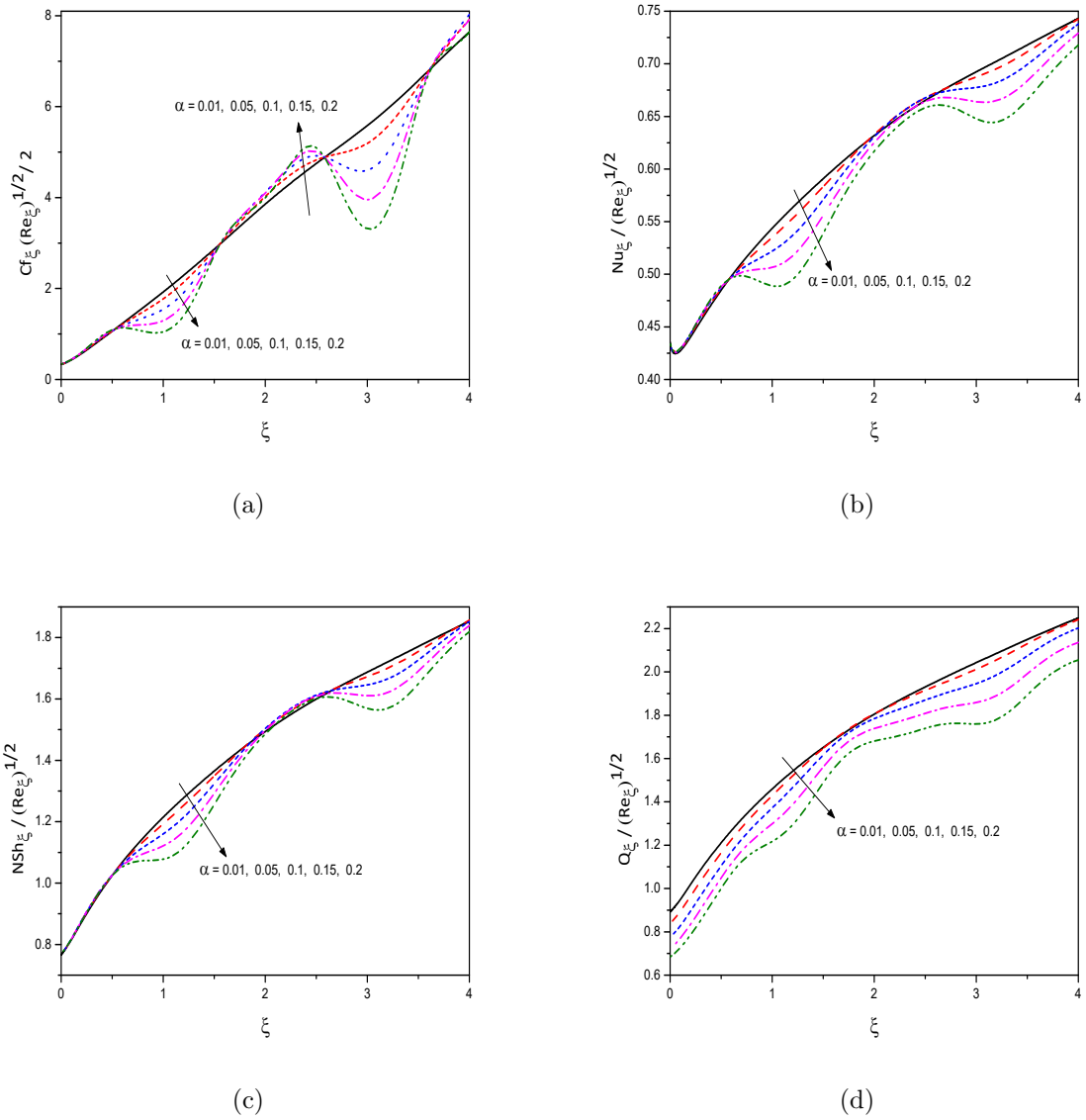

Figure 8.4: "Effect of the amplitude of the wavy surface α on the profiles of (a) $Cf_\xi(Re_\xi^{1/2})/2$ (b) $\frac{Nu_\xi}{Re_\xi^{1/2}}$ (c) $\frac{NSh_\xi}{Re_\xi^{1/2}}$ (d) $\frac{Q_\xi}{Re_\xi^{1/2}}$".

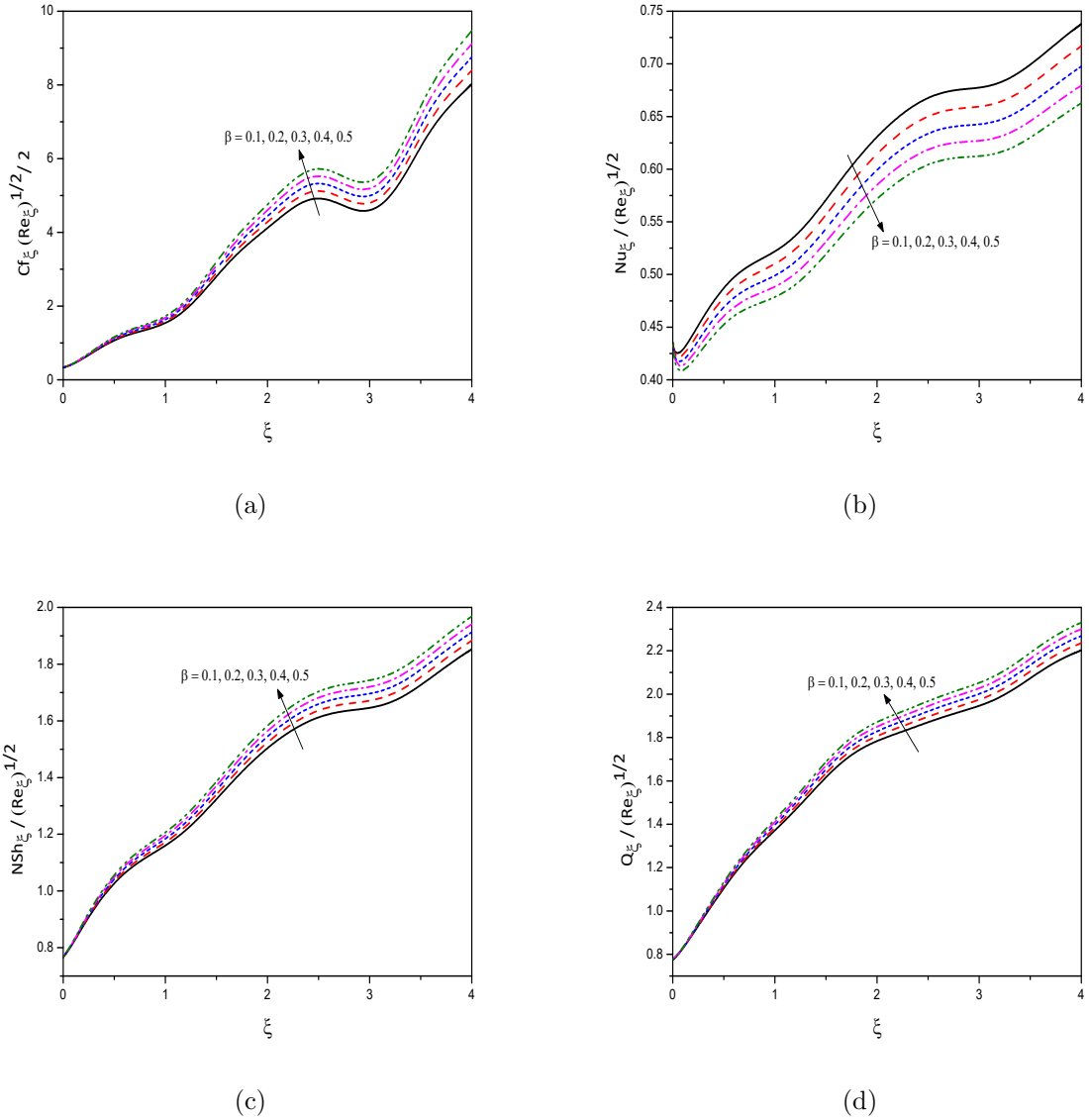

Figure 8.5: "Effect of the thermal conductivity parameter β on the profiles of (a) $Cf_\xi(Re_\xi^{1/2})/2$ (b) $\frac{Nu_\xi}{Re_\xi^{1/2}}$ (c) $\frac{NSh_\xi}{Re_\xi^{1/2}}$ (d) $\frac{Q_\xi}{Re_\xi^{1/2}}$".

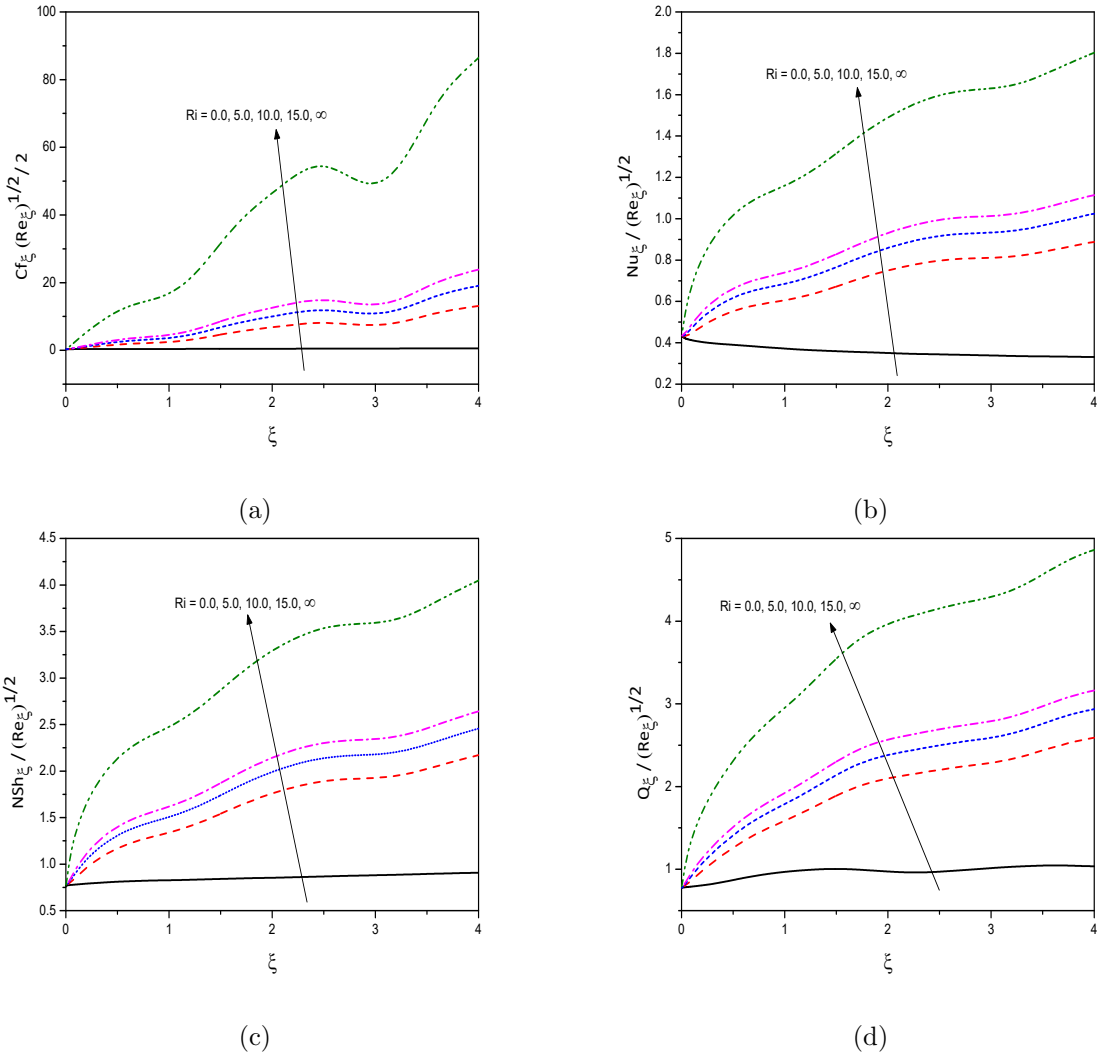

Figure 8.6: "Effect of the mixed convection parameter Ri on the profiles of (a) $Cf_\xi(Re_\xi^{1/2})/2$ (b) $\frac{Nu_\xi}{Re_\xi^{1/2}}$ (c) $\frac{NSh_\xi}{Re_\xi^{1/2}}$ (d) $\frac{Q_\xi}{Re_\xi^{1/2}}$".

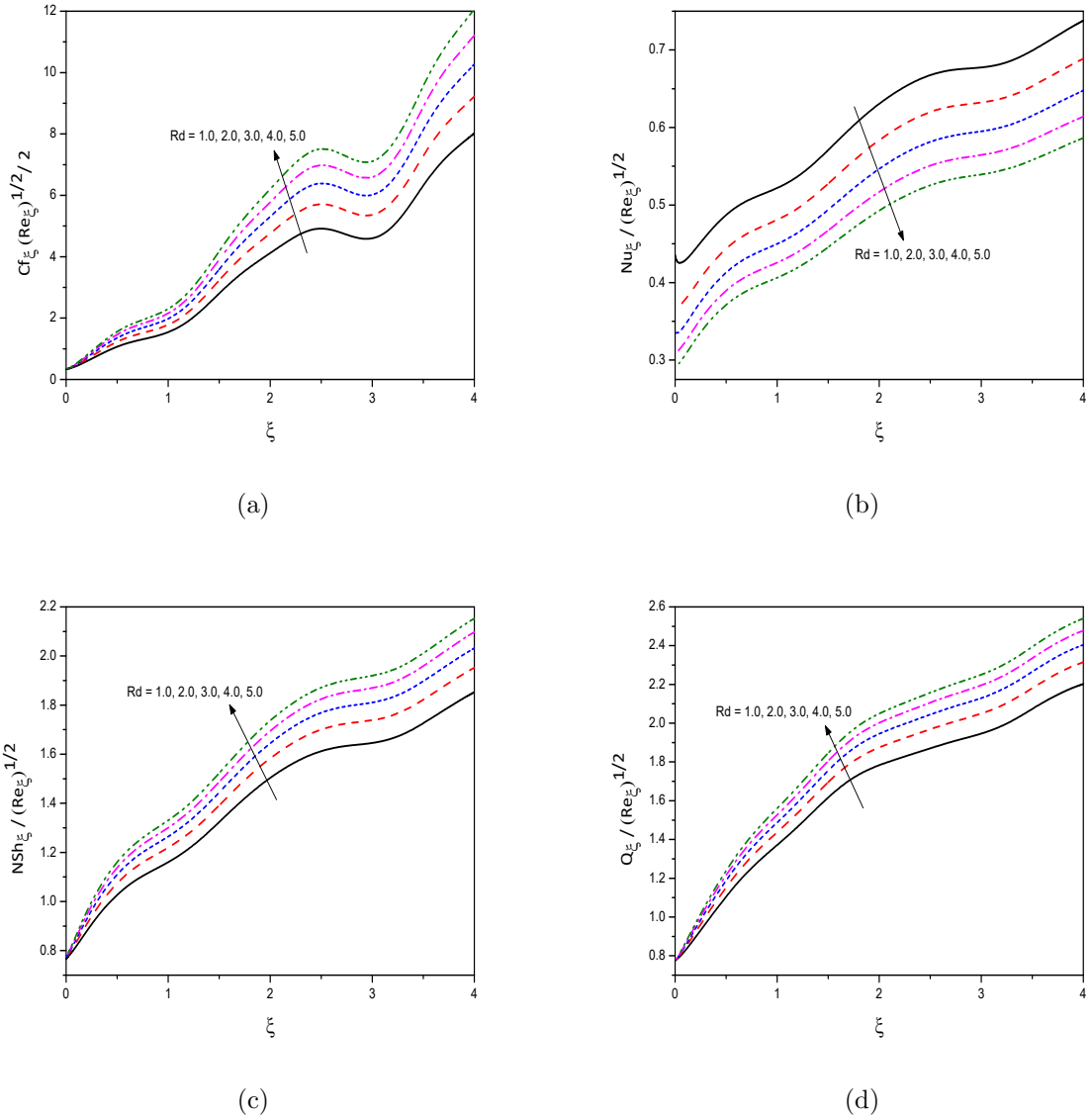

Figure 8.7: "Effect of the radiation parameter R_d on the profiles of (a) $Cf_\xi(Re_\xi^{1/2})/2$ (b) $\frac{Nu_\xi}{Re_\xi^{1/2}}$ (c) $\frac{NSh_\xi}{Re_\xi^{1/2}}$ (d) $\frac{Q_\xi}{Re_\xi^{1/2}}$".

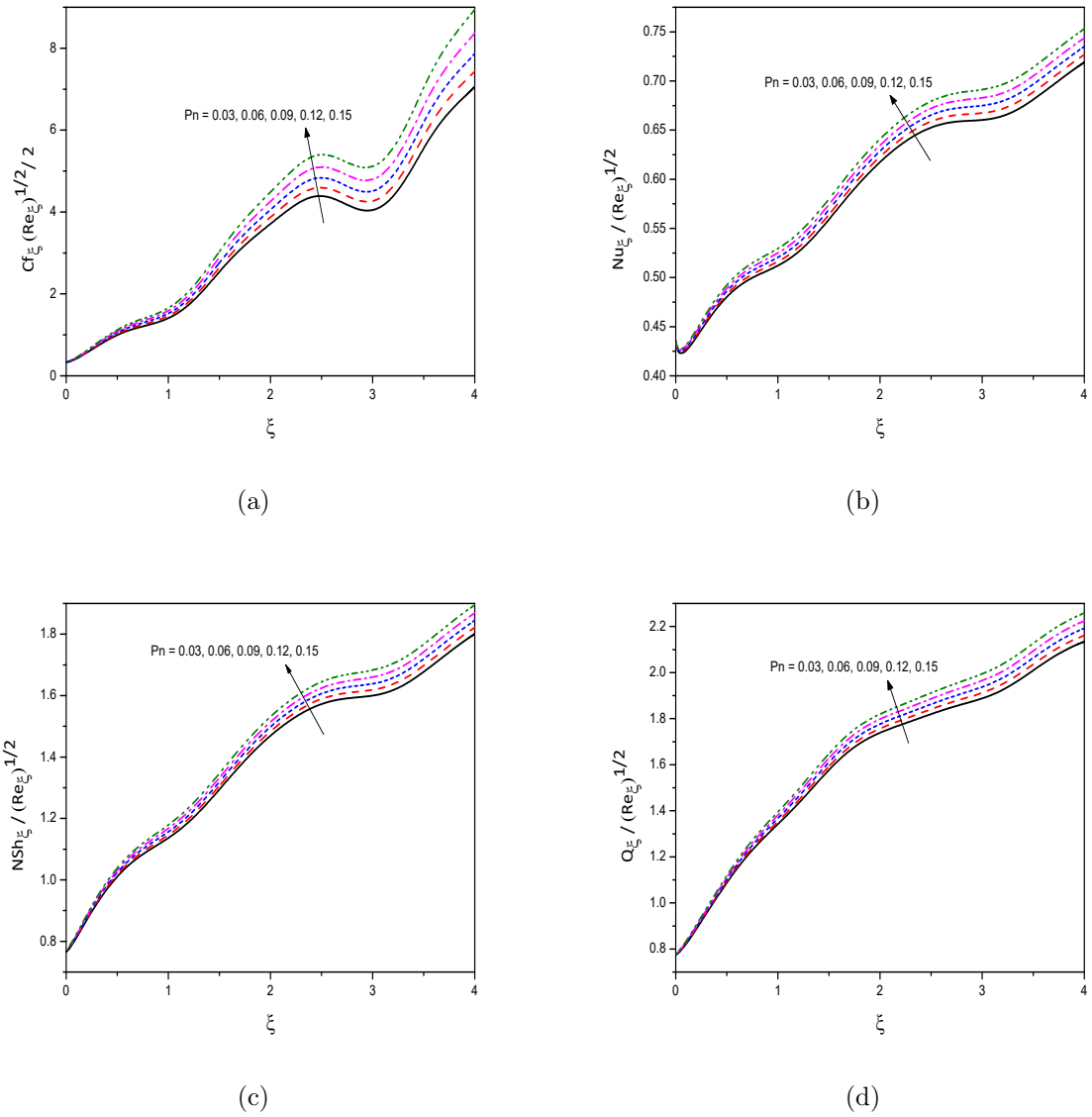

Figure 8.8: "Effect of the Pearson number P_n on the profiles of (a) $Cf_\xi(Re_\xi^{1/2})/2$ (b) $\frac{Nu_\xi}{Re_\xi^{1/2}}$ (c) $\frac{NSh_\xi}{Re_\xi^{1/2}}$ (d) $\frac{Q_\xi}{Re_\xi^{1/2}}$".

Chapter 9

Bioconvection in a Nanofluid Past a Moving Inclined Wavy Surface with Convective Boundary Conditions [1]

9.1 Introduction

The problem of forced convection flow and heat transfer past a continuously moving flat plate is a classic fluid mechanics problem that has fascinated the interest of many researchers, not only because of its numerous practical applications in various extrusion processes but also because of its fundamental role as a fundamental flow problem in Newtonian and non-Newton boundary layer theory. The study of fluids through moving inclined wavy surfaces has not gained much attention from researchers. Rees and Pop [99] analyzed the boundary layer flow and heat transfer on a continuous moving wavy surface. Hossain and Pop [47] discussed the influence of MHD on boundary-layer flow on a moving wavy surface. Wang and Chen [126] discussed the influence of the increased area of a continuously moving wavy plate in a quiescent fluid on its surface compared with a flat plate upon the aerosol particles floating in the fluid. Thumma *et al.* [120] presented a mathematical model of magnetohydrodynamic natural convective boundary layer flow of nanofluids past a stationary and moving inclined porous plate taking into account suction effects. Yacob *et al.* [129, 130] analyzed the steady flow and heat transfer in a nanofluid across a wedge that is either static or moving. Aboeldahab *et al.* [2] considered the free convection effects on MHD boundary layer flow and

[1] Communicated to "**International Journal of Applied Mechanics and Engineering**"

heat transfer over a continuous moving wavy surface in porous media. Mehmood *et al.* [72] computed the heat transfer enhancement due to nanofluid and surface the texture of the moving rough plate. Mehmood *et al.* [71] investigated the second law of thermodynamics in a convective heat transfer phenomena over a continuous horizontally moving wavy surface.

This chapter aims to study the bioconvection in a nanofluid past a moving inclined wavy surface with convective boundary conditions. The bivariate pseudo-spectral local linearisation (BPSLLM) approach is used to solve the partial differential equations, which govern the flow. The influence of pertinent parameters on the Nusselt number, nanoparticle Sherwood number, and density number of the microbes are presented.

9.2 Mathematical Formulation

Consider an incompressible, steady, two-dimensional and laminar mixed convection nanofluid flow containing motile microorganismsalong a moving inclined wavy surface The flow model and coordinate system are depicted in Fig. 2.1. It is assumed that, the wavy surface is moving tangentially to itself with a constant speed U_w.

The equations governing the flow considered are [19, 14]

$$\frac{\partial U}{\partial X}+\frac{\partial V}{\partial Y}=0 \tag{9.1}$$

$$\rho_{f\infty}\left(U\frac{\partial U}{\partial X}+V\frac{\partial U}{\partial Y}\right)=-\frac{\partial P}{\partial X}+\mu\left(\frac{\partial^2 U}{\partial X^2}+\frac{\partial^2 U}{\partial Y^2}\right)+[(1-\phi_\infty)\beta_T\rho_{f\infty}(T-T_\infty) -(\rho_p-\rho_{f\infty})(\phi-\phi_\infty)-\gamma\Delta\rho M]\,g\sin A \tag{9.2}$$

$$\rho_{f\infty}\left(U\frac{\partial V}{\partial X}+V\frac{\partial V}{\partial Y}\right)=-\frac{\partial P}{\partial Y}+\mu\left(\frac{\partial^2 V}{\partial X^2}+\frac{\partial^2 V}{\partial Y^2}\right)+[(1-\phi_\infty)\beta_T\rho_{f\infty}(T-T_\infty) -(\rho_p-\rho_{f\infty})(\phi-\phi_\infty)-\gamma\Delta\rho M]\,g\cos A \tag{9.3}$$

$$U\frac{\partial T}{\partial X}+V\frac{\partial T}{\partial Y}=\alpha_m\left(\frac{\partial^2 T}{\partial X^2}+\frac{\partial^2 T}{\partial Y^2}\right)+\gamma\left\{D_B\left(\frac{\partial\phi}{\partial X}\frac{\partial T}{\partial X}+\frac{\partial\phi}{\partial Y}\frac{\partial T}{\partial Y}\right) +\frac{D_T}{T_\infty}\left[\left(\frac{\partial T}{\partial X}\right)^2+\left(\frac{\partial T}{\partial Y}\right)^2\right]\right\} \tag{9.4}$$

$$U\frac{\partial \phi}{\partial X}+V\frac{\partial \phi}{\partial Y}=D_B\left(\frac{\partial^2 \phi}{\partial X^2}+\frac{\partial^2 \phi}{\partial Y^2}\right)+\frac{D_T}{T_\infty}\left(\frac{\partial^2 T}{\partial X^2}+\frac{\partial^2 T}{\partial Y^2}\right) \tag{9.5}$$

$$U\frac{\partial M}{\partial X}+V\frac{\partial M}{\partial Y}+\frac{\partial}{\partial X}\left(M\widetilde{V}\right)+\frac{\partial}{\partial Y}\left(M\widetilde{V}\right)=D_n\left(\frac{\partial^2 M}{\partial X^2}+\frac{\partial^2 M}{\partial Y^2}\right) \tag{9.6}$$

The associated boundary conditions are :

$$\left.\begin{array}{l} U\hat{t}_y-V\hat{t}_x=0, \quad U\hat{t}_x+V\hat{t}_y=U_w, \quad -k(\hat{n}\cdot\nabla T)=h_f[T_f-T], \\ \phi=\phi_w, \quad M=M_w \quad \text{at} \quad Y=Y_w=\sigma(X), \\ U\to 0, \quad T\to T_\infty, \quad \phi\to\phi_\infty \quad M\to M_\infty \quad \text{as} \quad Y\to\infty \end{array}\right\} \tag{9.7}$$

where $(\hat{t}_x,\hat{t}_y)$ is the unit tangent to the surface an is given by $(\frac{1}{\sqrt{1+\sigma_x^2}},\frac{\sigma_x}{\sqrt{1+\sigma_x^2}})$

The wavy surface is converted to a plane surface using the following non-dimensional transformations [131]

$$\left.\begin{array}{l} \xi=\dfrac{X}{L}, \quad \eta=\dfrac{Y-\sigma}{L\xi^{\frac{1}{2}}}\sqrt{Re}, \quad \psi=\dfrac{LU_w\xi^{\frac{1}{2}}f(\xi,\eta)}{\sqrt{Re}}, \quad p=\dfrac{P}{\rho U_w^2}, \\ \theta(\xi,\eta)=\dfrac{T-T_\infty}{T_f-T_\infty}, \quad \phi(\xi,\eta)=\dfrac{\Phi-\Phi_\infty}{\Phi_w-\Phi_\infty}, \quad \chi(\xi,\eta)=\dfrac{M}{M_w} \end{array}\right\} \tag{9.8}$$

where

$$Gr=\frac{(1-\Phi_\infty)\,g\beta_T\,(T_w-T_\infty)\,L^3}{\nu^2} \quad and \quad Re=\frac{U_wL}{\nu}$$

are the Grashof number and Reynolds number. Here ψ is the stream function defined in 2.10 of Chapter2.

Substituting Eq. (9.8) in the governing equations (9.1) to (9.6) and invoking the boundary layer approximation, we get the following non-dimensional equations.

$$\left(1+\sigma_\xi^2\right)f'''+\frac{1}{2}ff''-\frac{\xi\sigma_\xi\sigma_{\xi\xi}}{\left(1+\sigma_\xi^2\right)}(f')^2+\frac{Ri\,(\theta-N_r\phi-R_b\chi)\,\xi}{(1+{\sigma_\xi}^2)}\,(\sin A+\sigma_\xi\cos A) = \xi\left[f'\frac{\partial f'}{\partial\xi}-\frac{\partial f}{\partial\xi}f''\right] \tag{9.9}$$

$$\frac{\left(1+\sigma_\xi^2\right)}{\Pr}\left[\theta''+N_b\phi'\theta'+N_t(\theta')^2\right]+\frac{1}{2}f\theta'=\xi\left[f'\frac{\partial\theta}{\partial\xi}-\theta'\frac{\partial f}{\partial\xi}\right] \tag{9.10}$$

$$\frac{\left(1+\sigma_\xi^2\right)}{Le}\left[\phi''+\frac{N_t}{N_b}\theta''\right]+\frac{1}{2}f\phi'=\xi\left[f'\frac{\partial\phi}{\partial\xi}-\phi'\frac{\partial f}{\partial\xi}\right] \tag{9.11}$$

$$\frac{\left(1+\sigma_\xi^2\right)}{Sc}\chi'' - \frac{Pe}{Sc}\left(1-\sigma_\xi\right)\left(\chi\phi'' + \chi'\phi'\right) + \frac{1}{2}f\chi' = \xi\left[f'\frac{\partial\chi}{\partial\xi} - \chi'\frac{\partial f}{\partial\xi}\right] \tag{9.12}$$

and

$$\left.\begin{aligned} &f'(\xi,0) = \frac{1}{\sqrt{1+\sigma_\xi^2}},\ f(\xi,0) = -2\xi\left.\frac{\partial f}{\partial\xi}\right|_{(\xi,0)},\ \theta'(\xi,0) = -\frac{Bi\xi^{\frac{1}{2}}(1-\theta)}{\sqrt{1+\sigma_\xi^2}},\ \phi(\xi,0)=1,\\ &\chi(\xi,0)=1, \quad f'(\xi,\infty)=0, \quad \theta(\xi,\infty)=0, \quad \phi(\xi,\infty)=0, \quad \chi(\xi,\infty)=\delta\chi \end{aligned}\right\} \tag{9.13}$$

The quantities Pr, Pe, Le, Sc, Ri, N_b, N_r, N_t, and R_b are same as in Chapter 2 and Chapter 5 and $Bi = \dfrac{h_f L}{k\sqrt{\mathrm{Re}}}$ is the Biot number.

The parameters, coefficient of skin friction, Nusselt number, nanoparticle Sherwood number, and motile microorganism density number in their non-dimensional form are given by

$$\begin{aligned} \frac{1}{2}(Cf_\xi)(Re_\xi^{1/2}) &= \sqrt{1+\sigma_\xi^2}f''(\xi,0), \qquad \frac{Nu_\xi}{Re_\xi^{1/2}} = -\sqrt{1+\sigma_\xi^2}\,\theta'(\xi,0),\\ \frac{NSh_\xi}{Re_\xi^{1/2}} &= -\sqrt{1+\sigma_\xi^2}\,\phi'(\xi,0), \qquad \frac{Q_\xi}{Re_\xi^{1/2}} = -\sqrt{1+\sigma_\xi^2}\,\chi'(\xi,0) \end{aligned} \tag{9.14}$$

9.3 Method of Solution

The set of equations (9.9) - (9.12) with (9.13) are solved using BPSLLM [82].

On implementing this technique to equations (9.9) - (9.12), (9.13) we obtain

$$a_{1,m}f'''_{m+1} + a_{2,m}f''_{m+1} + a_{3,m}f'_{m+1} + a_{4,m}f_{m+1} + a_{5,m}\frac{\partial f'_{m+1}}{\partial\xi} + a_{6,m}\frac{\partial f_{m+1}}{\partial\xi} = R_{1,m} \tag{9.15}$$

$$b_{1,m}\theta''_{m+1} + b_{2,m}\theta'_{m+1} + b_{3,m}\theta_{m+1} + b_{4,m}\frac{\partial\theta_{m+1}}{\partial\xi} = R_{2,m} \tag{9.16}$$

$$c_{1,m}\phi''_{m+1} + c_{2,m}\phi'_{m+1} + c_{3,m}\phi_{m+1} + c_{4,m}\frac{\partial\phi_{m+1}}{\partial\xi} = R_{3,m} \tag{9.17}$$

$$d_{1,m}\chi''_{m+1} + d_{2,m}\chi'_{m+1} + d_{3,m}\chi_{m+1} + d_{4,m}\frac{\partial\chi_{m+1}}{\partial\xi} = R_{4,m} \tag{9.18}$$

where the coefficients are

$$a_{1,m} = 1+\sigma_\xi^2, \quad a_{2,m} = \frac{1}{2}f_m + \xi\frac{\partial f_m}{\partial\xi}, \quad a_{3,m} = -\left[\frac{\xi\sigma_\xi\sigma_{\xi\xi}}{1+\sigma_\xi^2}\right]2f'_m - \xi\frac{\partial f'_m}{\partial\xi},$$

$$a_{4,m} = \frac{1}{2} f''_m, \quad a_{5,m} = -\xi f'_m, \quad a_{6,m} = \xi f''_m,$$

$$R_{1,m} = \xi f''_m \frac{\partial f_m}{\partial \xi} - \frac{\xi \sigma_\xi \sigma_{\xi\xi}}{1+\sigma_\xi^2}\left(f'_m\right)^2 + \frac{1}{2} f_m f''_m - \xi f'_m \frac{\partial f'_m}{\partial \xi},$$
$$- \frac{Ri\,(\theta_m - N_r\,\phi_m - R_b\,\chi_m)\,\xi}{(1+{\sigma_\xi}^2)}\,(\sin A + \sigma_\xi \cos A)$$

$$b_{1,m} = \frac{(1+{\sigma_\xi}^2)}{\mathrm{Pr}}, \quad b_{2,m} = \frac{1+\sigma_\xi^2}{\mathrm{Pr}} N_b \phi'_m + \frac{1+\sigma_\xi^2}{\mathrm{Pr}} 2 N_t \theta'_m + \frac{1}{2} f_{m+1} + \xi \frac{\partial f_{m+1}}{\partial \xi},$$

$$b_{3,m} = 0, \quad b_{4,m} = -\xi f'_{m+1}, \quad R_{2,m} = \frac{1+\sigma_\xi^2}{\mathrm{Pr}} N_t (\theta'_m)^2,$$

$$c_{1,m} = \frac{1+\sigma_\xi^2}{Le}, \quad c_{2,m} = \frac{1}{2} f_{m+1} + \xi \frac{\partial f_{m+1}}{\partial \xi}, \quad c_{3,m} = 0, \quad c_{4,m} = -\xi f'_{m+1},$$

$$R_{3,m} = -\frac{1+\sigma_\xi^2}{Le} \frac{N_t}{N_b} \theta''_{m+1},$$

$$d_{1,m} = \frac{1+\sigma_\xi^2}{Sc}, \quad d_{2,m} = \frac{1}{2} f_{m+1} + \xi \frac{\partial f_{m+1}}{\partial \xi} - (1-\sigma_\xi) \frac{Pe}{Sc} \phi'_{m+1},$$

$$d_{3,m} = -(1-\sigma_\xi) \frac{Pe}{Sc} \phi''_{m+1}, \quad d_{4,m} = -\xi f'_{m+1}, \quad R_{4,m} = 0.$$

and

$$\left.\begin{array}{l} f'_{m+1}(\xi,0) = \dfrac{1}{\sqrt{1+\sigma_\xi^2}}, \;\; f_{m+1}(\xi,0) = -2\xi \left.\dfrac{\partial f}{\partial \xi}\right|_{(\xi,0)}, \;\; \theta'_{m+1}(\xi,0) = -\dfrac{Bi \xi^{\frac{1}{2}} (1-\theta)}{\sqrt{1+\sigma_\xi^2}}, \\ \phi_{m+1}(\xi,0) = 1\,, \quad \chi_{m+1}(\xi,0) = 1 \\ f'_{m+1}(\xi,\infty) = 0, \quad \theta_{m+1}(\xi,\infty) = 0, \quad \phi_{m+1}(\xi,\infty) = 0, \quad \chi_{m+1}(\xi,\infty) = \delta\chi \end{array}\right\} \quad (9.19)$$

In both η and ξ the pseudo-spectral process yields(Chapter : 2),

$$A^{(1)}\mathbf{F}_i + \gamma^{(1)}_{5,i} \sum_{j=0}^{M} \mathbf{d}_{i,j} \mathbf{D}\mathbf{F}_j + \gamma^{(1)}_{6,i} \sum_{j=0}^{M} \mathbf{d}_{i,j} \mathbf{F}_j = \mathbf{R}_{1,i} \quad (9.20)$$

$$A^{(2)}\mathbf{\Theta}_i + \gamma^{(2)}_{4,i} \sum_{j=0}^{M} \mathbf{d}_{i,j} \mathbf{\Theta}_j = \mathbf{R}_{2,i} \quad (9.21)$$

$$A^{(3)}\mathbf{\Phi}_i + \gamma^{(3)}_{4,i} \sum_{j=0}^{M} \mathbf{d}_{i,j} \mathbf{\Phi}_j = \mathbf{R}_{3,i} \quad (9.22)$$

$$A^{(4)}\chi_i + \gamma_{4,i}^{(4)} \sum_{j=0}^{M} \mathbf{d}_{i,j}\chi_j = \mathbf{R}_{4,i} \tag{9.23}$$

where

$$\begin{aligned} A^{(1)} &= \gamma_{1,i}^{(1)}\mathbf{D}^3 + \gamma_{2,i}^{(1)}\mathbf{D}^2 + \gamma_{3,i}^{(1)}\mathbf{D} + \gamma_{4,i}^{(1)}\mathbf{I}, \\ A^{(2)} &= \gamma_{1,i}^{(2)}\mathbf{D}^2 + \gamma_{2,i}^{(2)}\mathbf{D} + \gamma_{3,i}^{(2)}\mathbf{I}, \\ A^{(3)} &= \gamma_{1,i}^{(3)}\mathbf{D}^2 + \gamma_{2,i}^{(3)}\mathbf{D} + \gamma_{3,i}^{(3)}\mathbf{I}, \\ A^{(4)} &= \gamma_{1,i}^{(4)}\mathbf{D}^2 + \gamma_{2,i}^{(4)}\mathbf{D} + \gamma_{3,i}^{(4)}\mathbf{I} \end{aligned}$$

Here $\gamma_{k,i}^{(1)}$, $\gamma_{k,i}^{(2)}$, $\gamma_{k,i}^{(3)}$, $\gamma_{k,i}^{(4)}$ and $\mathbf{R}_{k,i}$ are N^{th} order diagonal matrices with diagonal elements as, $a_{k,m}(\zeta_r, \tau_i)$, $b_{k,m}(\zeta_r, \tau_i)$, $c_{k,m}(\zeta_r, \tau_i)$, $d_{k,m}(\zeta_r, \tau_i)$ and $R_{k,m}(\zeta_r, \tau_i)$ for $r = 1, 2, 3, \cdots N$ respectively and $\mathbf{I}$ refers the identity matrix.

Equation (9.20) in the form of matrix is

$$\begin{bmatrix} A_{0,0}^{(1)} & A_{0,1}^{(1)} & A_{0,2}^{(1)} & \cdots & A_{0,M}^{(1)} \\ A_{1,0}^{(1)} & A_{1,1}^{(1)} & A_{1,2}^{(1)} & \cdots & A_{1,M}^{(1)} \\ A_{2,0}^{(1)} & A_{2,1}^{(1)} & A_{2,2}^{(1)} & \cdots & A_{2,M}^{(1)} \\ \vdots & \vdots & \vdots & \vdots & \vdots \\ A_{M,0}^{(1)} & A_{M,1}^{(1)} & A_{M,2}^{(1)} & \cdots & A_{M,M}^{(1)} \end{bmatrix} \begin{bmatrix} \mathbf{F}_0 \\ \mathbf{F}_1 \\ \mathbf{F}_2 \\ \vdots \\ \mathbf{F}_M \end{bmatrix} = \begin{bmatrix} \mathbf{R}_{1,0} \\ \mathbf{R}_{1,1} \\ \mathbf{R}_{1,2} \\ \vdots \\ \mathbf{R}_{1,M} \end{bmatrix} \tag{9.24}$$

where

$$\begin{aligned} A_{i,j}^{(1)} &= A^{(1)} + \gamma_{5,i}^{(1)}\mathbf{d}_{i,i}\mathbf{D} + \gamma_{6,i}^{(1)}\mathbf{d}_{i,i}\mathbf{I}, \quad for \quad i = j; \\ A_{i,j}^{(1)} &= \gamma_{5,i}^{(1)}\mathbf{d}_{i,j}\mathbf{D} + \gamma_{6,i}^{(1)}\mathbf{d}_{i,j}\mathbf{I}, \quad for \quad i \neq j \end{aligned} \tag{9.25}$$

Similarly, (9.21) to (9.23) can also be written in the form of matrix equations. We solve these equations, iteratively, using suitable initial approximation.

9.4 Computational Results and Discussion

In the present study, we focus our discussion on analyzing the inclination angle effect A, amplitude α, mixed convection parameter Ri, bioconvection Peclet number Pe, bioconvection Schmidt number Sc, bioconvection Rayleigh number Rb, Biot number Bi, and microorganisms slip parameter $\delta\chi$ on the coefficient of skinfriction $Cf_\xi\sqrt{Re_\xi}$, Nusselt number $Nu_\xi/\sqrt{Re_\xi}$, nanoparticle Sherwood number $NSh_\xi/\sqrt{Re_\xi}$ and density number of motile mi-

crobes $Q_\xi/\sqrt{Re_\xi}$. The values of the parameters are fixed as $\mathrm{Pr} = 10, Le = 5, N_b = 0.05, N_t = 0.01, N_r = 0.03, R_b = 0.05, Pe = 2.0, Ri = 3.0, bi = 0.5, Sc = 2.0, \alpha = 0.01, A = \pi/4$ and $\delta\chi = 0.01$ unless otherwise mentioned.

Figure 9.1 refers to the effects of bioconvection Peclet number Pe on various physical parameters for given values of other required parameters in the discussion as mentioned above. It is found that the parameters are escalating for a raise in the bioconvection Peclet number Pe, i.e., a raise of particle movements cause the improvement of all dimensionless parameters under consideration. This is evident from the figures 9.1(a) to 9.1(d).

It is observed from the figure 9.2 that, variation of the parameters under consideration such as, $Cf_\xi\sqrt{Re_\xi}$, $Nu_\xi/\sqrt{Re_\xi}$, $NSh_\xi/\sqrt{Re_\xi}$ and $Q_\xi/\sqrt{Re_\xi}$ for different values of bioconvection Schmidt number Sc, behave similarly to that of bioconvection Peclet number Pe.

Figure 9.3 delineates the effect of the angle of the wavy surface A on required parameters. The raise in the angle of inclination has positive effect on the coefficient of skinfriction $Cf_\xi\sqrt{Re_\xi}$, Nusselt number $Nu_\xi/\sqrt{Re_\xi}$, nanoparticle Sherwood number $NSh_\xi/\sqrt{Re_\xi}$ and density number of motile microorganisms $Q_\xi/\sqrt{Re_\xi}$. Hence the transfer rate of all the physical quantities is more for verticle surface compared to horizontal surface. This is clear from the figures 9.3(a), 9.3(b), 9.3(c) and 9.3(d).

Figure 9.4 elucidates the typical behaviour of $Cf_\xi\sqrt{Re_\xi}$, $Nu_\xi/\sqrt{Re_\xi}$, $NSh_\xi/\sqrt{Re_\xi}$ and $Q_\xi/\sqrt{Re_\xi}$ with respect to amplitude of the wavy surface α. We found both increasing and decreasing nature in the profiles of the Skin friction parameter and density number of motile microbes for an increase in α, which we can observe in figures 9.4(a) and 9.4(d). The Nusselt number and nanoparticle Sherwood number are decreasing for an increase in α (9.4(b), 9.4(c)).

The Biot number Bi's effect on physical parameters under consideration is portrayed in figure 9.5. It is found from the figures 9.5(a), 9.5(b) that, the parameters skin friction $Cf_\xi\sqrt{Re_\xi}$, heat transfer rate $Nu_\xi/\sqrt{Re_\xi}$ are increasing with an increase in Bi. The figure 9.5(c) represents the behaviour of nanoparticle mass transfer rate $NSh_\xi/\sqrt{Re_\xi}$ with respect to Bi. It is found that the nanoparticle mass transfer rate is decreasing in the first half of the channel (up to $\xi = 4.4$) and increasing in the second half of the channel, whenever Bi increases. Similar behaviour is found for the density of motile microorganisms in figure 9.5(d), i.e., the density of motile microorganisms is decreasing in the first half of the channel (up to $\xi = 3.4$) and increasing in the second half of the channel.

The influence of Ri, mixed convection parameter, is portrayed in figures 9.6(a) - 9.6(d),

and it is similar to the behaviour of Biot number Bi. The increase of mixed convection parameter results in the enhancement of the dimensionless parameters $Cf_\xi\sqrt{Re_\xi}$, $Nu_\xi/\sqrt{Re_\xi}$. Where as the parameters $NSh_\xi/\sqrt{Re_\xi}$ and $Q_\xi/\sqrt{Re_\xi}$ are decreasing in the first quarter of the channel (up to $\xi = 1$ for both nanoparticle Sherwood number and density of motile microbes) and increasing in the remaining part of the channel.

Figure 9.7 shows the effect of Rb, bioconvection Rayleigh number, on $Cf_\xi\sqrt{Re_\xi}$, $Nu_\xi/\sqrt{Re_\xi}$, $NSh_\xi/\sqrt{Re_\xi}$ and $Q_\xi/\sqrt{Re_\xi}$. It is observed from figures 9.7(a) to 9.7(d), that the parameters' values falls, for a raise in bioconvection Rayleigh number. The presence of nanoparticles movement in the base fluid is a cause for this. These nanoparticles moves in the fluid arbitrarily, and the fluid temperature gradually rises.

The variation of physical quantities with the microorganism slip parameter $\delta\chi$ is depicted in figure 9.8. It is found that not much variation or very small variation in the profiles of $Cf_\xi(Gr_\xi)^{\frac{1}{4}}$, $Nu_\xi/(Gr_\xi)^{\frac{1}{4}}$, and $Q_\xi/(Gr_\xi)^{\frac{1}{4}}$ is observed. An increase in the parameter $\delta\chi$, decreases the coefficient of skin friction, local heat transfer rate, local nanoparticle mass transfer rate and local motile microorganism density number.

9.5 Conclusions

In this chapter, an analysis is presented to study the bioconvection in a nanofluid flow over a moving inclined sinusoidal surface with convective boundary conditions. The nonlinear equations are linearized employing local linearization procedure and the resultant system is solved by a bivariate pseudo-spectral collocation method. Important observations are itemized below:

- An increase in the bioconvection Peclet number, bioconvection Schmidt number and angle of wavy surface enhance the skin friction coefficient, heat transfer rate, nanoparticle mass transfer rate and density of motile microorganisms. A reverse trend is noticed for the influence of bioconvection Rayleigh number.
- The influence of microorganism slip parameter is to decrease the coefficient of skin friction, nanoparticle mass transfer rate, and density of motile organisms.
- The Biot number and mixed convection parameter are behaving similarly. Both heat transfer rate and surface drag are increasing for a rise in Bi, Ri. The nanoparticle

Sherwood number and motile microorganisms density are decreasing at the beginning and increasing across the channel.

- The heat transfer rate and nanoparticle Sherwood number are decreasing for a rise in slip parameter

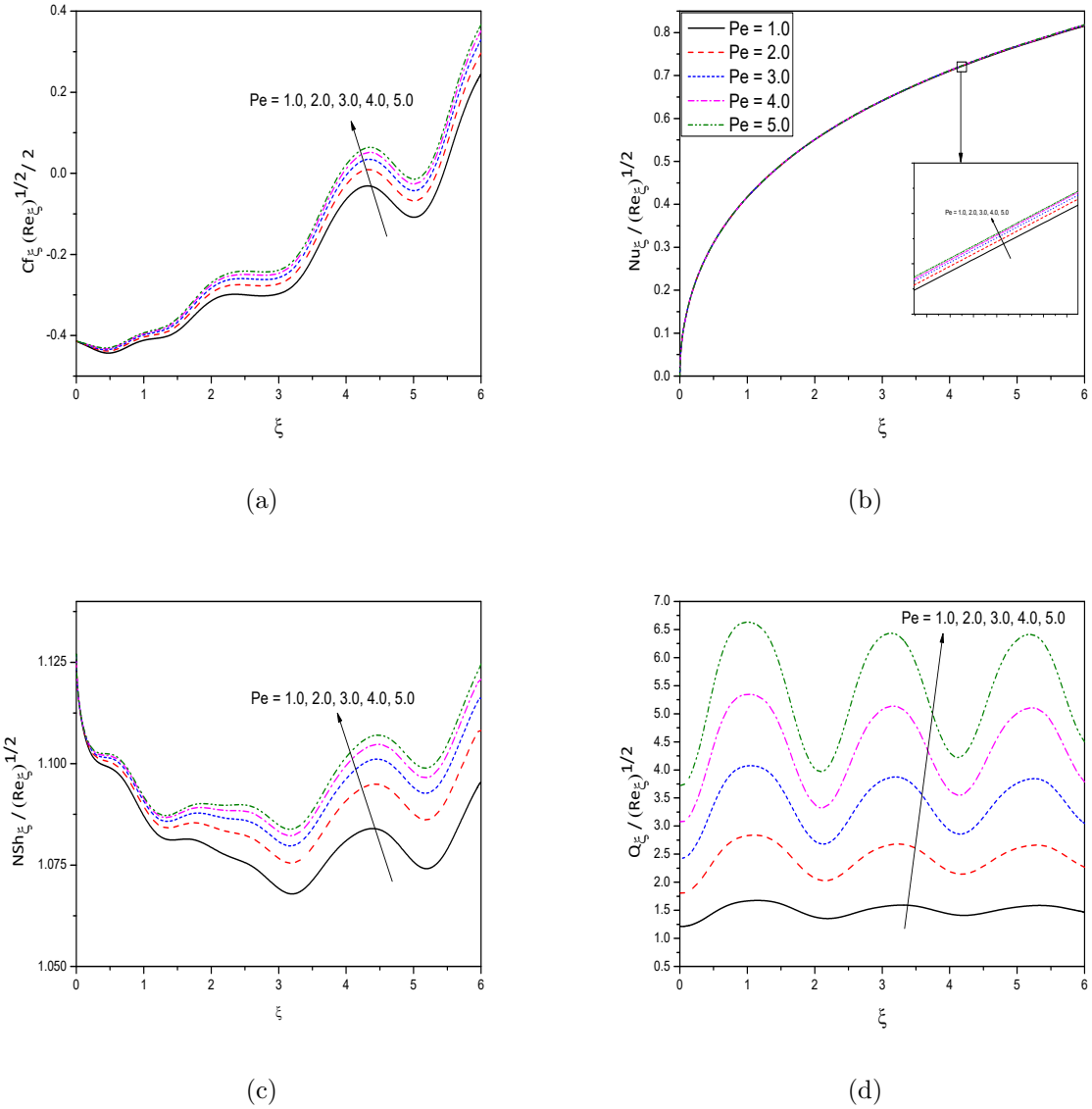

Figure 9.1: "Effect of the bioconvection Peclet number Pe on the profiles of (a) $Cf_\xi(Re_\xi^{1/2})/2$ (b) $\frac{Nu_\xi}{Re_\xi^{1/2}}$ (c) $\frac{NSh_\xi}{Re_\xi^{1/2}}$ (d) $\frac{Q_\xi}{Re_\xi^{1/2}}$".

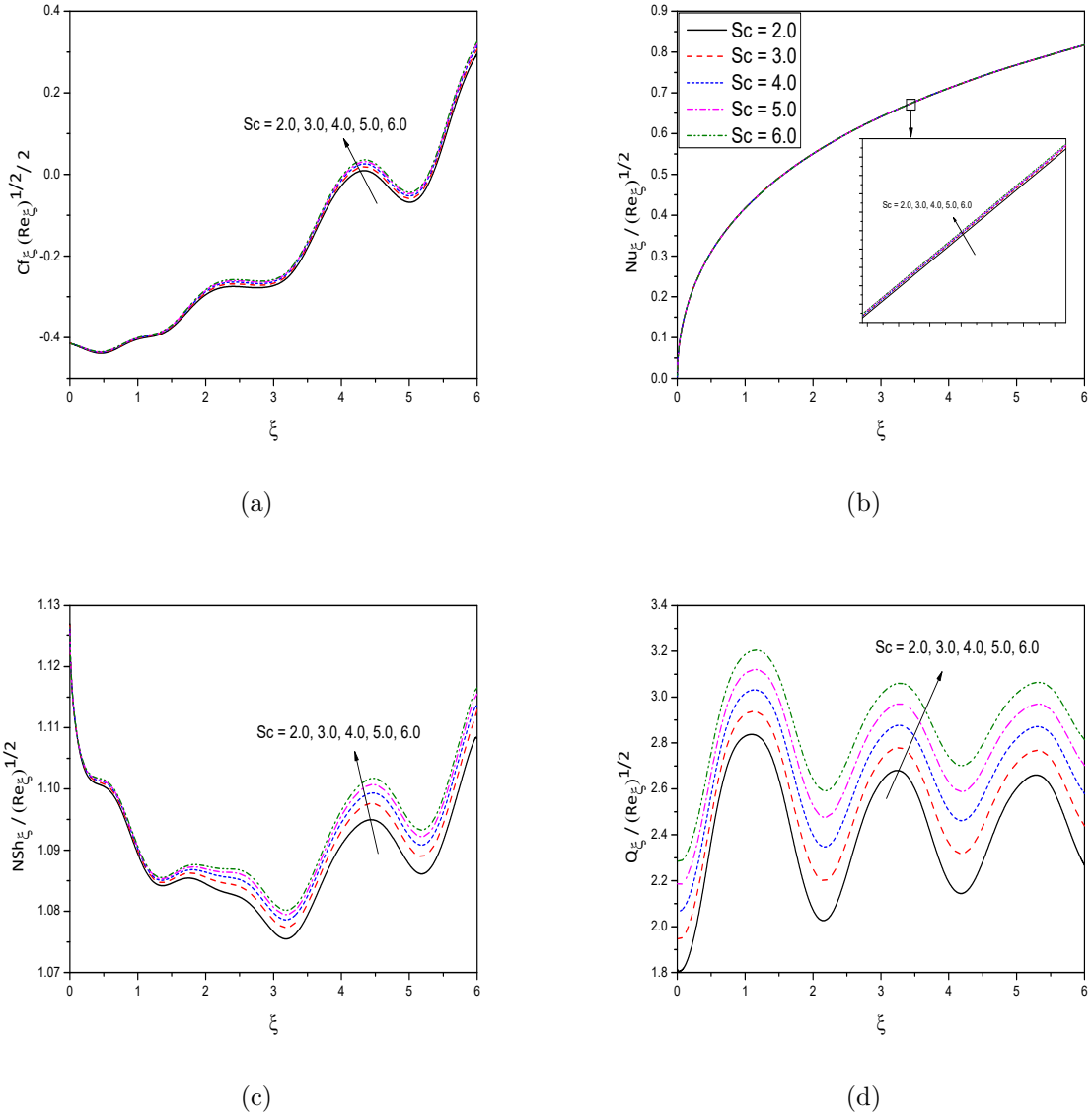

Figure 9.2: "Effect of the bioconvection Schmdt number Sc on the profiles of (a) $Cf_\xi(Re_\xi^{1/2})/2$ (b) $\frac{Nu_\xi}{Re_\xi^{1/2}}$ (c) $\frac{NSh_\xi}{Re_\xi^{1/2}}$ (d) $\frac{Q_\xi}{Re_\xi^{1/2}}$".

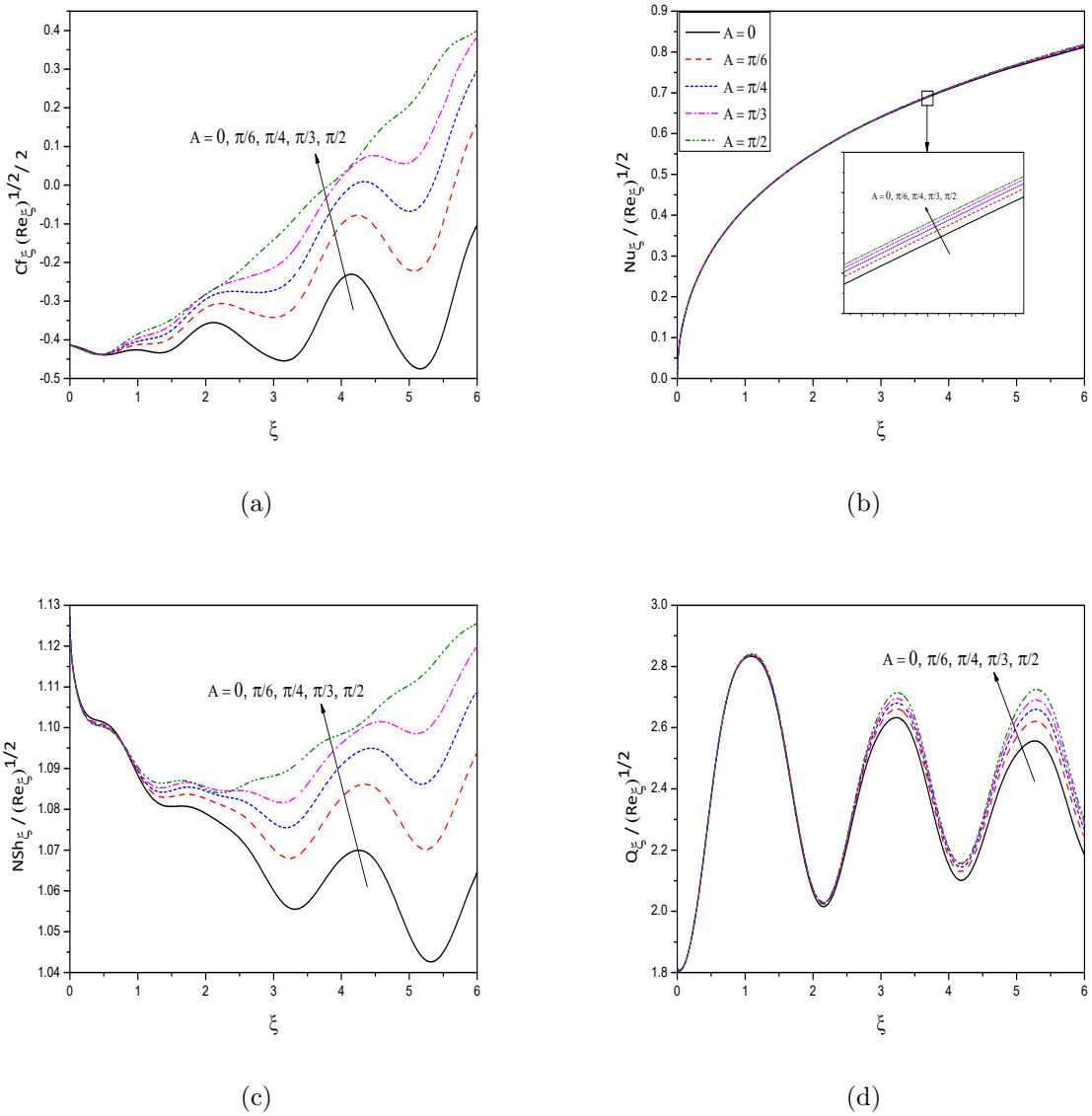

Figure 9.3: "Effect of the angle of inclination A on the profiles of (a) $Cf_\xi(Re_\xi^{1/2})/2$ (b) $\frac{Nu_\xi}{Re_\xi^{1/2}}$ (c) $\frac{NSh_\xi}{Re_\xi^{1/2}}$ (d) $\frac{Q_\xi}{Re_\xi^{1/2}}$".

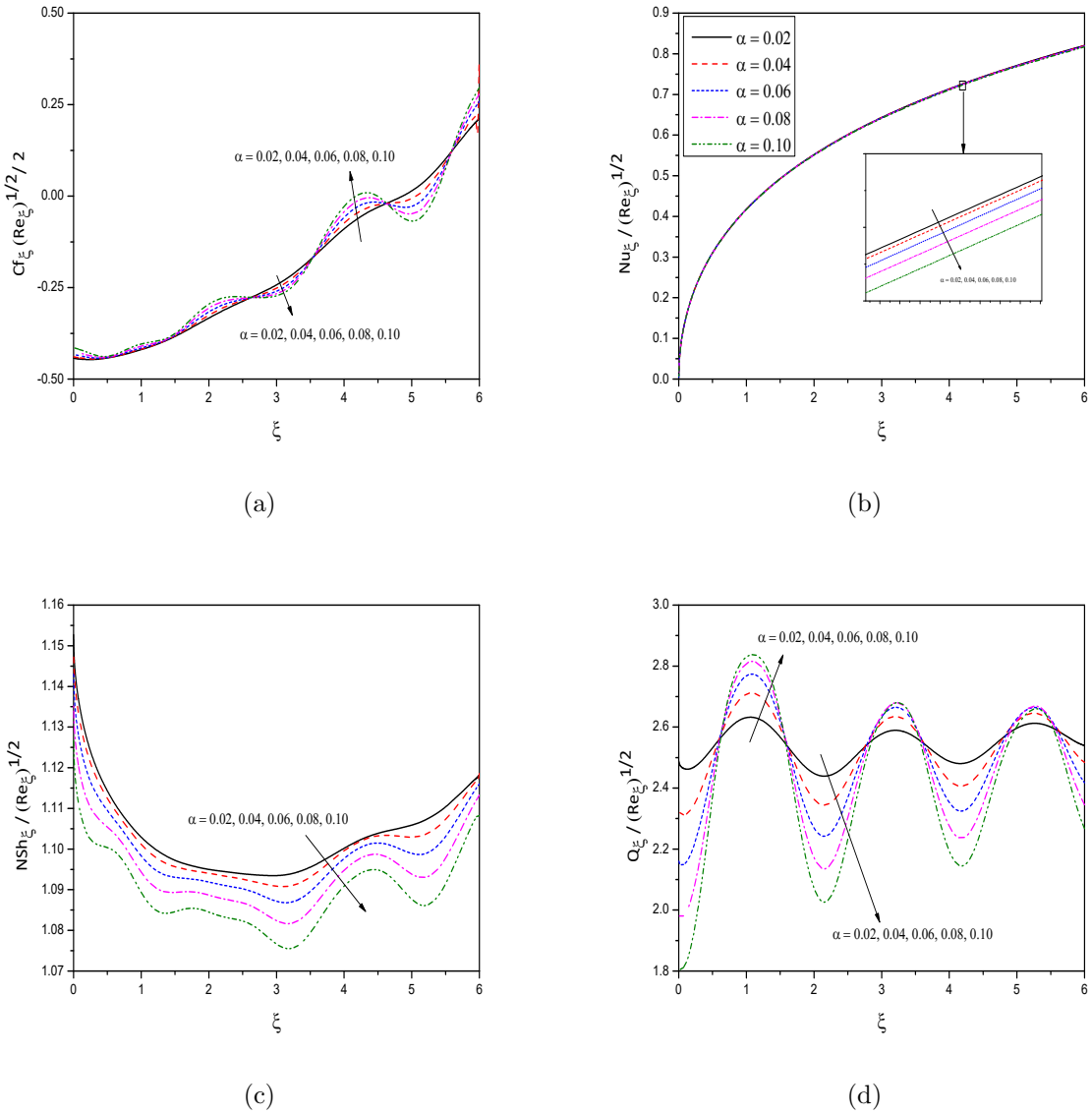

Figure 9.4: "Effect of the amplitude of the wavy surface α on the profiles of (a) $Cf_\xi(Re_\xi^{1/2})/2$ (b) $\frac{Nu_\xi}{Re_\xi^{1/2}}$ (c) $\frac{NSh_\xi}{Re_\xi^{1/2}}$ (d) $\frac{Q_\xi}{Re_\xi^{1/2}}$".

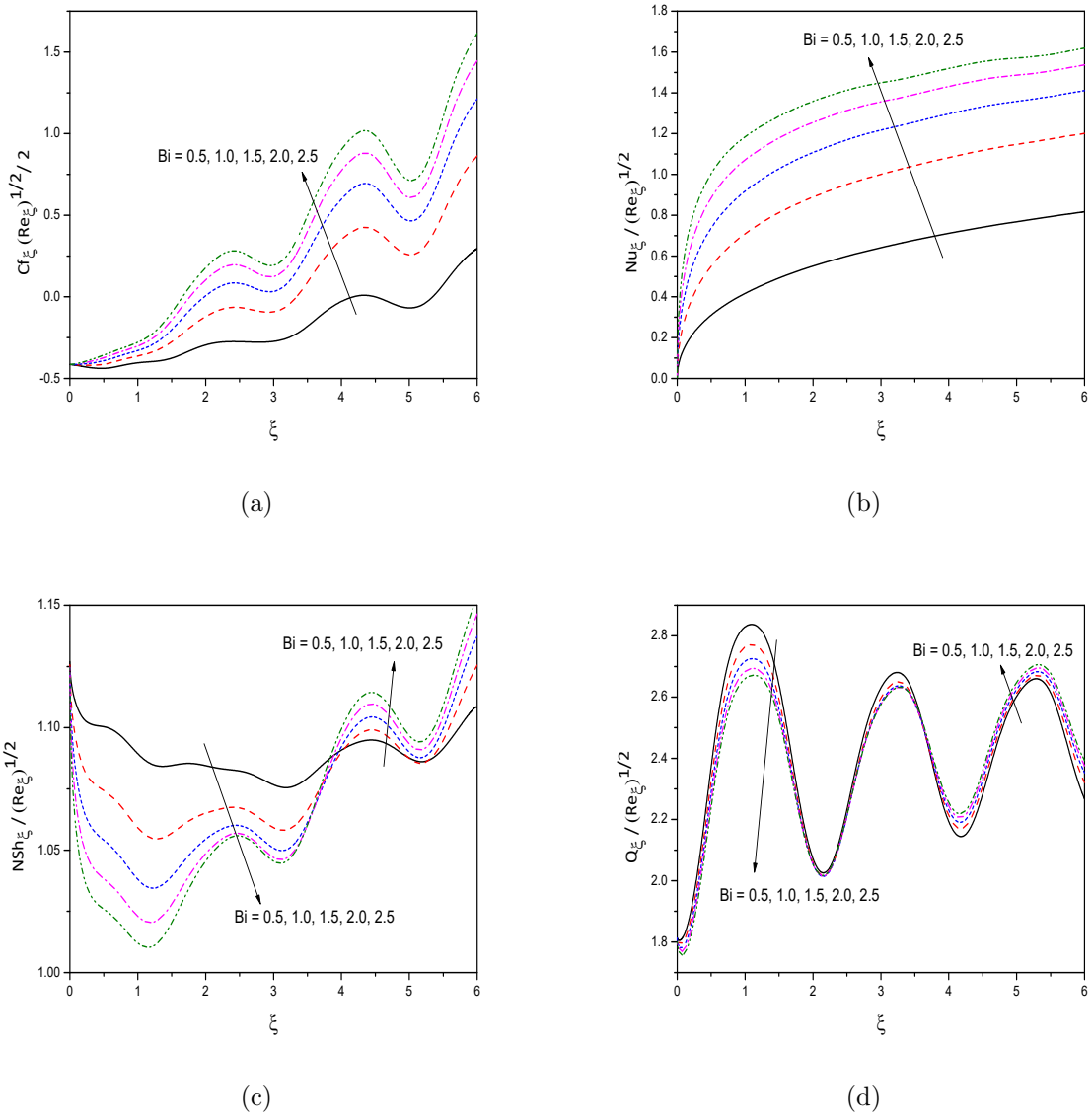

Figure 9.5: "Effect of the Biot number Bi on the profiles of (a) $Cf_\xi(Re_\xi^{1/2})/2$ (b) $\frac{Nu_\xi}{Re_\xi^{1/2}}$ (c) $\frac{NSh_\xi}{Re_\xi^{1/2}}$ (d) $\frac{Q_\xi}{Re_\xi^{1/2}}$".

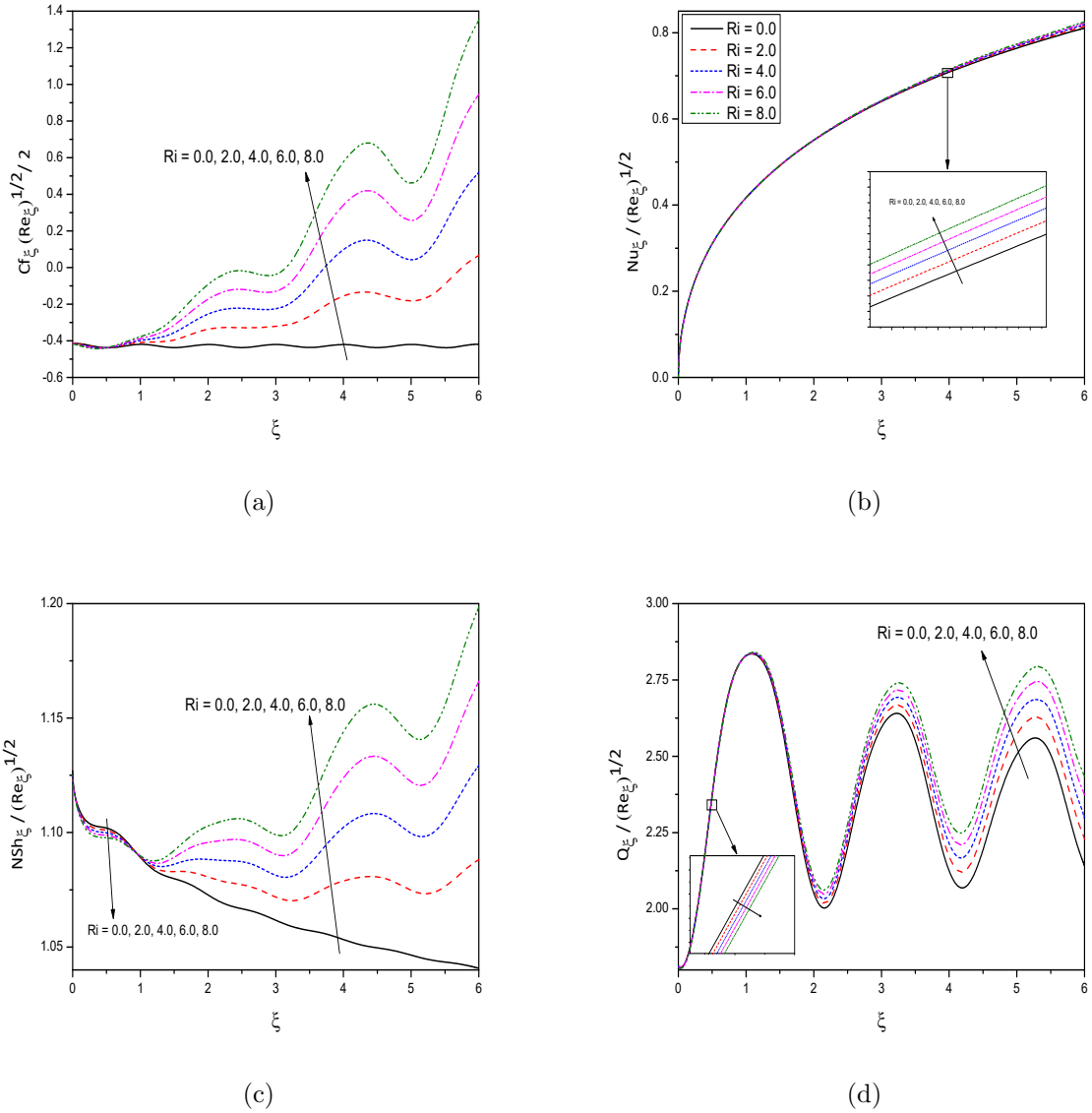

Figure 9.6: "Effect of the mixed convection parameter Ri on the profiles of (a) $Cf_\xi(Re_\xi^{1/2})/2$ (b) $\frac{Nu_\xi}{Re_\xi^{1/2}}$ (c) $\frac{NSh_\xi}{Re_\xi^{1/2}}$ (d) $\frac{Q_\xi}{Re_\xi^{1/2}}$".

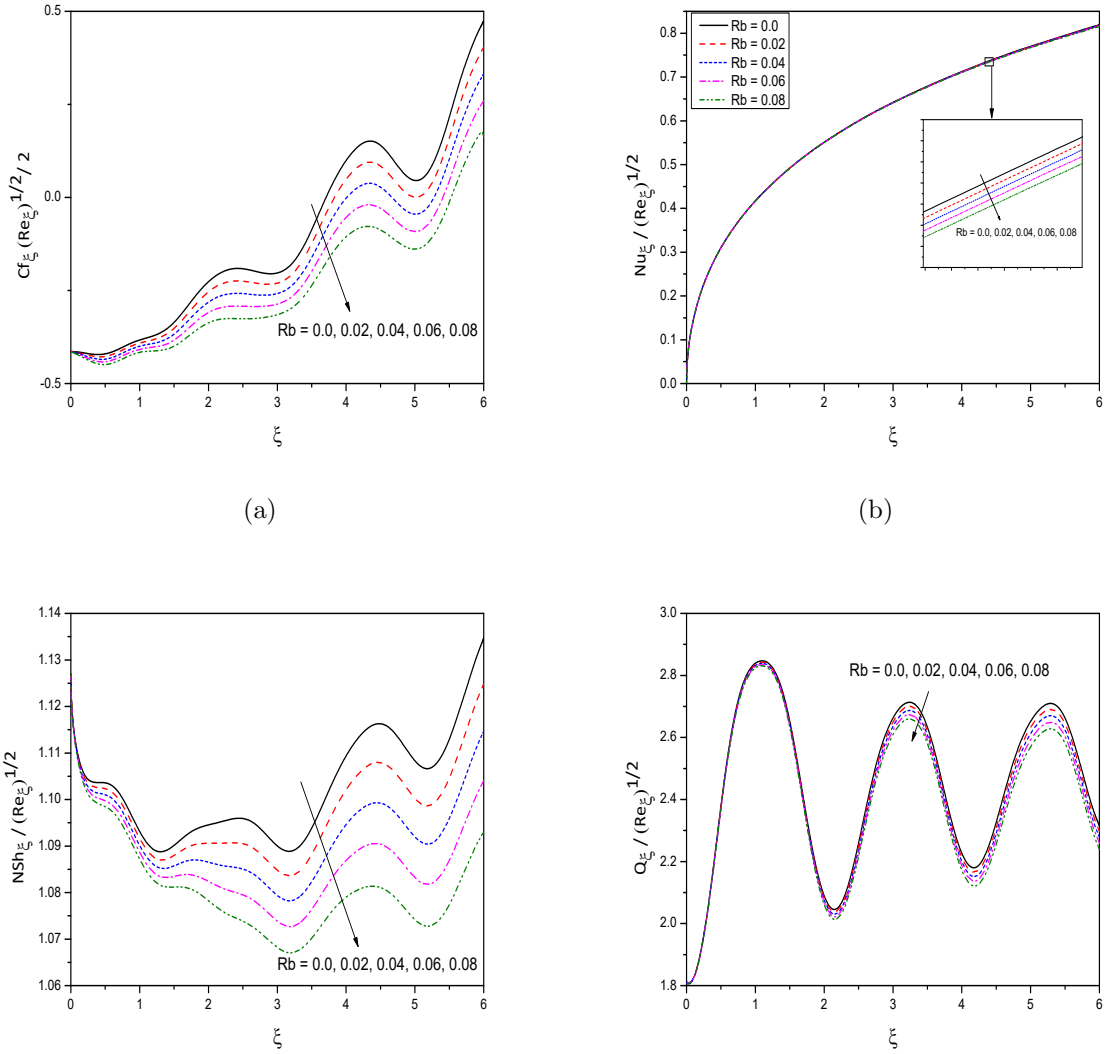

Figure 9.7: "Effect of the bioconvection Rayleigh number R_b on the profiles of (a) $Cf_\xi(Re_\xi^{1/2})/2$ (b) $\frac{Nu_\xi}{Re_\xi^{1/2}}$ (c) $\frac{NSh_\xi}{Re_\xi^{1/2}}$ (d) $\frac{Q_\xi}{Re_\xi^{1/2}}$".

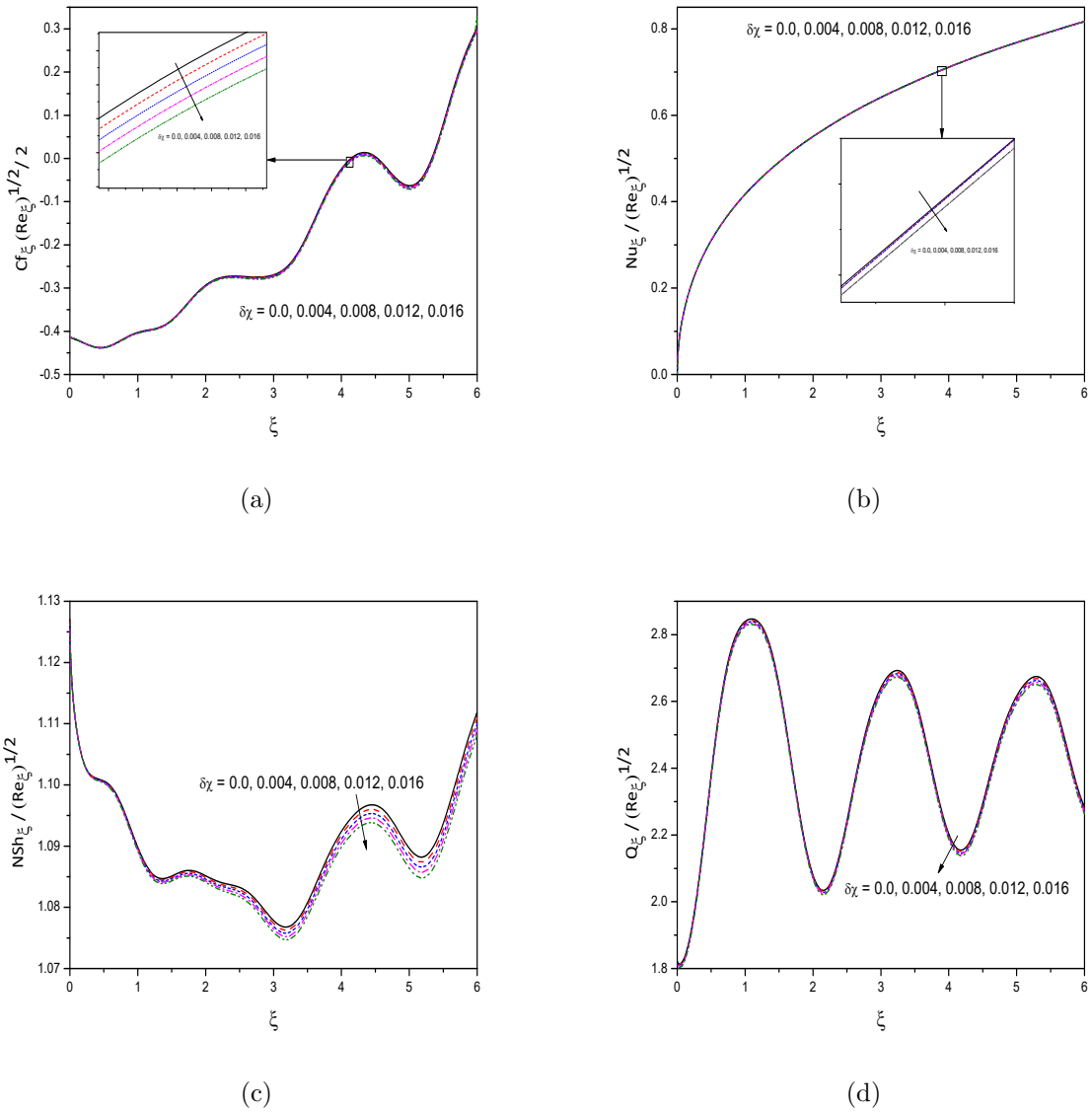

Figure 9.8: "Effect of the microorganism slip parameter $\delta\chi$ on the profiles of (a) $Cf_\xi(Re_\xi^{1/2})/2$ (b) $\frac{Nu_\xi}{Re_\xi^{1/2}}$ (c) $\frac{NSh_\xi}{Re_\xi^{1/2}}$ (d) $\frac{Q_\xi}{Re_\xi^{1/2}}$".

Chapter 10

Summary and Conclusions

In this thesis, the bioconvection flow of nanofluids past an Inclined Wavy Surface is studied.

The governing partial differential equations of the flow in Chapters - 2 through Chapters - 9 are transformed into a system of nonlinear ordinary differential equations using suitable transformations. The resulting non-linear ordinary differential equations were linearized and solved using the bivariate pseudo-spectral local linearisation method. The effects of various geometrical and fluid parameters on the skin friction coefficient, Nusselt number, Sherwood number, nanoparticle Sherwood number, and density of motile microorganisms are presented through graphs and discussed. The important observations made from this study are listed below :

- In all the cases, increasing the bioconvection Peclet number Pe, regular double-diffusive buoyancy ratio N_c, and bioconvection Schmidt number Sc improves the coefficient of skin friction, heat transfer rate, mass transfer rate, nanoparticle mass transfer rate, and motile microbe density.
- The influence of the bioconvection Rayleigh number R_b and the nanofluid buoyancy ratio N_r reduces skin friction, heat transfer rate, mass transfer rate, nanoparticle mass transfer rate, and motile microbe density.
- The skin friction, local heat, and nanoparticle mass transfer coefficients, and density of motile microorganisms are enhanced by the angle of inclination A of the wavy surface to the horizontal.
- Concerning the amplitude of the wavy surface α, the parameters behave as expected. It is observed that both increasing and decreasing nature in the profiles dependent

on the parameter ξ since there is an increase in amplitude. For an increase in α, the parameter profiles are observed to be growing and decreasing in a periodic nature. In general, it concludes that increasing the wave amplitude roughens the surface more.

- The skin friction coefficient, nanoparticle Sherwood number, and density number of motile microorganisms all rise when the variable thermal conductivity parameter β increases, whereas the Nusselt number drops.

- An increase in the variable viscosity parameter ϵ decreases the heat transfer rate, nanoparticle mass transfer rate, and motile microbe density number, but does not affect the skin friction coefficient.

- When the mixed convection parameter Ri is increased, the profiles of coefficient of skin friction, Nusselt number, nanoparticle Sherwood number, and density of motile microbes all increase.

- The Joule heating parameter J_0 and the Eckert number Ec diminish the local heat transfer rate. Whereas it is discovered that an increase in J_0 leads to an increase in local nanoparticle mass transfer rate and density of motile microorganisms.

- Increased magnetic induction parameter Ha improves the nanoparticle Sherwood number NSh and motile microbe density Qx and decreases the local heat transfer rate.

- The Radiation parameter Rd has the impact of reducing heat transfer and increasing other physical quantities such as skin friction, nanoparticle Sherwood number, and motile microbe density.

- The heat transfer rate, coefficient of skin friction, nanoparticle mass transfer rate, and density of motile microorganisms are all reduced when the temperature parameter $delta$, response rate parameter σ_1, and fitted rate constant n are increased. However, there is a general trend for an increase in the Pearson number P_n.

- A rise in the Biot number Bi leads to an increase in the Nusselt number, skin friction. However, for an increase in the Biot number Bi, the nanoparticle Sherwood number and density of motile microorganisms decrease first and then increase across the channel.

The work presented in the thesis can be extended to analyze the various effects like MHD, Hall effect, Hall and Ion slip, viscous dissipation, binary chemical reaction, etc. Further, this work can be extended by studying the analysis in various non-Newtonian fluids like Casson fluids, Jeffrey fluids, Power-law fluids, and the geometry can be changed to an oscillatory

vertical plate, inclined plate, through pipes, and an exponentially stretching sheet. This work can also be extended to porous media.

In the recent past, the study of stability analysis has attracted the curiosity of many researchers. Thus, the work presented in the thesis can be extended to study the stability of bioconvection flows in Newtonian and/or non-Newtonian fluids.

Bibliography

[1] IA Abbas and M Marin. Analytical solution of thermoelastic interaction in a half-space by pulsed laser heating. *Physica E: Low-Dimensional Systems and Nanostructures*, 87:254–260, 2017.

[2] EM Aboeldahab, Mahmoud KS, and R Adel. free convection effects on mhd boundary layer flow and heat transfer over a continuous moving wavy surface in porous media. *Int J of Applied Mathematics and Physics*, 3(2):221–229, 2011.

[3] S Ahmad and S Nadeem. Analysis of activation energy and its impact on hybrid nanofluid in the presence of hall and ion slip currents. *Applied Nanoscience*, 10(12):5315–5330, 2020.

[4] SE Ahmed and MM Abd El-Aziz. Effect of local thermal non-equilibrium on unsteady heat transfer by natural convection of a nanofluid over a vertical wavy surface. *Meccanica*, 48(1):33–43, 2013.

[5] SE Ahmed and A Mahdy. Laminar mhd natural convection of nanofluid containing gyrotactic microorganisms over vertical wavy surface saturated non-darcian porous media. *Applied Mathematics and Mechanics*, 37(4):471–484, 2016.

[6] NS Akbar and ZH Khan. Variable fluid properties analysis with water based cnt nanofluid over a sensor sheet: Numerical solution. *Journal of Molecular Liquids*, 232:471–477, 2017.

[7] NA Amirsom, Md Uddin, Md Faisal Md Basir, Ali Kadir, BO Anwar, et al. Computation of melting dissipative magnetohydrodynamic nanofluid bioconvection with second-order slip and variable thermophysical properties. *Applied Sciences*, 9(12):2493, 2019.

[8] S Amit and PK Kundu. Passive control nanoparticles in doublediffusive free convection nanofluid flow over an inclined permeable plate. *Heat TransferAsian Research*, 49(1):289–306, 2020.

[9] IL Animasaun, AO Oyem, et al. Effect of variable viscosity, dufour, soret and thermal conductivity on free convective heat and mass transfer of non-darcian flow past porous flat surface. *American Journal of Computational Mathematics*, 4(04):357, 2014.

[10] A Arefmanesh, A Aghaei, and H Ehteram. Mixed convection heat transfer in a cuo–water filled trapezoidal enclosure, effects of various constant and variable properties of the nanofluid. *Applied Mathematical Modelling*, 40(2):815–831, 2016.

[11] SA Arrhenius. ber die reaktionsgeschwindigkeit bei der inversion von rohrzucker durch suren. *Z. Phys. Chem.*, 4:226–48, 1889.

[12] M Azam, T Xu, and M Khan. Numerical simulation for variable thermal properties and heat source/sink in flow of cross nanofluid over a moving cylinder. *International Communications in Heat and Mass Transfer*, 118:104832, 2020.

[13] AK Barik, SK Mishra, SR Mishra, and PK Pattnaik. Multiple slip effects on mhd nanofluid flow over an inclined, radiative, and chemically reacting stretching sheet by means of fdm. *Heat TransferAsian Res.*, 49.

[14] CK Batchelor and GK Batchelor. *An introduction to fluid dynamics*. Cambridge university press, 2000.

[15] N Begum, S Siddiqa, and MA Hossain. Nanofluid bioconvection with variable thermophysical properties. *Journal of Molecular Liquids*, 231:325–332, 2017.

[16] FA Bhat and A Samanta. Linear stability of a contaminated fluid flow down a slippery inclined plane. *Physical Review E*, 98(3):033108, 2018.

[17] MM Bhatti, A Shahid, T Abbas, SZ Alamri, and R Ellahi. Study of activation energy on the movement of gyrotactic microorganism in a magnetized nanofluids past a porous plate. *Processes*, 8(3):328, 2020.

[18] M Bilal, M Sagheer, and S Hussain. Numerical study of magnetohydrodynamics and thermal radiation on williamson nanofluid flow over a stretching cylinder with variable thermal conductivity. *Alexandria engineering journal*, 57(4):3281–3289, 2018.

[19] J Buongiorno. Convective transport in nanofluids. *Journal of heat transfer*, 128(3):240–250, 2006.

[20] C Canuto, MY Hussaini, A Quarteroni, A Thomas Jr, et al. *Spectral methods in fluid dynamics*. Springer Science & Business Media, 2012.

[21] T Cebeci and P Bradshaw. *Physical and computational aspects of convective heat transfer*. Springer Science & Business Media, 2012.

[22] AJ Chamkha, M Mujtaba, A Quadri, and C Issa. Thermal radiation effects on mhd forced convection flow adjacent to a non-isothermal wedge in the presence of a heat source or sink. *Heat and Mass Transfer*, 39(4):305–312, 2003.

[23] AJ Chamkha, AM Rashad, PK Kameswaran, and MMM Abdou. Radiation effects on natural bioconvection flow of a nanofluid containing gyrotactic microorganisms past a vertical plate with streamwise temperature variation. *Journal of Nanofluids*, 6(3):587–595, 2017.

[24] CY Cheng. Double diffusive natural convection along an inclined wavy surface in a porous medium. *International communications in heat and mass transfer*, 37(10):1471–1476, 2010.

[25] CY Cheng. Natural convection heat transfer from an inclined wavy plate in a bidisperse porous medium. *International communications in heat and mass transfer*, 43:69–74, 2013.

[26] S Childress, M Levandowsky, and EA Spiegel. Pattern formation in a suspension of swimming microorganisms: equations and stability theory. *Journal of Fluid Mechanics*, 69(3):591–613, 1975.

[27] CC Cho. Mixed convection heat transfer and entropy generation of cu-water nanofluid in wavy-wall lid-driven cavity in presence of inclined magnetic field. *International Journal of Mechanical Sciences*, 151:703–714, 2019.

[28] SUS Choi and JA Eastman. Enhancing thermal conductivity of fluids with nanoparticles. Technical report, Argonne National Lab., IL (United States), 1995.

[29] YM Chu, MI Khan, NB Khan, S Kadry, SU Khan, I Tlili, and MK Nayak. Significance of activation energy, bio-convection and magnetohydrodynamic in flow of third grade fluid (non-newtonian) towards stretched surface: A buongiorno model analysis. *International Communications in Heat and Mass Transfer*, 118:104893, 2020.

[30] SJD D'Alessio, JP Pascal, H A Jasmine, and KA Ogden. Film flow over heated wavy inclined surfaces. *Journal of fluid mechanics*, 665:418, 2010.

[31] K Das, T Chakraborty, and PK Kundu. Lie group transformation for double-diffusive free convection nanofluid flow over an inclined plane. *Proceedings of the National Academy of Sciences, India Section A: Physical Sciences*, 89(2):387–396, 2019.

[32] SK Das, SUS. Choi, W Yu, and T Pradeep. *Nanofluids: Science and Technology*. Wiley Interscience, New Jersey, 2007.

[33] R Dhanai, P Rana, and L Kumar. Lie group analysis for bioconvection mhd slip flow and heat transfer of nanofluid over an inclined sheet: Multiple solutions. *Journal of the Taiwan Institute of Chemical Engineers*, 66:283–291, 2016.

[34] M Dhlamini, PK Kameswaran, P Sibanda, SS Motsa, and H Mondal. Activation energy and binary chemical reaction effects in mixed convective nanofluid flow with convective boundary conditions. *Journal of Computational Design and Engineering*, 6(2):149–158, 2019.

[35] WS Don and A Solomonoff. Accuracy and speed in computing the chebyshev collocation derivative. *SIAM Journal on Scientific Computing*, 16(6):1253–1268, 1995.

[36] JA Eastman, SUS Choi, Sheng Li, W Yu, and LJ Thompson. Anomalously increased effective thermal conductivities of ethylene glycol-based nanofluids containing copper nanoparticles. *Applied physics letters*, 78(6):718–720, 2001.

[37] L Godson, B Raja, DM Lal, and S Wongwises. Experimental investigation on the thermal conductivity and viscosity of silver-deionized water nanofluid. *Experimental Heat Transfer*, 23(4):317–332, 2010.

[38] RSR Gorla and M Kumari. Effect of melting on free convection along a vertical wavy surface in a nanofluid. *Journal of Nanofluids*, 5.

[39] M Goyal and R Bhargava. Simulation of natural convective boundary layer flow of a nanofluid past a convectively heated inclined plate in the presence of magnetic field. *Int. J. Appl. Comput. Math.*, 4.

[40] Z Guo. A review on heat transfer enhancement with nanofluids. *Journal of Enhanced Heat Transfer*, 27:1–70, 2020.

[41] Z Haddad, E Abu-Nada, HF Oztop, and A Mataoui. Natural convection in nanofluids: are the thermophoresis and brownian motion effects significant in nanofluid heat transfer enhancement? *International Journal of Thermal Sciences*, 57:152–162, 2012.

[42] M Hassan, M Marin, A Alsharif, and R Ellahi. Convective heat transfer flow of nanofluid in a porous medium over wavy surface. *Physics Letters A*, 382(38):2749–2753, 2018.

[43] T Hayat, S Qayyum, A Alsaedi, and A Shafiq. Inclined magnetic field and heat source/sink aspects in flow of nanofluid with nonlinear thermal radiation. *International Journal of Heat and Mass Transfer*, 103:99–107, 2016.

[44] T Hayat, M Waqas, SA Shehzad, and A Alsaedi. Mixed convection flow of viscoelastic nanofluid by a cylinder with variable thermal conductivity and heat source/sink. *International Journal of Numerical Methods for Heat & Fluid Flow*, 2016.

[45] M Heydari and H Shokouhmand. Numerical study on the effects of variable properties and nanoparticle diameter on nanofluid flow and heat transfer through micro-annulus. *International Journal of Numerical Methods for Heat & Fluid Flow*, 2017.

[46] MA Hossain, S Kabir, and DAS Rees. Natural convection of fluid with variable viscosity from a heated vertical wavy surface. *Zeitschrift für angewandte Mathematik und Physik ZAMP*, 53(1):48–57, 2002.

[47] M.A. Hossain and I Pop. Magnetohydrodynamic boundary layer flow and heat transfer on a continuous moving wavy surface. *Archives of Mechanics*, 48(5):813–823, 1996.

[48] S Hussain, A Aziz, T Aziz, and CM Khalique. Slip flow and heat transfer of nanofluids over a porous plate embedded in a porous medium with temperature dependent viscosity and thermal conductivity. *Applied Sciences*, 6(12):376, 2016.

[49] M Ijaz and M Ayub. Nonlinear convective stratified flow of maxwell nanofluid with activation energy. *Heliyon*, 5(1):e01121, 2019.

[50] M Ijaz Khan and F Alzahrani. Activation energy and binary chemical reaction effect in nonlinear thermal radiative stagnation point flow of walter-b nanofluid: Numerical computations. *International Journal of Modern Physics B*, 34(13):id.2050132, 2020.

[51] MS Iqbal, I Mustafa, A Ghaffari, and Usman. A computational analysis of dissipation effects on the hydromagnetic convective flow of hybrid nanofluids along a vertical wavy surface. *Heat Transfer*, DOI:10.1002/htj.22265, 2021.

[52] M Irfan. Study of brownian motion and thermophoretic diffusion on non-linear mixed convection flow of carreau nanofluid subject to variable properties. *Surfaces and Interfaces*, 23:100926, 2021.

[53] M Irfan, MA Farooq, A Aslam, A Mushtaq, and ZH Shamsi. Magnetohydrodynamic time-dependent bio-nanofluid flow in a porous medium with variable thermophysical properties. *Mathematical Problems in Engineering*, 2021, 2021.

[54] T Javed, H Ahmad, and A Ghaffari. Influence of radiation on vertical wavy surface with constant heat flux: Using keller box scheme. *Alexandria Engineering Journal*, 55(3):2221–2228, 2016.

[55] KH Kabir, MA Alim, and LS Andallah. Effects of stress work on mhd natural convection flow along a vertical wavy surface with joule heating. *Journal of Applied Fluid Mechanics*, 8(2), 2015.

[56] PK Kameswaran, B Vasu, PVSN Murthy, and RSR Gorla. Mixed convection from a wavy surface embedded in a thermally stratified nanofluid saturated porous medium with non-linear boussinesq approximation. *International Communications in Heat and Mass Transfer*, 77:78–86, 2016.

[57] JO Kessler. Hydrodynamic focusing of motile algal cells. *Nature*, 313(5999):218–220, 1985.

[58] R Khademi, A Razminia, and VI Shiryaev. Conjugate-mixed convection of nanofluid flow over an inclined flat plate in porous media. *Applied Mathematics and Computation*, 366:124761, 2020.

[59] M Khan, M Irfan, and WA Khan. Impact of nonlinear thermal radiation and gyrotactic microorganisms on the magneto-burgers nanofluid. *International Journal of Mechanical Sciences*, 130:375–382, 2017.

[60] MI Khan, F Haq, T Hayat, A Alsaedi, and MU Rahman. Natural bio-convective flow of sisko nanofluid subject to gyrotactic microorganisms and activation energy. *Physica Scripta*, 94(12):125203, 2019.

[61] MI Khan, F Haq, SA Khan, T Hayat, and MI Khan. Development of thixotropic nanomaterial in fluid flow with gyrotactic microorganisms, activation energy, mixed convection. *Computer methods and programs in biomedicine*, 187:105186, 2020.

[62] AV Kuznetsov. Non-oscillatory and oscillatory nanofluid bio-thermal convection in a horizontal layer of finite depth. *Eur. J. Mech. B/Fluids*, 30.

[63] AV Kuznetsov. Nanofluid bioconvection in porous media: oxytactic microorganisms. *J. Porous Media*, 15:233–248, 2012.

[64] AV Kuznetsov and DA Nield. Double-diffusive natural convective boundary-layer flow of a nanofluid past a vertical plate. *International Journal of Thermal Sciences*, 50(5):712–717, 2011.

[65] S Li and JA Eastman. Measuring thermal conductivity of fluids containing oxide nanoparticles. *J. Heat Transf*, 121(2):280–289, 1999.

[66] HT Lin and LK Lin. Similarity solutions for laminar forced convection heat transfer from wedges to fluids of any prandtl number. *International journal of heat and mass transfer*, 30(6):1111–1118, 1987.

[67] VM Magagula. *Bivariate pseudospectral collocation algorithms for nonlinear partial differential equations.* PhD thesis, 2016.

[68] AH Mahmoudi and E Abu-Nada. Combined effect of magnetic field and nanofluid variable properties on heat transfer enhancement in natural convection. *Numerical Heat Transfer, Part A: Applications*, 63(6):452–472, 2013.

[69] S Manjunatha, BA Kuttan, S Jayanthi, A Chamkha, and BJ Gireesha. Heat transfer enhancement in the boundary layer flow of hybrid nanofluids due to variable viscosity and natural convection. *Heliyon*, 5(4):e01469, 2019.

[70] A Mehmood and MS Iqbal. Effect of heat absorption in natural convection nanofluid flow along a vertical wavy surface. *Journal of Molecular Liquids*, 224:1326–1331, 2016.

[71] A Mehmood, MS Iqbal, S Khan, and S Munawar. Entropy analysis in moving wavy surface boundary-layer. *Thermal Science*, 23(1):233–241, 2019.

[72] A Mehmood, S Iqbal, MS, and I Mustafa. Cooling of moving wavy surface through mhd nanofluid. *Zeitschrift fur Naturforschung A*, 71(7):583–593, 2016.

[73] A Mehmood, S Khan, and MS Iqbal. Entropy generation due to a moving isothermal wavy surface in nanofluid. *International Journal of Exergy*, 28(4):317–332, 2019.

[74] D Mei, Y Zhu, X Xu, and F Xing. Energy conservation and heat transfer enhancement for mixed convection on the vertical galvanizing furnace. *Thermal Science*, 24(2 Part B):1055–1065, 2020.

[75] Y Menni, AJ Chamkha, , and A Azzi. Nanofluid flow in complex geometries –a review. *Journal of Nanofluids*, 8:893–916, 2019.

[76] JH Merkin. Natural-convection boundary-layer flow on a vertical surface with newtonian heating. *International Journal of Heat and Fluid Flow*, 15(5):392–398, 1994.

[77] MA Mjankwi, VG Masanja, EW Mureithi, and MN James. Unsteady mhd flow of nanofluid with variable properties over a stretching sheet in the presence of thermal radiation and chemical reaction. *International Journal of Mathematics and Mathematical Sciences*, 2019, 2019.

[78] MP Mkhatshwa, SS Motsa, and P Sibanda. Mhd bioconvective radiative flow of chemically reactive casson nanofluid from a vertical surface with variable transport properties. *International Journal of Ambient Energy*, pages 1–19, 2020.

[79] A Mojtabi and MC Charrier-Mojtabi. Double-diffusive convection in porous media. *Handbook of Porous media*, 2:269–320, 2005.

[80] RJ Moreau. *Magnetohydrodynamics*, volume 3. Springer Science & Business Media, 1990.

[81] SS Motsa. A new spectral local linearization method for nonlinear boundary layer flow problems. *Journal of Applied Mathematics*, 2013, 2013.

[82] SS Motsa, Ch RamReddy, and Ch Venkata Rao. Non-similarity solution for soret effect on natural convection over the vertical frustum of a cone in a nanofluid using new bivariate pseudo-spectral local linearisation method. *Applied Mathematics and Computation*, 314:439–455, 2017.

[83] SG Moulic and LS Yao. Natural convection along a vertical wavy surface with uniform heat flux. *Journal of heat transfer*, 111:1106–1108, 1989.

[84] I Mustafa and T Javed. Heat transfer in natural convection flow of nanofluid along a vertical wavy plate with variable heat flux. *Thermal Science*, 23(1):179–190, 2019.

[85] S Nandal and R Bhargava. Numerical study of variable fluid properties and magnetic field on convectively heated inclined plate utilizing nanofluids. *International Journal of Applied and Computational Mathematics*, 3(4):3305–3320, 2017.

[86] Z Narankhishig, J Ham, H Lee, and H Cho. Convective heat transfer characteristics of nanofluids including the magnetic effect on heat transfer enhancement - a review. *Applied Thermal Engineering*, 193:116987, 2021.

[87] M Narayana, P Sibanda, SS Motsa, and PG Siddheshwar. On double-diffusive convection and cross diffusion effects on a horizontal wavy surface in a porous medium. *Boundary Value Problems*, 2012(1):1–22, 2012.

[88] DA Nield and AV Kuznetsov. The cheng–minkowycz problem for natural convective boundary-layer flow in a porous medium saturated by a nanofluid. *International Journal of Heat and Mass Transfer*, 52(25-26):5792–5795, 2009.

[89] BC Pak and YI Cho. Hydrodynamic and heat transfer study of dispersed fluids with submicron metallic oxide particles. *Experimental Heat Transfer an International Journal*, 11(2):151–170, 1998.

[90] TJ Pedley, NA Hill, and JO Kessler. The growth of bioconvection patterns in a uniform suspension of gyrotactic micro-organisms. *Journal of Fluid Mechanics*, 195:223–237, 1988.

[91] TJ Pedley and JO Kessler. Hydrodynamic phenomena in suspensions of swimming micro-organisms. *Annu. Rev. Fluid Mech*, 24:313–358, 1992.

[92] JR Platt. Bioconvection patterns in cultures of free-swimming organisms. *Science*, 133(3466):1766–1767, 1961.

[93] DVK Prasad, GSK Chaitanya, and RS Raju. Double diffusive effects on mixed convection casson fluid flow past a wavy inclined plate in presence of darcian porous medium. *Results in Engineering*, 3:100019, 2019.

[94] N Purohit, S Jakhar, P Gullo, and MS Dasgupta. Heat transfer and entropy generation analysis of alumina/water nanofluid in a flat plate pv/t collector under equal pumping power comparison criterion. *Renewable Energy*, 120:14–22, 2018.

[95] K Rafique, MI Anwar, M Misiran, I Khan, SO Alharbi, P Thounthong, and KS Nisar. Numerical solution of casson nanofluid flow over a non-linear inclined surface with soret and dufour effects by keller-box method. *Frontiers in Physics*, 7:139, 2019.

[96] ZZ Rashed, SE Ahmed, and MA Sheremet. Mhd buoyancy flow of nanofluids over an inclined plate immersed in uniform porous medium in the presence of solar radiation. *Journal of Mechanics,*, 35(4):563–576, 2019.

[97] MM Rashidi, M Nasiri, M Khezerloo, and N Laraqi. Numerical investigation of magnetic field effect on mixed convection heat transfer of nanofluid in a channel with sinusoidal walls. *Journal of Magnetism and Magnetic Materials*, 401:159–168, 2016.

[98] PS Reddy and P Sreedevi. Mhd boundary layer heat and mass transfer flow of nanofluid through porous media over inclined plate with chemical reaction. *Multidiscipline Modeling in Materials and Structures*, 17(2):317–336, 2020.

[99] DAS Rees and I Pop. Boundary layer flow and heat transfer on a continuous moving wavy surface. *Acta Mechanica*, 112:149–158, 1995.

[100] KU Rehman, AA Malik, M Tahir, and MY Malik. Undersized description on motile gyrotactic micro-organisms individualities in mhd stratified water-based newtonian nanofluid. *Results in physics*, 8:981–987, 2018.

[101] NC Roy. Magnetohydrodynamic natural flow of a nanofluid due to sinusoidal surface temperature variations. *Phys.Fluids,*, 32:id No. 022003, 2020.

[102] NC Roy and S Siddiqa. Effect of nanofluid on heat transfer enhancement for mixed convection flow over a corrugated surface. *Journal of Non-Equilibrium Thermodynamics*, 45(4):373–383, 2020.

[103] T Sajid, M Sagheer, S Hussain, and M Bilal. Darcy-forchheimer flow of maxwell nanofluid flow with nonlinear thermal radiation and activation energy. *AIP Advances*, 8(3):035102, 2018.

[104] AR Sarhan, MR Karim, ZK Kadhim, and J Naser. Experimental investigation on the effect of vertical vibration on thermal performances of rectangular flat plate. *Experimental Thermal and Fluid Science*, 101:231–240, 2019.

[105] SM Sebdani, M Mahmoodi, and SM Hashemi. Effect of nanofluid variable properties on mixed convection in a square cavity. *International Journal of Thermal Sciences*, 52:112–126, 2012.

[106] A Shahid, HL Huang, CM Khalique, and MM Bhatti. Numerical analysis of activation energy on mhd nanofluid flow with exponential temperature-dependent viscosity past a porous plate. *Journal of Thermal Analysis and Calorimetry*, 143(3):2585–2596, 2021.

[107] GA Sheikhzadeh, ME Qomi, N Hajialigol, and A Fattahi. Numerical study of mixed convection flows in a lid-driven enclosure filled with nanofluid using variable properties. *Results in Physics*, 2:5–13, 2012.

[108] A Shenoy, M Sheremet, and I Pop. *Convective flow and heat transfer from wavy surfaces: viscous fluids, porous media, and nanofluids*. CRC press, 2016.

[109] N Shukla, P Rana, S Kuharat, OA Bég, et al. Non-similar radiative bioconvection nanofluid flow under oblique magnetic field with entropy generation. *Journal of Applied and Computational Mechanics*, 2020.

[110] S Siddiqa, MN Abrar, MA Hossain, and RSR Gorla. Double diffusive natural convection flow over a wavy surface situated in a non-absorbing medium. *International Journal of Heat and Mass Transfer*, 109:200–208, 2017.

[111] S Siddiqa, N Begum, MA Hossain, and RSR Gorla. Numerical solutions of free convection flow of nanofluids along a radiating sinusoidal wavy surface. *International Journal of Heat and Mass Transfer*, 126:899–907, 2018.

[112] S Siddiqa, M Sulaiman, MA Hossain, S Islam, and RSR Gorla. Gyrotactic bioconvection flow of a nanofluid past a vertical wavy surface. *International Journal of Thermal Sciences*, 108:244–250, 2016.

[113] H Sithole, H Mondal, VM Magagula, P Sibanda, and SS Motsa. Bivariate spectral local linearisation method (bsllm) for unsteady mhd micropolar-nanofluids with homogeneous–heterogeneous chemical reactions over a stretching surface. *International Journal of Applied and Computational Mathematics*, 5(1):12, 2019.

[114] R Sivaraj, IL Animasaun, AS Olabiyi, S Saleem, and N Sandeep. Gyrotactic microorganisms and thermoelectric effects on the dynamics of 29 nm cuo-water nanofluid over an upper horizontal surface of paraboloid of revolution. *Multidiscipline Modeling in Materials and Structures*, 2018.

[115] EM Sparrow and RD Cess. *Radiation Heat Transfer: Augmented Edition*. Routledge, 2018.

[116] D Srinivasacharya, B Mallikarjuna, and R Bhuvanavijaya. Effects of thermophoresis and variable properties on mixed convection along a vertical wavy surface in a fluid saturated porous medium. *Alexandria Engineering Journal*, 55(2):1243–1253, 2016.

[117] D Srinivasacharya and P Vijay Kumar. Mixed convection along an inclined wavy surface in a nanofluid saturated porous medium with wall heat flux. *Journal of Nanofluids*, 5.

[118] D Srinivasacharya and P Vijay Kumar. Mixed convection over an inclined wavy surface embedded in a nanofluid saturated porous medium. *Int J of Numerical Methods for Heat Fluid Flow*, 25(8):1774–1792, 2015.

[119] D Srinivasacharya and P Vijay Kumar. Radiation effect on natural convection over an inclined wavy surface embedded in a non-darcy porous medium saturated with a nanofluid. *Journal of Porous Media*, 18(8), 2015.

[120] T Thumma, A Chamkha, and SR Sheri. Mhd natural convective flow of nanofluids past stationary and moving inclined porous plate considering temperature and concentration gradients with suction. *International Journal of Numerical Methods for Heat & Fluid Flow*, 2017.

[121] RK Tiwari and MK Das. Heat transfer augmentation in a two-sided lid-driven differentially heated square cavity utilizing nanofluids. *International Journal of heat and Mass transfer*, 50(9-10):2002–2018, 2007.

[122] LN Trefethen. *Spectral methods in MATLAB*. SIAM, 2000.

[123] TH Tsai, DS Liou, Kuo. LS, and PH Chen. Rapid mixing between ferro-nanofluid and water in a semi-active y-type micromixer. *Sens. Actuators*, 153:267–273, 2009.

[124] A Tulu and W Ibrahim. Mixed convection hybrid nanofluids flow of mwcnts–al2o3/engine oil over a spinning cone with variable viscosity and thermal conductivity. *Heat Transfer*, 50(4):3776–3799, 2021.

[125] MJ Uddin, WA Khan, SR Qureshi, and OA Bég. Bioconvection nanofluid slip flow past a wavy surface with applications in nano-biofuel cells. *Chinese Journal of Physics*, 55(5):2048–2063, 2017.

[126] CC Wang and CK Chen. Thermophoretic deposition of particles from a boundary layer flow onto a continuously moving wavy surface. *Acta mechanica*, 181(3):139–151, 2006.

[127] G Wang, Z Zhang, R Wang, and Z Zhu. A review on heat transfer of nanofluids by applied electric field or magnetic field. *Nanomaterials*, 10.

[128] Y Xuan and Q Li. Heat transfer enhancement of nanofluids. *International Journal of heat and fluid flow*, 21(1):58–64, 2000.

[129] NA Yacob, A Ishak, R Nazar, and I Pop. Falkner–skan problem for a static and moving wedge with prescribed surface heat flux in a nanofluid. *International Communications in Heat and Mass Transfer*, 38(2):149–153, 2011.

[130] NA Yacob, A Ishak, and I Pop. Falkner–skan problem for a static or moving wedge in nanofluids. *International Journal of Thermal Sciences*, 50(2):133–139, 2011.

[131] LS Yao. Natural convection along a vertical wavy surface. *Journal of heat transfer*, 105(3):465–468, 1983.

[132] KA Yih. Mhd forced convection flow adjacent to a non-isothermal wedge. *International Communications in Heat and Mass Transfer*, 26(6):819–827, 1999.

[133] A Zeeshan, A Majeed, MJ Akram, and F Alzahrani. Numerical investigation of MHD radiative heat and mass transfer of nanofluid flow towards a vertical wavy surface with viscous dissipation and joule heating effects using keller-box method. *Mathematics and Computers in Simulation*, 190:1080–1109, 2021.

[134] R Zhou, X Ling, H Peng, and L Yang. Thermal characteristics of the combined flat plate heat receiver in solar power tower plant. *Energy*, 165:275–289, 2018.

[135] M Ziaei-Rad, A Kasaeipoor, MM Rashidi, and G Lorenzini. A similarity solution for mixed-convection boundary layer nanofluid flow on an inclined permeable surface. *Journal of Thermal Science and Engineering Applications*, 9(2), 2017.